Application of untargeted lipidomics in biomarker studies related to gut health, obesity, and neurodegenerative disorders

(腸の健康、肥満、神経変性疾患に関連するバイオマーカー研究における非標的リピドミクスの応用)

北海道大学大学院 国際食資源学院

国際食資源専攻 博士後期課程

Hokkaido University Graduate School of Global Food Resources

Division of Global Food Resources Doctoral Course

Jayashankar Jayaprakash

Dedication

This thesis is dedicated to my beloved father, P. Jayaprakash; my mother, B. Vasantha Kumari; my brother, J. Chandrakanth; and my cherished friends, S. Mruthyunjaya and Chandramouli, whose unwavering love, support, and encouragement have been my greatest source of strength throughout this journey.

Acknowledgement

I would like to express my deepest gratitude to my supervisor, **Dr. Siddabasave Gowda Bomme Gowda**, for his exceptional guidance, unwavering support, and insightful mentorship throughout my doctoral research. His constant encouragement, constructive feedback, and thoughtful discussions have been pivotal in shaping both my research and my personal growth. I am truly fortunate to have had the opportunity to work under his mentorship, which has made this academic journey deeply enriching.

I am sincerely thankful to Dr. Divyavani Gowda, Dr. Parasuraman Perumalsamy, Dr. Hitoshi Chiba, and Dr. Shu-Ping Hui for their valuable suggestions, support, and encouragement throughout my research.

I also extend my heartfelt thanks to my lab mates, Ms. Lipsa Rani Nath and Mr. Madhuvanahalli Sundaraswamy Punith, for their continuous support, collaboration, and camaraderie that made the lab environment both motivating and enjoyable. Their positive and friendly atmosphere in the lab not only kept me focused and motivated but also inspired me to push the boundaries of my research, constantly fuelling my passion and determination.

I am grateful to Prof. P. Mallu P, Dr. C. S. Karthik, Dr. S. Sandeep, and Dr. S. Nanjundaswamy, J.S.S. Science and Technology University, for their support and encouragement during my stay in Japan.

I would also like to extend my sincere thanks to all the members of the Laboratory of Advanced Lipid Analysis (LALA).

My special thanks to Ms. S. Kavyashree for her constant encouragement, kindness, and emotional support. Her presence has been a source of strength and positivity throughout this journey

Finally, I gratefully acknowledge the support provided by the DX fellowship, Hokkaido University.

Table of contents

Abstract

Lipids are a structurally and functionally diverse group of essential biomolecules that play significant roles in maintaining cellular structure, regulating energy metabolism, and mediating signal transduction. Lipids are also involved in various physiological processes such as cell proliferation, apoptosis, immune responses, and inflammation, making them critical determinants of health and disease. Dysregulation of lipid metabolism is increasingly recognized as a hallmark of various diseases, including gut dysbiosis, obesity, and neurodegeneration. Altered lipid profiles also play crucial roles in the pathophysiology of these disorders, highlighting the need for detailed lipid-level investigations. The growing field of lipidomics, particularly untargeted approaches using high-resolution mass spectrometry, offers powerful tools for profiling lipid alterations and elucidating the complex roles of lipids in health and disease. Lipidomics enables the discovery of disease-specific lipid fingerprints and metabolic pathways, offering deep insights into disease mechanisms and aiding in the identification of novel lipid biomarkers for early diagnosis of the disease. Despite their significance, comprehensive lipidomic analyses across multiple disease conditions remain limited in biomarker research. This thesis addresses the gap by employing an untargeted liquid chromatography coupled mass spectrometry (LC/MS)-based lipidomics strategy across multiple biological contexts to uncover novel lipid biomarkers associated with metabolic and neurodegenerative disorders, including exploring the therapeutic potential of natural bioactive lipids as anti-obesity agents.

Chapter one provides an overview of lipids, their classification, and their essential roles in health and disease. The chapter also highlights the use of an untargeted LC/MS technique to profile lipid alterations in complex biological systems, emphasizing the significance of lipidomics in biomarker research. The chapter highlights the current limitations in applying comprehensive lipidomic analyses across multiple disease contexts for novel biomarker discovery. This chapter establishes a foundation for understanding how lipidomic analysis can be leveraged to investigate disease mechanisms and discover novel biomarkers for early diagnosis, therapeutic monitoring, and disease stratification.

In Chapter two, an untargeted LC/MS-based lipidomics technique was used to investigate the sex-specific effects of ethanol on the colonic lipidome in a murine model. A total of 186 lipid species were identified, revealing distinct lipidomic profiles between pair-fed and ethanol-fed groups in male mice compared to female mice. This study offers new insights into the sex-dependent lipidomic responses to alcohol-induced gut-dysbiosis, highlighting potential lipid biomarkers such as PG (O-15:1/15:0) and PE (O-18:2/15:0) in both sexes upon ethanol exposures.

Chapter three transition to human samples, leading to the identification of novel gut microbial lipids. Through untargeted LC/MS analysis, 26 isomeric lipid species, including short- and medium-chain esters of hydroxy fatty acids (SFAHFAs and MFAHFAs), were detected. Notably, two new MFAHFAs were identified and characterized for the first time in human fecal samples. These findings provide the first evidence on unique microbial lipids, opening new avenues for exploring their physiological roles.

Chapter four describes the use of untargeted lipidomics in exploring lipid alterations in neurodegenerative disorders. Lipidomic analysis of saliva, plasma, and fecal samples from stage-specific groups of Alzheimer's disease (AD) revealed dynamic alterations in lipid profiles across disease stages in older adults. The study identified medium-chain fatty acids containing triacylglycerol as a potential early-stage non-invasive lipid biomarker for mild cognitive impairment patients. In parallel, brain lipidome alterations in AD, Parkinson's disease (PD), and Huntington's disease (HD) reveal distinct lipid profiles and highlight disease-specific lipid biomarker such as AHexCer (d(O-18:1)18:1/15:0;O), PC (O-22:5/19:3), and PS (O-17:0/22:6) that could aid in distinguishing these neurodegenerative disorders.

Chapter five focused on analyzing plasma samples of pre-adolescent children in the Hokkaido region using high-resolution LC/MS to explore lipidomic variations associated with sex, age, and overweight status. The untargeted lipidomics approach enabled the characterization of 219 lipid species, revealing distinct patterns across developmental stages and weight groups. The study revealed that overweight status influences plasma lipid composition in early childhood and identified TG (10:0/10:0/18:1) as a potential lipid biomarker associated with childhood obesity.

Chapter 6 investigates the therapeutic potential of seaweed-derived bioactive lipids by identifying a natural sphingomyelin synthase (SMS) inhibitor from *Undaria pinnatifida* (wakame). Through a combination of structural characterization techniques and *in-vitro* SMS assays, FA 20:5 was confirmed as the potent bioactive compound in wakame extract responsible for the inhibition of both SMS1 and SMS2. This study highlights the discovery of natural anti-obesity agents, offering new insights into lipid metabolism-related therapeutic strategies.

Overall, this thesis demonstrates the broad applicability of untargeted lipidomics in uncovering lipid biomarkers across gut dysbiosis, obesity, and neurodegenerative disorders. By integrating multi-disease approaches, this work advances our understanding of lipid dysregulation and its role in disease pathogenesis, offering new avenues for diagnosis and intervention.

Abbreviations

MS	Mass Spectrometry
LIPID MAPS	Lipid Metabolites and Pathways Strategy
FAs	Fatty Acyls
GPs	Glycerophospholipids
GLs	Glycerolipids
SPs	Sphingolipids
STs	Sterol Lipids
PRs	Prenol Lipids
SAs	Saccharolipids
PKs	Polyketides
CVD	Cardiovascular Diseases
NDs	Neurodegenerative Disorders
SFAs	Saturated Fatty Acids
MUFAs	Mono-Unsaturated Fatty Acids
PUFAs	Polyunsaturated Fatty Acids
SCFAs	Short-chain Fatty Acids
MCFAs	Medium-chain Fatty Acids
LCFAs	Long-chain Fatty Acids
MGs	Monoacylglycerols
DGs	Diacylglycerols
TGs	Triacylglycerols
T2D	Type 2 Diabetes
PC	Phosphatidylcholine
PE	Phosphatidylethanolamine
PS	Phosphatidylserine
PI	Phosphatidylinositol
PG	Phosphatidylglycerol
CL	Cardiolipin
Cer	Ceramide

SM	Sphingomyelin
LPS	Lipopolysaccharides
CoA	Coenzyme A
AD	Alzheimer's Disease
PD	Parkinson's Disease
HD	Huntington's disease
NMR	Nuclear Magnetic Resonance
TLC	Thin-layer chromatography
GC	Gas Chromatography
LC	Liquid Chromatography
HRMS	High-Resolution Mass Spectrometry
QTOF	Quadrupole Time-of-Flight
QqQ	Tripe Quadrapole
RT	Retention Time
LC/MS	Liquid Chromatography/Mass Spectrometry
UHPLC/MS	Ultra-High-Performance Liquid Chromatography/Mass Spectrometry
CEs	Cholesteryl Esters
AAHFAs	Acyl Alpha esters of Hydroxy Fatty Acids
HPLC	High Performance Liquid Chromatography
LTQ-Orbitrap-MS	Linear Ion Trap Orbitrap Mass Spectrometry
ALD	Alcohol-associated Liver Disease
TNF	Tumor Necrosis Factor
IL	Interleukin
FFAs	Free Fatty Acids
PLs	Phospholipids
PF	Pair Fed
EF	Ethanol Fed
IS	Internal Standard
ESI	Electrospray Ionization
ANOVA	Analysis of Variance

PCA	Principal Component Analysis
SIMCA	Soft Independent Modeling by Class Analogy
SD	Standard Deviation
FAHFAs	Fatty Acid esters of Hydroxy Fatty Acids
SFAHFAs	Short-chain Fatty Acid esters of Hydroxy Fatty Acids
LPC	Lysophosphatidylcholine
LPG	Lysophosphatidylglycerols
HexCer	Hexosyl Ceramide
HBMP	Hemibismonoacylglycerophosphate
PLS-DA	Partial Least-Squares Discriminant Analysis
WT	Wild-Type
HFD	High-Fat Diet
9-PAHSA	Palmitic Acid esters of 9-Hydroxy Stearic Acid
EPA	Eicosapentaenoic Acid
Nrf2	Nuclear response factor-2
AA	Acetic Acid
PA	Propionic Acid
BA	Butyric Acid
Pla2g2a	Phospholipase A2
MiaGB	Microbiome in Aging of Gut and Brain
m/z	Mass to Charge ratio
EIC	Extracted Ion Chromatogram
EA	Enanthic Acid
CLA	Caprylic Acid
LA	Lignoceric acid
CAG	Cytosine-Adenine-Guanine
Aβ	Amyloid-β
MCI	Mild Cognitive Impairment
CSF	Cerebrospinal Fluid
HV	Healthy volunteers

BHT	Butylated Hydroxytoluene
OPLS-DA	Orthogonal Partial Least Squares Discriminant Analysis
VIP	Variable Importance in Projection
SEM	Standard Error of the Mean
LPE	Lysophosphatidylethanolamine
TG-MCFAs	Triacylglycerols containing Medium Chain Fatty Acids
DG-MCFAs	Diacylglycerols containing Medium Chain Fatty Acids
ROC	Receiver Operating Characteristic
AUC	Area Under Curve
BMI	Body Mass Index
UW	Underweight
NW	Normalweight
OW	Overweight
FC	Fold Change
CI	Cognitive Impairment
KEGG	Kyoto Encyclopedia of Genes and Genomes
Acyl-CoA	Acetyl coenzyme A
G3P	Glycerol-3-Phosphate
LPA	Lysophosphatidic Acid
PA	Phosphatidic Acid
CDP-DG	Cytidine Diphosphate Diacylglycerol
Ser	Serine
LPs	Lysophospholipids
HDL-C	High-Density Lipoprotein Cholesterol
LDL-C	Low-Density Lipoprotein Cholesterol
sPLS-DA	Sparse Partial Least Squares Discriminant Analysis
S-plot	Score Plot
POW	Percentage of Overweight
SMS	Sphingomyelin Synthase
GA	Ginkgolic Acid

BSA	Bovine Serum Albumin
ppm	Parts Per Million
TMS	Tetramethylsilane
Hz	Hertz
J	Coupling Constants
EtOAc	Ethyl Acetate
Et_2O	Diethyl Ether
DMSO	Dimethyl Sulfoxide
MD	Molecular Dynamics
RMSF	Root Mean Square Fluctuations
RMSD	Root Mean Square Deviation
PTLC	Preparative Thin Layer Chromatography
D609	Tricyclodecan-9-yl-xanthogenate

Chapter 1

General Introduction

1.1 Overview of lipids and their classification

Lipids are a highly diverse and widely distributed class of hydrophobic or amphipathic molecules that are insoluble in water but soluble in organic solvents [1]. These molecules are vital to biological systems and are among the major constituents in various daily products such as food, pharmaceuticals, and cosmetics. Their unique physicochemical properties and diverse bioactive potential make them essential for various physiological processes and industrial applications, as shown in **Figure 1.1** [2]. Lipids are essential molecules that serve as major structural components of cellular membranes and are actively involved in numerous physiological processes. These include cell signaling, immune modulation, energy production and storage, protein folding and trafficking, as well as the maintenance of cellular and systemic homeostasis [3].

Recent advancements in analytical techniques, particularly in mass spectrometry (MS) and chromatographic separation, have significantly enhanced the precise identification, structural elucidation, and quantification of thousands of lipid species across various biological systems [4]. To bring order to the immense structural and functional diversity of lipid molecules, the Lipid Metabolites and Pathways Strategy (LIPID MAPS) consortium introduced a widely accepted classification system that organizes lipids based on their source, chemical structure, and biological functions. According to the LIPID MAPS structure database, over 49,667 lipid molecular species have been identified as of April 9, 2025 (https://www.lipidmaps.org/), encompassing both manually curated entries and structures generated through computational methods [1].

These lipids are systematically classified into eight major categories, such as fatty acyls (FAs), glycerolipids (GLs), glycerophospholipids (GPs), sphingolipids (SPs), sterol lipids (STs), prenol lipids (PRs), saccharolipids (SLs), and polyketides (PKs) encompassing both manually curated entries and structures generated through computational methods [5]. Structural representations of these lipid subclasses are illustrated in **Figure 1.2**, which underscores the chemical diversity and functional specialization across lipid classes.

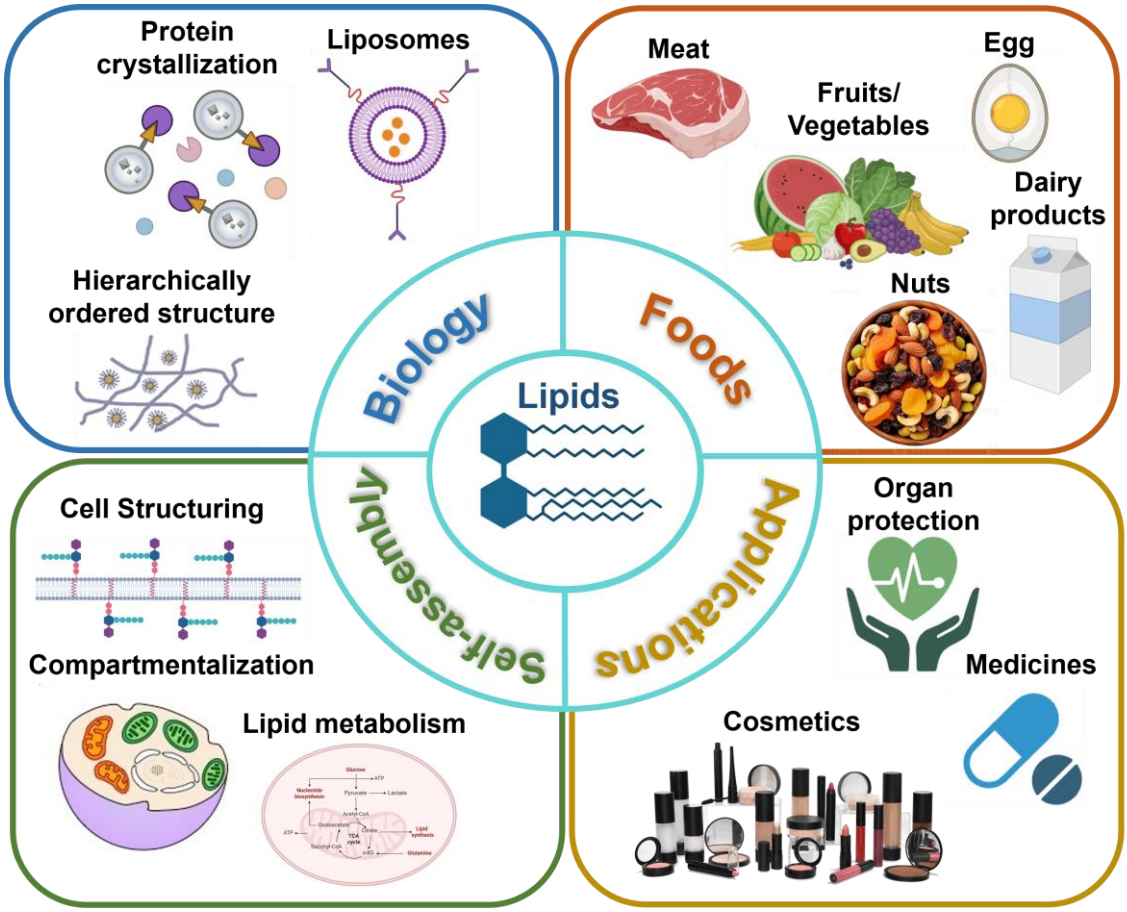

Figure 1.1: Overview of lipid applications across various fields.

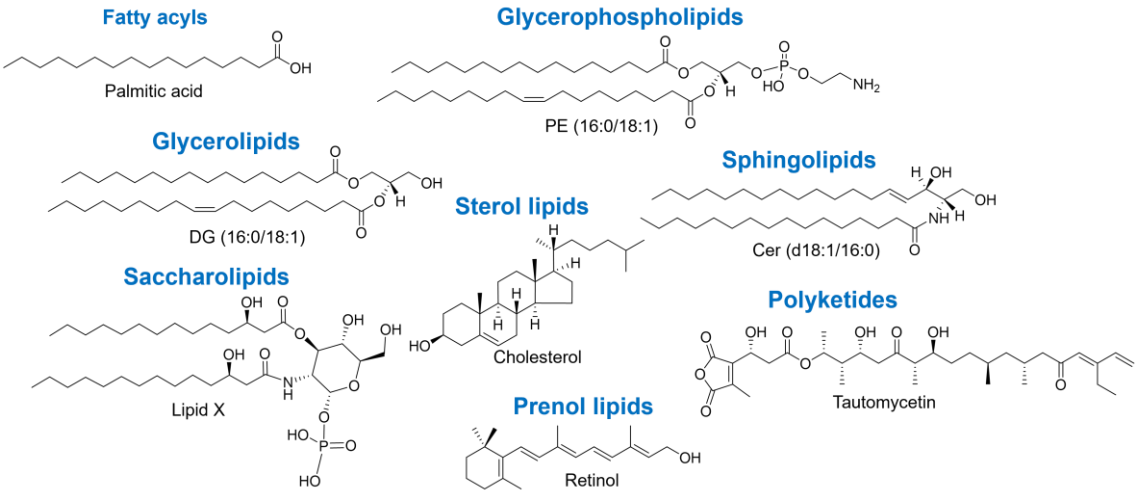

Figure 1.2: Representative structures of the 8 main sub-classes of lipids.

1.2 Lipids in Health and Disease

Lipids are vital components of human health, providing a primary energy source and playing key roles in numerous biological functions. They are critical for cell structure, function, and energy, as well as for organs and body insulation and protection. Beyond their role as energy reservoirs, lipids are involved in structural organization and compartmentalization of cellular organelles, cell differentiation, protection, induction, and resolution of acute and chronic inflammation [6]. Dysregulation in lipid metabolism has been reported in various diseases, such as cancer, obesity, diabetes, cardiovascular diseases (CVD), and neurodegenerative disorders (NDs) [7]. This highlights the roles of lipids in various biological conditions and suggests that lipids might be potential therapeutic targets in health and disease.

1.2.1 Fatty Acyls

FAs are fundamental building blocks of complex lipids, characterized by a hydrocarbon chain attached to a terminal carboxyl group. These molecules include various types of fatty acids, such as saturated fatty acids (SFAs), monounsaturated fatty acids (MUFAs), and polyunsaturated fatty acids (PUFAs), as well as their oxidized and conjugated forms. FAs are crucial for a wide range of biological processes, including energy storage, cellular structure maintenance, and regulation of signaling pathways [8]. Short- and medium-chain fatty acids (SCFAs and MCFAs), along with more abundant long-chain fatty acids (LCFAs), are found in both animal and plant tissues, where they contribute to cellular metabolism [9].

SFAs have been linked to CVD due to their increasing tendency to aggregate tightly in aqueous environments, leading to the deposition of lipid plaques on arterial walls [10]. On the other hand, PUFAs are particularly important as signaling molecules that help maintain physiological homeostasis [11]. Specifically, ω-6 PUFAs (eg., FA 18:2 and FA 20:4) are involved in cell signaling and are known for their pro-inflammatory effect, while ω-3 PUFAs (eg., FA 18:3 and FA 20:5) have demonstrated beneficial effects in managing chronic inflammation and metabolic disorders [12-13]. Furthermore, oxidation products of PUFAs, such as eicosanoids, serve as important signaling molecules involved in metabolic regulation.

1.2.2 Glycerolipids

GLs are a class of lipids composed of a glycerol backbone esterified to one, two, or three fatty acyl chains, forming mono-, di-, and tri-acylglycerols (MGs, DGs, and TGs), respectively. These molecules are primarily found in adipose tissue and serve as an important reservoir of metabolic energy [4]. Among them, TGs are the most abundant GLs and represent the major energy source of the human body upon oxidation [14]. These molecules are stored in the adipose tissue until extra energy is required. During energy-demand periods, TGs are hydrolyzed by lipases to release free fatty acids and glycerol into the bloodstream, which also provides thermal insulation [15]. Besides their role in energy storage, excessive accumulation of TGs in adipose tissue leads to obesity, associated with an increased risk of metabolic disorders such as type 2 diabetes (T2D), CVD, and certain cancers [16-18].

1.2.3 Glycerophospholipids

GPs are a major class of membrane lipids composed of a glycerol backbone esterified with two fatty acid chains and a phosphate group linked to a polar head group. GPs include phosphatidylcholine (PC), phosphatidylethanolamine (PE), phosphatidylserine (PS), phosphatidylinositol (PI), phosphatidylglycerol (PG), and cardiolipin (CL). These molecules are fundamental constituents of biological membranes, where they play critical roles in maintaining membrane structure, fluidity, and stability, cell signaling, lipid metabolism, and mitochondrial function. These features allow the membrane to support key processes such as vesicular trafficking, signal transduction, and molecular transport [19,20]. Alterations in GPs metabolism have been linked to various health issues, including CVD, NDs, pulmonary, and mitochondrial dysfunctions [21-23, 19].

1.2.4 Sphingolipids

SPs are a class of complex lipids characterized by a sphingoid base, such as sphingosine, linked to a fatty acid and polar head group. SPs are essential structural components of cell membranes, which play a critical role in cellular signaling, membrane stability, and intercellular communication [24]. They are typically enriched in neural tissue and can be found in the outer layer of membranes, where they form lipid rafts associated microdomains involved in signal transduction, cell recognition, immune

response, and stabilization [10]. Functionally, SPs have been reported to have multiple biological functions. In the central nervous system, they are crucial for brain development and neuronal function. In the gastrointestinal tract, they regulate the oral absorption of dietary nutrients. In immune systems, SPs have been reported to function in the differentiation, maturation, and functional responses of immune cells, including B and T lymphocytes [25-27]. SPs are broadly categorized into ceramides (Cer), sphingomyelins (SM), and glycosphingolipids. Among these, SM and Cer are known to regulate the activity of protein kinases and phosphatases, while glycosphingolipids, including gangliosides, act as specific receptors for hormones and other molecules on cell surfaces [10, 28]. Alterations in SPs metabolism have been associated with various pathological conditions, particularly NDs, highlighting their importance in maintaining neural health [29].

1.2.5 Sterol lipids

STs are composed of a rigid structure derived from cyclopentanoperhydrophenanthrene, consisting of three 6-membered and one 5-membered fused, non-planar rings. This unique structure provides stability and rigidity, which is essential for their biological functions. STs play a crucial role in maintaining the structural integrity of cellular membranes, modulating membrane fluidity and permeability [20]. Among them, cholesterol is the most abundant and well-characterized STs, serving not only as a structural component of animal cell membranes but also as a regulator of membrane dynamics [30]. Beyond their structural roles, STs function as precursors for the biosynthesis of several important biomolecules, including steroid hormones, bile acids, and vitamin D. These derivatives are involved in a wide range of physiological processes such as metabolic regulation, immune responses, fluid and electrolyte homeostasis, and reproductive function [10].

1.2.6 Prenol lipids

PRs are a diverse class of lipids derived from the polymerization of two or more isoprene units, typically composed of five-carbon building blocks. This class includes biologically significant subgroups such as carotenoids, retinoids, and quinones. These lipids are involved in several essential physiological processes. For instance, ubiquinones and plastoquinones serve critical roles in electron transport during cellular respiration and

photosynthesis, respectively [31]. Additionally, many PRs act as precursors for vitamins and hormones, such as vitamin A (retinol), vitamin E (tocopherol), and vitamin K (phylloquinone). Beyond their metabolic roles, PRs play an important role in cell protection under oxidative stress [31, 32].

1.2.7 Saccharolipids

SLs represent a distinctive class of lipids in which fatty acid chains are directly linked to a sugar backbone. These lipids are predominantly found in bacterial membranes and are known for their potent biological activities, particularly their ability to stimulate the immune system through endotoxin effects [33]. One of the most widely known SLs is lipid A, a bioactive component of lipopolysaccharides (LPS), which serves as a critical molecule for host immune recognition of Gram-negative bacterial infections [34]. SLs exhibit remarkable structural variability across different bacterial species, which can influence their immunogenic properties. Emerging studies suggest that SLs structures may play beneficial roles in modulating immune responses, including enhancing the efficacy of colorectal cancer immunotherapy by improving antigen and tumor recognition [35].

1.2.8 Polyketides

PKs are a diverse group of secondary metabolites synthesized through the condensation of propionyl-coenzyme A (CoA) and methylmalonyl-CoA [10]. These molecules exhibit a broad range of potent biological activities, including antibacterial, antiparasitic, antitumor, cholesterol-lowering, and immunosuppressive effects. Due to their diverse therapeutic properties, polyketides have garnered significant attention as valuable sources for the development of novel pharmacological agents [36].

1.3 Role of Lipidomics in the Omics Research

Lipidomics is a specialized branch of metabolomics dedicated to the comprehensive analysis and characterization of lipid species and their dynamic roles in biological systems. The term “lipidome”, referring to the entire collection of chemically distinct lipid molecular species in a cell, organ, or biological system, was first appeared in a peer-reviewed publication in 2001 [37]. The field of lipidomics formally emerged in 2003 and was defined as “the full characterization of lipid molecular species and of their

biological roles with respect to expression of proteins involved in lipid metabolism and function, including gene regulation" [38]. Lipidomics has gained increasing attention from both academic researchers and clinical scientists, and it is now regarded as a crucial tool for investigating a wide range of diseases and physiological processes, such as atherosclerosis, Alzheimer's disease (AD), and certain types of cancer. Furthermore, lipidomics is increasingly applied across diverse fields, offering new insights into complex biological systems and disease mechanisms [39].

The structural diversity and complexity of lipids pose significant challenges in analytical chemistry, particularly in their comprehensive characterization and quantification. To address this complexity, techniques such as MS and nuclear magnetic resonance (NMR) spectroscopy have become indispensable tools for the detailed analysis of lipid molecular species. On the other hand, various separation technologies, such as thin-layer chromatography (TLC), gas chromatography (GC), liquid chromatography (LC), supercritical fluid chromatography, and capillary electrophoresis, are essential tools for the comprehensive analysis of lipids in complex biological matrices [40]. These separation methods are commonly coupled with MS to enhance the sensitivity and specificity of lipidomic analyses.

Two principal approaches are employed in lipidomic analysis using MS: targeted lipidomics and untargeted (or global) lipidomics. Targeted lipidomics is particularly focused on the precise quantification of specific lipid species, typically those involved in one or several lipid pathways. The most widely utilized techniques in targeted lipidomics are multiple reaction monitoring and parallel-reaction monitoring acquisition modes, which provide high sensitivity and specificity by monitoring predefined precursor-product ion transitions for selected lipid targets [41]. In contrast, untargeted lipidomics, also referred to as global lipidomics, seeks to provide a comprehensive and unbiased analysis of the lipidome within a biological matrix. This approach is particularly advantageous for elucidating the structural composition of lipids due to its high mass resolution and accuracy [42]. Untargeted lipidomics is especially valuable for discovering novel lipids and identifying changes associated with disease interventions that are overlooked in targeted approaches.

Untargeted lipidomics workflows typically employ high-resolution MS (HRMS) platforms, such as quadrupole time-of-flight (QTOF), Orbitrap, and triple quadrupole (QqQ) MS, often coupled with LC. These advanced techniques enhance sensitivity, detection limits, and the structural elucidation of lipid species, enabling the detection of thousands of lipids in a single analysis [43]. This allows for a comprehensive understanding of lipid diversity and dynamic alterations across various diseases. Data processing and annotation are also critical components of lipidomics. Software platforms such as MS-DIAL support initial lipid identification by leveraging integrated spectral library matching, which incorporates accurate mass, retention time (RT), and MS/MS fragmentation pattern comparisons to ensure reliable lipid annotation.

The application of untargeted lipidomics serves as the central methodology for exploring disease-related lipid alterations across metabolic disorders, NDs, cardiovascular conditions, and gastrointestinal health, making it an ideal platform for understanding disease mechanisms and discovering lipid biomarkers for early diagnosis, disease stratification, and therapeutic monitoring [44].

1.4 Untargeted lipidomics- a tool for biomarker discovery

The concept of biomarker discovery involves identifying molecular indicators that can predict disease risk, aid in early diagnosis, monitor disease progression, or evaluate therapeutic response. In this context, LC/MS-based untargeted lipidomics techniques are increasingly applied to biomarker discovery, which provides a comprehensive platform for detecting perturbations in lipid metabolic pathways, enabling the profiling of thousands of lipid species across multiple classes. This makes it an ideal platform for identifying novel lipid biomarkers for diagnosing various diseases [43, 44].

Recent advances in LC/MS-based untargeted lipidomics have significantly improved the sensitivity and facilitated the detection of low-abundance lipids that may serve as early indicators of diseases. Lipid-based biomarkers have been increasingly reported across various domains. For instance, studies have shown that ultra-high-performance LC/MS (UHPLC/MS)-based untargeted lipidomics identified a panel of 10 plasma lipids as a “biomarker” to distinguish AD patients from controls, of which 6 were identified as long-chain cholesteryl esters (CEs), with approximately 80% accuracy [45]. Similarly, in childhood obesity, untargeted serum lipidomics revealed elevated levels of

PC, CE, TGs, and branched chain amino acids that distinguish obese children from healthy controls, potentially serving as potential biomarkers and used to study obesity pathomechanisms in adolescents [46]. Apart from applications in human diseases, the strategy of lipidomics-driven biomarker discovery has also been used to identify novel lipid mediators involved in gut health. Koelmel et al. (2020) used untargeted lipidomics alongside 16S rRNA sequencing to identify acyl alpha esters of hydroxy fatty acids (AAHFAs) as microbiota-specific lipids, with significant reductions observed in antibiotic-treated mice [47]. However, previous studies have successfully demonstrated the potential of untargeted lipidomics in identifying biomarkers for various conditions, but they are often limited to sample type and validation across diverse populations. In contrast, the present thesis overcomes some of these limitations by employing a multi-matrix approach, incorporating both human and animal models, and aiming to uncover novel lipids and discover lipid biomarkers relevant to gut health, obesity, and NDs.

1.5 Significance and Aim of the Thesis

The increasing global prevalence of metabolic and NDs, alongside growing recognition of gut health, highlights the urgent need for improved diagnostic strategies and a deeper mechanistic understanding of disease progression. Lipids, being key structural and signaling molecules, play critical roles in cellular communication, metabolic regulation, and physiological function- all of which are central to the pathophysiology of gut health, obesity, and neurodegeneration. Lipid dysregulation has been observed across these conditions, suggesting the potential of lipid molecules as sensitive indicators of disease onset and progression.

Despite rapid advancements in untargeted lipidomics, significant gaps remain in identifying lipid-based biomarkers with high translational potential across multiple disease states. Untargeted LC/MS-based lipidomics, involving the comprehensive and unbiased analysis of the entire lipidome using HRMS, has emerged as a powerful tool for discovering novel lipid biomarkers. This study integrates a series of studies applying LC/MS-based untargeted lipidomics across animal models and human populations, spanning different life stages and pathological conditions. These investigations aim to identify novel lipid mediators and signatures that contribute to disease pathogenesis and

may serve as early lipid biomarkers for diagnosis, monitoring, or risk stratification, as depicted in **Figure 1.3**.

This thesis aims to harness the power of LC/MS-based untargeted lipidomics to discover novel lipid biomarkers across a spectrum of health conditions, including gut dysbiosis, childhood obesity, and NDs. By utilizing high-performance LC (HPLC) coupled with linear ion trap-Orbitrap-MS (LTQ-Orbitrap-MS), the study seeks to comprehensively profile lipid metabolites across diverse biological samples. Firstly, the study investigates gut dysbiosis by performing untargeted lipidomic profiling of colon content samples from ethanol-treated mice, aiming to uncover lipid biomarkers associated with intestinal health. Secondly, to explore the lipid alterations in childhood obesity, the study examines plasma lipid profiles from preadolescent children to identify weight-specific lipid biomarkers that could serve as an early indicator of metabolic risk. Lastly, the study focuses on analyzing lipidomic alterations in saliva, plasma, fecal, and brain tissue samples from individuals affected by NDs to discover novel lipid biomarkers for early diagnosis, disease monitoring, and therapeutic development.

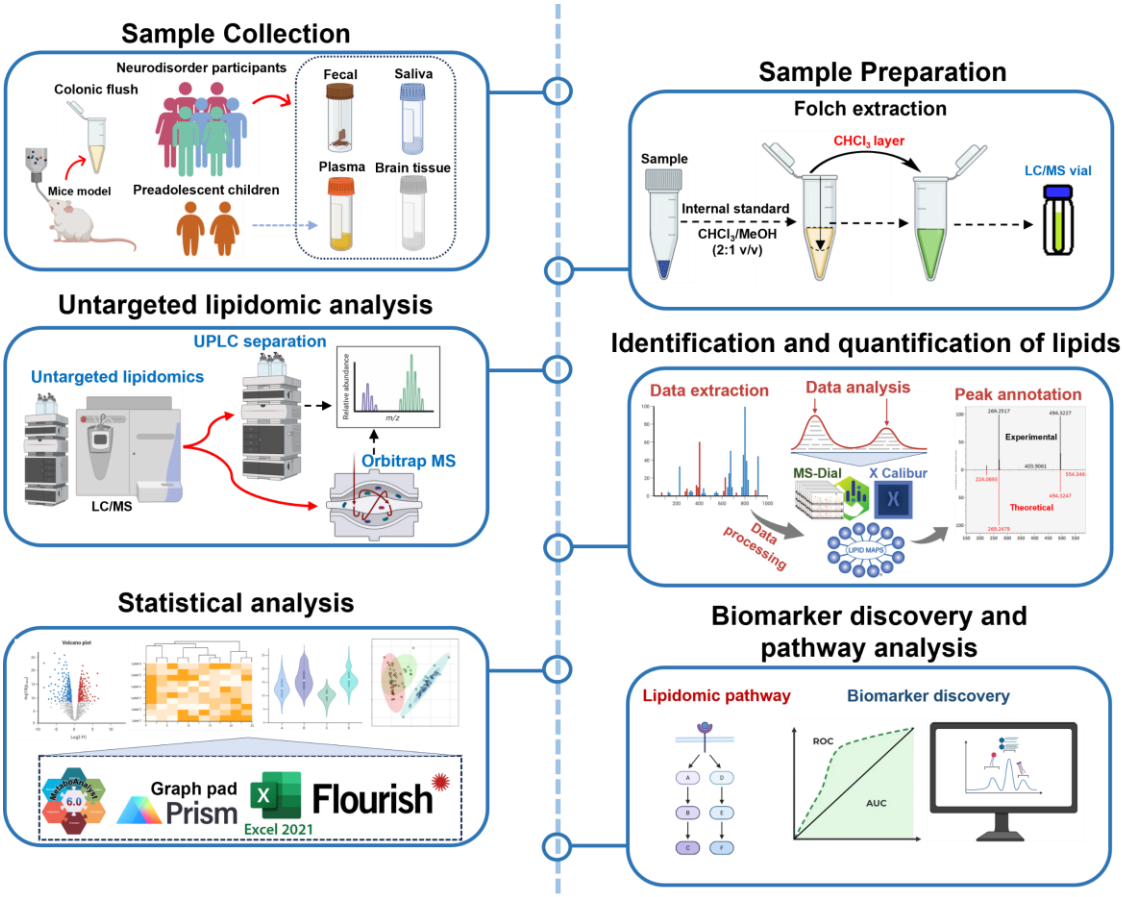

Figure 1.3: Study design for untargeted lipidomics workflow in lipid biomarker research.

1.6 References:

1. Fahy, E., Cotter, D., Sud, M., & Subramaniam, S. (2011). Lipid classification, structures and tools. Biochimica et Biophysica Acta (BBA)-Molecular and Cell Biology of Lipids, 1811(11), 637-647.
2. Kulkarni, C. V. (2012). Lipid crystallization: from self-assembly to hierarchical and biological ordering. Nanoscale, 4(19), 5779-5791.
3. Mouritsen, O. G. (2005). Life-as a matter of fat (Vol. 538). Springer-Verlag Berlin Heidelberg.
4. Wenk, M. R. (2005). The emerging field of lipidomics. Nature reviews Drug discovery, 4(7), 594-610.
5. Conroy, M. J., Andrews, R. M., Andrews, S., Cockayne, L., Dennis, E. A., Fahy, E., Guad, C., Griffith, W. J., Jukes, G., Kochin, M., Mendivelso, K., Lopez-Clavijo, A. F., Ready, C., Subramaniam, S., & O'Donnell, V. B. (2024). LIPID MAPS: update to databases and tools for the lipidomics community. Nucleic Acids Research, 52(D1), D1677-D1682.
6. Amin, K. A., Homeida, A. M., El Mazoudy, R. H., Hashim, K. S., & Garelnabi, M. (2019). Dietary lipids in health and disease. Journal of Lipids, 2019, 5729498.
7. Leuti, A., Fazio, D., Fava, M., Piccoli, A., Oddi, S., & Maccarrone, M. (2020). Bioactive lipids, inflammation and chronic diseases. Advanced Drug Delivery Reviews, 159, 133-169.
8. Jenkins, B., West, J. A., & Koulman, A. (2015). A review of odd-chain fatty acid metabolism and the role of pentadecanoic acid (C15: 0) and heptadecanoic acid (C17: 0) in health and disease. Molecules, 20(2), 2425-2444.
9. Schönfeld, P., & Wojtczak, L. (2016). Short-and medium-chain fatty acids in energy metabolism: the cellular perspective. Journal of lipid research, 57(6), 943-954.
10. Bou Khalil, M., Hou, W., Zhou, H., Elisma, F., Swayne, L. A., Blanchard, A. P., Yao, Z., Bennett, A. A. L., & Figeys, D. (2010). Lipidomics era: accomplishments and challenges. Mass spectrometry reviews, 29(6), 877-929.
11. Simopoulos, A. P. (2016). An increase in the omega-6/omega-3 fatty acid ratio increases the risk for obesity. Nutrients, 8(3), 128.

12. Serhan, C. N., & Chiang, N. (2013). Resolution phase lipid mediators of inflammation: agonists of resolution. Current opinion in pharmacology, 13(4), 632-640.
13. Valenzuela, P. L., Carrera-Bastos, P., Gálvez, B. G., Ruiz-Hurtado, G., Ordovas, J. M., Ruilope, L. M., & Lucia, A. (2021). Lifestyle interventions for the prevention and treatment of hypertension. Nature Reviews Cardiology, 18(4), 251-275.
14. Yen, C. L. E., Stone, S. J., Koliwad, S., Harris, C., & Farese Jr, R. V. (2008). Thematic review series: glycerolipids. DGAT enzymes and triacylglycerol biosynthesis. Journal of lipid research, 49(11), 2283-2301.
15. Yen, C. L. E., Nelson, D. W., & Yen, M. I. (2015). Intestinal triacylglycerol synthesis in fat absorption and systemic energy metabolism. Journal of lipid research, 56(3), 489-501.
16. Gross, R. W., & Han, X. (2007). Lipidomics in diabetes and the metabolic syndrome. Methods in enzymology, 433, 73-90.
17. Lowe, M. E. (2002). The triglyceride lipases of the pancreas. Journal of lipid research, 43(12), 2007-2016.
18. Rosen, E. D., & Spiegelman, B. M. (2006). Adipocytes as regulators of energy balance and glucose homeostasis. Nature, 444(7121), 847-853.
19. Van Meer, G., Voelker, D. R., & Feigenson, G. W. (2008). Membrane lipids: where they are and how they behave. Nature reviews Molecular cell biology, 9(2), 112-124.
20. Hunte, C., & Richers, S. (2008). Lipids and membrane protein structures. Current opinion in structural biology, 18(4), 406-411.
21. van Meer G. (2005). Cellular lipidomics. The EMBO journal, 24(18), 3159–3165.
22. Tzelepi, V., Gika, H., Begou, O., & Timotheadou, E. (2023). The contribution of lipidomics in ovarian cancer management: a systematic review. International Journal of Molecular Sciences, 24(18), 13961.
23. Brzozowski, J. S., Jankowski, H., Bond, D. R., McCague, S. B., Munro, B. R., Predebon, M. J., ... & Weidenhofer, J. (2018). Lipidomic profiling of extracellular vesicles derived from prostate and prostate cancer cell lines. Lipids in health and disease, 17, 1-12.
24. Hannun, Y. A., & Obeid, L. M. (2008). Principles of bioactive lipid signalling: lessons from sphingolipids. Nature reviews Molecular cell biology, 9(2), 139-150.

25. Dasgupta, S., & Ray, S. K. (2017). Diverse biological functions of sphingolipids in the CNS: ceramide and sphingosine regulate myelination in developing brain but stimulate demyelination during pathogenesis of multiple sclerosis. Journal of neurology and psychology, 5(1), 10-13188.

26. Kurek, K., Łukaszuk, B., Piotrowska, D. M., Wiesiołek, P., Chabowska, A. M., & Żendzian-Piotrowska, M. (2013). Metabolism, physiological role, and clinical implications of sphingolipids in gastrointestinal tract. BioMed research international, 2013(1), 908907.

27. Zhang, X., Matsuda, M., Yaegashi, N., Nabe, T., & Kitatani, K. (2020). Regulation of necroptosis by phospholipids and sphingolipids. Cells, 9(3), 627.

28. Liebisch, G., Vizcaíno, J. A., Köfeler, H., Trötzmüller, M., Griffiths, W. J., Schmitz, G., Spener, F., & Wakelam, M. J. (2013). Shorthand notation for lipid structures derived from mass spectrometry. Journal of lipid research, 54(6), 1523-1530.

29. Platt, F. M., Boland, B., & van der Spoel, A. C. (2012). Lysosomal storage disorders: The cellular impact of lysosomal dysfunction. Journal of Cell Biology, 199(5), 723-734.

30. Bloch, K. E. (1983). Sterol, structure and membrane function. Critical Reviews in Biochemistry, 14(1), 47-92.

31. Fahy, E., Subramaniam, S., Brown, H. A., Glass, C. K., Merrill Jr, A. H., Murphy, R. C., Raetz, C. R. H., Russell, D. W., Seyama, Y., Shaw, W., Shimizy, T., Spener, F., Meer, G. V., VanNieuwenhze, M. S., White, S. H., Witztum, J. L., & Dennis, E. A. (2005). A comprehensive classification system for lipids. European journal of lipid science and technology, 107(5), 337-364.

32. Martano, C., Mugoni, V., Dal Bello, F., Santoro, M. M., & Medana, C. (2015). Rapid high performance liquid chromatography–high resolution mass spectrometry methodology for multiple prenol lipids analysis in zebrafish embryos. Journal of Chromatography a, 1412, 59-66.

33. Park, J., Choi, J., Kim, D. D., Lee, S., Lee, B., Lee, Y., ... & Oh, Y. K. (2021). Bioactive lipids and their derivatives in biomedical applications. Biomolecules & Therapeutics, 29(5), 465.

34. Raetz, C. R., & Whitfield, C. (2002). Lipopolysaccharide endotoxins. Annual review of biochemistry, 71(1), 635-700.

35. Song, W., Tiruthani, K., Wang, Y., Shen, L., Hu, M., Dorosheva, O., Qiu, K., Kinghorn, K. A., Liu, R., & Huang, L. (2018). Trapping of lipopolysaccharide to promote immunotherapy against colorectal cancer and attenuate liver metastasis. Advanced materials, 30(52), 1805007.

36. Dutta, S., Whicher, J. R., Hansen, D. A., Hale, W. A., Chemler, J. A., Congdon, G. R., Narayan A. R. H., Håkansson, K., Sherman, D. H., Smith, J. L., & Skiniotis, G. (2014). Structure of a modular polyketide synthase. Nature, 510(7506), 512-517.

37. Kishimoto, K., Urade, R., Ogawa, T., & Moriyama, T. (2001). Nondestructive quantification of neutral lipids by thin-layer chromatography and laser-fluorescent scanning: suitable methods for "lipidome" analysis. Biochemical and biophysical research communications, 281(3), 657-662.

38. Spener, F., Lagarde, M., Géloên, A., & Record, M. (2003). What is lipidomics?. European Journal of Lipid Science and Technology, 105(9), 481-482.

39. Li, M., Yang, L., Bai, Y., & Liu, H. (2014). Analytical methods in lipidomics and their applications. Analytical chemistry, 86(1), 161-175.

40. Li, M., Zhou, Z., Nie, H., Bai, Y., & Liu, H. (2011). Recent advances of chromatography and mass spectrometry in lipidomics. Analytical and bioanalytical chemistry, 399, 243-249.

41. Xu, T., Hu, C., Xuan, Q., & Xu, G. (2020). Recent advances in analytical strategies for mass spectrometry-based lipidomics. Analytica chimica acta, 1137, 156-169.

42. Rustam, YH, & Reid, GE (2018). Analytical challenges and recent advances in mass spectrometry based lipidomics. Analytical chemistry , 90 (1), 374-397.

43. Cajka, T., & Fiehn, O. (2016). Toward merging untargeted and targeted methods in mass spectrometry-based metabolomics and lipidomics. Analytical chemistry, 88(1), 524-545.

44. Hu, C., van der Heijden, R., Wang, M., van der Greef, J., Hankemeier, T., & Xu, G. (2009). Analytical strategies in lipidomics and applications in disease biomarker discovery. Journal of Chromatography B, 877(26), 2836-2846.

45. Proitsi, P., Kim, M., Whiley, L., Pritchard, M., Leung, R., Soininen, H., ... & Legido-Quigley, C. (2015). Plasma lipidomics analysis finds long chain cholesteryl esters to be associated with Alzheimer's disease. Translational psychiatry, 5(1), e494-e494.

46. Szczerbinski, L., Wojciechowska, G., Olichwier, A., Taylor, M. A., Puchta, U., Konopka, P., Paszko, A., Citko, A., Goscik, J., Fiehn, O., Fan, S., Wasilewska, A., Taranta-Jansz, K., & Kretowski, A. (2022). Untargeted metabolomics analysis of the serum metabolic signature of childhood obesity. Nutrients, 14(1), 214.

47. Yasuda, S., Okahashi, N., Tsugawa, H., Ogata, Y., Ikeda, K., Suda, W., Arai, H., Hattori, M., & Arita, M. (2020). Elucidation of gut microbiota-associated lipids using LC-MS/MS and 16S rRNA sequence analyses. Iscience, 23(12).

Chapter 2

Exploring ethanol-induced colonic lipidome alterations in sex-specific mice models using untargeted LC/MS

2.1 Introduction

Alcohol consumption is a major contributor to global morbidity and mortality, exerting detrimental effects across various organ systems, notably the liver, gut, and brain, ultimately leading to multisystemic disorders [1, 2]. Chronic alcohol intake significantly increases the risk of alcohol-associated liver disease (ALD), driven by oxidative stress, increased intestinal permeability, and systemic endotoxemia [3]. Extensive research using both animal and human models has consistently demonstrated a strong link between alcohol use and gut microbiota disruption, commonly referred to as gut dysbiosis [1, 4]. This dysbiosis, along with alcohol-induced disruption of tight junction proteins in the intestinal epithelium, facilitates the translocation of bacterial endotoxins into the mucosa, triggering immune dysfunction and systemic inflammation. This response is marked by elevated levels of pro-inflammatory cytokines such as tumor necrosis factor (TNF)-α and interleukin (IL)-1β, which further impair gut barrier integrity [5, 6]. Central to this process is the gut-liver axis, a bidirectional communication pathway between the gut and liver that mediates the transport of digestive and bacterial metabolites, amplifying liver damage in the presence of gut dysfunction [7].

The intestinal mucosal barrier plays a critical role in gut immune function, maintained by intercellular tight junctions between neighbouring enterocytes [8]. Alcohol exposure significantly alters the gut metabolome, leading to alterations in key metabolic profiles, particularly lipids such as free fatty acids (FFAs), SCFAs, bile acids, and amino acids [9]. FFAs, derived from the lipolysis of adipose tissue and various cell types, play essential roles as signaling molecule precursors and building blocks for various lipids, including phospholipids (PLs) present in cell membranes [10, 11]. Studies have shown that these lipids have been implicated in the pathogenesis of ALD, influencing both pro-inflammatory and inflammation-resolving lipid signaling pathways, and thereby represent promising therapeutic targets for ALD [12]. In contrast, SCFAs- especially butyrate- exert beneficial effects on gut barrier function by potentially reducing intestinal permeability when present in appropriate concentrations [13].

Previous studies on lipid metabolism in alcohol-induced gut dysbiosis have provided limited insight into the broader relationship between ethanol-induced gut dysbiosis and host lipid metabolism, particularly with respect to sex-specific differences. Previous studies on ethanol-induced alterations in lipid metabolism have focused on

specific lipid classes by employing techniques such as LC coupled with QqQ and QTOF/MS analysis [14, 15]. These studies have demonstrated that alcohol consumption can significantly alter the gut microbiota and associated lipid metabolism. However, they are limited in scope as they do not capture the full spectrum of lipidomic changes, particularly in relation to the sex-specific effect of ethanol on gut lipid metabolism, which remains unclear. To address this gap, the present study aims to systematically investigate the comprehensive lipidome of the effect of alcohol-induced gut dysbiosis in a mice model of both sexes using HPLC coupled with LTQ-Orbitrap-MS was employed to enable broad and high-resolution lipid profiling (**Figure 2.1**). To our knowledge, this is the first study to systematically explore the sex-specific effects of ethanol on gut lipid metabolism, shedding light on the intricate interplay between alcohol consumption and lipid alterations. This may pave the way for a deeper understanding of the underlying mechanisms and potential therapeutic strategies to address alcohol-related pathologies in a sex-specific context.

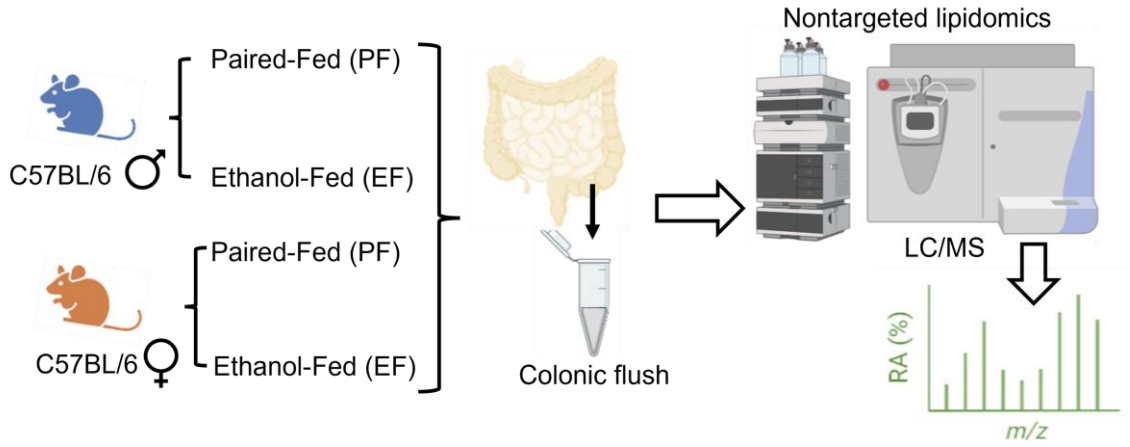

Figure 2.1: Schematic overview of colon content lipidomic analysis in pair-fed (PF) and ethanol-fed (EF) mice.

2.2 Materials and Methods

2.2.1 Chemicals and reagents

The solvents used in the study, including methanol, 2-propanol, and a mobile-phase additive of 1 M aqueous ammonium acetate, were sourced from Wako Pure Chemical Industries, Ltd. (Osaka, Japan). HPLC-grade chloroform was obtained from Sigma-Aldrich (MO). Deuterium-labeled internal standard (IS), namely EquiSPLASH

(Lot: 330731-1EA-013) and oleic acid-d9, were procured from Avanti Polar Lipids (Alabaster, AL).

2.2.2 Animal samples

Adult male and female C57BL/6 mice, aged 8 to 10 weeks, were used for the study. These animals were bred and maintained in the institutional core facility at the University of Tennessee Health Science Center (UTHSC). All animal studies reported in this work were approved by the Institutional Animal Care and Use Committee (IACUC). The mice were housed under a 12-hour light/dark cycle, with unrestricted access to standard laboratory food and water. Each cage housed two animals under controlled environmental conditions [16].

2.2.3 Chronic ethanol feeding

To simulate chronic alcohol exposure, mice were administered a Lieber–DeCarli liquid diet (Dyets Inc., Bethlehem, PA), which included a gradual increase in ethanol-fed (EF) concentration over four weeks (0% for 2 days, 1% for 2 days, 2% for 2 days, 4% for 1 week, 5% for 1 week, and 6% for 1 week). Control mice were pair-fed (PF) an isocaloric maltodextrin diet (BioServ, NJ). The diet intake (mL/g BW/day) for male mice (PF: 0.68, EF: 0.66) and female mice (PF: 0.73, EF: 0.72) was recorded, respectively. Body weight was monitored throughout the study. At the end of the 4-week feeding period, both PF and EF mice (n = 4 for each group) of both sexes were euthanized. Colonic contents were then flushed with 3 mL of 0.9% saline and stored at −80°C until lipid extraction.

2.2.4 Lipid extraction

Lipid extraction from colonic flush samples of both male (PF, EF) and female (PF, EF) mice was performed using the Folch extraction method with slight modifications [17]. Briefly, 100 µL of colonic flush from each mouse was mixed with 100 µL of methanol and 100 µL of IS solution (comprising oleic acid-d9 at 100 µg/mL and EquiSPLASH Lipidomic mix at 10 µg/mL in methanol) in a 2 mL Eppendorf tube. Next, 400 µL of chloroform was added, and the mixture was vortexed at 3500 rpm for 5 min. The samples were then centrifuged at 15,000 rpm for 10 min to separate the layers. The lower chloroform layer, containing the lipids, was transferred to a new 2 mL Eppendorf tube. To the residue, 400 µL of chloroform was added again and vortexed for 1 min, followed

by centrifugation for 10 min. The chloroform layer was transferred to the same new 2 mL Eppendorf tube [18]. The combined extract was evaporated at 4°C for 3 hours using a centrifuge evaporator. Finally, the extract was redissolved in 100 μL of methanol, followed by vortexing and centrifugation for 10 min at 15,000 rpm, and transferred to LC/MS vials.

2.2.5 Lipidomic analysis by HPLC/LTQ-Orbitrap MS

Lipid analysis was performed using an LTQ-Orbitrap-MS (Thermo-Fisher Scientific Inc., San Jose, CA) coupled with an HPLC based on the LC-20AD ultra fluid LC system (Shimadzu Corp., Kyoto, Japan). Lipids were separated using an Atlantis T3 C18 column (2.1 mm × 150 mm, 3 μM, Waters, Milford, MA) at a flow rate of 0.2 mL/min with a mobile-phase gradient consisting of aqueous 10 mM ammonium acetate (A), isopropanol (B), and methanol (C). The column was maintained at 40°C throughout the analysis. These LC/MS conditions were consistent with our previous studies. The mobile phase composition was adjusted as follows: 30% B and 35% C from 0 to 1 min, 75% B and 15% C from 1 to 9 min, 82.5% B and15% C from 9 to 21 min, 95% B and 5% C from 21 to 25 min, 30% B and 35% C from 25 to 26 min, and 30% B and 35% C from 26 to 30 min. On the other hand, the positive mode analysis used a distinct linear gradient: 30% B and 35% C from 0 to 1 min, 82.5% B and 15% C from 1 to 9 min, followed by a steady state of 95% B and 5% C from 9 to 15 min, 95% B and 5% C from 15 to 25 min. A brief return to 30% B and 35% C was made from 25 to 26 min, and finally, the composition was kept constant at 30% B and 35% C from 26 to 30 min.

MS analysis was performed using an LTQ-Orbitrap-MS (Thermo Fisher Scientific Inc., San Jose, CA) operating in both positive and negative ionization modes. Instrumental parameters were consistent with those described in our previously published studies [20]. For the electrospray ionization (ESI), the capillary temperature was maintained at 330 °C, with nitrogen sheath and auxiliary gas flow rates set at 50 and 20 arbitrary units, respectively. In negative ion mode, the source and capillary voltages were set to 3 kV and 10 V, respectively, and the scan range was *m/z* 160–1900. In positive ion mode, these voltages were adjusted to 4 kV and 25 V, respectively, with a scan range of *m/z* 150–1950. Full MS (MS^1) spectra were acquired in Fourier transform mode at a

resolving power of 60,000. Additionally, low-resolution MS/MS spectra were collected in the ion trap mode using a collision energy of 40 V [21].

2.2.6 LC/MS data processing and lipid quantification

Data processing was carried out using MS-DIAL software version 4.9, which was instrumental in performing key steps such as peak detection, alignment, deconvolution, annotation, and integration of peak areas [22]. The parameters applied included a minimum peak height threshold of 1000 amplitude, a maximum charge number of 2, a smoothing level of 3 scans, and a minimum peak width of 5 scans. Additional settings included a mass slice width of 0.1 Da, a σ window value of 0.5, and an identification score threshold of 80 % to ensure reliable lipid annotation. Further, signal intensity 5-fold greater than the blank was selected with RT alignment and MS^1 tolerance 0.1 min and 0.015 Da, respectively. Lipid identification was validated by comparing the RT characteristics and percentage matching between the reference and experimental MS/MS spectra. The software enabled high-throughput, accurate identification of lipid species. For the relative quantification of lipid molecular species, we followed the established lipidomics protocols. This involved calculating the peak area ratios of the identified lipids to the internal standard. These ratios were subsequently multiplied by the known concentration of the IS and normalized to the sample volume to estimate the relative abundance of each lipid species.

2.2.7 Statistical analysis

The dataset analysis comprised lipid molecular species detected in both positive and negative ion modes. Data visualization was performed using Microsoft Excel 2021, and graphs were created with GraphPad Prism version 8.0.1. Statistical analysis involved one-way analysis of variance (ANOVA) with Tukey's multiple comparison test, with significance set at $p < 0.05$. Principal component analysis (PCA) was conducted using soft independent modeling by class analogy (SIMCA) 14.1 (Umetrics), with score plots used to assess group similarities and loading plots (model coefficients vs covariance) to identify key discriminating lipid features. One-way ANOVA was also performed using MetaboAnalyst 5.0 (https://www.metaboanalyst.ca), following the user guidelines. All results are expressed as mean ± standard deviation (SD).

2.3 Results

2.3.1 Sex-specific lipid profiling and multivariate analysis in ethanol-treated mice

Male and female mice were categorized into PF and EF groups. Following sacrifice, colonic contents were collected and subjected to total lipid extraction, followed by untargeted lipidomic profiling using HPLC/LTQ-Orbitrap-MS. A total of 186 lipid molecular species were identified and characterized based on accurate mass measurements and MS/MS fragmentation patterns using MS-DIAL software. Relative lipid concentrations were determined using IS normalization. The results of one-way ANOVA and PCA on all quantified lipid species are presented in **Figure 2.2. Figure 2.2A** highlights statistically significant and non-significant lipid metabolites based on one-way ANOVA results, with $p < 0.05$. Out of 186 metabolites, 158 lipid molecular species were statistically significant. **Figure 2.2B** displays the multivariate PCA score plot of annotated lipids from both male and female PF and EF groups. The first two components together explained 69.2% of the total variance, with component 1 accounting for 40.5%.

The PCA results revealed distinct clustering between the male PF and EF groups, highlighting a clear separation in their lipidomic profiles. In contrast, female PF and EF groups exhibited overlapping clusters, suggesting minimal differences in their lipid composition. **Figure 2C** illustrates the corresponding loading plot, which displays the variables contributing to the observed group separation in the PCA. The loading plot shows how different lipid species are distributed and how they contribute to the variation between samples. Lipid molecules with high positive or negative loading scores exert the greatest influence on the components. Lipid molecular species that largely influence the group separation in the PCA score plot along components 1 and 2 are shown in **Figure 2.2C**, indicating their pivotal role in group separation. These findings identify specific lipids responsible for the observed separation in the two-dimensional PCA plot.

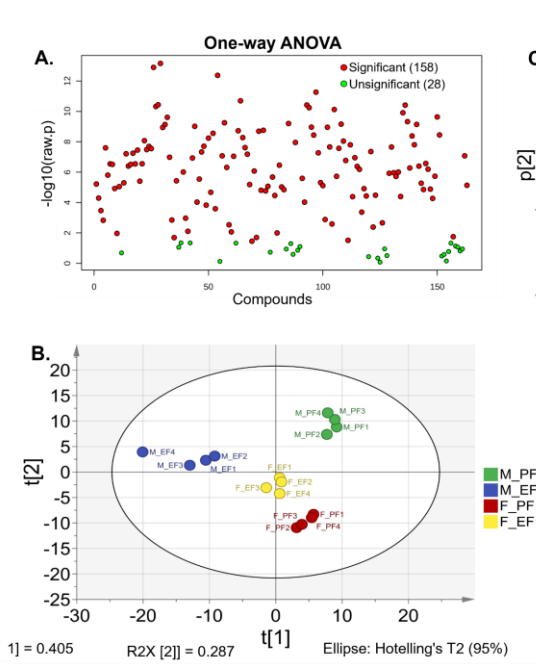

Lipid$	p[1]	p[2]	Lipid#	p[1]	p[2]
PG (O-16:1/18:1)	0.078	-0.050	PG (15:0/15:0)	0.027	0.128
HBMP 54:4	0.073	0.085	FA 16:0;(2OH)	0.018	0.128
HBMP 52:4	0.063	0.038	PE (14:0/15:0)	0.013	0.127
AAHFA 3:0/22:0;O	0.062	0.105	PG (16:0/18:1)	0.013	0.127
HBMP 51:4	0.044	0.060	PG (O-16:1/16:0)	0.018	0.126
HexCer (40:0;4O)	-0.113	0.003	FAHFA 22:1/18:0;O	0.020	-0.129
HexCer (38:0;4O)	-0.112	0.010	TG (O-21:1/17:0/18:1)	0.005	-0.126
HexCer (42:1;4O)	-0.112	0.004	Cer (42:1;2O)	0.018	-0.126
Cer (36:0;3O)	-0.112	0.000	FAHFA 18:1/18:0;O	0.034	-0.126
HexCer (40:1;4O)	-0.112	-0.002	Cer (42:0;2O)	0.032	-0.125

Figure 2.2. Multivariant analysis of lipid metabolites in PF (n = 4) and EF (n = 4) colonic flush samples of male and female mice. **A.** One-way ANOVA analysis of 186 lipid species identified across the groups (Tukey's honestly significant difference with $p < 0.05$). **B.** Principal Component Analysis (PCA) score plot highlighting the distinct differences between the four cohorts. **C.** PCA loading plot and scores of lipid metabolites from both sexes. Lipid species with large positive and negative contributions to components p[1] and p[2] are marked by the symbols $ and #, respectively.

2.3.2 Sex-specific changes in top altered lipids and fatty acyls: A hierarchical cluster correlation analysis

Figure 2.3A presents the results of the cluster correlation analysis for the top 50 lipids that exhibited significant changes between the PF and EF groups in both sexes, based on their *p*-values. Lipids with higher concentrations are represented by intense red, while those with lower concentrations are shown in blue. In male mice, alcohol feeding caused notable changes in the colonic lipid profile compared to females. Specific lipids such as FA 20:1 to fatty acid esters of hydroxy fatty acids (FAHFA 16:0/18:0;O), including several hexosyl ceramide (HexCer 34:1;3O, HexCer 34:0;4O, HexCer 40:0;4O, and HexCer 38:0;4O) were significantly increased in the EF group of males compared to the PF group. In contrast, female mice displayed higher levels of lipids such as FA 20:2, FA

22:5, FA 15:1, and Cer (Cer (35:0;3O), Cer (48:1;4O), Cer (33:0;3O)) in the EF group than in the PF group. Conversely, lipids like FAHFA 16:0/18:0;O, FAHFA 18:2/18:0;O, FAHFA 18:1/18:0;O, and FAHFA 22:1/18:0;O were decreased in the EF group of females, as shown at the top of the heatmap. **Figure 2.3B** shows the cluster correlation analysis results for various FAs, including FFAs, HFAs, FAHFA, and AAHFA (also known as short chain fatty acid esters of HFAs (SFAHFA)). As mentioned earlier, several FFAs, such as SFAs (e.g., FA 24:0), MUFAs (e.g., FA 20:1), PUFAs (e.g., FA 22:6), and FA 18:1;(2OH), were increased in the EF group of male mice. Meanwhile, female mice exhibited higher levels of FA 20:2, FA 22:5, and AAHFA 3:0/24:1;O in the EF group compared to the PF group.

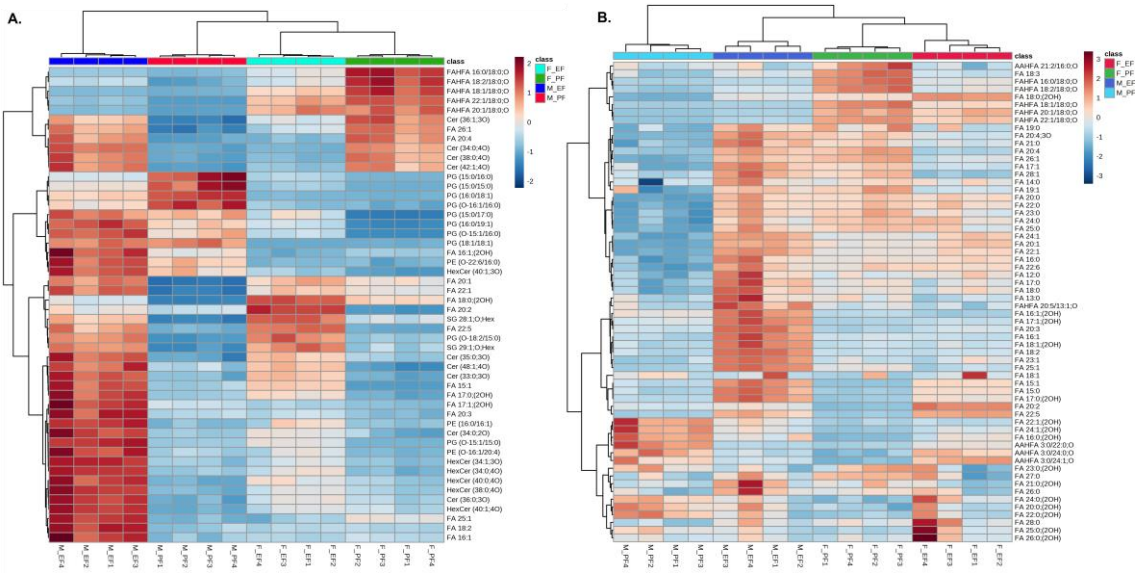

Figure 2.3: Hierarchical cluster correlation analysis of lipidomic alterations in the colonic flush samples from both male and female mice in the PF (n = 4) and EF (n = 4) groups representing **A.** Significantly altered lipids (p < 0.05) and **B.** Fatty acyls (clustering method: ward, distance measure: Euclidean).

2.3.3 Sex-specific alterations in glycerophospholipids and sphingolipids: A hierarchical cluster correlation approach

Figure 2.4 presents the results of hierarchical cluster correlation analysis for GPs and SPs visualized as heatmaps. In both male and female mice, the GPs, particularly PE, located at the bottom of the heatmap in **Figure 2.4A**, were found to be at higher levels in the EF group compared to the PF group. Additionally, lipid species such as PG (O-

16:1/18:1), lysophosphatidylcholine (eg., LPC 16:0), and lysophosphatidylglycerols (eg., LPG O-18:0) were decreased, whereas certain PE and PG species (i.e., PE (O-18:2/15:0), PG (O-18:2/15:0), PE (O-18:1/18:1), PE (O-16:1/15:0), and PE (O-16:1/18:1)) were increased in the EF group of female mice compared to the PF group. The analysis of SPs, as shown in **Figure 2.4B**, revealed that many Cer and HexCer were increased in the EF group of male mice compared to the PF group. For female mice, specific Cer (i.e., Cer (49:1;4O), Cer (50:1;4O), Cer (51:1;4O)) and HexCer (i.e., HexCer (42:0;4O), HexCer (42:0;3O), HexCer (43:0;4O), HexCer (44:0;4O)) showed increased levels in the EF group. Significant changes in SP levels, specifically in male mice, by the effect of ethanol on gut lipid metabolism, suggest that the SP pathway is a potential target for further investigations involving alcohol-induced effects.

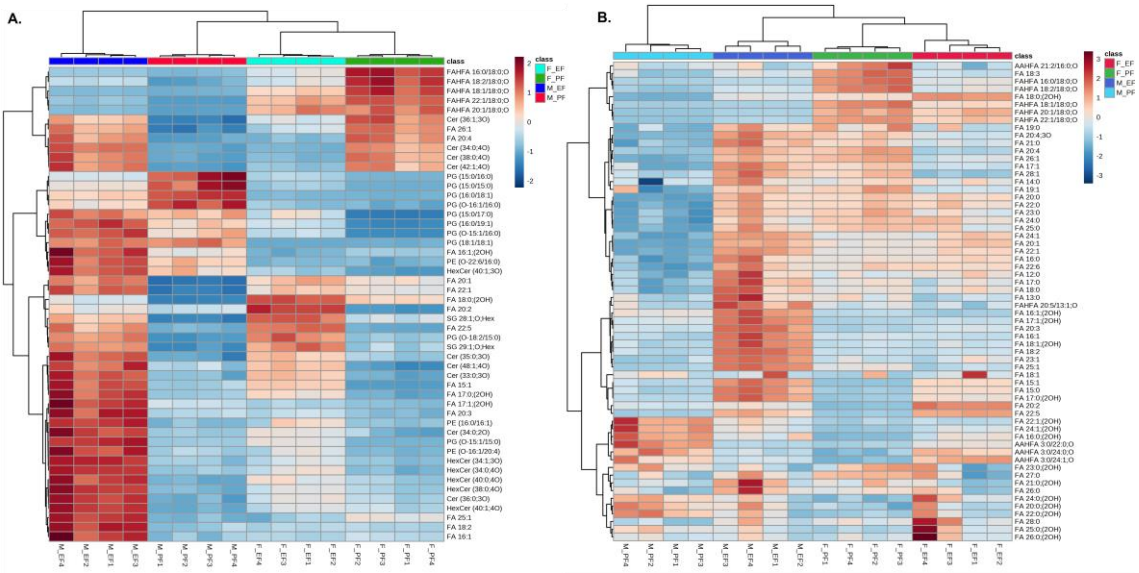

Figure 4: Hierarchical cluster correlation analysis of lipidomic alterations in the colonic flush samples from both male and female mice in the PF (n = 4) and EF (n = 4) groups, representing **A.** Glycerophospholipids (GPs) and **B.** Sphingolipids (SPs) (clustering method: ward, distance measure: Euclidean).

2.3.4 Identifying sex-specific lipid biomarkers for the impact of ethanol on gut metabolism using volcanic plots

A volcanic plot represents the graph of $-\log_{10}(p\text{-value})$ vs $\log_2$ (fold change), was used to highlight lipid molecular species that showed significant alterations. The volcanic plots for the lipid profiles of male and female mice's colon content are presented in **Figure**

2.5. The data clearly demonstrate that several lipid species, such as PE (O-18:2/15:0) and PG (O-15:1/15:0), and many others, were significantly upregulated (marked in red on the right) in the EF group of male mice compared to the PF group (**Figure 2.5A**). Conversely, certain lipids, like AAHFA 3:0/22:0;O and PG (15:0/16:0), shown in blue on the left, were downregulated in the EF group compared to the PF group. In female mice, lipids, including FA 15:1, FA 22:5, FA 20:2, PG (O-15:1/16:0), PG (0–15:1/15:0), and many other lipid species, were notably increased in the EF group, as shown in **Figure 2.5B**. In contrast, several lipids, such as PG (O-16:1/18:1), FA 18:3, FA 20:4, and many other lipids, were decreased in the EF group, with these lipids appearing in blue on the plot. Interestingly, both PE (O-18:2/15:0) and PG (O-15:1/15:0) were elevated in the colon contents of both male and female mice in the EF group, suggesting these lipids may serve as common markers for alcohol's impact on gut metabolism across both sexes.

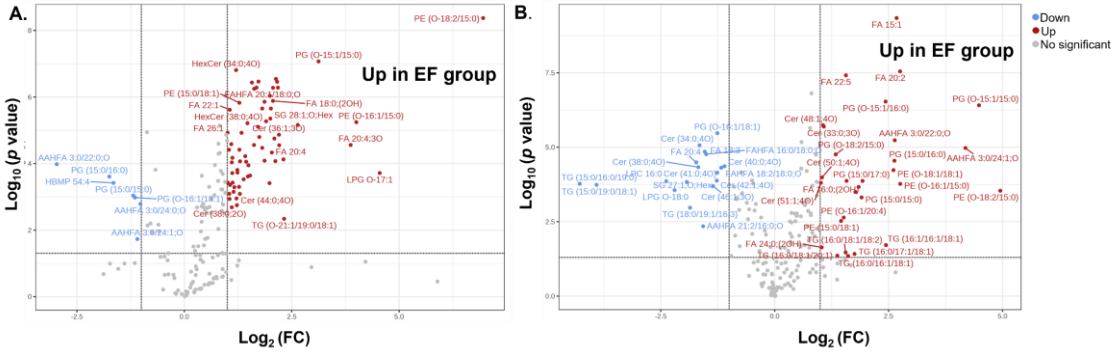

Figure 2.5: Volcano plot showing significantly altered lipids (t-test, $p < 0.05$) in the colonic flush samples of **A.** Male mice in the PF vs EF group (n = 4). **B.** Female mice in the PF vs EF group (n = 4).

2.2.5 Variation in lipid subclass levels induced by the effect of ethanol feeding

Figure 2.6 illustrates the changes in lipid subclasses due to ethanol feeding in both male and female mice. The bar graph shows the concentration of each lipid subclass as the sum of the individual lipid species within the respective groups. In both sexes, the concentration of PE lipids was increased in the EF group compared to the PF group of both sexes, with a more pronounced increase observed in male mice. Conversely, PG and hemibismonoacylglycerophosphate (HBMP) levels were significantly decreased in EF group of male mice, but no significant changes were seen in females. FAHFA levels were significantly decreased in the EF group of female mice, while no significant changes were

detected in the male mice. The short-chain fatty acid-derived lipid AAHFA was significantly decreased in male mice but exhibited an opposite trend in female mice. SPs such as Cer were increased in the EF group of male mice, whereas no such change was observed in female mice. HexCer showed a significant elevation in both sexes in the EF group compared to the PF group. Furthermore, the FAs compositions were analyzed at the SFAs, MUFAs, and PUFAs levels. As shown in Figure 6, in all cases, male EF mice had higher concentrations compared with the PF group, whereas female mice did not show any significant differences in all cases. In conclusion, the increased levels of PE, Cer, HexCer, and FA, along with decreased PG and HBMP, represent specific markers of ethanol's impact on gut lipid metabolism. In female mice with increased PE, HexCer, and decreased FAHFA, AAHFA appears to be the marker of the ethanol-induced effects on the gut.

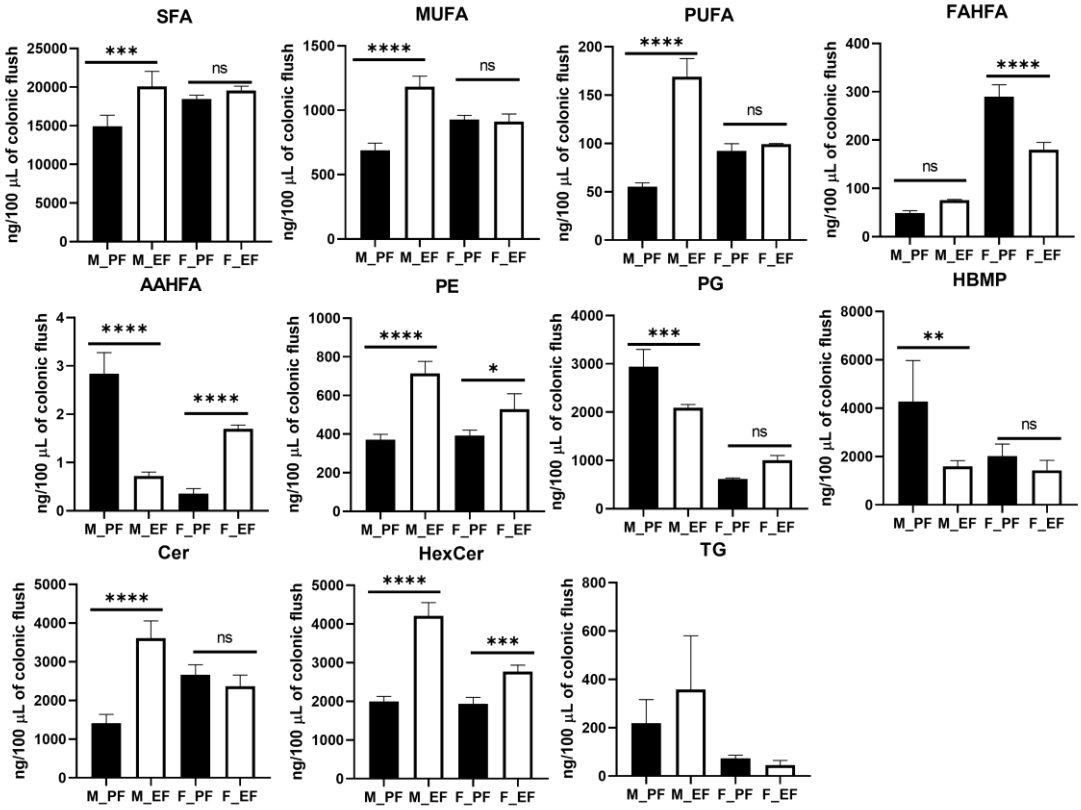

Figure 2.6: Alterations in the total lipidome at the subclass level in the PF (n = 4) and EF (n = 4) groups of both sexes (Ordinary one-way ANOVA, ****p < 0.0001, ***p <0.001, **p <0.01, *p< 0.05, (ns).)

2.3 Discussion

Ethanol consumption significantly impacts the gut barrier, which has major implications for the development and progression of gut dysbiosis. Alcohol is known to disrupt the balance of gut microbiota and increase intestinal mucosal permeability, allowing harmful microbial products such as LPS to enter the bloodstream [23, 24]. This condition, often referred to as "leaky gut," is associated with various diseases, including ALD, alcoholic steatohepatitis, and inflammatory bowel disease [25, 26]. Lipids are vital for gut metabolism, particularly in maintaining the integrity of the gut barrier. In a healthy gut, a variety of lipids, such as PLs, cholesterol, and various FFAs, are present, contributing to cell membrane stability and barrier function [27]. Ethanol-induced dysbiosis can disrupt lipid metabolism, with studies showing that alcohol alters gut microbiota composition, leading to increased levels of LPS and other lipid derivatives [28]. Multivariate PCA showed distinct group separations in the score plot. To confirm these findings, partial least-squares discriminant analysis (PLS-DA) was performed, and the results, which also indicated a large separation between the PF and EF groups, are shown in the **Appendix Figure 2.1.** Both PCA and PLS-DA results demonstrated similar group distinctions.

As depicted in **Figure 2.3**, significant increases in SFAs [FA 26:0, FA 13:0, FA 21:0 (2OH), FA 12:0, and FA 17:0] and MUFAs [FA 16:1, FA 17:1 (2OH), FA 18:1 (2OH), FA 23:1, FA 25:1] were observed in the male EF group compared to the PF group. However, no such changes were seen between the PF and EF groups in female mice for SFAs and MUFAs. Previous studies have emphasized the critical role of FFAs metabolism in the progression and development of ALD [10, 29]. Several studies show that FFAs have been implicated in the development of alcohol-induced gut dysbiosis, a condition where ethanol intake disrupts gut microbiota balance and potentially contributes to gastrointestinal disorders [30]. In a previous animal study, it was suggested that maintaining intestinal levels of FFAs, particularly SFAs, could help sustain gut barrier integrity [31]. Additionally, PUFAs like FA 18:2, FA 20:3, and FA 22:6 were increased in the male EF group, while FA 20:2 and FA 22:5 were increased in female mice under similar conditions. The increase in MUFAs and PUFAs in the male liver samples fed with ethanol aligns with our findings in colonic flushes [14]. Furthermore, a previous study using both wild-type (WT) and fat-1 mice exposed to ethanol feeding showed

significantly higher levels of total ω-6 PUFAs in both the WT-ethanol and fat-1-ethanol groups [32].

FAHFAs are emerging endogenous lipids recognized for their anti-inflammatory and antidiabetic effects [33]. In our study, we observed a decrease in FAHFA 18:1/18:0;O, FAHFA 20:1/18:0;O, and FAHFA 22:1/18:0;O in the EF group of female mice. Conversely, AAHFA 3:0/24:1;O levels were increased in these mice. In male mice, the levels of AAHFA (3:0/24:0;O) and AAHFA (3:0/22:0;O) decreased in the EF group. AAHFAs, also referred to as SFAHFA, were previously identified in our lab and have been shown to be decreased in the colon contents of male rats on a high-fat diet (HFD), while they increase in male mice infected with the influenza virus [34, 19]. Additionally, recent *in-vitro* studies have demonstrated that *Bacteroides acidifies* can promote FAHFA levels through Spearman correlation analysis with the mouse gut microbiota [35]. GPs are vital components of cellular membranes and play a crucial role in cellular functions. The modulation of GPs is influenced by alcohol-induced gut dysbiosis [36]. In this study, total PE levels were found to increase in both male and female EF groups (**Figure 2.4**), whereas PG and HBMP levels were notably decreased in the male mice EF group. A previous study in male mice fed ethanol for 5 weeks showed decreased PG in the liver in the EF group compared with controls [37].

Previous studies have highlighted the bioactive roles of SPs in various pathological conditions, including cancer, inflammation, obesity, and NDs, observed in both human and animal models [38, 39]. In this study, an increase in SPs, particularly Cer in male EF mice, and HexCer levels in both male and female EF groups was noted. These findings align with a prior study that reported an increase in Cer levels in the liver of EF mice exhibiting dysbiosis [40]. However, no significant differences in the total TG content in the colon were observed between PF and EF groups for both sexes, as shown in **Appendix Figure 2.2**. A previous study found that occludin knockout mice exposed to ethanol exhibited increased colon permeability and enhanced TG accumulation in the liver compared to WT mice [41]. This research provides valuable insight into lipid class variations in both PF and EF groups across sexes, as well as a detailed lipid composition analysis. Nevertheless, certain limitations must be addressed in future studies, such as the semiquantitative nature of the concentrations reported here, rather than absolute levels. Additional validation with a larger sample size of fresh animals may be needed to confirm

these results. While various molecular species of SPs, GPs, and FAs were detected in the EF samples of both male and female mice, the precise mechanisms behind their metabolism remain unclear.

2.4 Conclusion

In summary, lipid profiling of colon flush samples from both male and female PF and EF mice was conducted to explore lipid metabolism in alcohol-associated disorders. Relative concentrations of lipid species were observed between PF and EF mice of both males and females. Statistical analysis indicated notable changes in FAs and SPs levels in male PF and EF groups. Both male and female EF groups showed elevated levels of GPs, especially PG (O-15:1/15:0) and PE (O-18:2/15:0), which were identified as common markers. Female EF mice exhibited a specific reduction in FAHFA, underlining the significance of this lipid species in alcohol-related disorders. Overall, significant differences in the lipidome were detected between the EF and PF diets. This study highlights the efficacy of untargeted lipid profiling using HPLC/LTQ-MS in analyzing global lipid profiles in PF and EF-fed mice. This research provides important insights into the sex-specific aspects of lipid metabolism in alcohol-related diseases, offering new perspectives on the potential mechanisms behind these conditions.

2.6 References

1. Rehm, J., Samokhvalov, A. V., & Shield, K. D. (2013). Global burden of alcoholic liver diseases. Journal of hepatology, 59(1), 160-168.
2. Mathurin, P., & Bataller, R. (2015). Trends in the management and burden of alcoholic liver disease. Journal of hepatology, 62(1), S38-S46.
3. Parlesak, A., Schäfer, C., Schütz, T., Bode, J. C., & Bode, C. (2000). Increased intestinal permeability to macromolecules and endotoxemia in patients with chronic alcohol abuse in different stages of alcohol-induced liver disease. Journal of hepatology, 32(5), 742-747.
4. Litwinowicz, K., Choroszy, M., & Waszczuk, E. (2020). Changes in the composition of the human intestinal microbiome in alcohol use disorder: a systematic review. The American Journal of Drug and Alcohol Abuse, 46(1), 4-12.
5. Bode, C., & Bode, J. C. (2003). Effect of alcohol consumption on the gut. Best practice & research Clinical gastroenterology, 17(4), 575-592.
6. Bala, S., Marcos, M., Kodys, K., Csak, T., Catalano, D., Mandrekar, P., & Szabo, G. (2011). Up-regulation of microRNA-155 in macrophages contributes to increased tumor necrosis factor α (TNFα) production via increased mRNA half-life in alcoholic liver disease. Journal of Biological Chemistry, 286(2), 1436-1444.
7. Zima, T., & Kalousová, M. (2005). Oxidative stress and signal transduction pathways in alcoholic liver disease. Alcoholism: Clinical and Experimental Research, 29, 110S-115S.
8. Suzuki, T. (2013). Regulation of intestinal epithelial permeability by tight junctions. Cellular and molecular life sciences, 70, 631-659.
9. Silva, Y. P., Bernardi, A., & Frozza, R. L. (2020). The role of short-chain fatty acids from gut microbiota in gut-brain communication. Frontiers in endocrinology, 11, 508738.
10. Jeon, S., & Carr, R. (2020). Alcohol effects on hepatic lipid metabolism. Journal of lipid research, 61(4), 470–479.
11. Van Meer, G., Voelker, D. R., & Feigenson, G. W. (2008). Membrane lipids: where they are and how they behave. Nature reviews Molecular cell biology, 9(2), 112-124.

12. Voutilainen, T., & Kärkkäinen, O. (2019). Changes in the human metabolome associated with alcohol use: a review. Alcohol and Alcoholism, 54(3), 225-234.
13. Binienda, A., Twardowska, A., Makaro, A., & Salaga, M. (2020). Dietary carbohydrates and lipids in the pathogenesis of leaky gut syndrome: An overview. International journal of molecular sciences, 21(21), 8368.
14. Fang, C., Zhou, Q., Liu, Q., Jia, W., & Xu, Y. (2022). Crosstalk between gut microbiota and host lipid metabolism in a mouse model of alcoholic liver injury by chronic baijiu or ethanol feeding. Food & Function, 13(2), 596-608.
15. Yasuda, S., Okahashi, N., Tsugawa, H., Ogata, Y., Ikeda, K., Suda, W., Arai, H., Hattori, M., & Arita, M. (2020). Elucidation of gut microbiota-associated lipids using LC-MS/MS and 16S rRNA sequence analyses. Iscience, 23(12).
16. Meena, A. S., Shukla, P. K., Rao, R., Canelas, C., Pierre, J. F., & Rao, R. (2023). TRPV6 deficiency attenuates stress and corticosterone-mediated exacerbation of alcohol-induced gut barrier dysfunction and systemic inflammation. Frontiers in Immunology, 14, 1093584.
17. Gowda, S. G. B., Gowda, D., Hou, F., Chiba, H., Parcha, V., Arora, P., Halade, G. V., & Hui, S. P. (2022). Temporal lipid profiling in the progression from acute to chronic heart failure in mice and ischemic human hearts. Atherosclerosis, 363, 30-41.
18. Gowda, S. G. B., Gao, Z. J., Chen, Z., Abe, T., Hori, S., Fukiya, S., Ishizuka, S., Yokota, A., Chiba, H., & Hui, S. P. (2020). Untargeted lipidomic analysis of plasma from high-fat diet-induced obese rats using UHPLC–linear trap Quadrupole–Orbitrap MS. Analytical Sciences, 36(7), 821-828.
19. B. Gowda, S. G., Gowda, D., Ohno, M., Liang, C., Chiba, H., & Hui, S. P. (2021). Detection and structural characterization of SFAHFA homologous series in mouse colon contents by LTQ-Orbitrap-MS and their implication in influenza virus infection. Journal of the American Society for Mass Spectrometry, 32(8), 2196-2205.
20. Gowda, S. G. B., Minami, Y., Gowda, D., Chiba, H., & Hui, S. P. (2022). Detection and characterization of lipids in eleven species of fish by non-targeted liquid chromatography/mass spectrometry. Food Chemistry, 393, 133402.
21. Gowda, S. G. B., Sasaki, Y., Hasegawa, E., Chiba, H., & Hui, S. P. (2022). Lipid fingerprinting of yellow mealwormTenebrio molitor by untargeted liquid chromatography-mass spectrometry. Journal of Insects as Food and Feed, 8(2), 157-168.

22. Gowda, S. G. B., Yifan, C., Gowda, D., Tsuboi, Y., Chiba, H., & Hui, S. P. (2022). Analysis of antioxidant lipids in five species of dietary seaweeds by liquid chromatography/mass spectrometry. Antioxidants, 11(8), 1538.

23. Bishehsari, F., Engen, P. A., Preite, N. Z., Tuncil, Y. E., Naqib, A., Shaikh, M., Rossi, M., Wilber, S., Green, S. J., Hamaker, B. R., Khazaie, K., Voigt, R. M., Forsyth, C. B., & Keshavarzian, A. (2018). Dietary fiber treatment corrects the composition of gut microbiota, promotes SCFA production, and suppresses colon carcinogenesis. Genes, 9(2), 102.

24. Mutlu, E. A., Gillevet, P. M., Rangwala, H., Sikaroodi, M., Naqvi, A., Engen, P. A., Kwasny, M., Lau, C. K., & Keshavarzian, A. (2012). Colonic microbiome is altered in alcoholism. American Journal of Physiology-Gastrointestinal and Liver Physiology, 302(9), G966-G978.

25. Mendes, B. G., & Schnabl, B. (2020). From intestinal dysbiosis to alcohol-associated liver disease. Clinical and molecular hepatology, 26(4), 595.

26. Salim, S. A. Y., & Söderholm, J. D. (2011). Importance of disrupted intestinal barrier in inflammatory bowel diseases. Inflammatory bowel diseases, 17(1), 362-381.

27. Cani, P. D., Bibiloni, R., Knauf, C., Waget, A., Neyrinck, A. M., Delzenne, N. M., & Burcelin, R. (2008). Changes in gut microbiota control metabolic endotoxemia-induced inflammation in high-fat diet–induced obesity and diabetes in mice. Diabetes, 57(6), 1470-1481.

28. Yan, A. W., E. Fouts, D., Brandl, J., Stärkel, P., Torralba, M., Schott, E., Tsukamoto, H., Nelson, K. E., Brenner, D. A., & Schnabl, B. (2011). Enteric dysbiosis associated with a mouse model of alcoholic liver disease. Hepatology, 53(1), 96-105.

29. Hwang, S., & Gao, B. (2019). How does your fat affect your liver when you drink?. The Journal of clinical investigation, 129(6), 2181-2183.

30. Hartmann, P., Seebauer, C. T., & Schnabl, B. (2015). Alcoholic liver disease: the gut microbiome and liver cross talk. Alcoholism: Clinical and Experimental Research, 39(5), 763-775.

31. Chen, P., Torralba, M., Tan, J., Embree, M., Zengler, K., Stärkel, P., Pijkeren, J. V., Depew, J., Loomba, R., Ho, S. B., Bajaj, J. S., Mutlu, E. A., Keshavarzian, A., Tsukamoto, H., Nelson, K. E., Fouts, D. E., & Schnabl, B. (2015). Supplementation of

saturated long-chain fatty acids maintains intestinal eubiosis and reduces ethanol-induced liver injury in mice. Gastroenterology, 148(1), 203-214.

32. Warner, D. R.., Warner, J. B., Hardesty, J. E., Song, Y. L., King, T. N., Kang, J. X., Chen, C.-Y., Xie, S., Yuan, F., Prodhan, M. A. I., Ma, X., Zhang, X., Rouchka, E. C., Maddipati, K. R., Whitlock, J., Li, E. C., Wang, G. P., McClain, C. J., & Kirpich, I. A. (2019). Decreased ω-6: ω-3 PUFA ratio attenuates ethanol-induced alterations in intestinal homeostasis, microbiota, and liver injury. Journal of lipid research, 60(12), 2034-2049.

33. Yore, M. M., Syed, I., Moraes-Vieira, P. M., Zhang, T., Herman, M. A., Homan, E. A., Patel, R. T., Lee, J., Chen, S., Peroni, O. D., Dhaneshwar, A. S., Hammarstedt, A., Smith, U., McGraw, T. E., Saghatelian, A., & Kahn, B. B. (2014). Discovery of a class of endogenous mammalian lipids with anti-diabetic and anti-inflammatory effects. Cell, 159(2), 318-332.

34. Gowda, S. G. B., Liang, C., Gowda, D., Hou, F., Kawakami, K., Fukiya, S., Yokota, A., Chiba, H., & Hui, S. (2020). Identification of short-chain fatty acid esters of hydroxy fatty acids (SFAHFAs) in a murine model by nontargeted analysis using ultra-high-performance liquid chromatography/linear ion trap quadrupole-Orbitrap mass spectrometry. Rapid communications in mass spectrometry, 34(17), e8831.

35. Yan, S., Zhu, Y., Li, L., Qin, S., Yuan, J., Chang, X., & Hu, S. (2023). Alginate oligosaccharide ameliorates azithromycin-induced gut microbiota disorder via Bacteroides acidifaciens-FAHFAs and Bacteroides-TCA cycle axes. Food & Function, 14(1), 427-444.

36. Wang, X., Li, L., Bian, C., Bai, M., Yu, H., Gao, H., ... & Zhao, R. (2023). Alterations and correlations of gut microbiota, fecal, and serum metabolome characteristics in a rat model of alcohol use disorder. Frontiers in Microbiology, 13, 1068825.

37. Koelmel, J. P., Tan, W. Y., Li, Y., Bowden, J. A., Ahmadireskety, A., Patt, A. C., Orlicky, D. J., Mathé, E., Kroeger, N. M., Thompson, D. C., Cochran, J. A., Golla, J. P., Kandyliari, A., Chen, Y., Charkoftaki, G., Guingab-Cagmat, J. D., Tsugawa, H., Arora, A., Veselkov, K., Kato, S., Otoki, Y., Nakagawa, K., Yost, R. A., Garrett, T. J., & Vasiliou, V. (2022). Lipidomics and redox Lipidomics indicate early stage alcohol-induced liver damage. Hepatology communications, 6(3), 513-525.

38. Gomez-Larrauri, A., Presa, N., Dominguez-Herrera, A., Ouro, A., Trueba, M., & Gomez-Muñoz, A. (2020). Role of bioactive sphingolipids in physiology and pathology. Essays in biochemistry, 64(3), 579-589.
39. Alaamery, M., Albesher, N., Aljawini, N., Alsuwailm, M., Massadeh, S., Wheeler, M. A., Chao, C. C., & Quintana, F. J. (2021). Role of sphingolipid metabolism in neurodegeneration. Journal of Neurochemistry, 158(1), 25-35.
40. Clugston, R. D., Jiang, H.; Lee, M. X., Piantedosi, R., Yuen, J. J., Ramakrishnan, R., Lewis, M. J., Gottesman, M. E., Huang, L.-S., Goldberg, I. J., Berk, P. D., & Blaner, W. S. (2011). Altered hepatic lipid metabolism in C57BL/6 mice fed alcohol: a targeted lipidomic and gene expression study [S]. Journal of lipid research, 52(11), 2021-2031.
41. Ballway, J. W., & Song, B. J. (2021). Translational approaches with antioxidant phytochemicals against alcohol-mediated oxidative stress, gut dysbiosis, intestinal barrier dysfunction, and fatty liver disease. Antioxidants, 10(3), 384.

Chapter 3

Identification and characterization of novel SFAHFAs and MFAHFAs in human fecal samples using untargeted LC/MS analysis

3.1 Introduction

The human gut is home to a highly diverse and dynamic community of microorganisms, collectively referred to as the gut microbiota. These microbial populations play a crucial role in maintaining host health and have been implicated in the pathogenesis of several diseases, including inflammatory bowel disease, celiac disease, and colorectal cancer [1–4]. One of the primary ways the gut microbiota influences host physiology is through the fermentation of dietary macronutrients, particularly carbohydrates and proteins. This process results in the production of a wide array of bioactive metabolites such as short-SCFAs, FFAs, bile acids, and various amino acid derivatives [5,6]. SCFAs, which are SFAs containing one to six carbon atoms, serve not only as essential energy sources for colonocytes but also as potent signaling molecules involved in gut homeostasis [1,7]. Beyond SCFAs, the gut microbiota also contributes to the biosynthesis of complex lipid structures, such as α-galactosylceramides and Cer-PLs conjugates, which have been recognized for their immunomodulatory functions [8–10]. A particularly noteworthy discovery in lipid biology occurred in 2014, with the identification of FAHFAs in mammalian adipose tissue. These endogenous lipids have attracted considerable interest due to their anti-inflammatory, antioxidant, anti-apoptotic, and insulin-sensitizing properties [11,12]. Further investigations have linked FAHFAs to immunological processes within the gut, particularly through their modulation in cancer cell environments. For instance, the presence of FAHFAs has been associated with reduced apoptosis in gut-derived tumor cells, suggesting a possible protective mechanism employed by tumors to evade immune surveillance [13]. Different isomers of FAHFAs frequently exhibit various biological properties; for example, stereo-palmitic acid esters of 9-hydroxy stearic acid (9-PAHSA) are more effective in enhancing insulin secretion and glucose uptake than their regioisomer species, while both exhibit anti-inflammatory properties [14]. Our prior work has shown that long-chain FAHFAs, such as eicosapentaenoic acid (EPA) and docosahexaenoic acid esters of 12-HSA, possess antioxidant activity through the activation of nuclear response factor-2 (Nrf2) activation [15,16].

Recent studies have explored the diverse biological functions of FAHFAs and their long-chain variants [11, 17]. However, much less is known about species featuring ester linkages at specific positions on the hydroxy fatty acid backbone, particularly at

carbon positions C2, C3, and C4. This represents a significant gap in the field, underscoring the need for further structural elucidation and functional characterization of these lipids. Addressing this, our research group recently identified a novel subclass of FAHFAs named SFAHFAs [18]. These lipids, primarily detected in the large intestine and cecum content of rats, suggest they originate from the gut microbiota [19,20]. SFAHFAs are synthesized from SCFAs such as acetic acid (AA), propionic acid (PA), butyric acid (BA), and valeric acid in combination with various 2-HFAs. Our earlier analyses characterized over 20 distinct isomeric forms of SFAHFAs, each comprising different SCFA and HFAs pairings. These molecules have emerged as important lipid species in gut-associated metabolic processes and diseases. For instance, we reported increased levels of specific SFAHFAs in the colon samples of mice infected with the influenza virus [21], while decreased levels of AA-derived SFAHFAs were observed in ethanol-treated male mice [22]. Cecum contents from laying hens with *Campylobacter jejuni* infection revealed elevated levels in SFAHFAs (4:0/25:0 and 5:0/26:0) at 24 weeks compared to the 8-week post-infection group [23]. Additionally, a decrease in SFAHFA (2:0/22:0, 2:0/23:0, 2:0/24:0, 2:0/24:1, and 4:0/24:0) levels was observed in the stool samples of Phospholipase A2, group IIA (*Pla2g2a*)-deficient mice [24]. These studies highlight the biological importance of SFAHFAs in various diseases through their impact on the gut microbiota. However, most research on identifying SFAHFAs has focused on murine samples, with limited research on their detection and characterization in human samples [18,21,25]. Thus, the present study signifies the first comprehensive identification and characterization of different SFAHFA analogs in human fecal samples using high-performance liquid chromatography HPLC coupled LTQ Orbitrap MS.

3.2 Materials and Methods

3.2.1 Chemicals and reagents

The materials used in this study, including solvents and IS, were the same as those described in **Chapter 2, Section 2.1**.

3.2.2 Sample information

Fecal samples from elderly individuals were obtained and stored at –80 °C freezer until further analysis. All procedures for human studies reported in this paper were approved by the University of South Florida (USF). The sample collection followed the

protocol outlined in the Microbiome in Aging of Gut and Brain (MiaGB) study [26]. Ethical approval for the study was granted by the Ethics Committee of the Department of Health Sciences, Hokkaido University (Approval No. 22-87).

3.2.3 Lipid extraction from human fecal samples

A 100 mg aliquot of human fecal sample (n=5) was placed in a 2 mL Eppendorf tube and mixed with 0.5 mL of ice-cold methanol containing 0.01% butylated hydroxytoluene (BHT) to prevent oxidation. The sample was homogenized using ceramic beads (1.4 mm, Fisherbrand, Fisher Scientific) in a Bead Mill 4 homogenizer (Fisherbrand, Tokyo, Japan) for 1 minute (two repeated 30s cycles). A 100 μL aliquot of the homogenate was used for the lipid extraction using the modified Folch technique, as described previously in **Chapter 2, Section 2.2.4.**

3.2.4 LC/MS analysis

The LC/MS conditions employed for lipid analysis in negative ion mode in this chapter were identical to those previously described in **Chapter 2, Section 2.2.5**.

3.2.6 LC/MS data processing and quantification

The processing of LC/MS data, lipid identification, and quantification procedures was carried out using MS-DIAL software (version 4.9), and as described previously in **Chapter 2, Section 2.2.6**. To improve confidence in lipid identifications, peak processing and integration were performed using Xcalibur 2.2 software (Thermo Fisher Scientific Inc.). This software also facilitated the verification of MS and MS/MS spectral features, including RT and fragmentation patterns, against authentic reference standards synthesized in our laboratory. Relative quantification of lipid species was carried out by knowing the amount of IS added and the weight of the samples utilized for the analysis.

3.2.7 Statistical analysis

The data processing and visualization have been done, as described previously in **Chapter 2, Section 2.2.7** The data are presented as the mean ± standard error of the mean (SEM, n=5).

3.3 Results

3.3.1 Identification of FAHFAs in human fecal samples using untargeted LC/MS

In this study, untargeted LC/MS was employed to screen and identify SFAHFAs in human fecal samples. To the best of our knowledge, this is the first report to describe the detection and structural characterization of SFAHFAs in human-derived samples. A total of 26 isomeric FAHFAs were identified, comprising both SFAHFAs and medium-chain variants, with saturated and unsaturated carbon chains in human fecal samples.

MCFAs, typically consisting of 7 to 14 carbon atoms, are SFAs known to be synthesized by gut microbiota [27]. In the FAHFA molecules, the HFA moiety can be either SFAs (lacking double bonds) or unsaturated FFAs (containing one or more double bonds) within the carbon backbone. A comprehensive list of the identified FAHFAs, including their RT, theoretical masses (*m/z*), experimental masses (*m/z*), and mass errors, is presented in **Table 3.1**. HRMS further confirmed the identification of these lipids with MS^n characterization. All the identified FAHFAs were detected and ionized in the negative mode to yield $[M–H]^-$ ion.

Table 3.1: Overview of detected short- and medium-chain esters of hydroxy fatty acids (SFAHFAs and MFAHFAs) in the present study with their retention time (RT), experimental masses (*m/z*), theoretical masses (*m/z*), and mass errors

Sl. no	Lipid species	RT (min)	Theoretical *m/z*	Experimental *m/z*	Mass error (ppm)
1	SFAHFA 2:0/20:0	9.41	369.3010	369.3011	0.27
2	SFAHFA 2:0/22:0	10.34	397.3323	397.3323	0
3	SFAHFA 2:0/23:0 or 3:0/22:0	10.67	411.3479	411.3481	0.48
4	SFAHFA 2:0/24:0 or 4:0/22:0	11.12	425.3636	425.3636	0
5	SFAHFA 3:0/24:0 or 4:0/23:0 or 2:0/25:0	11.37	439.3792	439.3795	0.68
6	SFAHFA 4:0/24:0 or 2:0/26:0	11.55	453.3949	453.3952	0.66
7	SFAHFA 5:0/24:0 or 4:0/25:0 or 3:0/26:0	11.83	467.4105	467.4106	0
8	SFAHFA 6:0/24:0	11.96	481.4262	481.4266	0.83
9	MFAHFA 7:0/24:0 or SFAHFA 6:0/25:0	12.15	495.4418	495.4422	0.80
10	MFAHFA 8:0/24:0 or	12.43	509.4575	509.4578	0.58

	7:0/25:0 or SFAHFA 6:0/26:0				
11	MFAHFA 7:0/26:0 or 8:0/25:0	12.65	523.4731	523.4729	-0.38
12	SFAHFA 2:0/24:1	10.44	423.3479	423.3477	-0.47
13	SFAHFA 3:0/24:1 or 2:0/25:1	10.73	437.3636	437.3634	-0.45
14	SFAHFA 4:0/24:1	11.01	451.3792	451.3794	0.44

3.3.2 Detailed characterization of unsaturated SFAHFAs in human fecal samples

The RT and mass spectral fragmentation of representative unsaturated SFAHFAs identified in human fecal samples were compared with those of synthetically prepared reference compounds, as shown in **Figure 3.1**. **Figure 3.1A** shows the extracted ion chromatogram (EIC) and detail fragmentation spectra of SFAHFA 2:0/24:1, both from the sample and the corresponding synthetic standard. The SFAHFA 2:0/24:1 detected in the sample ionized to yield an $[M–H]^-$ ion at m/z 423.3477. In the MS^2 spectrum, the appearance of fragment ions at m/z 381 $[M–H–42]^-$ and m/z 363 ($[M–H–60]^-$) validate the occurrence of acetate esterification to the HFA. Subsequent MS^3 analysis revealed a characteristic loss of 46 Da (HCOOH), confirming the presence of a hydroxy group at the C2 position, thereby validating the compound to be SFAHFA 2:0/24:1. Comparable fragmentation patterns were also observed for the synthetic standard of SFAHFA 2:0/24:1, as well as for other unsaturated SFAHFA species. The EIC and mass spectral fragmentation for both the standard and sample SFAHFA 3:0/24:1 are presented in **Figure 3.1B**. This compound ionizes to yield an $[M–H]^-$ ion at m/z 437.3634. The MS^2 spectrum displayed fragment ions at m/z 381 $[M–H–56]^-$ and m/z 363 $[M–H–74]^-$, indicative of propionate esterification to the HFA moiety. Additionally, MS^3 spectra revealed a characteristic loss of 46 Da (HCOOH), confirming the presence of a hydroxy group at the C2 position and validating the identification of the compound as SFAHFA 3:0/24:1. This lipid species was observed to co-elute with its isomeric form of SFAHFA 2:0/25:1, as evidenced by the fragment ions in the MS^2 spectra. A similar fragmentation pattern was observed for the standard SFAHFA 3:0/24:1. The EIC and detailed mass fragmentation for SFAHFA 4:0/24:1, detected in both the sample and standard, are shown in **Figure 3.1C**. SFAHFA 4:0/24:1 ionized to yield $[M–H]^-$ ion at m/z 451.3794. The MS^2 spectrum

exhibited fragment ions at m/z 381 $[M–H–70]^-$ and m/z 363 $[M–H–88]^-$, indicating the esterification of butyrate to an HFA. Furthermore, MS^3 analysis revealed a characteristic loss of 46 Da (HCOOH), confirming the presence of a hydroxy group at the C2 position and validating the structure as SFAHFA 4:0/24:1. This fragmentation pattern was also consistent with that of the corresponding standard SFAHFA 4:0/24:1. This study is the first to identify and structurally characterize unsaturated SFAHFAs in human fecal samples, with comparative analysis against synthetically prepared standard compounds.

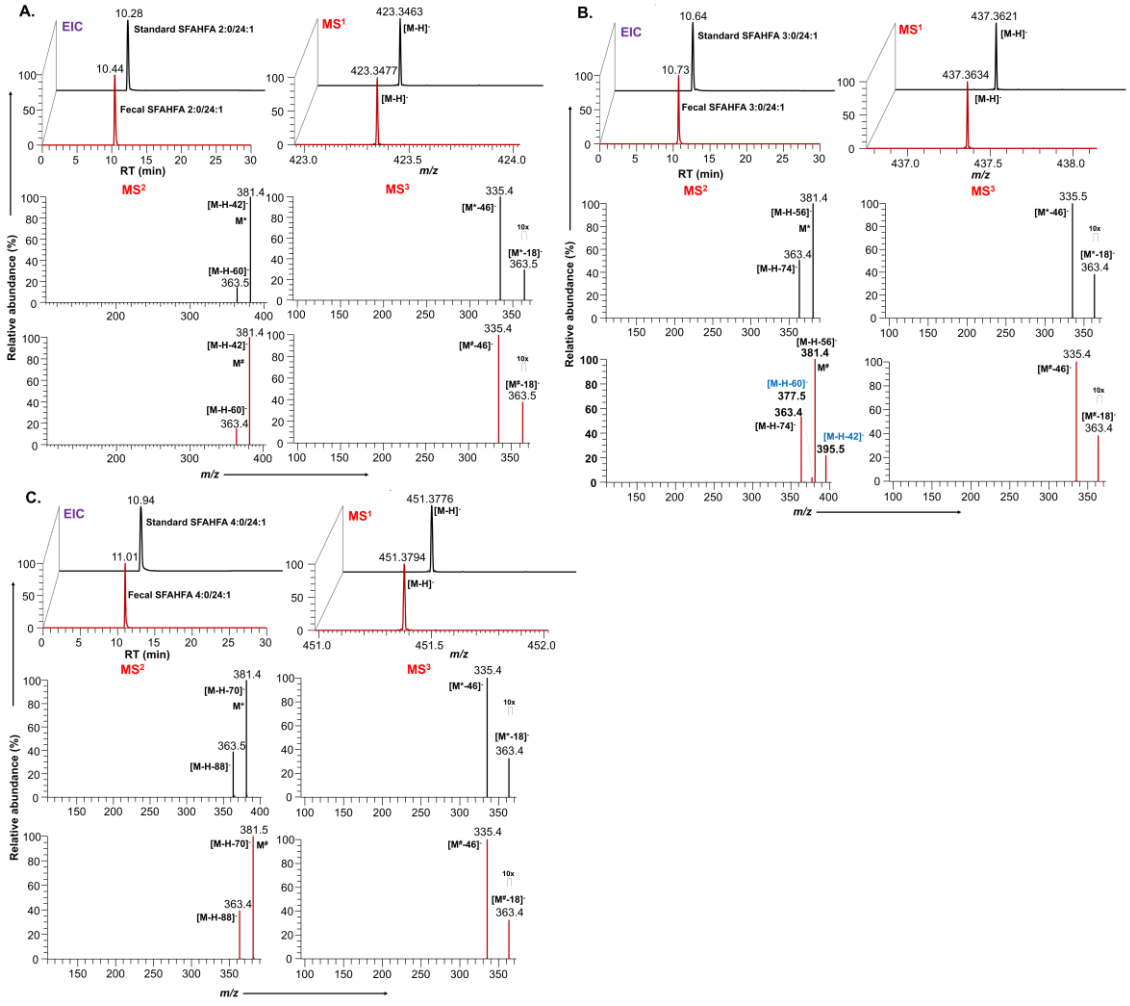

Figure 3.1: Representative extracted ion chromatogram (EIC) and mass spectral fragmentation of SFAHFAs standard and their detection in fecal samples. **A.** SFAHFA 2:0/24:1. **B.** SFAHFA 3:0/24:1. **C.** SFAHFA 4:0/24:1. (Spectra from the standards and fecal samples are displayed in black and red, respectively.)

3.3.3 In-depth characterization of a novel class of saturated MFAHFAs in human fecal samples

The RT and mass spectral fragmentation patterns of representative saturated medium chain- FAHFA (MFAHFA) species identified in human fecal samples were compared with those of synthetically MFAHFAs, as shown in **Figure 3.2**. The EIC and detailed mass spectral fragmentation of MFAHFA 7:0/24:0, detected in both the sample and the corresponding standard, are presented in **Figure 3.2A**. In the sample, MFAHFA 7:0/24:0 ionized to yield an $[M–H]^-$ ion at m/z 495.4422. MS^2 analysis of the precursor ion underwent further ionization to produce fragment ions at m/z 383 $[M–H–112]^-$ and m/z 365 $[M–H–130]^-$, corresponding to the losses of neutral molecules such as $CH_3(CH_2)_4CHCO$ and $CH_3(CH_2)_5COOH$, respectively. The presence of these fragment ions confirms that the esterified moiety in this MFAHFA species is enanthic acid (EA). Additionally, the MS^3 spectrum of the m/z 383 fragment ion yielded further fragment ions at m/z 365 and m/z 337, corresponding to the loss of 18 Da (H_2O) and 46 Da (HCOOH), respectively. These losses confirm that the hydroxyl group in lignoceric acid (LA) is positioned at the C2 location. A similar fragmentation pattern was observed for the standard MFAHFA 7:0/24:0. This lipid species co-eluted with an isomeric form of SFAHFA 6:0/25:0, as indicated by fragment ions in the MS^2 spectra.

The EIC and detailed mass spectral fragmentation of MFAHFA 8:0/24:0, detected in both the sample and the corresponding standard, are presented in **Figure 3.2B**. In the sample, SFAHFA 8:0/24:0 ionized to yield $[M–H]^-$ ion at m/z 509.4578. Further MS^2 analysis of the precursor ion yielded fragment ions at m/z 383 $[M–H–126]^-$ and m/z 365 $[M–H–144]^-$, corresponding to the losses of neutral molecules such as $CH_3(CH_2)_5CHCO$ and $CH_3(CH_2)_6COOH$, respectively. The appearance of these fragment ions confirms that the esterified moiety in this MFAHFA species is caprylic acid (CLA). The MS^3 spectrum of the m/z 383 fragment ion produced subsequent ions at m/z 365 and m/z 337, corresponding to the losses of 18 Da (H_2O) and 46 Da (HCOOH), respectively. These losses confirm that the hydroxyl group in LA is positioned at the C2 location. A similar fragmentation pattern was observed for the standard MFAHFA 8:0/24:0. This molecular species co-eluted with isomeric mixtures of MFAHFA 7:0/25:0 and SFAHFA 6:0/26:0, as confirmed by the presence of characteristic fragment ions in the mass spectra. This study is the first to report the detection and comprehensive mass spectral characterization of

EA- and CLA-esterified MFAHFAs in human fecal samples, along with comparative analysis against synthetic standards. The EIC, MS^1, MS^2, and MS^3 fragmentation data of the identified SFAHFAs and MFAHFAs are presented in the supplementary figures (**Appendix Figures 3.1 and 3.2**).

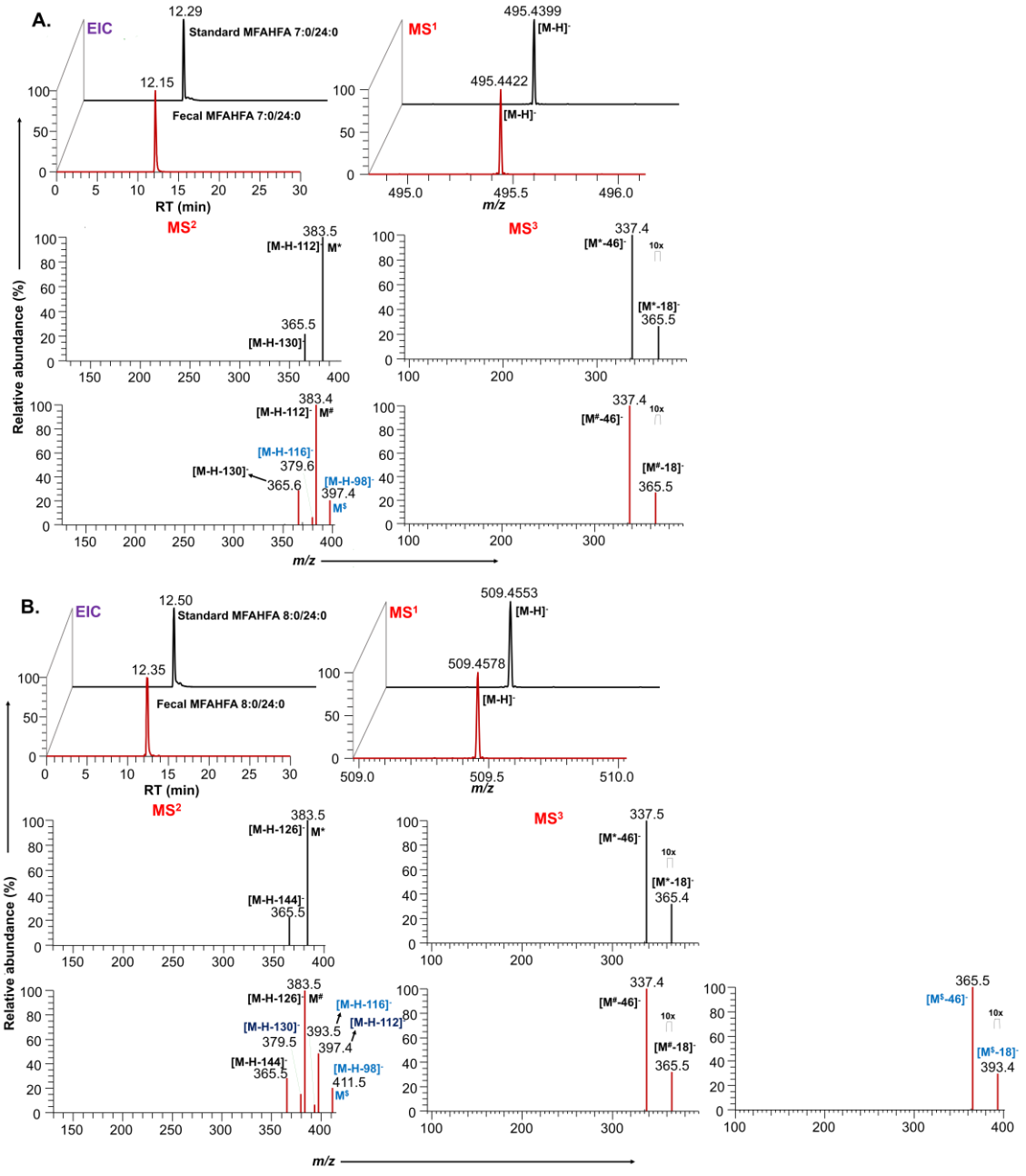

Figure 3.2: Representative EIC and mass spectral fragmentation of novel saturated MFAHFAs standard and their detection in fecal samples. **A.** MFAHFA 7:0/24:1. **B.** MFAHFA 8:0/24:1. (Spectra from the standards and fecal samples are displayed in black and red, respectively.)

3.3.4 Quantitative Analysis of SFAHFAs and MFAHFAs in Human Fecal Samples

The identified SFAHFAs and MFAHFAs species in human fecal samples were relatively quantified using an IS. **Figure 3.3** illustrates the relative abundance of these lipid species. Among the saturated species, SFAHFA 2:0/24:0 or 4:0/22:0 were the most predominant in the fecal samples (**Figure 3.3A**). A similar pattern was observed for the unsaturated SFAHFAs (**Figure 3.3B**), with SFAHFA 2:0/24:1 showing a marked increase in abundance compared to other species. The findings of the current study are summarized in **Figure 3.4**, which presents a proposed biosynthetic pathway for the synthesis of SFAHFAs and MFAHFAs. Notably, elevated levels of SFAHFA 2:0/24:0 and SFAHFA 2:0/24:1 were observed in the participants' fecal samples, indicating that these lipid species may serve as promising candidates for future functional and mechanistic investigations. The distinct class of MFAHFAs is present at lower abundances in human fecal samples compared to other lipid species, and their biosynthetic origin remains unclear. Our findings indicate that the biosynthesis of these novel MFAHFAs may be influenced by the gut microbiota, highlighting the need for further mechanistic studies to elucidate their biological roles. This is the first study to report the detection, identification, and in-depth mass spectral characterization of SFAHFAs and MFAHFAs in human fecal samples, along with comparative fragmentation analysis using synthetic standards. Nonetheless, the study has several limitations that should be addressed in future research. These include the semi-quantitative nature of the reported concentrations, which do not reflect absolute abundance, and multiple isomeric species complicating our chromatographic method's separation of certain FAHFAs.

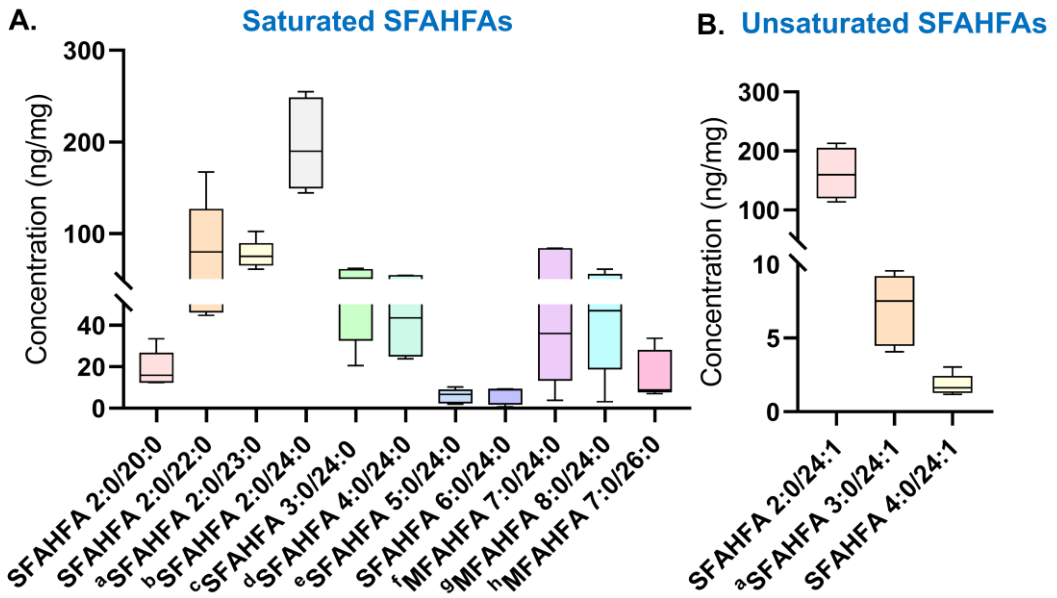

Figure 3.3: Relative abundance of SFAHFAs and MFAHFAs identified in human fecal samples. Data are presented as mean ± standard error (n = 5). **A.** Saturated SFAHFAs and MFAHFAs (a: SFAHFA 2:0/23:0 or 3:0/22:0, b: SFAHFA 2:0/24:0 or 4:0/22:0, c: SFAHFA 3:0/24:0 or 4:0/23:0 or 2:0/25:0, d: SFAHFA 4:0/24:0 or 2:026:0, e: SFAHFA 5:0/24:0 or 4:0/25:0 or 3:0/26:0, f: MFAHFA 7:0/24:0 or SFAHFA 6:0/25:0, g: MFAHFA 8:0/24:0 or 7:0/25:0 or SFAHFA 6:0/26:0, h: MFAHFA 7:0/26:0 or 8:0/25:0). **B.** Unsaturated SFAHFAs (a: SFAHFA 3:0/24:1 or 2:0/25:1).

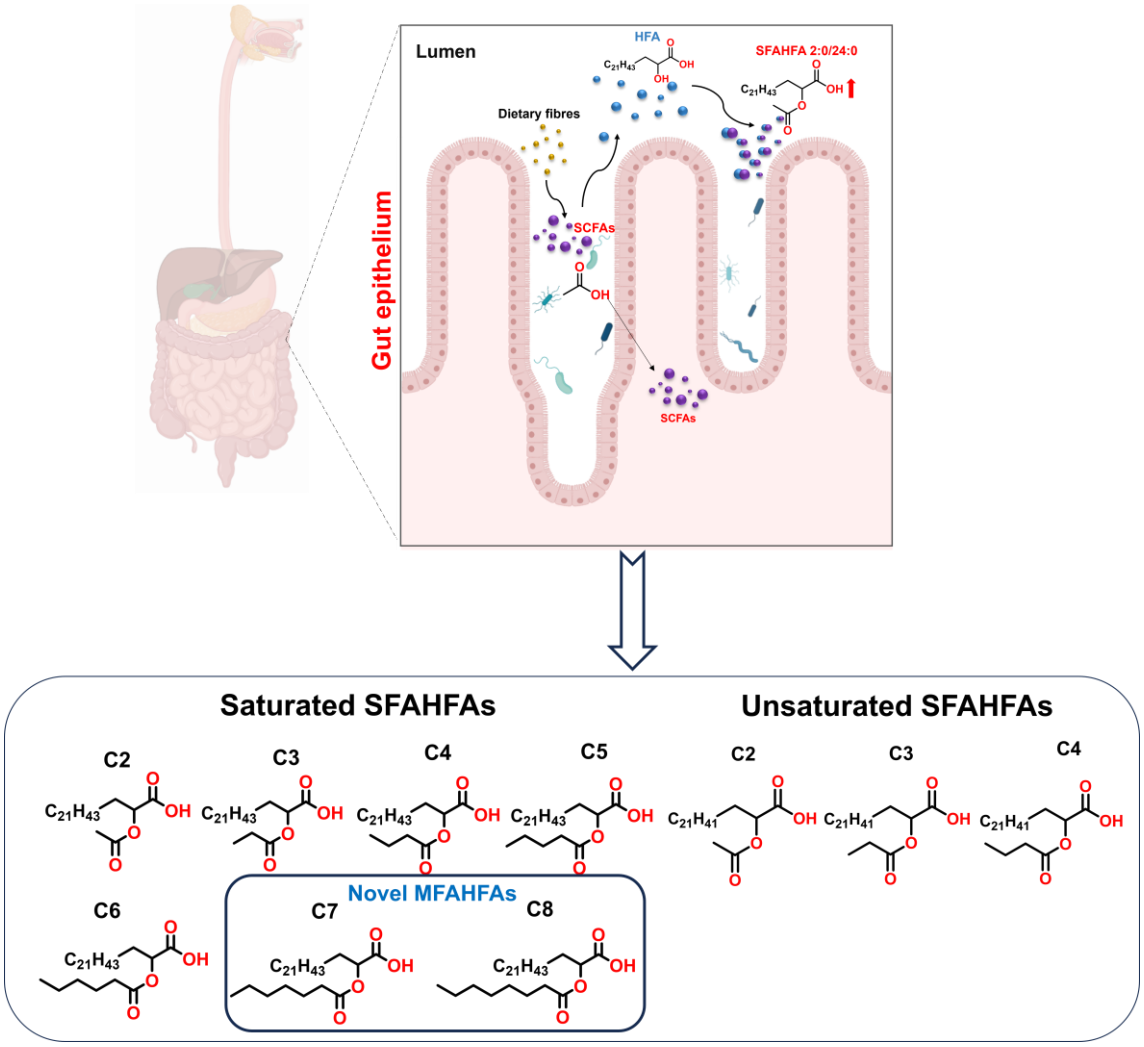

Figure 3.4: Proposed biosynthetic pathways of SFAHFAs and MFAHFAs detected in human fecal samples

3.4 Discussion

The gut and its metabolites play a crucial role in maintaining overall health by influencing metabolic, immune, and inflammatory processes. Identifying and understanding the complex array of metabolites produced by the gut microbiota is essential for uncovering their impact on various diseases and developing potential biomarkers for early diagnosis. Advancements in lipidomics, particularly through untargeted LC/MS techniques, have revolutionized for more accurate profiling of gut-derived metabolites, providing new insights into gut health and its link to various disorders [28]. SFAHFAs represent a recently identified and novel lipid class within the broader FAHFAs family and are increasingly known for their potential role in modulating

the gut microbiota. In 2020, this novel class of isomeric lipids was first identified and characterized in murine models through untargeted LC/MS analysis [18]. Later, these studies revealed that SFAHFAs have a significant role in the pathophysiology of influenza virus infection [21]. Rist et al. reported elevated levels of various SFAHFAs in the colonic contents of weaned piglets subjected to low-protein diet supplementation compared to those on a standard-protein diet [29]. Additionally, the presence of SFAHFAs has been observed in antibiotic-treated mice, with evidence supporting their biosynthesis by the gut microbiota [30]. Recently, SFAHFAs have been identified in human stool samples from healthy individuals; however, the study did not provide a comprehensive characterization of these lipids [31]. The present study is the first to report the detailed identification and structural characterization of both saturated and unsaturated FAHFAs, including SFAHFAs and MFAHFAs, in human fecal samples.

Utilizing LC coupled HRMS analysis, we identified 26 isomeric FAHFAs and confirmed their structural features by comparing fragmentation patterns with synthesized standards. Notably, the detection of unique lipid species, such as MFAHFA 7:0/24:0 and MFAHFA 8:0/24:0, points to a broader spectrum of gut-derived lipids than previously documented, expanding our understanding of the lipidomic diversity in the human gut. Our identification of unsaturated SFAHFAs, such as 2:0/24:1, 3:0/24:1, and 4:0/24:1 (**Figure 3.1**), is consistent with the fragmentation patterns observed in our previous study, demonstrating comparable retention behaviors and MS/MS profiles [21]. Additionally, the discovery of saturated MFAHFAs, including 7:0/24:0 and 8:0/24:0 (**Figure 3.2**), expands the diversity of FAHFAs and enhances the spectrum of gut-derived lipids. These lipid species may originate from microbial fermentation of dietary lipids, as MCFAs are recognized byproducts of gut microbial metabolism [32]. The co-elution and overlapping fragmentation patterns of MFAHFAs with their isomeric SFAHFAs present a chromatographic challenge, preventing the clear distinction of structural isomers. This issue could be addressed through isotope-labelling experiments [33], which is not considered in this study.

The relative concentrations of the identified SFAHFAs and MFAHFAs in human fecal samples showed that SFAHFA 2:0/24:0 or 4:0/22:0, as well as SFAHFA 2:0/24:1, were significantly elevated among the saturated and unsaturated species, respectively (**Figure 3.3**). These findings align with a previous study that showed elevated levels of

SFAHFAs (4:0/22:0), (3:0/22:0), and (3:0/24:0) in human stool samples [31]. In our prior research, we developed an improved method for detecting SFAHFAs in murine samples. The results revealed that the levels of PA- and AA-derived SFAHFAs were significantly higher in the cecum samples from the control mice compared to those from the HFD group [34]. Yasuda et al. demonstrated that the levels of SFAHFAs (also referred to as acyl α-hydroxyl fatty acids) were reduced in fecal samples from antibiotic-treated mice compared to the control group. This suggests a positive correlation between the gut bacteria, specifically *Bacteroidales* and *Clostridiales*, and the production of SFAHFAs in the gut microbiota [30]. Additionally, previous studies have reported that dietary magnesium supplementation enhances the levels of MCFAs, particularly EA and CLA, in human stool samples [35].

3.5 Conclusion

In this study, we performed comprehensive identification and mass spectral characterization of FAHFA-derived lipid species, including SFAHFAs and MFAHFAs, in human fecal samples using advanced LC/MS techniques. Notably, we discovered two novel MFAHFA species- EA and CLA esters of long-chain hydroxy fatty acids (C24 and C26)—detected for the first time in human fecal samples. Among the characterized lipids, SFAHFA 2:0/24:0 or 4:0/22:0 and SFAHFA 2:0/24:1 were found to be the most abundant saturated and unsaturated species, respectively, offering novel insights into gut-associated lipid metabolism. This study represents the first report of both known and previously unreported FAHFA species in human fecal samples, opening a new avenue for lipidomics research. Future studies are essential to elucidate the microbial and host-derived origins, biochemical functions, and metabolic pathways of MFAHFAs, thereby advancing our understanding of their potential roles in human health.

3.6 References:

1. Mirzaei, R., Dehkhodaie, E., Bouzari, B., Rahimi, M., Gholestani, A., Hosseini-Fard, S. R., Keyvani, H., Teimoori, A., & Karampoor, S. (2022). Dual role of microbiota-derived short-chain fatty acids on host and pathogen. Biomedicine & Pharmacotherapy, 145, 112352.
2. Basson, A., Trotter, A., Rodriguez-Palacios, A., & Cominelli, F. (2016). Mucosal interactions between genetics, diet, and microbiome in inflammatory bowel disease. Frontiers in immunology, 7, 290.
3. Di Cagno, R., Rizzello, C. G., Gagliardi, F., Ricciuti, P., Ndagijimana, M., Francavilla, R., Guerzoni, M. E., Crecchio, C., Gobbetti, M., & De Angelis, M. (2009). Different fecal microbiotas and volatile organic compounds in treated and untreated children with celiac disease. Applied and environmental microbiology, 75(12), 3963–3971.
4. Chen G. Y. (2018). The Role of the Gut Microbiome in Colorectal Cancer. Clinics in colon and rectal surgery, 31(3), 192–198.
5. Muegge, B. D., Kuczynski, J., Knights, D., Clemente, J. C., González, A., Fontana, L., Henrissat, B., Knight, R., & Gordon, J. I. (2011). Diet drives convergence in gut microbiome functions across mammalian phylogeny and within humans. Science (New York, N.Y.), 332(6032), 970–974.
6. Niccolai, E., Baldi, S., Ricci, F., Russo, E., Nannini, G., Menicatti, M., Poli, G., Taddei, A., Bartolucci, G., Calabrò, A. S., Stingo, F. C., & Amedei, A. (2019). Evaluation and comparison of short chain fatty acids composition in gut diseases. World journal of gastroenterology, 25(36), 5543–5558.
7. Binienda, A., Twardowska, A., Makaro, A., & Salaga, M. (2020). Dietary Carbohydrates and Lipids in the Pathogenesis of Leaky Gut Syndrome: An Overview. International journal of molecular sciences, 21(21), 8368.
8. An, D., Oh, S. F., Olszak, T., Neves, J. F., Avci, F. Y., Erturk-Hasdemir, D., Lu, X., Zeissig, S., Blumberg, R. S., & Kasper, D. L. (2014). Sphingolipids from a symbiotic microbe regulate homeostasis of host intestinal natural killer T cells. Cell, 156(1-2), 123–133.

9. Imai, T., Matsumura, T., Mayer-Lambertz, S., Wells, C. A., Ishikawa, E., Butcher, S. K., Barnett, T. C., Walker, M. J., Imamura, A., Ishida, H., Ikebe, T., Miyamoto, T., Ato, M., Ohga, S., Lepenies, B., van Sorge, N. M., & Yamasaki, S. (2018). Lipoteichoic acid anchor triggers Mincle to drive protective immunity against invasive group A Streptococcus infection. Proceedings of the National Academy of Sciences of the United States of America, 115(45), E10662–E10671.
10. Brown, E. M., Ke, X., Hitchcock, D., Jeanfavre, S., Avila-Pacheco, J., Nakata, T., Arthur, T. D., Fornelos, N., Heim, C., Franzosa, E. A., Watson, N., Huttenhower, C., Haiser, H. J., Dillow, G., Graham, D. B., Finlay, B. B., Kostic, A. D., Porter, J. A., Vlamakis, H., Clish, C. B., … Xavier, R. J. (2019). Bacteroides-Derived Sphingolipids Are Critical for Maintaining Intestinal Homeostasis and Symbiosis. Cell host & microbe, 25(5), 668–680.e7.
11. Yore, M. M., Syed, I., Moraes-Vieira, P. M., Zhang, T., Herman, M. A., Homan, E. A., Patel, R. T., Lee, J., Chen, S., Peroni, O. D., Dhaneshwar, A. S., Hammarstedt, A., Smith, U., McGraw, T. E., Saghatelian, A., & Kahn, B. B. (2014). Discovery of a class of endogenous mammalian lipids with anti-diabetic and anti-inflammatory effects. Cell, 159(2), 318–332.
12. Kolar, M. J., Nelson, A. T., Chang, T., Ertunc, M. E., Christy, M. P., Ohlsson, L., Härröd, M., Kahn, B. B., Siegel, D., & Saghatelian, A. (2018). Faster Protocol for Endogenous Fatty Acid Esters of Hydroxy Fatty Acid (FAHFA) Measurements. Analytical chemistry, 90(8), 5358–5365.
13. Rodríguez, J. P., Guijas, C., Astudillo, A. M., Rubio, J. M., Balboa, M. A., & Balsinde, J. (2019). Sequestration of 9-Hydroxystearic Acid in FAHFA (Fatty Acid Esters of Hydroxy Fatty Acids) as a Protective Mechanism for Colon Carcinoma Cells to Avoid Apoptotic Cell Death. Cancers, 11(4), 524.
14. Aryal, P., Syed, I., Lee, J., Patel, R., Nelson, A. T., Siegel, D., Saghatelian, A., & Kahn, B. B. (2021). Distinct biological activities of isomers from several families of branched fatty acid esters of hydroxy fatty acids (FAHFAs). Journal of lipid research, 62, 100108.
15. B Gowda, S. G., Fuda, H., Tsukui, T., Chiba, H., & Hui, S. P. (2020). Discovery of Eicosapentaenoic Acid Esters of Hydroxy Fatty Acids as Potent Nrf2 Activators. Antioxidants (Basel, Switzerland), 9(5), 397.

16. B Gowda, S. G., Tsukui, T., Fuda, H., Minami, Y., Gowda, D., Chiba, H., & Hui, S. P. (2021). Docosahexaenoic Acid Esters of Hydroxy Fatty Acid Is a Novel Activator of NRF2. International journal of molecular sciences, 22(14), 7598.
17. Kokotou M. G. (2020). Analytical Methods for the Determination of Fatty Acid Esters of Hydroxy Fatty Acids (FAHFAs) in Biological Samples, Plants and Foods. Biomolecules, 10(8), 1092.
18. Gowda, S. G. B., Liang, C., Gowda, D., Hou, F., Kawakami, K., Fukiya, S., Yokota, A., Chiba, H., & Hui, S. P. (2020). Identification of short-chain fatty acid esters of hydroxy fatty acids (SFAHFAs) in a murine model by nontargeted analysis using ultra-high-performance liquid chromatography/linear ion trap quadrupole-Orbitrap mass spectrometry. Rapid communications in mass spectrometry : RCM, 34(17), e8831.
19. Dalile, B., Van Oudenhove, L., Vervliet, B., & Verbeke, K. (2019). The role of short-chain fatty acids in microbiota-gut-brain communication. Nature reviews. Gastroenterology & hepatology, 16(8), 461–478.
20. Serra, S., De Simeis, D., Castagna, A., & Valentino, M. (2020). The fatty-acid hydratase activity of the most common probiotic microorganisms. Catalysts, 10(2), 154.
21. B Gowda, S. G., Gowda, D., Ohno, M., Liang, C., Chiba, H., & Hui, S. P. (2021). Detection and Structural Characterization of SFAHFA Homologous Series in Mouse Colon Contents by LTQ-Orbitrap-MS and Their Implication in Influenza Virus Infection. Journal of the American Society for Mass Spectrometry, 32(8), 2196–2205.
22. Gowda, S. G. B., Nath, L. R., Li, Y., Jayaprakash, J., Gowda, D., & Hui, S. P. (2024). Sex-specific effect of ethanol on colonic short-chain fatty acids and derivatives in the mouse model using targeted LC/MS. Medical Mass Spectrometry, 8(1), 11-18.
23. Asakura, H., Nakayama, T., Yamamoto, S., Izawa, K., Kawase, J., Torii, Y., & Murakami, S. (2021). Long-Term Grow-Out Affects Campylobacter jejuni Colonization Fitness in Coincidence With Altered Microbiota and Lipid Composition in the Cecum of Laying Hens. Frontiers in veterinary science, 8, 675570.

24. Miki, Y., Taketomi, Y., Kidoguchi, Y., Yamamoto, K., Muramatsu, K., Nishito, Y., Park, J., Hosomi, K., Mizuguchi, K., Kunisawa, J., Soga, T., Boilard, E., B Gowda, S. G., Ikeda, K., Arita, M., & Murakami, M. (2022). Group IIA secreted phospholipase A2 controls skin carcinogenesis and psoriasis by shaping the gut microbiota. JCI insight, 7(2), e152611.
25. Gowda, S. G. B., Hou, F., Gowda, D., Chiba, H., Kawakami, K., Fukiya, S., Yokota, A., & Hui, S. P. (2024). Synthesis and quantification of short-chain fatty acid esters of hydroxy fatty acids in rat intestinal contents and fecal samples by LC-MS/MS. Analytica chimica acta, 1288, 342145.
26. James, A. S., Adil, N. A., Goltz, D., Tangudu, D., Chaudhari, D. S., Shukla, R., Kumar, V., Kumar, A., Masternak, M. M., Holland, P., Labyak, C., Golden, A., Dangiolo, M., Arikawa, A. Y., Kociolek, J., Fraser, A., Williams, C., Agronin, M., Aymat, M., Jain, S., … Yadav, H. (2024). Abnormalities in gut virome signatures linked with cognitive impairment in older adults. Gut microbes, 16(1), 2431648.
27. Gregor, A., Auernigg-Haselmaier, S., Trajanoski, S., König, J., & Duszka, K. (2021). Colonic Medium-Chain Fatty Acids Act as a Source of Energy and for Colon Maintenance but Are Not Utilized to Acylate Ghrelin. Nutrients, 13(11), 3807.
28. Okahashi, N., Ueda, M., Yasuda, S., Tsugawa, H., & Arita, M. (2021). Global profiling of gut microbiota-associated lipid metabolites in antibiotic-treated mice by LC-MS/MS-based analyses. STAR protocols, 2(2), 100492.
29. Rist, V. T., Weiss, E., Eklund, M., & Mosenthin, R. (2013). Impact of dietary protein on microbiota composition and activity in the gastrointestinal tract of piglets in relation to gut health: a review. Animal : an international journal of animal bioscience, 7(7), 1067–1078.
30. Yasuda, S., Okahashi, N., Tsugawa, H., Ogata, Y., Ikeda, K., Suda, W., Arai, H., Hattori, M., & Arita, M. (2020). Elucidation of Gut Microbiota-Associated Lipids Using LC-MS/MS and 16S rRNA Sequence Analyses. iScience, 23(12), 101841.
31. Folz, J., Culver, R. N., Morales, J. M., Grembi, J., Triadafilopoulos, G., Relman, D. A., Huang, K. C., Shalon, D., & Fiehn, O. (2023). Human metabolome variation along the upper intestinal tract. Nature metabolism, 5(5), 777–788.

32. Dodd, D., Spitzer, M. H., Van Treuren, W., Merrill, B. D., Hryckowian, A. J., Higginbottom, S. K., Le, A., Cowan, T. M., Nolan, G. P., Fischbach, M. A., & Sonnenburg, J. L. (2017). A gut bacterial pathway metabolizes aromatic amino acids into nine circulating metabolites. Nature, 551(7682), 648–652.
33. Zhu, Q. F., Yan, J. W., Zhang, T. Y., Xiao, H. M., & Feng, Y. Q. (2018). Comprehensive Screening and Identification of Fatty Acid Esters of Hydroxy Fatty Acids in Plant Tissues by Chemical Isotope Labeling-Assisted Liquid Chromatography-Mass Spectrometry. Analytical chemistry, 90(16), 10056–10063.
34. B Gowda, S. G., Gowda, D., Liang, C., Li, Y., Kawakami, K., Fukiya, S., Yokota, A., Chiba, H., & Hui, S. P. (2020). Chemical Labeling Assisted Detection and Identification of Short Chain Fatty Acid Esters of Hydroxy Fatty Acid in Rat Colon and Cecum Contents. Metabolites, 10(10), 398.
35. Fan, L., Zhu, X., Sun, S., Yu, C., Huang, X., Ness, R., Dugan, L. L., Shu, L., Seidner, D. L., Murff, H. J., Fodor, A. A., Azcarate-Peril, M. A., Shrubsole, M. J., & Dai, Q. (2022). Ca:Mg ratio, medium-chain fatty acids, and the gut microbiome. Clinical nutrition (Edinburgh, Scotland), 41(11), 2490–2499.

Chapter 4

Integrated lipidomic analysis of patient samples for biomarker discovery in neurodegenerative disease using untargeted LC/MS

4.1 Introduction

NDs are a group of chronic and progressive conditions involving the selective loss of neurons and their association, leading to motor, cognitive, and behavioral impairments [1]. The key pathological features of these disorders include protein misfolding, the formation of aggregates, synaptic dysfunction, and neuronal death [2]. AD, Parkinson's disease (PD), and Huntington's disease (HD) are the most prevalent NDs and major causes of disability in aging populations globally [3]. PD is the second most complex progressive ND following AD, it affects to the dopaminergic neurons in the substantia nigra, resulting in α-synuclein accumulation and the formation of Lewy bodies, which underlie its motor and non-motor symptoms [4]. Similarly, HD is a hereditary disorder caused by cytosine-adenine-guanine (CAG) trinucleotide expansions in the huntingtin gene, producing a toxic protein that drives neuronal loss in the striatum and cortex [5]. While these diseases generally manifest during mid to late life, they are often preceded by prolonged periods of slow progression, during which molecular alterations occur well before clinical symptoms become evident [6].

However, AD remains the most common progressive NDs and the primary cause of dementia in older populations, which is marked by gradual memory loss and cognitive decline [7]. In the 21st century, AD has become an ever-growing burden on the public health system and economy [8]. The World Health Organization estimates that over 55 million people suffer from dementia globally (https://www.who.int/news-room/fact-sheets/detail/dementia (accessed on 11th December 2024)). In the absence of the development of effective therapeutic interventions, this number is expected to increase to 152 million by 2050 (https://www.alz.co.uk/research/world-report-2018). The hallmark pathological characteristics of AD include the accumulation of phosphorylated tau (p-tau) proteins and amyloid-β (Aβ) peptides in the brain [9]. The disease progresses gradually, beginning with an asymptomatic stage, a preclinical stage, followed by the onset of mild cognitive impairment (MCI), ultimately leading to the development of dementia [10]. The early stages of AD, often characterized by MCI, represent a crucial period for intervention to address and modify the risk factors that contribute to cognitive decline and dementia [11]. MCI affects over 15% of the population, and its prevalence increases with age [12]. Identifying the increased risk of AD in its early stages (MCI) is essential for timely preventive interventions [13]. Unfortunately, early detection of AD remains a significant

challenge because of the lack of effective treatments and limited potential for preventing its progression [14, 15]. This highlights the importance of identifying innovative and reliable biomarkers for the early diagnosis of AD.

The current diagnostic biomarkers for NDs rely on invasive sampling, neuropsychological evaluations, and neuroimaging techniques; however, these approaches often lack disease specificity [16,17]. Lipidomic techniques have significant potential for identifying novel diagnostic lipid biomarkers of NDs at a certain time [18]. Lipids are particularly significant as they constitute approximately 50% of the brain's dry weight [19]. Lipids are involved in multiple functions of neuronal membranes, including proliferation, apoptosis, structural support, and cell signaling, and influence neurodegeneration and cognitive decline [20]. Alterations in brain lipid metabolism disrupt the membrane integrity and impair synaptic function, contributing to Aβ aggregation and tau hyperphosphorylation [21]. Dysregulation of lipid homeostasis in several classes of lipids is associated with the development of NDs and many other injuries of the central nervous system via alterations in the composition of PLs, plasmalogens, Cer, gangliosides, and sulfatides in the brain [22,23]. Given their critical involvement in various biological processes, lipids have attracted attention as potential biomarkers for early diagnosis of disease progression [24].

Existing studies on lipid metabolism and the pathogenesis of NDs development face challenges in fully elucidating the complex association between AD, PD, and HD and their changes in the host lipid homeostasis [25], particularly in the context of the MCI stage in older adults with AD patients [26]. LC/MS is a widely used technique for the lipidomic analysis of different biological samples and the simultaneous characterization of hundreds of lipids, which are crucial for the identification of metabolic factors in the early detection of AD, PD, and HD pathophysiology [27,28]. Previous studies have explored significant alterations in specific lipid classes, particularly SM, CE, PC, LPC, PE, lysophosphatidylethanolamine (LPE), PI, MG, TG, and DG, in plasma samples of AD patients using LC coupled to TOF and Q-exactive Plus Orbitrap/MS [29,30]. Furthermore, lipidomic profiling of cerebrospinal fluid (CSF) samples from patients with AD using LC with Q Exactive Plus Hybrid Quadrupole-Orbitrap MS demonstrated a significant reduction in PG, monoHexCer, SM, PI, PC, PE, and CE levels in the MCI and dementia groups compared with those in the control groups [20]. Additionally, brain

tissue lipidome analysis of AD patients showed significant upregulation of PS and TG molecular species in mild and severe AD groups, respectively [31]. Another study using LC coupled with Synapt XS HRMS for plasma lipidome analysis in AD and PD patients reported significant alterations in SPs and GPs. These lipid changes not only distinguished healthy controls from diseased individuals but also effectively differentiated PD from AD cases [28].

However, previous studies on dysregulated lipid metabolism in the pathophysiology of NDs progression have been limited to plasma, CSF samples and largely restricted their comparisons to a single disease state versus healthy controls. Therefore, exploration of lipid biomarkers in readily accessible, non-invasive clinical samples such as saliva and fecal samples can be highly beneficial for designing interventions in the early stage (MCI) of disease progression. To the best of our knowledge, a systematic approach to studying the salivary and fecal lipid profiles in patients with MCI and dementia has been lacking; sex- and weight-specific variations remain unclear. In this study, we utilized HPLC/LTQ-Orbitrap-MS to systematically investigate the comprehensive lipidome of saliva, plasma, and fecal samples obtained from healthy individuals and patients with MCI and dementia to determine potent lipid biomarkers in the early stage of MCI. Furthermore, we extended our investigation to brain tissues from patients with AD, PD, and HD, enabling the assessment of disease-, region-, and sex-specific lipid alterations across advanced stages of neurodegeneration and gaining insights into AD, PD, and HD potent differential lipid biomarkers. Together, this two-tiered approach—from bio fluids to brain tissue—offers new insights into the systemic and localized lipid dysregulation underlying NDs progression and highlights potential early lipid biomarkers, as well as lipid species associated with disease severity and type. The detailed study design is depicted in **Figure 4.1.** This study is the first to conduct such a comprehensive lipidomic analysis of saliva, plasma, and fecal samples for lipid biomarker analysis in the diagnosis of AD in its early stage (MCI). In parallel, we analyzed brain tissue samples to uncover disease-specific lipid alterations across AD, PD, and HD disorders. In addition, we explored sex-, weight-, and region-specific lipid alterations in disease progression.

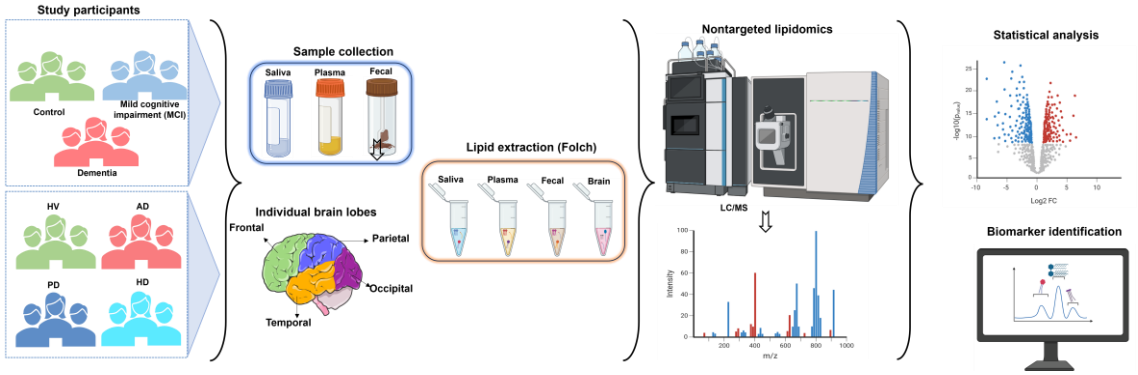

Figure 4.1: Integrated study design for lipidomic analysis of invasive (plasma) and non-invasive (saliva, fecal) clinical samples from healthy individuals, MCI, and dementia patients, as well as brain tissue samples from Healthy volunteers (HV), Alzheimer's disease (AD), Huntington's disease (HD), and Parkinson's disease (PD) patients.

4.2 Materials and Methods

4.2.1 Chemicals and reagents

The materials used in this study, including solvents and internal standards, were the same as those described in **Chapter 2, Section 2.1**.

4.2.2 Sample information

The saliva, plasma, and fecal samples from healthy individuals, MCI patients, and dementia patients of older adults were collected and stored in a freezer at -80°C until further analysis. The study details are consistent with those provided in **Chapter 3, Section 3.2.2.** The brain tissue samples from each lobe were collected from healthy volunteers, AD, HD, and PD patients.

4.2.3 Extraction of lipids

Saliva, plasma, and fecal samples from healthy individuals, MCI, and dementia patients of older adults were subjected to total lipid extraction. Briefly, saliva samples (150-200 µL) and plasma samples (50 µL) were transferred into a 2 mL Eppendorf tube, to which ice-cold methanol (100 µL, with 0.01% BHT) was added. Lipid extraction from both saliva and plasma was performed using a modified Folch method, as described in **Chapter 2, Section 2.2.4.** Fecal lipid extraction followed a similar protocol, as outlined in **Chapter 3, Section 3.2.4**. In case of brain tissue samples from healthy volunteers (HV), AD, PD, and HD participants, 200 µL aliquots of homogenate from each brain lobe were

mixed with ice-cold methanol (100 µL, with 0.01% BHT). Lipids were extracted using the same modified Folch method with a $CHCl_3$: MeOH: Milli-Q ratio of 2:1:0.5 as described in **Chapter 2, Section 2.2.4.**

4.2.4 Untargeted analysis by LC/MS

The LC/MS conditions employed for lipid analysis in both negative and positive ion modes in this chapter were identical to those previously described in **Chapter 2, Section 2.2.5**.

4.2.5 Lipid annotation and quantification

The processing of LC/MS data, lipid identification, and quantification procedures were carried out using MS-DIAL software (version 4.9) as described previously in **Chapter 2, Section 2.2.6**. To improve the confidence in lipid identifications, peak processing and integration were performed using Xcalibur 2.2 software (Thermo Fisher Scientific Inc.), as described previously in **Chapter 3, Section 3.2.6**.

4.2.6 Statistical analysis

The data processing and visualization have been done, as described previously in **Chapter 2, Section 2.2.7**. To thoroughly evaluate the data variation, PCA and orthogonal partial least squares discriminant analysis (OPLS-DA) were performed using MetaboAnalyst 6.0. (https://www.metaboanalyst.ca), Heatmaps were generated following the provided user instructions. Score plots were created to evaluate the similarity among different groups, whereas variable importance in projection (VIP) and loading plots (model coefficients versus covariance) were used to identify key lipid features distinguishing each group. OPLS-DA is a supervised multivariate analysis technique that enhances classification accuracy with reduced overfitting compared to other multivariate analyses [32]. Statistical analyses were conducted using one-way and two-way ANOVA and Tukey's multiple comparison test to determine significant differences ($p < 0.05$). The Mann-Whitney U test was also used to assess statistical differences between the two groups ($p < 0.05$). All data are expressed as the mean ± SEM.

4.3 Results

4.3.1. Saliva, plasma, and fecal lipidome profiling in cognitive impairment cohorts

4.3.1.1 Multivariate analysis of saliva, plasma, and fecal lipidome

In this pilot study, an untargeted lipidomic tactic was employed to profile the structural lipids in saliva, plasma, and fecal samples from healthy individuals and CI (MCI and dementia) patients of older adults using HPLC/LTQ-Orbitrap-MS. Detailed demographic characteristics of the participants involved in this work are presented in **Table 4.1**.

Table 4.1: Demographic data shows the characteristics of the participants across control, MCI, and dementia groups included in the study

	Saliva			**Plasma**			**Fecal**		
Groups	**Control**	**MCI**	**Dementia**	**Control**	**MCI**	**Dementia**	**Control**	**MCI**	**Dementia**
No of Participants (n)	81	37	6	60	26	4	87	37	4
Age in years (mean ± SD)	69.9 ± 8.2	74.7 ± 9.8	81.8 ± 9.2	69.9 ± 8.6	72.6 ± 8.7	78.2 ± 8.9	69.8 ± 8.1	74.8 ± 9.7	83.7 ± 7.8
Gender									
Male (n)	21	15	4	17	11	3	23	14	3
Female (n)	60	22	2	43	15	1	64	23	1
BMI (kg/m^2)[a]									
Overweight (OW) (BMI: 25 to 29.9 kg/m2)	50	20	4	33	11	2	53	20	3
Normal weight (NW) (BMI: 18.5 to 24.9 kg/m2)	29	17	2	26	15	2	32	17	1
Underweight (UW) (BMI: ≤18.5 kg/m2)	2	-	-	1	-	-	2	-	-
MOCA score (mean ± SD)	27.7 ± 1.2	22.9 ± 1.8	15.1 ± 3.7	27.8 ± 1.2	23.0 ± 1.8	13.7 ± 3.8	27.7 ± 1.3	22.8 ± 1.8	16.7 ± 1.5

Multivariate analysis was conducted to elucidate the stage-specific (control, MCI, and dementia) group differences in the saliva, plasma, and fecal lipidomes of older adults (**Figure 4.2).** The result of the OPLS-DA analysis of all lipid molecular species identified in the stage-specific groups of saliva samples is shown in **Figure 4.2A.** For instance, the score plot shows minor group separation between the control and MCI groups, accounting for 45.6% of the total variance in the model (**Figure 4.2Ai**). Furthermore, the VIP plot shows that GLs are responsible for this minor group separation with a VIP score of >2, indicating a high VIP score for the identification of plausible biomarker candidates (**Appendix Figure 4.1A)**. The score plot in **Figure 4.2Aii** reveals limited group separation between the control and dementia groups, with the model accounting for 48% of the total variance. This variation is driven by GLs and GPs (**Appendix Figure 4.1A)**. By contrast, the score plot of the MCI and dementia groups shows minor group separation, as shown in **Figure 4.2Aiii,** with the model explaining 56.2% of the total variance. The GLs are the key contributors to this differentiation, as evidenced by their high VIP scores (VIP > 2) (**Appendix Figure 4.1A)**. The OPLS-DA analysis of all lipid molecular species identified in the stage-specific groups of plasma samples is shown in **Figure 4.2B**. The score plot depicted in **Figure 4.2Bi** demonstrates minor group separation between the control and MCI groups, with the model explaining 32.4% of the total variance. The VIP plot shows that GPs and GLs are the primary lipid metabolites contributing to the group separation (**Appendix Figure 4.1B)**. Similarly, the score plots shown in **Figures 4.2Bii** and **4.2Biii** illustrate minor group separation between the control vs. dementia and MCI vs. dementia groups, with the total variance of the models 27.7% and 37.8%, respectively. The VIP plots highlight that GPs, STs, and SPs are the major lipid metabolites in the observed separations (**Appendix Figure 4.1B).** The results of the OPLS-DA analysis of all lipids molecular species identified in fecal samples across stage-specific groups are shown in **Figure 4.2C**. The score plot in **Figure 4.2Ci** reveals slight differences in the lipidome profile between the control and MCI groups, with the model explaining 13.1% of the total variance. The VIP plot emphasizes that GLs and FAs are responsible for this group separation (**Appendix Figure 4.1C**). The score plots in **Figures 4.2Cii and 4.2Ciii** depict minor group separations between the control vs. dementia and MCI vs. dementia groups with the total variance of the models accounting for 14.7% and 15.9%,

respectively. The VIP plot highlights FAs, GLs, and SPs as the major metabolites responsible for this group separation (**Appendix Figure 4.1C**).

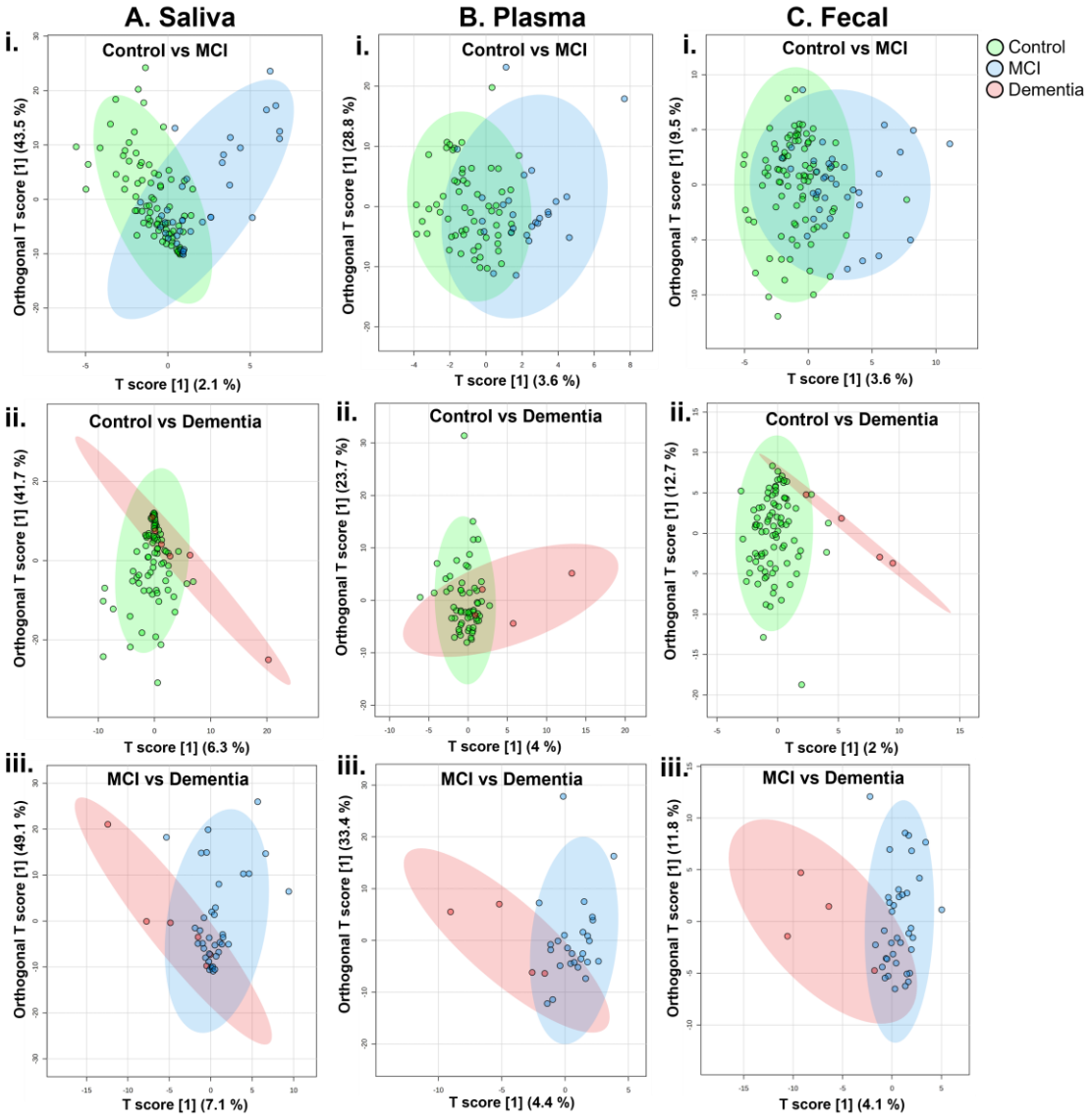

Figure 4.2: Multivariate analysis of all lipids molecular species identified in saliva, plasma, and fecal samples of control, mild cognitive impairment (MCI), and dementia groups of older adults. **A.** Orthogonal partial least square discriminate analysis (OPLS-DA) score plot of the saliva samples representing: **(i)** control vs MCI groups, **(ii)** control vs dementia groups, **(iii)** MCI vs dementia groups. **B.** OPLS-DA score plot of the plasma samples representing: **(i)** control vs MCI groups, **(ii)** control vs dementia groups, **(iii)** MCI vs dementia groups. **C.** OPLS-DA score plot of the fecal samples representing: **(i)** control vs MCI groups, **(ii)** control vs dementia groups, **(iii)** MCI vs dementia groups.

4.3.1.2 Distribution of lipid classes and fatty acyl compositions in older adults' saliva, plasma, and fecal samples.

Figure 4.3 illustrates the percentage distribution of major lipid classes, relative concentrations of FAs levels, and the ω-6: ω-3 ratio in stage-specific groups of older adults across saliva, plasma, and fecal samples. In total, 266, 217, and 260 lipid metabolites were detected in the saliva, plasma, and fecal samples, respectively, spanning five major lipid classes: FAs, GPs, GLs, SPs, and STs. The stage-specific group distribution of these lipid classes across the saliva, plasma, and fecal samples of older adults is presented in **Figure 4.3A**, highlighting the distinct variations in the lipid composition across different sample types and disease stages. In the saliva samples, FAs are predominant in each group compared to other lipid classes, followed by GLs, GPs, and SPs (**Figure 4.3Ai**). The MCI group had the highest proportion of GLs (31.9%), while the control group showed higher SPs (4.5%). Conversely, the dementia group exhibited a slightly higher distribution of FAs (50.2%) and GPs (20.5%) than the control and MCI groups. In plasma samples, the GPs content was abundant in each group compared to the other lipid classes, followed by GLs and FAs (**Figure 3Aii**). The control group showed the highest percentage of GP content (44.6 %) compared to the MCI and dementia groups. By contrast, the MCI group showed the highest percentage of FAs (15.3%), whereas the dementia group had the highest percentage of GLs (31.8%). FAs dominated the lipid class distribution across all groups in the fecal samples, followed by GLs and GPs. The dementia group exhibited a slightly higher proportion of FAs (95.7%) than the control and MCI groups. Interestingly, the MCI group had a higher percentage of GLs (3.1%) than the control and dementia groups. By contrast, the dementia group exhibited a slightly higher distribution of FAs (95.7%) compared to the control and MCI groups. The MCI and dementia groups displayed a similar percentage distribution of GPs (1.8%).

SFAs, MUFAs, and PUFAs are categorized as a subclass of FAs. The carbon chains of SFAs are indicated by no double bonds, whereas the carbon chains of MUFAs contain one double bond, and the carbon chains of PUFAs contain two or more double bonds. The bar graph in **Figure 4.3B** illustrates the relative distributions of SFAs, MUFAs, and PUFAs in the saliva, plasma, and fecal samples across the control, MCI, and dementia groups. Surprisingly, no statistically significant differences were detected in the overall levels of SFAs, MUFAs, and PUFAs across the stage-specific groups in the saliva, plasma,

and fecal samples. However, a slight increase in the levels of SFAs, MUFAs, and PUFAs was noted in the saliva and plasma samples of the MCI group (**Figure 4.3Bi and 4.3Bii**). By contrast, SFA levels in fecal samples were slightly lower in the MCI group than in the control group. Conversely, MUFAs and PUFA levels in fecal samples decreased with disease progression. (**Figure 4.3Biii**).

The PUFAs were further categorized into ω-3 PUFAs, where the double bond is located on the C3 from the methyl end, and ω-6, where the double bond is at C6 from the methyl end of the fatty acid chain. The results for the ω-6: ω-3 ratio across the stage-specific groups of the saliva, plasma, and fecal samples are shown in **Figure 4.3C**. In saliva samples, the control group exhibited a significantly higher ω-6: ω-3 ratio of approximately 18:1 compared to the MCI group. By contrast, no significant differences in the ω-6: ω-3 ratio were detected among the control and MCI groups of plasma samples. Notably, fecal samples from the dementia group displayed a significantly higher ω-6: ω-3 ratio of approximately 27:1 compared to the control and MCI groups.

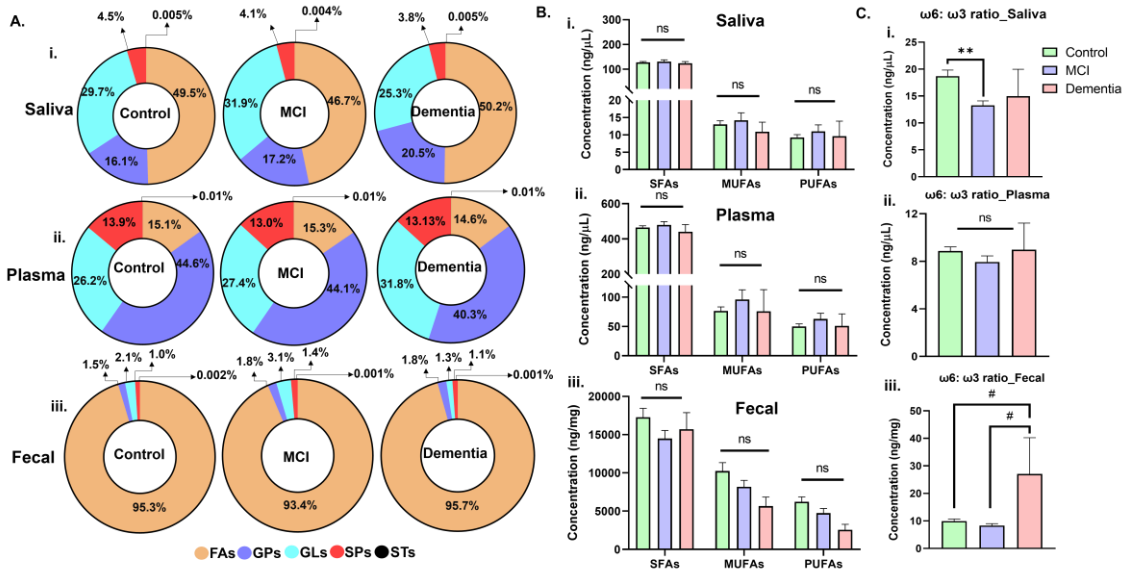

Figure 4.3: Distribution of major lipid classes and fatty acyl levels in control, MCI, and dementia groups of saliva, plasma, and fecal samples. **A.** Donut chart showing the percentage distribution of major lipid classes in stage-specific groups of older adults, (i) saliva, (ii) plasma, and (iii) fecal samples. **B.** Changes in SFAs, MUFAs, and PUFAs levels in stage-specific groups of older adults, (i) saliva, (ii) plasma, and (iii) fecal samples. **C.** ω-6: ω-3 ratio in stage-specific groups of, (i) saliva, (ii) plasma, and (iii) fecal samples.

(Ordinary one-way ANOVA with Tukey's multiple comparison tests, #p<0.0001, **p<0.01, and p>0.05 (ns), saturated fatty acids (SFAs), monounsaturated fatty acids (MUFA), and polyunsaturated fatty acids (PUFAs)).

4.3.1.3 Volcanic plot analysis of stage-specific groups of older adults in saliva, plasma, and fecal samples

Figure 4.4 shows a volcanic plot representing the graph of $-\log_{10}$(p-value) vs. $\log_2$(fold change) related to the significantly altered lipid molecular species in the stage-specific groups of saliva, plasma, and fecal samples. The red color on the right side of the plot indicates upregulation, and the blue color on the left side of the plot indicates downregulation of the lipid molecular species in each group. Volcano plots representing lipidome alterations in the saliva samples of the stage-specific groups are presented in **Figure 4.4A**. The results clearly show that several TG molecular species, particularly oleic acid or linoleic-acid-composed TG, oxidized TG, and FAs such as FA 20:5, FA 22:5, and FA 20:4, were upregulated in the MCI group compared to the control group (**Figure 4.4Ai)**. In comparison between the control and dementia groups shows that GPs such as LPE 22:5, LPE 20:4, and PI (18:0/20:4) were upregulated in the dementia group compared to the control group (**Figure 4.4Aii**). **Figure 4.4Aiii** shows that TG (22:0/18:1:18:2), TG (22:0/18:2:18:2), and LPI 24:0 were upregulated in the dementia group compared to the MCI group. Volcanic plots of plasma lipidome alterations in the stage-specific groups are shown in **Figure 4.4B** and indicate the upregulation of FA 12:0, FA 20:4, FA 20:5, FA 22:5, LPC 14:0, LPE 22:5, LPC 22:5, and many other lipid molecular species in the MCI group. Conversely, CE 18:2 was downregulated in the MCI group relative to the control group (**Figure 4.4Bi**). In the comparison between the control and dementia groups, LPC 16:1, PI (16:0/20:5), HexCer (d18:0/21:0;O), HexCer (d18:0/15:0;O), and several other lipid molecular species were upregulated in the dementia group compared to the control group (**Figure 4.4Bii). Figure 4.4Biii** highlights the upregulation of CE 18:1 and CE 18:2 in the dementia group compared to the MCI group. Volcanic plots depicting fecal lipid alterations in stage-specific groups are presented in **Figure 4.4C.** The results clearly show that most of the TG and DG molecular species, particularly the TG- and DG-containing medium-chain fatty acids (TG-MCFAs and DG-MCFAs), as well as many other lipid molecular species, were upregulated in the

MCI group. By contrast, FAHFAs and many other lipid molecular species are downregulated in the MCI group compared to those in the control group, as shown in **Figure 4.4Ci**. In comparison between the control and dementia groups showed that upregulation of lipid species such as LPE 18:1, LPE 16:0, and TG (16:0/20:0/18:1) was observed in the dementia group compared to the control group (**Figure 4.4Cii**). **Figure 4.4Ciii** reveals the upregulation of several FAHFAs and other lipid molecular species in the dementia group. However, TG (16:0/18:2/18:3), TG (18:1/18:1/18:2), and TG (16:0/18:1/18:2) levels are downregulated in the dementia group than in the MCI group**.** **Appendix Figure 4.2A-C** shows the heatmaps of the top 50 altered lipid molecular species in stage-specific groups across the saliva, plasma, and fecal samples of older adults.

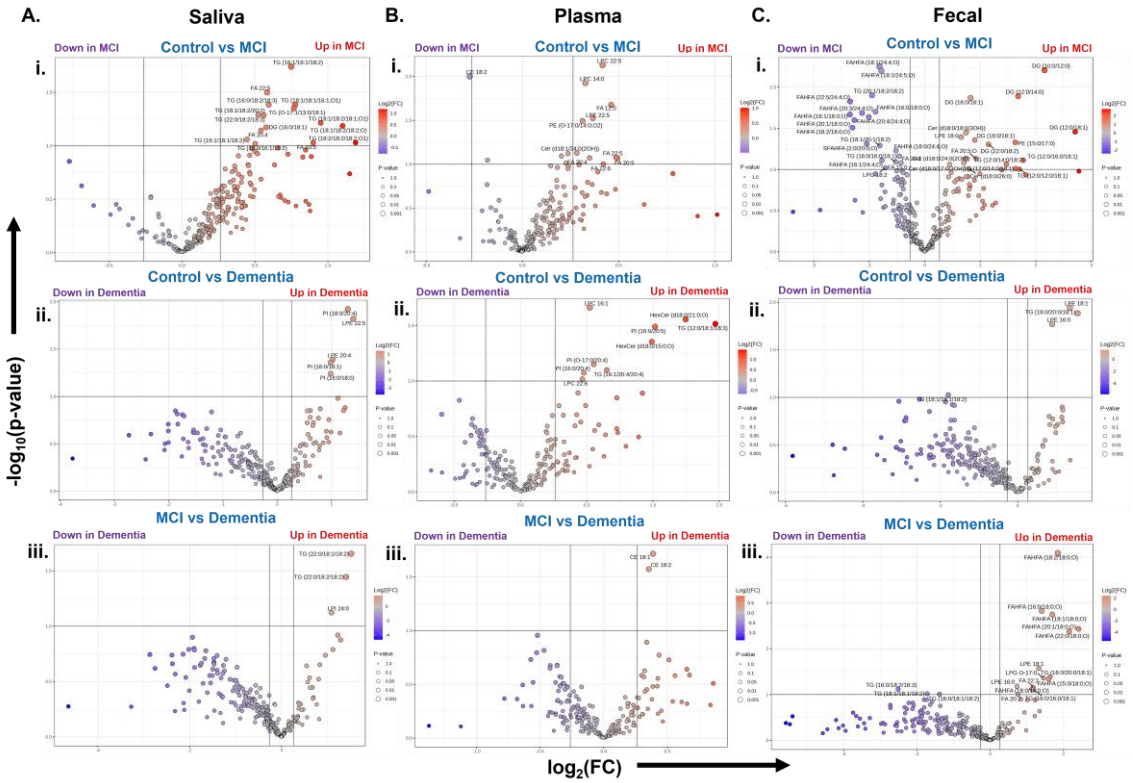

Figure 4.4: Volcanic plot representing significantly altered lipids (t-test, $p < 0.1$) in the control, MCI, and dementia groups of saliva, plasma, and fecal samples. **A.** Volcanic plot for significantly altered lipids in saliva samples for, (i) control vs MCI groups. (ii) control vs dementia groups. (iii) MCI vs dementia groups. **B.** Volcanic plot for significantly altered lipids in plasma samples for: (i) control vs MCI groups. (ii) control vs dementia

groups. (iii) MCI vs dementia groups. **C.** Volcanic plot for significantly altered lipids in fecal samples for: (i) control vs MCI groups. (ii) control vs dementia groups. (iii) MCI vs dementia groups.

4.3.1.4 Identification of lipid biomarkers for early-stage diagnosis of MCI patients in older adults.

Receiver operating characteristic (ROC) analysis was conducted to evaluate the diagnostic potential of lipid metabolites that were significantly altered between the control and MCI groups in the saliva, plasma, and fecal samples of older adults (**Figure 4.5A)**. The selection of lipid metabolites for ROC analysis was performed using MetaboAnalyst 6.0.

Among the altered lipid metabolites in saliva samples between control and MCI groups, FA 18:3 exhibited high discriminatory potential, with an area under the curve (AUC) value of 0.6947 (**Figure 4.5Ai**). By contrast, FA 22:5 and CE 18:2 demonstrated moderate diagnostic effects, with AUC values of 0.5526 and 0.5475, respectively (**Figure 4.5Aii – 4.5Aiii**). Altered lipid metabolites in plasma samples from control and MCI groups demonstrated good diagnostic potential for CE 18:2, with a high AUC value of 0.6865 (**Figure 4.5Aiv**). However, FA 22:5 and FA 18:3 showed moderate diagnostic effects, with AUC values of 0.6090 and 0.5840, respectively (**Figure 4.5Av – 4.4Avi**). Similarly, in fecal samples, CE 18:2 demonstrated a high diagnostic value, with an AUC value of 0.6095 (**Figure 4.5Avii**). However, FA 18:3 and FA 22:5 exhibited moderate diagnostic potency, with AUC values of 0.5166 and 0.5026, respectively (**Figure 4.5Aviii – 4.5Aix**).

The variation of the TG-MCFAs and DG-MCFAs molecular species between the control, MCI, and dementia groups in the saliva, plasma, and fecal samples is further examined in **Figure 4.5B.** The bar graph shows the Mean ± SEM of the relative concentrations of the individual TG-MCFAs and DG-MCFAs species in the respective saliva, plasma, and fecal samples groups. In saliva samples, the levels of TG-MCFAs were found to decrease with disease progression for patients in both the MCI and dementia groups compared to the control group as shown in **Figure 4.5Bi**. In the plasma samples, a slight increase in TG-MCFAs was observed in patients in the MCI group compared to the control and dementia groups (**Figure 4.5Bii).** Conversely, in fecal

samples, both TG-MCFAs and DG-MCFAs levels were elevated in the MCI group compared to those in the control group, suggesting the potential excretion of these lipids in MCI patients (**Figure 4.5Biii).** These findings suggest that specific lipid metabolites, including FA 18:3, FA 22:5, CE 18:2, and TG-MCFAs, may serve as promising non-invasive lipid biomarkers for the early-stage (MCI) disease progression.

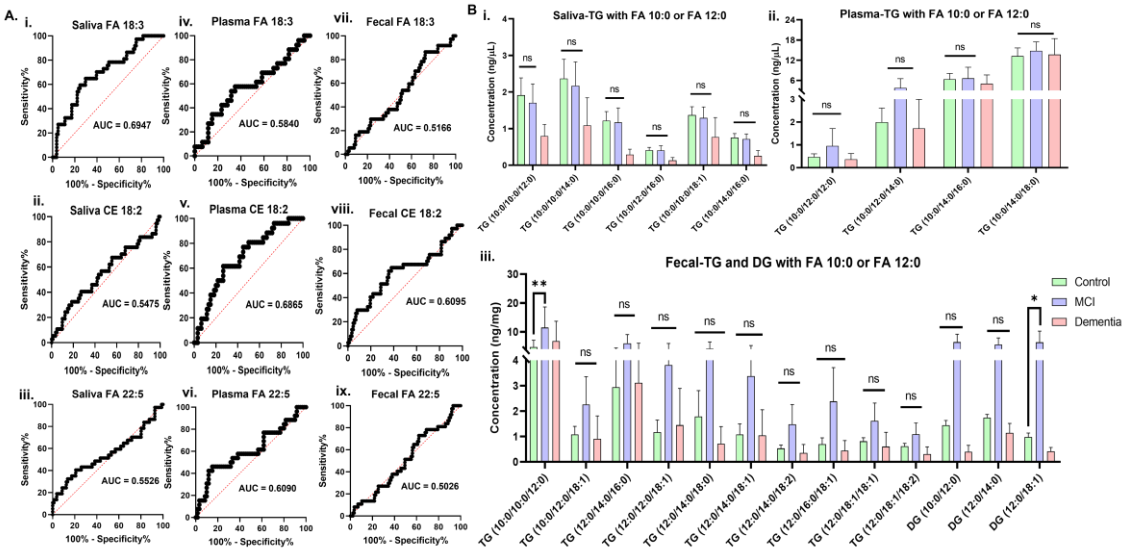

Figure 4.5: Receiver operating characteristics (ROC) analysis and triacylglycerols and diacylglycerol containing medium chain fatty acid (TG-MCFAs and DG-MCFAs) levels in stage-specific groups of saliva, plasma, and fecal samples **A.** ROC analysis for significantly altered lipid species in control vs MCI groups of, (i-iii) saliva samples. (iv-vi) plasma samples, and (vii-xi) fecal samples **B.** Bar plots representing: (i) Changes in TG-MCFAs levels in stage-specific groups of saliva samples, (ii) Changes in TG-MCFAs levels in stage-specific groups of plasma samples, (iii) Changes in TG-MCFAs and DG-MCFAs levels in stage-specific groups of fecal samples (Ordinary two-way ANOVA with Tukey's multiple comparison tests, **p<0.01, *p<0.1, and p>0.05 (ns), triacylglycerols (TGs), and diacylglycerols (DGs).

4.3.1.5 Sex-specific lipid fingerprinting in MCI patients of saliva, plasma, and fecal samples of older adults.

A recent study has highlighted sex-based differences in the prevalence of MCI and dementia, with females reportedly at a higher risk than males [33]. To investigate sex-specific lipid alterations associated with MCI, we analyzed saliva, plasma, and fecal

samples from male and female participants categorized into control and MCI groups. The results of multivariate OPLS-DA analysis of the sex-specific lipid distribution in the saliva, plasma, and fecal samples of control and MCI groups are shown in **Figure 4.6A**. The score plot illustrates the minor group separation between the control and MCI groups among both male and female participants in saliva samples, explaining 13.5% and 50.4% of the total variance in the model, respectively (**Figure 4.6 Ai and Aii**). The VIP plot shows that GPs, GLs, and FAs are the primary lipid metabolites contributing to group separation (**Appendix Figure 4.3A)**. In plasma samples, the score plot depicted in **Figure 4.6Aiii** demonstrates a clear group separation between the control and MCI groups of male participants, accounting for 28.6% of the total variance in the model. GPs, FAs, and SPs are the key contributors to this major differentiation, as evidenced by their high VIP scores (> 2) (**Appendix Figure 4.3B)**. By contrast, the score plot of the female participants exhibited only minor group separation, indicating minimal lipid compositional differences, with 31.5% of the total variance in the model (**Figure 4.6Aiv**). This variation is driven by GPs and STs (**Appendix Figure 4.3B**). For fecal samples, both male and female participants showed minor group separation between the control and MCI groups, with the model explaining 17.9% and 12.4% of the total variance, respectively (**Figure 4.6Av and Avi)**. The VIP plot shows that GLs, FAs, and SPs are the primary lipid metabolites contributing to group separation (**Appendix Figure 4.3BC**).

Figure 4.6B presents volcanic plots illustrating sex-specific lipid alteration in the control and MCI groups of saliva, plasma, and fecal samples in terms of $-\log_{10}$ (p-value) vs. $\log_2$ (fold change) values. The volcano plot results for saliva samples show no differences between the control and MCI groups for male participants (**Figure 4.6Bi**). However, for female participants, specific lipids such as FA 18:3 and oleic acid or linoleic acid-composed TGs are upregulated in the MCI group compared to those in the control group (**Figure 4.6Bii**). For plasma samples, male participants with MCI showed upregulation of PI (20:4/17:1;O1), LPC 14:0, and other lipid molecular species, whereas HexCer (d18:1/23:1;O) was downregulated (**Figure 4.6Biii**). For female participants, several lipids were differentially expressed, with the upregulation of LPC 22:5, LPE 22:5, FA 12:0, HexCer (d18:0/21:0;O), LPC 22:6, and PS (18:0/18:1), and the downregulation of CE 18:1 and CE 18:2 observed in patients with the MCI compared to control groups (**Figure 4.6Biv**). Fecal samples revealed distinct sex-specific lipid alterations in control

and MCI groups. The volcano plot results for male participants show upregulation of FA 22:5;(2OH), FA 24:0;(2OH), FA 25:0;(2OH), and downregulation of TG (16:0/16:1/18:1), FAHFA (18:1/24:5;O), and PG (O-18:2/16:0) in the MCI group compared to the control group (**Figure 4.6Bv**). However, for female participants, FA 10:0, PE (15:0/17:0), TG- and DG-MCFAs, and many other lipid molecular species are significantly upregulated in the MCI group, while FAHFAs and other lipid molecular species were downregulated in the MCI group compared to the control patients (**Figure 4.6Bvi**).

To further elucidate the significant lipid alterations between the control and MCI groups, we examined the upregulated and down-regulated lipid molecular species in male and female participants across saliva, plasma, and fecal samples, as shown in **Figure 4.6C**. Bar graphs depict the mean ± SEM of the relative concentrations of these significantly altered lipid species in the respective groups. In saliva samples, FA 18:3 was notably elevated in female participants with MCI compared to males. However, no other lipid species demonstrated significant differences between the male and female participants in the saliva samples (**Figure 4.6Ci – 4.6Civ).** In plasma samples, LPC 22:5 was significantly increased in female participants, while PI (20:4/17:1;O1) was significantly elevated in male participants of the MCI group compared to the control group. Conversely, HexCer (d18:1/23:1;O) and CE 18:2 were significantly decreased in male and female participants, respectively, in patients with MCI compared to the control group (**Figure 4.6Cv – 4.6Cviii).** In fecal samples, FAHFA (18:1/24:4;O) levels were significantly decreased in female participants of the MCI group. However, no other lipid species exhibited significant differences between male and female participants in fecal samples (**Figure 4.6Cix – 4.6Cxii**). **Appendix Figure 4.4A-C,** provided in the Supporting Information show the heatmaps of the top 50 altered lipid molecular species in male and female participants of control and MCI groups across saliva, plasma, and fecal samples of older adults.

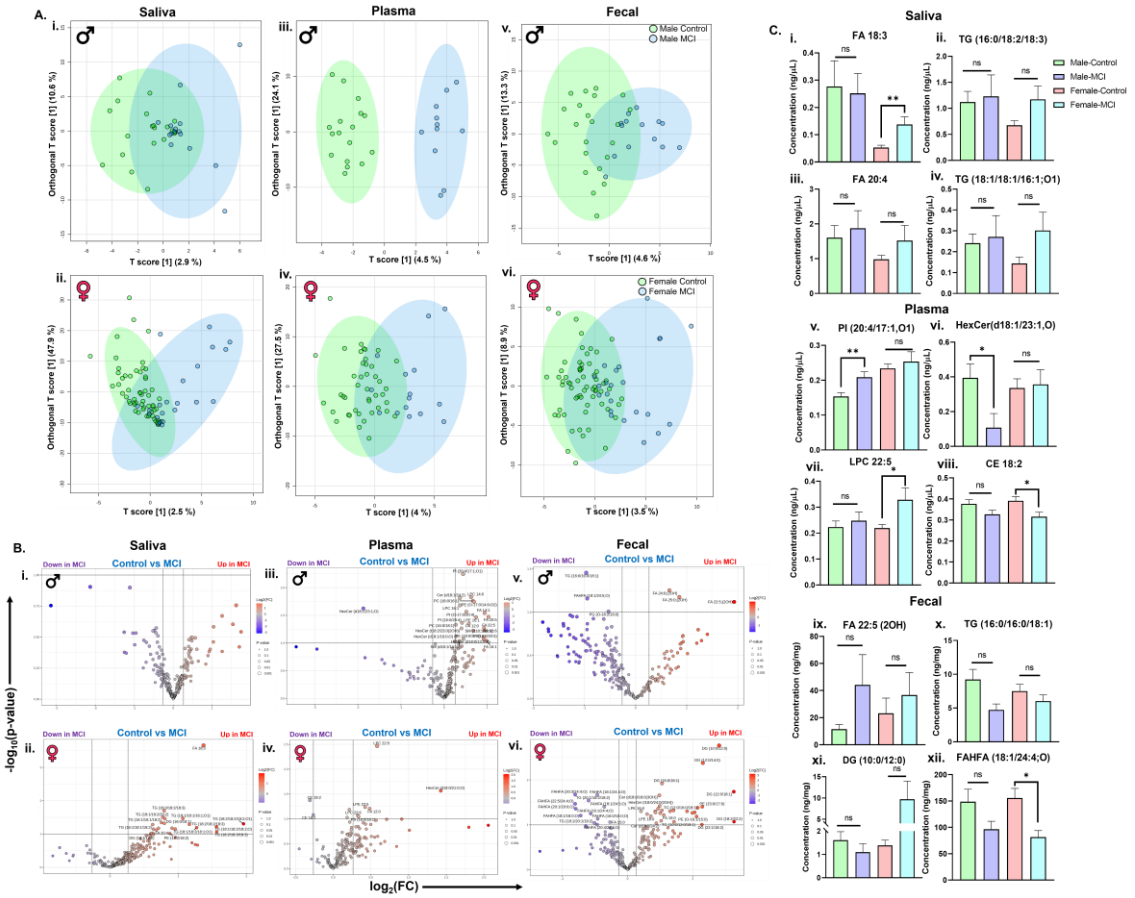

Figure 4.6: Sex-specific lipidome alternation in control and MCI groups of saliva, plasma, and fecal samples**. A.** Multivariate orthogonal partial least square discriminate analysis (OPLS-DA) score plot analysis of control and MCI groups for: (i) male saliva samples, (ii) female saliva samples, (iii) male plasma samples, (iv) female plasma samples, (v) male fecal samples, and (vi) female fecal samples. **B.** Volcanic plot representing significantly altered lipids (t-test, $p < 0.1$) in the control and MCI groups for (i) male saliva samples, (ii) female saliva samples, (iii) male plasma samples, (iv) female plasma samples, (v) male fecal samples, and (vi) female fecal samples. **C.** Bar graph representing significantly altered lipids among male and female participants in the control and MCI groups of, (i-vi) saliva samples, (v-viii) plasma samples, and (ix-xii) fecal samples (Mann-Witney U tests, **p<0.01, *p<0.1, and p>0.05 (ns))

4.3.1.6 Bodyweight-specific lipidome alteration in MCI patients of saliva, plasma, and fecal samples of older adults.

Body mass index (BMI) is a standard measure used to assess the height/weight characteristics of adults, categorizing them into underweight (UW), normal-weight (NW),

and overweight (OW) groups [34]. The participants with BMI < 18.5, BMI 18.5 ~ 24.9, and BMI ≥ 25 were grouped as underweight (UW), normal weight (NW), and overweight (OW), respectively.

Body-weight-specific lipid alterations associated with MCI in the saliva, plasma, and fecal samples of older adults in the NW and OW groups were analyzed. UW participants were not considered in this analysis because of the discrepancies in the sample size. The results of multivariate OPLS-DA analysis of bodyweight-specific lipid distribution in patients with MCI across saliva, plasma, and fecal samples are presented in **Figure 4.7A**. The score plot illustrates the minor group separation between the control and MCI groups among both NW and OW participants for saliva samples, explaining 60.3% and 50.5% of the total variance in the model, respectively (**Figures 4.7Ai and Aii**). The VIP plot indicated that GLs and FAs are the primary lipid metabolites contributing to the group separation (**Appendix Figure 4.5A)**. For plasma samples, the score plots (**Figures 4.7Aiii and 4.7Aiv**) show a subtle separation between the control and MCI groups for both NW and OW participants, with minimal differences in lipid composition. The model explains 34.1% of the total variance, with GPs, FA, and SPs identified as the key contributors to the observed separation (**Appendix Figure 4.5B**). By contrast, the fecal samples show minor group separation between the control and MCI groups for both NW and OW participants, with the model accounting for 18.7% and 13% of the total variance, respectively (**Figure 4.7Av and 4.7Avi**). The VIP plot shows that GPs, GLs, and FAs are the primary lipid metabolites contributing to group separation (**Appendix Figure 4.5C**).

Figure 4.7B presents volcano plots illustrating body-weight-specific lipid alterations in the saliva, plasma, and fecal samples of the control and MCI groups, with data expressed as $-\log_{10}$ (p-value) vs. $\log_2$ (fold change) values. For NW participants, the volcano plot results for saliva samples show upregulation of FA 18:3, FA 20:4, FA 22:5, and many other lipid molecular species in the MCI group compared to the control group. Conversely, TG (17:1/18:1/20:1) was downregulated in the MCI group compared to the control group (**Figure 4.7Bi**). However, for OW participants, oleic acid or linoleic acid-containing TG molecular species are upregulated in the MCI group compared to the control group (**Figure 4.7Bii**). The volcano plot results for plasma samples show upregulation of the LPC 14:0, LPE 22:5, and many other lipid molecular species in the

MCI group compared to the control group of NW participants. Conversely, CE 18:1 and CE 18:2 were downregulated in the MCI group compared to the control group of NW participants (**Figure 4.7Biii**). However, for OW participants, LPC 22:6, LPE 18:3, and LPC 16:1 are upregulated, and HexCer (d18:1/23:1;O) is downregulated in the MCI group compared to the control group (**Figure 4.7Biv**). The volcano plot results for fecal samples show upregulation of DG molecular species, particularly DG-MCFAs, and many other lipid molecular species, and significant downregulation of FAHFAs, and FAs in the MCI group compared to the control group of NW participants (**Figure 4.7Bv**). By contrast, for OW participants, LPE 18:0, PE (15:0/17:0), HexCer (t18:0/24:0(2OH)), and DG (10:0/12:0) are upregulated in the MCI group. However, FAHFA (18:1/24:4;O) and FAHFA (18:1/24:5;O) are downregulated in the MCI group compared to the control group (**Figure 4.7Bvi**).

We further investigated the significant alterations in the up- and down-regulated lipid molecular species in the saliva, plasma, and fecal samples of patients with MCI across NW and OW participants, as illustrated in **Figure 4.7C**. The bar graph illustrates the Mean ± SEM of the relative concentrations of the significantly altered lipid molecular species in the respective groups. In saliva samples, FA 18:3 was significantly increased in the MCI group of both NW and OW groups. However, no other lipid species displayed significant differences between NW and OW participants in the saliva samples (**Figure 4.7Ci – 4.7Civ**). In the plasma samples, LPC 14:0 was significantly increased in the NW participants with MCI compared to OW participants, while CE 18:2 was significantly lower in the NW participants of the MCI group compared to the OW group. However, other species showed no significant differences between NW and OW participants of plasma samples (**Figure 4.7Cv – 4.7Cviii)**. In fecal samples, FAHFA (18:1/24:4;O) and TG (16:0/16:0/18:1) levels were significantly decreased for both NW and OW participants in the MCI group. However, other species showed no significant differences between NW and OW participants of fecal samples (**Figure 4.7Cix – 4.7Cxii)**. **Appendix Figure 4.6A-C** shows the heatmaps of the top 50 altered lipid molecular species in control and MCI groups of NW and OW participants across saliva, plasma, and fecal samples of older adults.

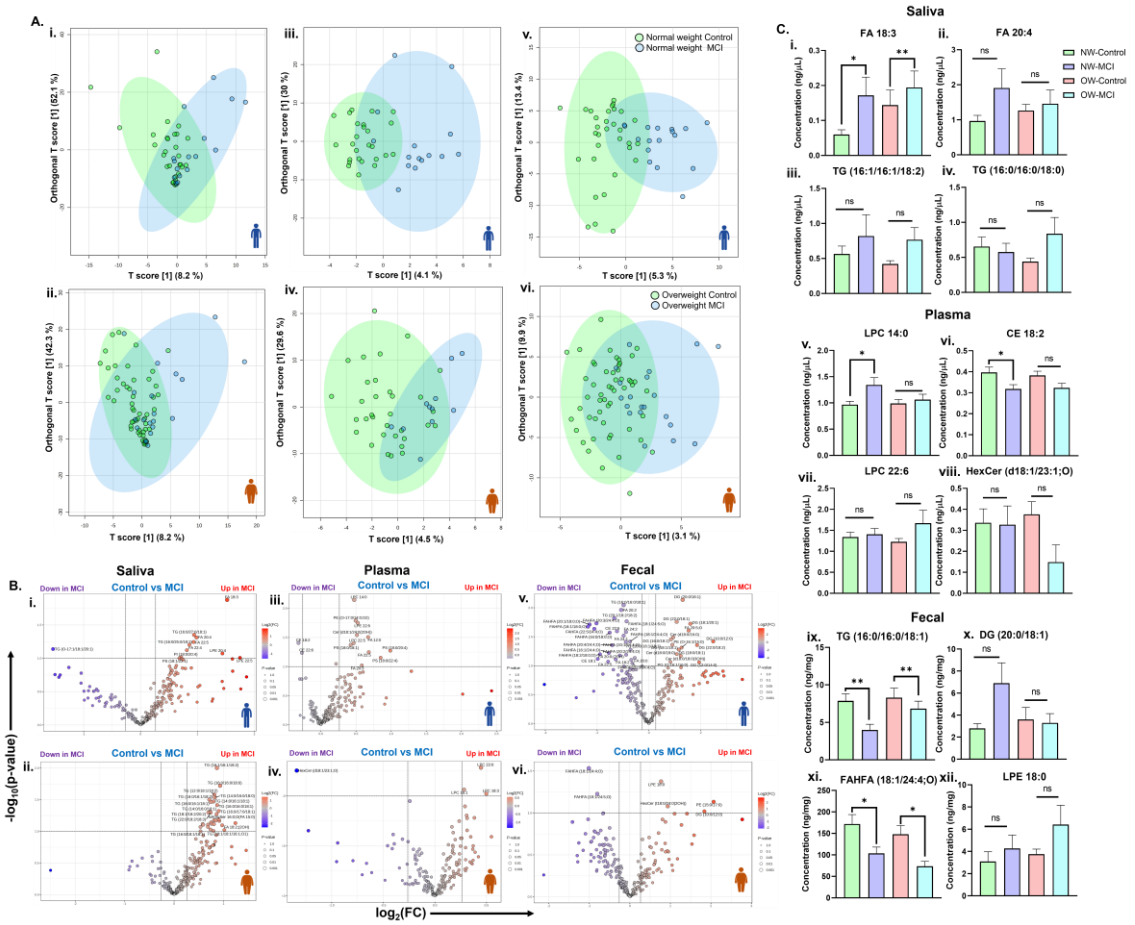

Figure 4.7: Weight-specific lipidome alternation in control and MCI groups of saliva, plasma, and fecal samples**. A.** Multivariate orthogonal partial least square discriminate analysis (OPLS-DA) score plot analysis of control and MCI groups for: (i) NW saliva samples, (ii) OW saliva samples, (iii) NW plasma samples, (iv) OW plasma samples, (v) NW fecal samples, and (vi) OW fecal samples. **B.** Volcanic plot representing significantly altered lipids (t-test, $p < 0.1$) in the control and MCI groups for (i) NW saliva samples, (ii) OW saliva samples, (iii) NW plasma samples, (iv) OW plasma samples, (v) NW fecal samples, and (vi) OW fecal samples. **C.** Bar graph representing significantly altered lipids among NW and OW participants in the control and MCI group of, (i-vi) saliva samples, (v-viii) plasma samples, and (ix-xii) fecal samples (Mann-Witney U tests, **p<0.01, *p<0.1, and p>0.05 (ns))

4.3.2 Comprehensive brain lipidome profiling in neurovegetative disorders

4.3.2.1 Multivariate analysis of brain lipidome

In this study, brain tissue samples from the frontal, temporal, parietal, and occipital regions were collected from healthy individuals and patients diagnosed with AD, PD, and HD. Total lipids were extracted from each brain region, followed by untargeted lipidomic analysis using HPLC/LTQ-Orbitrap-MS. Detailed demographic characteristics of the participants involved in this work are presented in **Table 4.2**.

Table 4.2: Characteristics of the participants across healthy volunteers (HV), Alzheimer's disease (AD), Parkinson's disease (PD), and Huntington's disease (HD) groups included in the study

Condition	Tissue samples of the cerebral cortices				Age (Years)	Analysis time
	Frontal	Temporal	Parietal	Occipital		
Healthy Volunteer (HV)	Male	Male	Male	Male	57	12.6
	Male	Male	Male	Male	76	22.2
	Male	Male	Male	Male	67	12.3
	Female	Female	Female	Female	73	18.5
	Female	Female	Female	Female	55	19.7
	Female	Female	Female	Female	75	15.4
Alzheimer's disease (AD)	Male	Male	Male	Male	76	9.8
	Male	Male	Male	Male	76	13.8
	Male	Male	Male	Male	81	15.8
	Female	Female	Female	Female	78	19.3
	Female	Female	Female	Female	66	15.7
	Female	Female	Female	Female	45	16.2
Parkinson's disease (PD)	Male	Male	Male	Male	82	13.0
	Male	Male	Male	Male	87	11.2
	Male	Male	Male	Male	73	30.6
	Female	Female	Female	Female	72	14.7
	Female	Female	Female	Female	64	16.2
	Female	Female	Female	Female	81	14.8
Huntington's disease (HD)	Male	Male	Male	Male	37	7.3
	Male	Male	Male	Male	77	15.3
	Male	Male	Male	Male	49	12.7
	Female	Female	Female	Female	68	11.0
	Female	Female	Female	Female	79	16.0
	Female	Female	Female	Female	69	8.6

Figure 4.8 represents the various classes of lipid species identified across the different brain regions and their corresponding multivariate analyses. The analysis of brain tissue samples from the frontal, parietal, occipital, and temporal regions identified a total of 291 lipid species across multiple lipid classes, as shown in **Figure 4.8A**. Among these, 40 were identified as FAs, followed by 38 PCs, 35 PEs, 22 PSs, 19 CLs, 18 PGs, 15 PIs, 13 Cer, 11 TGs, 10 SMs, 14 HexCer, and AHexCer. The multivariate PCA score plot of annotated lipid species from the different regions of brain tissue samples across HV, HD, PD, and AD groups is illustrated in **Figure 4.8B**. Principal components 1 and 2 together accounted for 80.8% of the total variance, with component 1 explaining 52.2% and component 2 contributing 28.6% of the variance.

The PCA analysis revealed minor separation between the HV and AD groups, indicating relatively subtle lipidomic differences. In contrast, a more distinct separation was observed between the HV and HD, PD groups. Interestingly, the HD and PD groups showed considerable overlap in their lipidomic profiles, suggesting shared alterations in lipid metabolism. **Appendix Figure 4.7A** presents the loading plot of the components that influence the group separations observed in the PCA. This plot highlights key lipid species, particularly FAs and GPs, that exhibit high positive or negative loading scores, contributing significantly to the variance and driving group separation along the first and second principal components. These results indicate that specific lipids play a crucial role in the observed group separation and in defining the distinct lipidomic profiles of the different disease groups. Further, the pairwise OPLS-DA analysis was performed to evaluate the lipidomic differences between the HV and each of their disease groups (AD, PD, and HD), allowing for individual assessment of disease-specific lipidomic alterations. The OPLS-DA score plot revealed a clear group separation between the HV and AD patients, as illustrated in **Figure 4.8C**. The two components of the T scores, T score 1 and T score 2, accounted for 28.6% of the total variance in the model, with T score 1 contributing 21.4% of the variance. This separation reflects significant alterations in lipid composition associated with AD pathology. Furthermore, the VIP plot shows that SPs and GPs are responsible for this clear group separation with a VIP score of >2, indicating a high VIP score for the identification of plausible biomarker candidates (**Appendix Figure 4.7B**). The OPLS-DA score plot in **Figure 4.8D** illustrates the clear group separation between the HV and HD patients. The model accounted for a total variance of 30.8%,

with T score 1 explaining 20.8% variance, respectively. This variation is driven by FAs and GPs, as identified in the corresponding VIP plot (**Appendix Figure 4.7C**). The OPLS-DA score plot depicted in **Figure 4.8E** reveals a clear group separation between the HV and PD patients, with the model accounting for a total variance of 43%, with T score 1 explaining 19.4% of the variance. The VIP plots highlight that FAs and GPs were the major metabolite contributors to this group separation (**Appendix Figure 4.7D**).

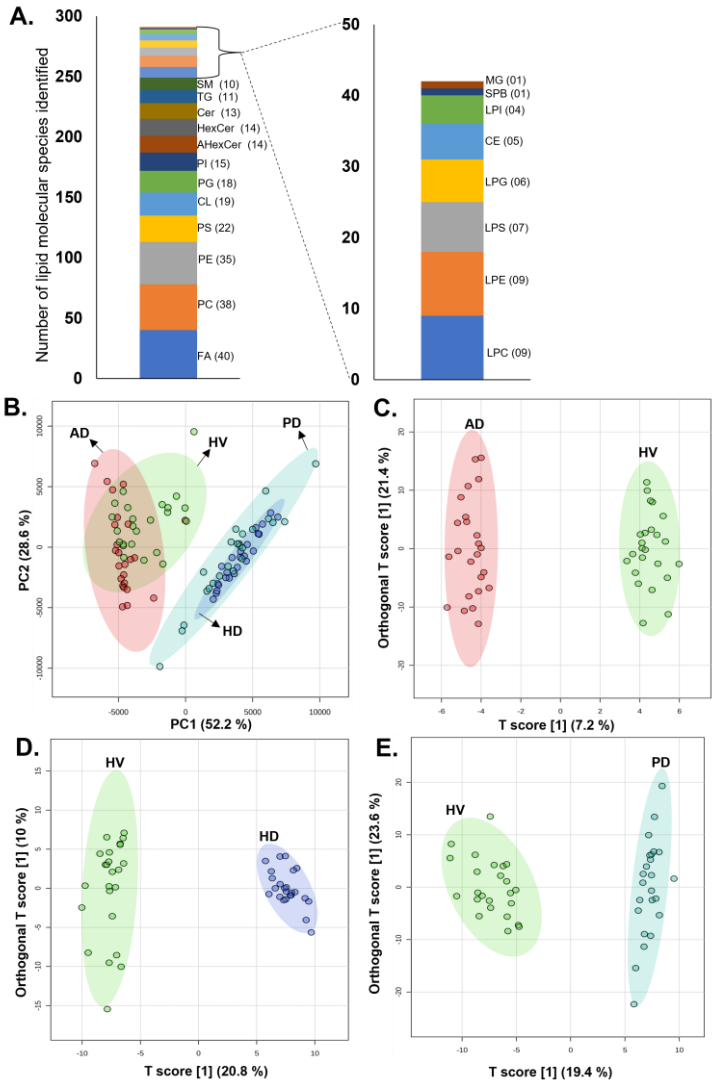

Figure 4.8: A. Different classes of lipid species were identified in brain tissue samples from HV, AD, HD, and PD patients. **B.** PCA score plot of the brain tissue samples from the HV, AD, HD, and PD groups of neurodegenerative patients. **C.** OPLS-DA score plot of the brain tissue samples from the HV and AD groups. **D.** OPLS-DA score plot of the

brain tissue samples from the HV and HD groups. **E.** OPLS-DA score plot of the brain tissue samples from the HV and PD groups.

4.3.2.2 Disease-specific alteration in brain lipidome across AD, PD, and HD

The volcano plot displays the distribution of significantly altered lipids between the HV and disease groups (AD, HD, and PD) of brain lipidome by plotting a graph of $-\log_{10}(p\text{-value})$ against $\log_2(\text{fold change})$, thereby highlighting lipids with both statistical significance and substantial fold changes (**Figure 4.9A**). Lipid species that are significantly upregulated in the disease group are represented in red on the right side, while those that are significantly downregulated appear in blue on the left side, reflecting group-specific alterations in lipid abundance. In the comparison between HV and AD groups, the volcano plot revealed a distinct upregulation of AHexCer (d(O-18:1)18:1/15:0;O) and PS (16:1/24:0;O) in the AD group compared to the HV group. However, several lipid species, such as LPC 17:2, PG (24:0/18:1;O2), LPC 18:2, PI (O-16:1/17:1), PC (O-22:5/19:3), and FA 22:4;(2OH), were found to be significantly decreased in the brain tissue samples of AD group. In the comparison between the HV vs HD groups, the volcano plot revealed a distinct upregulation of lipid species, including PC (O-22:5/17:3), PS (O-17:0/22:6), FA 18:0, and many other lipid species in the HD group. Conversely, lipids such as AHexCer (d(O-18:1)18:1/15:0;O), AHexCer (d(O-18:1)18:2/24:1;O), AHexCer (d(O-18:1)18:3/26:1;O), and many other lipid molecular species are downregulated in the HD group compared to the HV group. A similar lipidome alteration was observed in the comparison between HV vs PD groups. The volcano plot revealed significant upregulation of several lipid species in the PD group, including PS (O-17:0/22:6), PC (O-22:5/17:3), and FA 18:0, along with other differentially expressed lipids. In contrast, a marked downregulation of specific lipids, such as AHexCer (d(O-18:1)18:1/15:0;O), and AHexCer (d(O-18:1)18:3/26:1;O), along with several other lipid molecular species, was observed in the PD group compared to HV group. Significantly altered lipid molecular species ($p < 0.05$) based on their fold change and p-value across HV vs AD, HD, and PD patients are shown in **Appendix Tables 4.1-4.3**.

The heat map depicting the top 30 significantly altered lipid species (based on p-value significance) across the HV, AD, HD, and PD groups is shown in **Figure 4.9B**. Lipid abundance is represented by a color gradient, with intense red indicating higher

concentrations and deep blue representing lower concentrations within each group. Compared to the HV group, the AD group displayed pronounced alterations in the brain lipidome. Notably, lipids such as AHexCer (d(O-18:1)18:1/15:0;O), AHexCer (d(O-18:1)18:2/24:1;O), AHexCer (d(O-18:1)18:3/26:1;O), and SM (d18:1/16:1) were significantly elevated in AD patients. In the HD group, a distinct increase was observed in lipid species including PS (18:0/22:4), PC (O-22:5/19:3), PC (O-22:5/17:3), FA 18:0, CL 70:0, and CL 74:5. In the case of the PD group, lipid species such as CL 70:0 and PC (O-22:5/19:3) exhibited similar trends to those observed in the HD group. In addition, several other lipid molecules, including FAs and CLs species exhibited in the top of the heatmap, were found to be increased in the PD group compared to the HV group.

ROC curve analysis was conducted to assess the diagnostic potential of the significantly altered lipid species in the AD, HD, and PD groups, as shown in **Figure 4.9C**. To further illustrate their discriminatory power, a bar graph representing the mean ± SEM of the relative concentrations of these lipids across the respective groups is also presented. Among the altered lipid metabolism in brain tissue samples of AD, HD, and PD groups, AHexCer (d(O-18:1)18:1/15:0;O) demonstrated the strongest diagnostic performance, showing an AUC value of 0.8125 in the AD group and a perfect 1.000 in both HD and PD groups. The bar graph depicting the relative abundance of this lipid revealed a significant increase in the AD group, whereas a marked decrease was observed in both HD and PD groups compared to the HV group. Another key lipid, PS (O-17:0/22:6), exhibited excellent diagnostic potential for HD (AUC = 1.000) and PD (AUC = 0.9167), but not for AD (AUC = 0.5126). Consistently, its levels were significantly increased in HD and PD groups, with no notable change observed in the AD group. Similarly, PC (O-22:5/19:3) showed a robust diagnostic performance across all three neurodegenerative disorders, with AUC values of 0.7465, 0.9479, and 0.8785 for AD, HD, and PD groups, respectively. However, its abundance displayed an inverse pattern-significantly decreased in AD but markedly increased in both HD and PD groups compared to HV. These findings suggest that while certain lipid species may be broadly altered across neurodegenerative disorders, their directionality and diagnostic relevance vary depending on the specific condition.

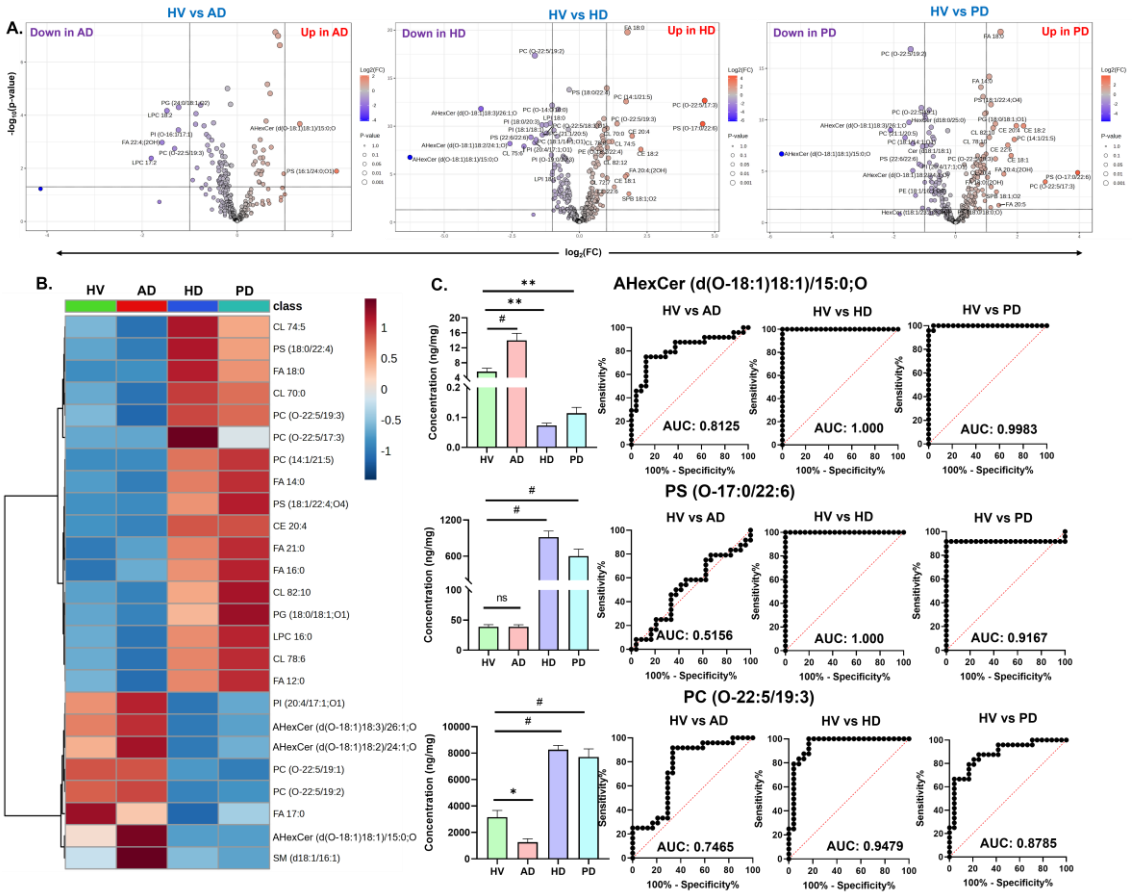

Figure 4.9: A. Volcanic plot representing significantly altered lipid levels ($p < 0.05$) in the brain samples of HV vs AD, HV vs HD, HV vs PD. **B.** Hierarchical cluster correlation analysis of the top 25 significantly altered lipids ($p < 0.05$) in HV, AD, HD, and PD groups. **C.** Bar graph and ROC analysis of significantly altered lipids in AD, HD, and PD groups (Ordinary one-way ANOVA, #p< 0.0001, ***p<0.001, **p<0.01, *p<0.05, 0.1(ns)). All data are represented as mean ± SEM.

4.3.2.3 Sex-specific brain lipid fingerprinting across AD, PD, and HD

To explore sex-specific lipidome variations associated with neurodegenerative disorders, we analyzed brain tissue samples from both male and female participants, stratified into HV, AD, HD, and PD groups. **Figure 4.10A** presents volcanic plots illustrating sex-specific lipid alteration in the HV and disease groups (AD, HD, and PD) of brain lipidome by plotting a graph of $-\log_{10}$(p-value) against $\log_2$(fold change). The volcano plot for HV vs AD groups reveals significant upregulation of AHexCer (d(O-18:1)18:1/15:0;O), and HexCer (d18:1/23:0;O) in the male participants of the AD group

compared with the HV group (**Figure 4.10A**). However, a few lipid molecules, such as PG (24:0/18:1;O2), LPC 17:2, PI (O-16:1/17:1), LPC 18:2, CL 81:6, PI (O-16:1/17:1), and PC (O-22:5/19:3), are downregulated in the male participants of the AD group compared with the HV group. In the case of female participants, AHexCer (d(O-18:1)18:1/15:0;O), AHexCer (d(O-18:1)18:2/24:1;O), SM (d18:1/18:1), and many other lipid molecular species were upregulated in the AD group. In contrast, the lipids LPC 18:2, LPC 17:2, LPC 22:6, and many other lipid molecules were downregulated in the AD group compared to the HV group, as described in **Figure 4.10A**.

In the comparison between the HV vs HD groups, the volcano plot revealed a distinct upregulation of lipid species, including PC (O-22:5/17:3), PS (O-17:0/22:6), FA 18:0, and several other lipid molecular species in the HD group of male participants. Conversely, lipids such as AHexCer (d(O-18:1)18:1/15:0;O), AHexCer (d(O-18:1)18:2/24:1;O), AHexCer (d(O-18:1)18:3/26:1;O), and many other lipid molecular species are downregulated in the HD group compared to the HV group **Figure 4.10A**). In female participants, a similar trend of upregulation was observed, with elevated levels of PC (O-22:5/19:3), PC (O-22:5/17:3), PS (O-17:0/22:6), FA 18:0, and many other lipid molecular species in the HD group compared to the HV group. In contrast, the lipids AHexCer (d(O-18:1)18:1/15:0;O), AHexCer (d(O-18:1)18:2/24:1;O), AHexCer (d(O-18:1)18:3/26:1;O), PC (O-22:5/19:2), and many other lipid molecules were downregulated in the HD group compared to the HV group, as described in **Figure 4.10A**.

Similarly, in the comparison between the HV vs PD groups, the volcano plot revealed a distinct upregulation of lipid species, including PC (O-22:5/17:3), PS (O-17:0/22:6), CE 18:1, FA 18:0, and many other lipid species in the PD group of male participants compared with the HV group. Conversely, lipids such as AHexCer (d(O-18:1)18:1/15:0;O), AHexCer (d(O-18:1)18:2/24:1;O), AHexCer (d(O-18:1)18:3/26:1;O), and many other lipid molecular species are downregulated in the PD group compared to the HV group (**Figure 4.10A**). In the case of female participants, the lipidomic alterations paralleled those in males, with upregulation of PC (O-22:5/17:3), PS (O-17:0/22:6), and many other lipid molecular species in the PD group compared with the HV group. Interestingly, AHexCer (d(O-18:1)18:1/15:0;O), and many other lipid molecular species showed marked downregulation in the PD group compared to the HV group, as described in **Figure 4.10A**.

To further elucidate the significant lipid alterations between the HV and disease groups (AD, HD, and PD), we investigated sex-specific changes in the relative concentrations of upregulated and downregulated lipid molecular species in brain tissue samples, as illustrated in **Figure 4.10B**. The bar graphs represent the mean ± SEM of the significantly altered lipid species across male and female participants.

In the AD group, AHexCer (d(O-18:1)18:1/15:0;O) was significantly elevated in female participants compared to the HV group, while no significant difference was observed in males. In contrast, SM (d18:1/18:1) was significantly increased in both male and female participants of AD group compared to the HV group (**Figure 4.10B)**. In the HD group, AHexCer (d(O-18:1)18:1/15:0;O) was significantly decreased in both sexes compared to the HV group. On the other hand, PS (O-17:0/22:6) showed a significant upregulation in the HD group of both sexes compared to the HV group (**Figure 4.10B)**. In the PD group, AHexCer (d(O-18:1)18:1/15:0;O) demonstrated a similar downregulation trend as observed in HD, being significantly decreased in the PD group of both sexes compared to the HV group. Conversely, PC (O-22:5/19:3) was significantly upregulated in both sexes within the PD group compared to the HV group (**Figure 4.10B)**.

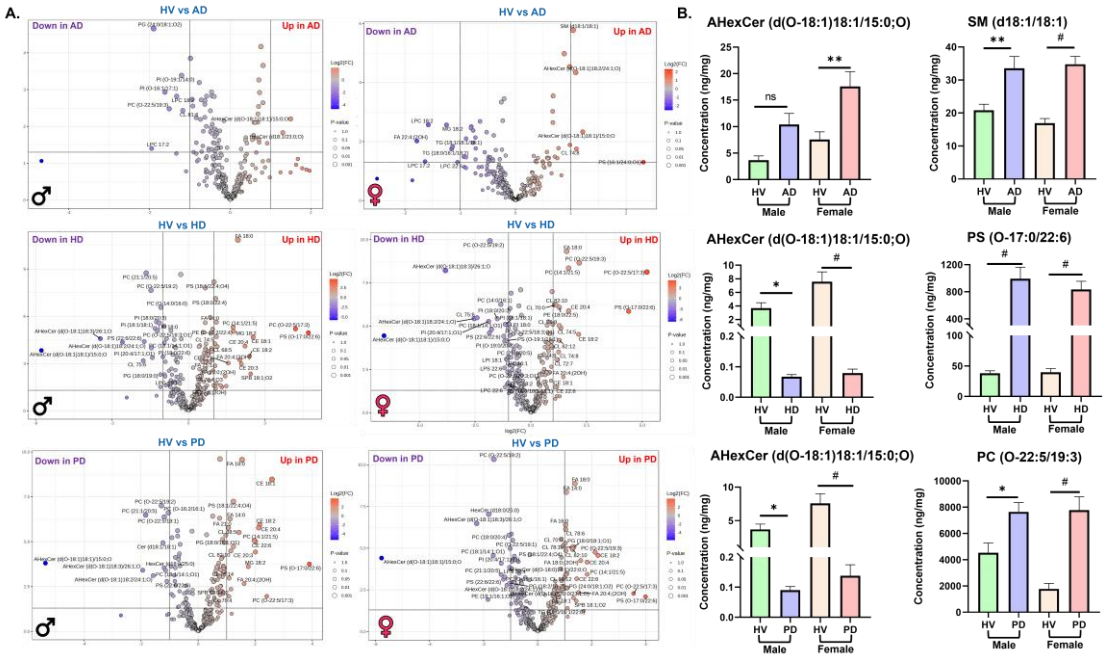

Figure 4.10: A. Volcanic plot representing significantly altered lipid levels ($p < 0.05$) in the brain samples of HV vs AD, HV vs HD, HV vs PD in male and female participants.

B. Bar graph representing significantly altered lipids in AD, HD, and PD groups in male and female participants (Ordinary one-way ANOVA, #p< 0.0001, ***p<0.001, **p<0.01, *p<0.05, 0.1(ns)). All data are represented as mean ± SEM.

4.3.2.4 Region-specific brain lipidome alterations in AD, PD, and HD

To investigate the spatial distribution of significantly altered lipid species across different brain regions, we constructed brain lobe-specific heatmaps complemented by bar graphs showing the relative abundances of these lipids in control (HV), AD, HD, and PD groups. As illustrated in **Figure 4.11**, the heatmaps highlight the differential expression of lipid species in distinct brain lobes (frontal, temporal, parietal, and occipital) for AD, HD, and PD groups. The bar graphs show the mean ± SEM of its concentration in each brain region, enabling direct comparison between disease and control groups.

The results revealed a disease-specific and region-specific alteration pattern for AHexCer (d(O-18:1)18:1/15:0;O). This lipid was markedly elevated in the AD group, particularly in the parietal lobe, showing the highest concentration, followed by a significant increase in the occipital lobe. In contrast, in both HD and PD groups, this lipid was significantly downregulated, with the occipital lobe being the primary region exhibiting a decrease. The spatial abundance of AHexCer (d(O-18:1)18:1/15:0;O) is illustrated as a brain lobe-specific heatmap in **Figure 4.11**.

For PS (O-17:0/22:6), a distinct pattern of upregulation was observed predominantly in the HD and PD groups, with no alterations detected in AD. Regional distribution analysis revealed a strong increase in HD, particularly in the parietal and occipital lobes (****$p < 0.0001$), followed by a moderate increase in the temporal lobe (***$p < 0.001$) and a mild elevation in the frontal lobe (**$p < 0.01$). In the PD group, this lipid showed the most prominent increase in the occipital lobe (****$p < 0.0001$), followed by the parietal lobe (***$p < 0.001$). In contrast, the AD group exhibited no statistically significant change in PS (O-17:0/22:6) levels across any of the brain regions examined. The spatial abundance of PS (O-17:0/22:6) is illustrated as a brain lobe-specific heatmap in **Figure 4.11**.

The expression pattern of PC (O-22:5/19:3) revealed marked elevation in both HD and PD groups compared to controls, with no significant alterations observed in the AD

group, although its levels were relatively lower. Region-wise analysis demonstrated a pronounced upregulation of PC (O-22:5/19:3) in the occipital lobe of HD participants (*p < 0.0001), followed by elevated levels in the temporal, parietal, and frontal lobes (***p < 0.0001). In the case of PD, this lipid also showed a significant increase in the occipital and parietal lobes (****p < 0.0001), while no significant differences were observed in the frontal and temporal lobes. This region-specific pattern underscores the potential involvement of PC (O-22:5/19:3) in the pathophysiology of HD and PD. The spatial abundance of PC (O-22:5/19:3) is illustrated as a brain lobe-specific heatmap in **Figure 4.11**. **Appendix Figure 4.8** shows the heatmaps of the top 50 altered lipid molecular species in region-specific groups across the brain tissue samples of HV, AD, HD, and PD participants.

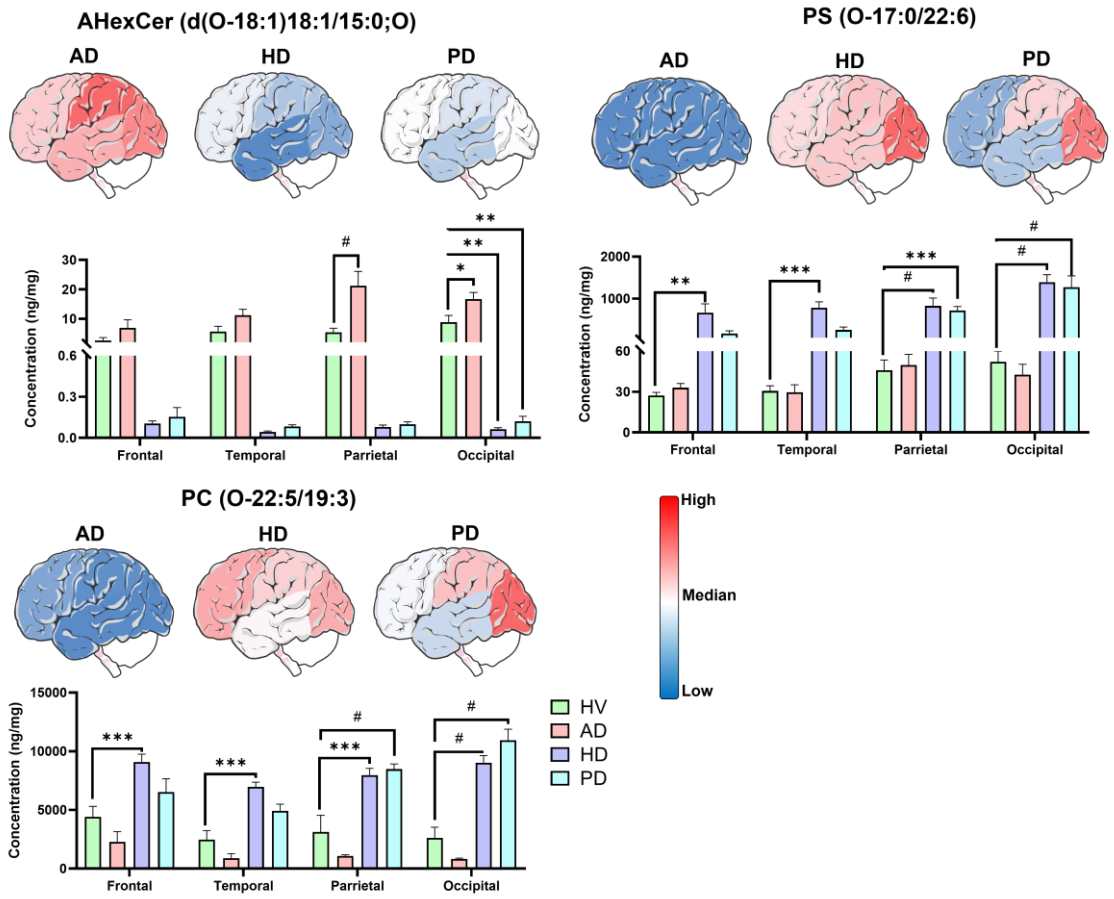

Figure 4.11: Top cluster view and bar graph representing significantly altered lipids in various brain lobes of AD, HD, and PD groups. (Ordinary two-way ANOVA with Tukey's

multiple comparisons test, #p< 0.0001, ***p<0.001, **p<0.01, *p<0.05, 0.1(ns)). All data are represented as mean ± SEM.

4.4 Discussion

Lipids are essential components of cellular membranes and play pivotal roles in maintaining neuronal structure, membrane fluidity, and synaptic function. Dysregulation in lipid metabolism has been implicated in various neurodegenerative disorders such as AD, PD, and HD [35]. Among various NDs, AD has become the most common and extensively studied NDs, especially due to its cognitive manifestations across stages from MCI to dementia. Similar to AD, PD and HD are the second most common and rare NDs, characterized by motor dysfunction and cognitive decline, respectively [36]. CI is a debilitating NDs that involves a steady decline in cognitive ability. The current methods for diagnosing CI at an early stage rely primarily on biomarkers related to amyloid accumulation, tau protein abnormalities, and signs of neurodegeneration [37]. Despite their use, these biomarkers do not offer sufficient specificity to accurately predict the course of the disease or the likelihood of progression in individual patients [38]. Recently, there has been a notable emergence of MS-based lipidomic techniques as significant technological platforms for characterizing system-level changes in lipids for NDs, which is critical for understanding the biological basis of AD, PD, and HD pathogenesis and suggests a potential discovery platform for identifying novel lipid biomarkers for the early diagnosis of disease progression [22]. While many studies have explored the lipidomics landscape in the pathogenesis of AD, PD, and HD, these analyses have been limited to invasive sample types and the type of disease [39-40].

To address these gaps, the present study applied a comprehensive untargeted lipidomics approach by combining both invasive and non-invasive sample types. We examined lipidomic alterations in saliva, plasma, and fecal samples across control, MCI, and dementia stages of AD to identify stage-specific lipid perturbations in older adults. Additionally, we also conducted in-depth region-specific lipidomic analysis of brain tissues from AD, PD, and HD patients, revealing both shared and disease-specific alterations. This integrative framework enhances our understanding of lipid involvement in neurodegeneration and may facilitate the identification of accessible biomarkers and potential therapeutic targets.

The results of this study are visualized in a lipid biosynthesis pathway analysis as depicted in **Figure 4.12,** based on Kyoto Encyclopedia of Genes and Genomes (KEGG) pathways. Acetyl coenzyme A (Acyl-CoA) plays a central role as a precursor molecule in the synthesis of various lipid classes. Acyl-CoA contributes to the formation of FAs, which are fundamental building blocks in lipid biosynthesis, along with CE, which belongs to the sterols subclass of lipids. Furthermore, FAs facilitate the synthesis of FAHFAs and SFAHFAs. Acyl-CoA, in combination with dihydroxyacetone phosphate (DHAP), and glycerol-3-phosphate (G3P), initiates the production of lysophosphatidic acid (LPA), which subsequently forms phosphatidic acid (PA), DG, and TG. PA interacts with cytidine diphosphate diacylglycerol (CDP-DG) to generate PLs and GPs. Additionally, Acetyl-CoA can be converted to palmitoyl-CoA. Palmitoyl CoA in combination with the amino acid serine (Ser) leads to the formation of 3-dehydro-sphinganine and dihydrosphingosine. These intermediates are used to produce Cer, a key component of the SPs class. Furthermore, Cer aids in the synthesis of HexCer and SM.

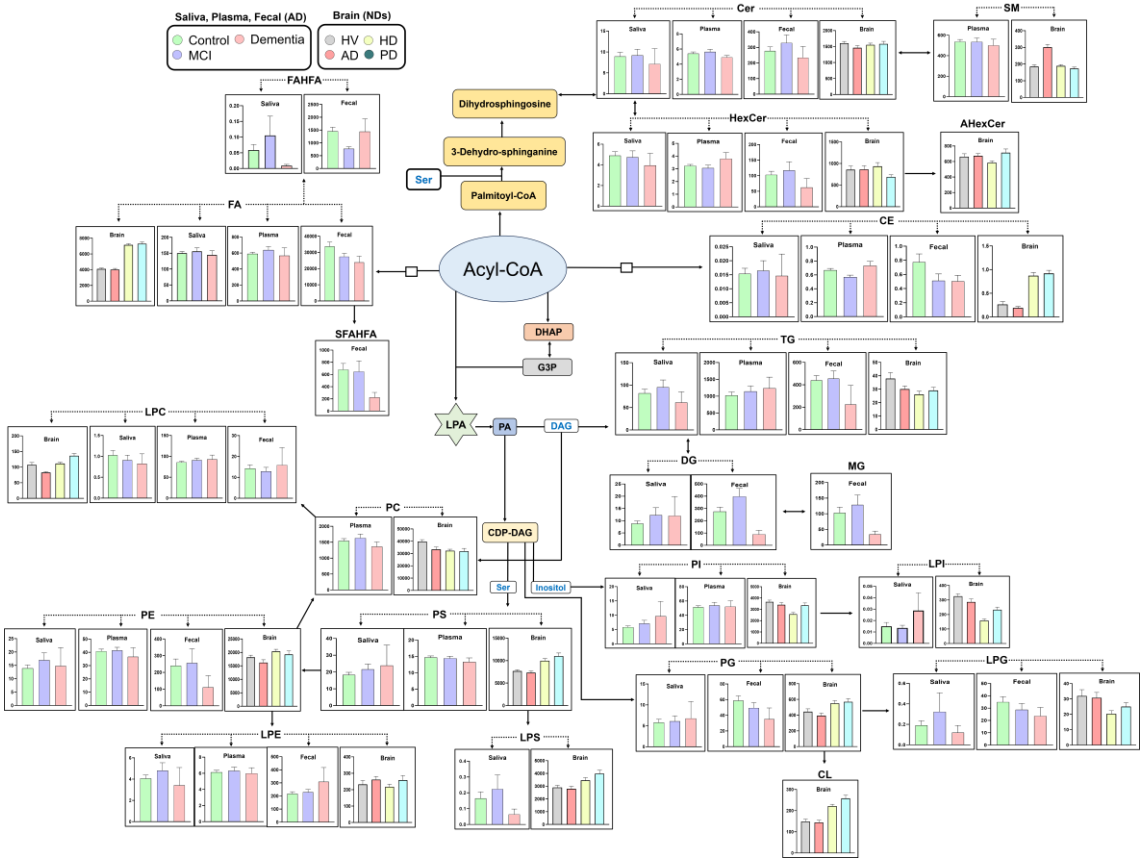

Figure 4.12: Analysis of lipid biosynthesis pathways was conducted across stage-specific cognitive impairment (CI) groups (MCI, dementia) and healthy individuals in saliva,

plasma, and fecal samples, as well as disease-specific neurodegenerative disorder groups (AD, PD, and HD) and healthy volunteers in the brain tissue samples. The data are represented as mean ± SEM. The Y-axis represents the concentration of the lipid subclass in ng/µL and ng/mg for saliva, plasma, fecal, and brain tissue samples. The X-axis represents control, MCI, and dementia as well as HV, AD, PD, and HD.

Our lipidomic analysis revealed variations in the specific lipid biosynthesis pathways between the stage-specific groups of saliva, plasma, and fecal samples of older adults, as well as distinct regional and disease-specific alterations in the brain lipidome of individuals with AD, PD, and HD. For example, the increasing and decreasing trend of FAs in stage-specific groups of older adults may be due to the dysregulation of the FAs metabolic pathway. Notably, FAs levels were significantly elevated in the brains of individuals with HD and PD, indicating disease-specific perturbations in lipid metabolism **(Figure 4.12**). This increase in FAs levels aligns with a previous study that reported dysregulated fatty acid metabolism in these NDs. Elevated FA levels in plasma and CSF samples, particularly saturated FAs, have been implicated in mitochondrial dysfunction and altered membrane dynamics in PD and HD, potentially contributing to mitochondrial dysfunction and altered membrane dynamics [41, 42]

FFAs are considered promising therapeutic agents that play key roles in neurogenesis, reducing neuronal inflammation and supporting neurotransmitter production, which are crucial for proper brain development [43]. As depicted in **Figure 4.3B**, SFA levels did not exhibit any significant differences among the control, MCI, and dementia groups across saliva, plasma, and fecal samples. However, most studies did not include saliva and fecal sample analyses. Our results on plasma samples are aligned with those of a previous study by Cunnane et al., which reported no significant changes in the total SFA levels between the control, MCI, and dementia groups of plasma samples [44]. A recent meta-analysis by Hosseini et al., reported no significant changes in most fatty acids between control and MCI groups in plasma/serum samples [45]. Furthermore, a previous study mentioned that maintaining dietary FAs intake may be an effective and precise prevention strategy for cognitive decline and may improve older adults' physiological and pathological status [46]. In the case of the brain lipidome, elevated levels of saturated fatty acid (FA 18:0) were observed in both PD and HD brain tissues (**Figure 4.9A**). These results are consistent with earlier findings showing increased FA

18:0 in the frontal cortex of PD patients, likely reflecting reduced n9-desaturase activity, which can disrupt membrane fluidity and impair neuronal signaling [47].

FFAs, such as MUFAs alternation, are associated with brain development, anti-inflammation, and cognitive preservation and are key components of neuronal membranes and influence membrane fluidity, receptor function, and signal transduction [48]. However, in our study, the levels of MUFAs and PUFAs were not significantly different between the saliva, plasma, and fecal samples of the control, MCI, and dementia groups. These findings agree with the results of a prior study, which indicated no significant differences in the total MUFA levels between the control and MCI groups across different sex categories in blood samples [49]. PUFAs appear to be crucial for normal brain function and cognitive health. Impairments in PUFA metabolism contribute to neuronal apoptosis, leading to the neuropsychological deficits commonly observed in dementia patients [50]. It has been found that patients with high ω-6 to ω-3 PUFA ratios are usually described as having a high risk of cognitive impairment [51]. A recent study found that lower ω-6 to ω-3 PUFA ratios predict better spatial memory and cognitive status in older adults [52]. Our study shows that the saliva samples display a significantly low ω-6 to ω-3 ratio in the MCI group, whereas fecal samples display a significantly higher ratio in the dementia group (**Figure 4.3C**). The elevated ratio in the fecal can be attributed to the dysregulation of PUFA metabolism in dementia patients, leading to increased excretion of these fatty acids [50]. This finding is consistent with another study that reported higher ω-6 to ω-3 PUFA ratios in blood samples, which were associated with accelerated cognitive decline and greater risk of dementia in elderly individuals [53].

Among all detected PUFAs, we found upregulation of ω-6 (FA 20:4) and ω-3 (FA 20:5, and FA 22:5) PUFAs in the MCI group compared to the control group of saliva and plasma samples (**Figure 4.4**). These results are consistent with previous studies that reported increased levels of FA 18:3 and FA 20:4 in the serum and plasma samples of AD patients [54, 55]. Another study suggested that a diet rich in ω-3 fatty acids may increase the levels of FA 20:5 and FA 22:5 in plasma samples of AD patients [56]. The upregulation of ω-3 PUFA in the MCI group of saliva and plasma samples may be influenced by diet, which is not considered in our study. Further, FA 20:5 was found to be upregulated in the brain tissue samples of PD patients (**Figure 4.9A**). These results are consistent with a

previous study on diet supplementation of FA 20:5, which increases the levels of FA 20:5 in the brain of rats exposed to the PD model [57].

FAHFAs are a new endogenous class of lipids involved in glucose homeostasis, insulin resistance, and anti-inflammatory functions [58]. SFAHFAs, that were previously identified in our laboratory [59]. In our study, FAHFAs and SFAHFAs (2:0/20:0;O) levels were lower in the MCI group than in the control group of the fecal samples. A previous study on brain tissue samples demonstrated a significant increase in the FAHFA levels for the dementia group [60]. Our results also showed similar observations in the fecal samples of the dementia group compared to the MCI group (**Figure 4.4**). This discrepancy in fecal samples may be attributed to differences in sample types, suggesting that the dysregulation of FAHFAs and SFAHFAs may vary across different samples or stages of AD pathology.

SPs were discovered to be structural components of cell membranes in the brain and act as cellular messengers [61]. Changes in sphingolipid metabolism have been linked to the development of various NDs, including AD and metabolic syndrome [62]. Interestingly, increased levels of serum ceramide were associated with an increased risk of AD [63]. In our study, dihydroxy Cer species comprising FA 18:0 and FA 18:1 were upregulated in fecal and plasma samples of the MCI group. However, HexCer (d18:0/21:0;O) and HexCer (d18:0/15:0;O) were upregulated in the plasma samples of the dementia group (**Figure 4.4**). These findings are consistent with those of a previous study that demonstrated the upregulation of Cer and HexCer in the plasma samples of AD patients [64]. The observed upregulation of Cer in brain tissue samples from AD patients may be attributed to the loss of tight regulation typically observed under normal conditions during Cer biosynthesis. In healthy individuals, Cer biosynthesis is tightly controlled. However, this regulation is disrupted during neurodegeneration in AD, leading to increased Cer levels (**Figure 4.12**) [65]. Elevated SM levels have been reported in the CSF of patients with prodromal AD [66], supporting our findings of notably high SM levels in the brain tissue samples of AD patients and confirming the relationship between sphingomyelins and AD CI (**Figure 4.12**). Additionally, the identified AHexCer (d(O-18:1)18:1/15:0;O) showed elevated levels in AD patients, whereas decreased levels were observed in both HD and PD patients, suggesting its potential as a differential biomarker among these disorders (**Figure 4.9C**). This finding is consistent with previous studies

reporting elevated HexCer levels in plasma and postmortem brain tissues of AD patients, indicating a positive association between HexCer accumulation and AD pathology [67, 68]. Another study reported the level of Hex1Cer (m19:0/21:2) was significantly higher and the total amount of Hex1Cer tended to higher, in AD urine indicating they are highly abundant in the vertebrate brain [69], and these results are consistent with our study on elevated level of AHexCer (d(O-18:1)18:1/15:0;O) in brain tissue samples of AD patients compared to HV. As ceramide accumulation is known to disrupt mitochondrial function and promote oxidative stress, the reduced AHexCer levels in HD and PD may reflect distinct pathological mechanisms in these diseases.

GPs are amphiphilic molecules that actively contribute to the function of ion channels, transporters, and receptors and regulate neuronal membrane activities, transport, and cellular proliferation [70]. A recent study reported that dysregulation of GPs metabolism in the brain is associated with AD progression [71]. In our study, GPs such as lysophospholipids (LPs) and PLs were upregulated in the fecal and saliva samples of the dementia group compared to those of the control and MCI groups, while for plasma samples, both LPs and PLs were upregulated in the MCI and dementia groups compared with those in the control group (**Figure 4.4**). These results are consistent with previous studies showing that higher levels of plasma PLs species are correlated with post-stroke CI [72]. An earlier examination of plasma samples revealed increased levels of PL species in AD patients [30]. The two most abundant classes of LPs, such as LPC and LPE are associated with brain inflammation. Our results are consistent with those of a previous study that reported increased levels of LPs in human and mouse AD brains. Accumulation of these LPs species is correlated with astrocytic activation and oxidative stress [73]. This can explain the upregulation of LPs in the plasma samples of the MCI group. A recent study highlighted the accumulation of GPs in brain samples of female AD mice. This finding can be attributed to various physiological and developmental factors, including changes in hormone levels, alterations in dietary habits, metabolic shifts associated with growth and development, and other biological processes that occur during puberty [74]. Abnormal PLs composition is a hallmark of NDs and primarily affects the cortical regions of the brain [75]. In our study, we observed a significant reduction in PC and LPC levels in the brain tissue samples of AD patients compared to HV. Conversely, in PD and HD brain tissues, PC levels were similarly decreased, while LPC levels were elevated relative

to HV (**Figure 4.12**). These findings are consistent with previous reports showing reduced PC levels in the plasma of AD patients and in post-mortem substantia nigra samples of PD patients [76, 77]. Another study reported that lower PC levels predict future cognitive impairment most acutely, but do not adequately discriminate between AD patients and cognitively normal controls [78]. Recent studies have reported elevated levels of PS and LPS in human parkin-mutant fibroblasts and in the plasma samples of PD patients [79, 80]. Our findings are in line with earlier research suggesting that increased levels of PS and its derivatives may be associated with impaired mitochondrial turnover and disrupted endoplasmic reticulum organization in PD and HD patients. Such alterations in membrane lipid composition could reflect broader dysregulation of cellular homeostasis in the pathogenesis of the disease. CLs are another GPs, mainly localized in the inner mitochondrial membrane, that play a crucial role in maintaining membrane fluidity and supporting the activity of mitochondrial electron transport chain enzymes [81]. In our study, elevated levels of CLs were observed in the brain tissue samples of both HD and PD patients compared to HV. These findings are consistent with previous reports demonstrating increased levels of PUFA-containing CLs in the plasma of rotenone-treated rats during the later stages of PD, suggesting a potential link between CL accumulation and mitochondrial dysfunction in neurodegeneration [82].

GLs, including TGs and DGs, play a central role in the maintenance of energy homeostasis and the stability and functionality of cell membranes, particularly in neurons and myelin sheaths [83]. Increased DG levels have previously been reported in the frontal cortex and plasma samples of AD patients, highlighting the potential link between DG dysregulation and AD pathology [30, 84]. Consistent with these findings, our analysis of fecal samples revealed a significant increase in the DG levels in the MCI group, suggesting a possible early disruption of DG metabolism (**Figure 4.4**). However, our data showed no significant upregulation of DGs in the saliva or plasma samples of stage-specific groups of older adults, in contrast to previous plasma-based findings [84]. This discrepancy may be due to the dynamic and compartment-specific nature of DG metabolism.

A recent investigation also revealed that increased levels of TG molecular species in CSF samples of AD patients are associated with an increased risk of severe obstructive sleep apnoea. Consistent with this finding, our analysis of saliva samples showed an

upregulation in the MCI group compared to the control group [85]. However, in fecal samples, TGs were significantly dysregulated in both MCI and dementia groups. Previous studies have also reported the accumulation of TGs in the blood circulation of AD mice, suggesting that severe hyperlipidemia is- a key vascular risk factor for AD development [18]. This accumulation precedes amyloid deposition in mouse models, further establishing the potential role of TGs in AD [86]. TG-MCFAs serve as a source of ketone bodies and are hydrolyzed by the lipases to produce MCFAs [87]. TG-MCFAs have been shown to support brain energy metabolism and potentially delay neuronal dysfunction in AD patients [88]. Furthermore, medium-chain triglyceride oil supplementation improves working memory in AD patients, emphasizing the therapeutic potential of TG-MCFAs [89]. In our study, TG-MCFAs (especially TG (10:0/10:0/12:0) were significantly higher in the MCI group than in the control group of fecal samples. However, these levels were lower in the MCI and dementia group than in the control group of saliva samples (**Figure 4.5B**). These results highlight the potential of TG-MCFAs as biomarkers of the early stages of cognitive decline, such as MCI. Similarly, DG-MCFAs have been reported to play a role in lipid metabolism, and a recent meta-analysis emphasized their role in postprandial lipid control [90]. Our results showed that DG-MCFAs were significantly increased in the fecal samples of the MCI group compared with the control group. However, no data are available on the implications of these mediators in CI stages. In the present study, TG levels were significantly lower in the brain tissue of AD patients compared to HV, with no notable changes in PD and HD (**Figure 4.12**). This aligns with previous reports showing reduced TG levels in urine samples from AD patients relative to controls, implying dysfunction in GLs metabolism in AD patients [91].

Cholesterol and its esters play important roles in amyloid genesis [92]. A recent investigation revealed that high cholesterol levels are positively correlated with an increased risk of dementia [93]. Meta-analyses have consistently reported that circulating and brain cholesterol levels are higher in AD patients compared to control groups [94]. Conversely, Zondermann et al. observed lower total cholesterol levels in serum samples from MCI and dementia-free participants than in those with dementia [95]. Consistent with these findings, our results demonstrated increased levels of CE 18:1 and CE 18:2 in the dementia group compared to the control group in the plasma samples. However, CE 18:2 levels were lower in the MCI group than in the control group of plasma samples.

This variation may reflect the dysregulation of cholesterol metabolism at different stages of cognitive decline (**Figure 4.12**). A study by Kreilaus et al. reported elevated levels of cholesterol ester concentrations in the caudate and putamen regions are positively associated with increased risk of HD [96]. These results are consistent with our findings on elevated levels of CE in both brain tissue samples of HD and PD patients compared to HV (**Figure 4.12**). The increase was more pronounced in the region-specific lipid disturbances in HD and PD patients.

This study provides valuable insights into the identification of diverse lipid classes in saliva, plasma, and fecal samples of older adults, categorized into control, MCI, and dementia groups, through a comprehensive analysis of lipid composition. Also, the brain lipidomic analysis of HV, AD, PD, and HD participants. However, this study has several limitations that must be acknowledged and addressed in future research. First, the lipid concentrations reported were semi-quantitative rather than absolute, which may have limited the precision of the findings. Second, lipid composition is influenced by various factors such as diet, physical activity, genetic predisposition, and family history, which were not considered in this study. Additionally, although major lipid molecular species, such as FAs, GLs, GPs, SPs, and STs, have been detected in saliva, plasma, fecal, and brain tissue samples from healthy and disease groups of older adults, the underlying mechanisms governing their metabolism remain unclear. Finally, the small sample size in the dementia group limited the ability to compare sex- and weight-specific lipid alterations in saliva, plasma, and fecal samples with those in other groups. In the case of brain tissue samples, the study was limited to a sample size of $n = 3$ per brain lobe and sex group, which may reduce statistical power and limit the generalizability of the findings.

4.5 Conclusion

This study presents a comprehensive lipidomic analysis of saliva, plasma, fecal, and brain tissue samples from older adults, covering various stages of CI and major NDs. A total of 266, 217, and 260 lipid metabolites were identified in saliva, plasma, and fecal samples from stage-specific groups of CI spanning five major lipid classes. Multivariate analysis and percentage distribution of major lipid classes revealed stage-specific lipid profiles in saliva, plasma, and fecal samples of older adults. Statistical analysis revealed significant

changes in the ω6 to ω3 ratios in the saliva and fecal samples of CI stages. ROC analysis identified potential lipid biomarkers with high specificity for FA 18:3, FA 22:5, and CE 18:2 of the MCI group. Furthermore, elevated levels of TG-MCFAs in fecal samples indicate early-stage lipid biomarkers for MCI. Sex- and weight-specific lipid alterations in MCI groups have also been studied. Further, the study expanded into a comprehensive brain lipidome profiling across region-specific samples from HV and AD, PD, and HD patients. A total of 291 lipid molecular species were identified in the brain tissue samples. Multivariate OPLS-DA analysis demonstrated clear group separation between HV and disease groups, indicating distinct disease-associated lipidomic profiles. Volcano plot analysis further highlighted the disease-specific upregulation and downregulation of key lipid species, reflecting lipidomic alterations in each disorder. ROC analysis identified several lipid species, including AHexCer (d(O-18:1)18:1/15:0;O), PC (O-22:5/19:3), and PS (O-17:0/22:6)- as potential biomarkers for the differential diagnosis of NDs in older adults. Additionally, statistical analysis revealed significant sex-specific and brain region–specific lipid alterations across HV and NDs, underscoring the influence of biological sex and anatomical location on disease-related lipid dysregulation. These findings emphasize the relevance of these lipid biomarkers across sexes and various brain lobes in distinguishing HV from NDs conditions. Together, these findings offer valuable insights into lipid dysregulation during early and progressive stages of NDs in older adults and provide a strong foundation for developing both non-invasive and disease-specific diagnostic markers.

References:

1. Jucker, M., & Walker, L. C. (2011). Pathogenic protein seeding in Alzheimer disease and other neurodegenerative disorders. Annals of neurology, 70(4), 532–540.
2. Skovronsky, D. M., Lee, V. M., & Trojanowski, J. Q. (2006). Neurodegenerative diseases: new concepts of pathogenesis and their therapeutic implications. Annual review of pathology, 1, 151–170.
3. Prusiner S. B. (2001). Shattuck lecture--neurodegenerative diseases and prions. The New England journal of medicine, 344(20), 1516–1526.
4. Tkachenko, K., González-Sáiz, J. M., & Pizarro, C. (2025). Untargeted Lipidomic Reveals Potential Biomarkers in Plasma Samples for the Discrimination of Patients Affected by Parkinson's Disease. Molecules (Basel, Switzerland), 30(4), 850.
5. Yilmaz, A., Akyol, S., Ashrafi, N., Saiyed, N., Turkoglu, O., & Graham, S. F. (2025). Lipidomics of Huntington's Disease: A Comprehensive Review of Current Status and Future Directions. Metabolites, 15(1), 10.
6. Katsuno, M., Sahashi, K., Iguchi, Y., & Hashizume, A. (2018). Preclinical progression of neurodegenerative diseases. Nagoya journal of medical science, 80(3), 289–298.
7. DeTure, M. A., & Dickson, D. W. (2019). The neuropathological diagnosis of Alzheimer's disease. Molecular neurodegeneration, 14(1), 32.
8. Proitsi, P., Kim, M., Whiley, L., Simmons, A., Sattlecker, M., Velayudhan, L., Lupton, M. K., Soininen, H., Kloszewska, I., Mecocci, P., Tsolaki, M., Vellas, B., Lovestone, S., Powell, J. F., Dobson, R. J., & Legido-Quigley, C. (2017). Association of blood lipids with Alzheimer's disease: A comprehensive lipidomics analysis. Alzheimer's & dementia : the journal of the Alzheimer's Association, 13(2), 140–151.
9. Bloom G. S. (2014). Amyloid-β and tau: the trigger and bullet in Alzheimer disease pathogenesis. JAMA neurology, 71(4), 505–508.
10. Porsteinsson, A. P., Isaacson, R. S., Knox, S., Sabbagh, M. N., & Rubino, I. (2021). Diagnosis of Early Alzheimer's Disease: Clinical Practice in 2021. The journal of prevention of Alzheimer's disease, 8(3), 371–386.

11. Petersen, R. C., Roberts, R. O., Knopman, D. S., Boeve, B. F., Geda, Y. E., Ivnik, R. J., Smith, G. E., & Jack, C. R., Jr (2009). Mild cognitive impairment: ten years later. Archives of neurology, 66(12), 1447–1455.

12. Bai, W., Chen, P., Cai, H., Zhang, Q., Su, Z., Cheung, T., Jackson, T., Sha, S., & Xiang, Y. T. (2022). Worldwide prevalence of mild cognitive impairment among community dwellers aged 50 years and older: a meta-analysis and systematic review of epidemiology studies. Age and ageing, 51(8), afac173.

13. François, M., Bull, C. F., Fenech, M. F., & Leifert, W. R. (2019). Current State of Saliva Biomarkers for Aging and Alzheimer's Disease. Current Alzheimer research, 16(1), 56–66.

14. Thambisetty, M., & Lovestone, S. (2010). Blood-based biomarkers of Alzheimer's disease: challenging but feasible. Biomarkers in medicine, 4(1), 65–79.

15. Morris, J. K., Honea, R. A., Vidoni, E. D., Swerdlow, R. H., & Burns, J. M. (2014). Is Alzheimer's disease a systemic disease?. Biochimica et biophysica acta, 1842(9), 1340–1349.

16. Brookmeyer, R., & Abdalla, N. (2018). Estimation of lifetime risks of Alzheimer's disease dementia using biomarkers for preclinical disease. Alzheimer's & dementia : the journal of the Alzheimer's Association, 14(8), 981–988.

17. Hane, F. T., Robinson, M., Lee, B. Y., Bai, O., Leonenko, Z., & Albert, M. S. (2017). Recent Progress in Alzheimer's Disease Research, Part 3: Diagnosis and Treatment. Journal of Alzheimer's disease : JAD, 57(3), 645–665.

18. Zhang, X., Liu, W., Zan, J., Wu, C., & Tan, W. (2020). Untargeted lipidomics reveals progression of early Alzheimer's disease in APP/PS1 transgenic mice. Scientific reports, 10(1), 14509.

19. O'Brien, J. S., & Sampson, E. L. (1965). Lipid composition of the normal human brain: gray matter, white matter, and myelin. Journal of lipid research, 6(4), 537–544.

20. Byeon, S. K., Madugundu, A. K., Jain, A. P., Bhat, F. A., Jung, J. H., Renuse, S., Darrow, J., Bakker, A., Albert, M., Moghekar, A., & Pandey, A. (2021). Cerebrospinal fluid lipidomics for biomarkers of Alzheimer's disease. Molecular omics, 17(3), 454–463.

21. Kao, Y. C., Ho, P. C., Tu, Y. K., Jou, I. M., & Tsai, K. J. (2020). Lipids and Alzheimer's Disease. International journal of molecular sciences, 21(4), 1505.

22. Huynh, K., Lim, W. L. F., Giles, C., Jayawardana, K. S., Salim, A., Mellett, N. A., Smith, A. A. T., Olshansky, G., Drew, B. G., Chatterjee, P., Martins, I., Laws, S. M., Bush, A. I., Rowe, C. C., Villemagne, V. L., Ames, D., Masters, C. L., Arnold, M., Nho, K., Saykin, A. J., … Meikle, P. J. (2020). Concordant peripheral lipidome signatures in two large clinical studies of Alzheimer's disease. Nature communications, 11(1), 5698.

23. Yadav, R. S., & Tiwari, N. K. (2014). Lipid integration in neurodegeneration: an overview of Alzheimer's disease. Molecular neurobiology, 50(1), 168–176.

24. Walter, A., Korth, U., Hilgert, M., Hartmann, J., Weichel, O., Hilgert, M., Fassbender, K., Schmitt, A., & Klein, J. (2004). Glycerophosphocholine is elevated in cerebrospinal fluid of Alzheimer patients. Neurobiology of aging, 25(10), 1299–1303.

25. Estes, R. E., Lin, B., Khera, A., & Davis, M. Y. (2021). Lipid Metabolism Influence on Neurodegenerative Disease Progression: Is the Vehicle as Important as the Cargo?. Frontiers in molecular neuroscience, 14, 788695.

26. Wood P. L. (2012). Lipidomics of Alzheimer's disease: current status. Alzheimer's research & therapy, 4(1), 5.

27. Ferré-González, L., Lloret, A., & Cháfer-Pericás, C. (2023). Systematic review of brain and blood lipidomics in Alzheimer's disease mouse models. Progress in lipid research, 90, 101223.

28. Tkachenko, K., González-Sáiz, J. M., & Pizarro, C. (2025). Untargeted Lipidomic Reveals Potential Biomarkers in Plasma Samples for the Discrimination of Patients Affected by Parkinson's Disease. Molecules (Basel, Switzerland), 30(4), 850.

29. Peña-Bautista, C., Álvarez-Sánchez, L., Roca, M., García-Vallés, L., Baquero, M., & Cháfer-Pericás, C. (2022). Plasma Lipidomics Approach in Early and Specific Alzheimer's Disease Diagnosis. Journal of clinical medicine, 11(17), 5030.

30. Liu, Y., Thalamuthu, A., Mather, K. A., Crawford, J., Ulanova, M., Wong, M. W. K., Pickford, R., Sachdev, P. S., & Braidy, N. (2021). Plasma lipidome is dysregulated in Alzheimer's disease and is associated with disease risk genes. Translational psychiatry, 11(1), 344.

31. Akyol, S., Ugur, Z., Yilmaz, A., Ustun, I., Gorti, S. K. K., Oh, K., McGuinness, B., Passmore, P., Kehoe, P. G., Maddens, M. E., Green, B. D., & Graham, S. F. (2021). Lipid Profiling of Alzheimer's Disease Brain Highlights Enrichment in Glycerol(phospho)lipid, and Sphingolipid Metabolism. Cells, 10(10), 2591.

32. Zhao, L., Duan, X., & Liu, H. (2023). Novel Grade Classification Tool with Lipidomics for Indica Rice Eating Quality Evaluation. Foods (Basel, Switzerland), 12(5), 944.

33. Podcasy, J. L., & Epperson, C. N. (2016). Considering sex and gender in Alzheimer disease and other dementias. Dialogues in clinical neuroscience, 18(4), 437–446.

34. Nuttall F. Q. (2015). Body Mass Index: Obesity, BMI, and Health: A Critical Review. Nutrition today, 50(3), 117–128.

35. Yadav, R. S., & Tiwari, N. K. (2014). Lipid integration in neurodegeneration: an overview of Alzheimer's disease. Molecular neurobiology, 50(1), 168–176.

36. Moberly, J. B., Attman, P. O., Samuelsson, O., Johansson, A. C., Knight-Gibson, C., & Alaupovic, P. (2002). Alterations in lipoprotein composition in peritoneal dialysis patients. Peritoneal dialysis international : journal of the International Society for Peritoneal Dialysis, 22(2), 220–228.

37. Sperling, R. A., Aisen, P. S., Beckett, L. A., Bennett, D. A., Craft, S., Fagan, A. M., Iwatsubo, T., Jack, C. R., Jr, Kaye, J., Montine, T. J., Park, D. C., Reiman, E. M., Rowe, C. C., Siemers, E., Stern, Y., Yaffe, K., Carrillo, M. C., Thies, B., Morrison-Bogorad, M., Wagster, M. V., & Phelps, C. H. (2011). Toward defining the preclinical stages of Alzheimer's disease: recommendations from the National Institute on Aging-Alzheimer's Association workgroups on diagnostic guidelines for Alzheimer's disease. Alzheimer's & dementia : the journal of the Alzheimer's Association, 7(3), 280–292.

38. Dumurgier, J., Hanseeuw, B. J., Hatling, F. B., Judge, K. A., Schultz, A. P., Chhatwal, J. P., Blacker, D., Sperling, R. A., Johnson, K. A., Hyman, B. T., & Gómez-Isla, T. (2017). Alzheimer's Disease Biomarkers and Future Decline in Cognitive Normal Older Adults. Journal of Alzheimer's disease : JAD, 60(4), 1451–1459.

39. Carrillo, F., Ghirimoldi, M., Fortunato, G., Palomba, N. P., Ianiro, L., De Giorgis, V., Khoso, S., Giloni, T., Pietracupa, S., Modugno, N., Barberis, E., Manfredi, M., & Esposito, T. (2025). Multiomics approach identifies dysregulated lipidomic and proteomic networks in Parkinson's disease patients mutated in TMEM175. NPJ Parkinson's disease, 11(1), 23.

40. Sakr, F., Dyrba, M., Bräuer, A., Teipel, S., & Alzheimer’s Disease Neuroimaging Initiative (2022). Association of Lipidomics Signatures in Blood with Clinical

Progression in Preclinical and Prodromal Alzheimer's Disease. Journal of Alzheimer's disease : JAD, 85(3), 1115–1127.

41. Fernández-Irigoyen, J., Cartas-Cejudo, P., Iruarrizaga-Lejarreta, M., & Santamaría, E. (2021). Alteration in the Cerebrospinal Fluid Lipidome in Parkinson's Disease: A Post-Mortem Pilot Study. Biomedicines, 9(5), 491.

42. McGarry, A., Gaughan, J., Hackmyer, C., Lovett, J., Khadeer, M., Shaikh, H., Pradhan, B., Ferraro, T. N., Wainer, I. W., & Moaddel, R. (2020). Cross-sectional analysis of plasma and CSF metabolomic markers in Huntington's disease for participants of varying functional disability: a pilot study. Scientific reports, 10(1), 20490.

43. Youdim, K. A., Martin, A., & Joseph, J. A. (2000). Essential fatty acids and the brain: possible health implications. International journal of developmental neuroscience : the official journal of the International Society for Developmental Neuroscience, 18(4-5), 383–399.

44. Cunnane, S. C., Schneider, J. A., Tangney, C., Tremblay-Mercier, J., Fortier, M., Bennett, D. A., & Morris, M. C. (2012). Plasma and brain fatty acid profiles in mild cognitive impairment and Alzheimer's disease. Journal of Alzheimer's disease : JAD, 29(3), 691–697.

45. Hosseini, M., Poljak, A., Braidy, N., Crawford, J., & Sachdev, P. (2020). Blood fatty acids in Alzheimer's disease and mild cognitive impairment: A meta-analysis and systematic review. Ageing research reviews, 60, 101043.

46. Li, P., Gao, Y., Ma, X., Zhou, S., Guo, Y., Xu, J., Wang, X., Van Halm-Lutterodt, N., & Yuan, L. (2022). Study on the Association of Dietary Fatty Acid Intake and Serum Lipid Profiles With Cognition in Aged Subjects With Type 2 Diabetes Mellitus. Frontiers in aging neuroscience, 14, 846132.

47. Fabelo, N., Martín, V., Santpere, G., Marín, R., Torrent, L., Ferrer, I., & Díaz, M. (2011). Severe alterations in lipid composition of frontal cortex lipid rafts from Parkinson's disease and incidental Parkinson's disease. Molecular medicine (Cambridge, Mass.), 17(9-10), 1107–1118.

48. Dakterzada, F., Jové, M., Cantero, J. L., Mota-Martorell, N., Pamplona, R., & Piñoll-Ripoll, G. (2024). The shift in the fatty acid composition of the circulating lipidome in Alzheimer's disease. Alzheimer's & dementia : the journal of the Alzheimer's Association, 20(5), 3322–3333.

49. Dhillon, V. S., Thomas, P., Lee, S. L., Deo, P., & Fenech, M. (2023). Red Blood Cell Fatty Acid Profiles Are Significantly Altered in South Australian Mild Cognitive Impairment and Alzheimer's Disease Cases Compared to Matched Controls. International journal of molecular sciences, 24(18), 14164.

50. Tan, Z. S., Harris, W. S., Beiser, A. S., Au, R., Himali, J. J., Debette, S., Pikula, A., Decarli, C., Wolf, P. A., Vasan, R. S., Robins, S. J., & Seshadri, S. (2012). Red blood cell ω-3 fatty acid levels and markers of accelerated brain aging. Neurology, 78(9), 658–664.

51. de Oliveira Otto, M. C., Wu, J. H. Y., Thacker, E. L., Lai, H. T. M., Lemaitre, R. N., Padhye, N., Song, X., King, I. B., Lopez, O., Siscovick, D. S., & Mozaffarian, D. (2023). Circulating Omega-3 and Omega-6 Fatty Acids, Cognitive Decline, and Dementia in Older Adults. Journal of Alzheimer's disease : JAD, 95(3), 965–979.

52. Loef, M., & Walach, H. (2013). The omega-6/omega-3 ratio and dementia or cognitive decline: a systematic review on human studies and biological evidence. Journal of nutrition in gerontology and geriatrics, 32(1), 1–23.

53. Baierle, M., Vencato, P. H., Oldenburg, L., Bordignon, S., Zibetti, M., Trentini, C. M., Duarte, M. M., Veit, J. C., Somacal, S., Emanuelli, T., Grune, T., Breusing, N., & Garcia, S. C. (2014). Fatty acid status and its relationship to cognitive decline and homocysteine levels in the elderly. Nutrients, 6(9), 3624–3640.

54. Cui, Y., Chen, X., Liu, L., Xie, W., Wu, Y., Wu, Q., & Wang, D. (2015). Gas chromatography-mass spectrometry analysis of the free fatty acids in serum obtained from patients with Alzheimer's disease. Bio-medical materials and engineering, 26 Suppl 1, S2165–S2177.

55. Iuliano, L., Pacelli, A., Ciacciarelli, M., Zerbinati, C., Fagioli, S., Piras, F., Orfei, M. D., Bossù, P., Pazzelli, F., Serviddio, G., Caltagirone, C., & Spalletta, G. (2013). Plasma fatty acid lipidomics in amnestic mild cognitive impairment and Alzheimer's disease. Journal of Alzheimer's disease : JAD, 36(3), 545–553.

56. Freund Levi, Y., Vedin, I., Cederholm, T., Basun, H., Faxén Irving, G., Eriksdotter, M., Hjorth, E., Schultzberg, M., Vessby, B., Wahlund, L. O., Salem, N., Jr, & Palmblad, J. (2014). Transfer of omega-3 fatty acids across the blood-brain barrier after dietary supplementation with a docosahexaenoic acid-rich omega-3 fatty acid preparation in

patients with Alzheimer's disease: the OmegAD study. Journal of internal medicine, 275(4), 428–436.

57. Luchtman, D. W., Meng, Q., & Song, C. (2012). Ethyl-eicosapentaenoate (E-EPA) attenuates motor impairments and inflammation in the MPTP-probenecid mouse model of Parkinson's disease. Behavioural brain research, 226(2), 386–396.

58. Wood P. L. (2020). Fatty Acyl Esters of Hydroxy Fatty Acid (FAHFA) Lipid Families. Metabolites, 10(12), 512.

59. Gowda, S. G. B., Liang, C., Gowda, D., Hou, F., Kawakami, K., Fukiya, S., Yokota, A., Chiba, H., & Hui, S. P. (2020). Identification of short-chain fatty acid esters of hydroxy fatty acids (SFAHFAs) in a murine model by nontargeted analysis using ultra-high-performance liquid chromatography/linear ion trap quadrupole-Orbitrap mass spectrometry. Rapid communications in mass spectrometry : RCM, 34(17), e8831.

60. Obis, E., Sol, J., Andres-Benito, P., Martín-Gari, M., Mota-Martorell, N., Galo-Licona, J. D., Piñol-Ripoll, G., Portero-Otin, M., Ferrer, I., Jové, M., & Pamplona, R. (2023). Lipidomic Alterations in the Cerebral Cortex and White Matter in Sporadic Alzheimer's Disease. Aging and disease, 14(5), 1887–1916.

61. Crivelli, S. M., Giovagnoni, C., Visseren, L., Scheithauer, A. L., de Wit, N., den Hoedt, S., Losen, M., Mulder, M. T., Walter, J., de Vries, H. E., Bieberich, E., & Martinez-Martinez, P. (2020). Sphingolipids in Alzheimer's disease, how can we target them?. Advanced drug delivery reviews, 159, 214–231.

62. Hussain, G., Wang, J., Rasul, A., Anwar, H., Imran, A., Qasim, M., Zafar, S., Kamran, S. K. S., Razzaq, A., Aziz, N., Ahmad, W., Shabbir, A., Iqbal, J., Baig, S. M., & Sun, T. (2019). Role of cholesterol and sphingolipids in brain development and neurological diseases. Lipids in health and disease, 18(1), 26.

63. Mielke, M. M., & Lyketsos, C. G. (2010). Alterations of the sphingolipid pathway in Alzheimer's disease: new biomarkers and treatment targets?. Neuromolecular medicine, 12(4), 331–340.

64. Chua, X. Y., Torta, F., Chong, J. R., Venketasubramanian, N., Hilal, S., Wenk, M. R., Chen, C. P., Arumugam, T. V., Herr, D. R., & Lai, M. K. P. (2023). Lipidomics profiling reveals distinct patterns of plasma sphingolipid alterations in Alzheimer's disease and vascular dementia. Alzheimer's research & therapy, 15(1), 214.

65. Filippov, V., Song, M. A., Zhang, K., Vinters, H. V., Tung, S., Kirsch, W. M., Yang, J., & Duerksen-Hughes, P. J. (2012). Increased ceramide in brains with Alzheimer's and other neurodegenerative diseases. Journal of Alzheimer's disease : JAD, 29(3), 537–547.
66. Kosicek, M., Zetterberg, H., Andreasen, N., Peter-Katalinic, J., & Hecimovic, S. (2012). Elevated cerebrospinal fluid sphingomyelin levels in prodromal Alzheimer's disease. Neuroscience letters, 516(2), 302–305.
67. Savica, R., Murray, M. E., Persson, X. M., Kantarci, K., Parisi, J. E., Dickson, D. W., Petersen, R. C., Ferman, T. J., Boeve, B. F., & Mielke, M. M. (2016). Plasma sphingolipid changes with autopsy-confirmed Lewy Body or Alzheimer's pathology. Alzheimer's & dementia (Amsterdam, Netherlands), 3, 43–50.
68. Blusztajn, J. K., Aytan, N., Rajendiran, T., Mellott, T. J., Soni, T., Burant, C. F., Serrano, G. E., Beach, T. G., Lin, H., & Stein, T. D. (2023). Cerebral Gray and White Matter Monogalactosyl Diglyceride Levels Rise with the Progression of Alzheimer's Disease. Journal of Alzheimer's disease : JAD, 95(4), 1623–1634.
69. Watanabe, Y., Kasuga, K., Tokutake, T., Kitamura, K., Ikeuchi, T., & Nakamura, K. (2021). Alterations in Glycerolipid and Fatty Acid Metabolic Pathways in Alzheimer's Disease Identified by Urinary Metabolic Profiling: A Pilot Study. Frontiers in neurology, 12, 719159.
70. Nitsch, R., Pittas, A., Blusztajn, J. K., Slack, B. E., Growdon, J. H., & Wurtman, R. J. (1991). Alterations of phospholipid metabolites in postmortem brain from patients with Alzheimer's disease. Annals of the New York Academy of Sciences, 640, 110–113.
71. Xu, S., Zhu, Z., Delafield, D. G., Rigby, M. J., Lu, G., Braun, M., Puglielli, L., & Li, L. (2024). Spatially and temporally probing distinctive glycerophospholipid alterations in Alzheimer's disease mouse brain via high-resolution ion mobility-enabled sn-position resolved lipidomics. Nature communications, 15(1), 6252.
72. Sabogal-Guáqueta, A. M., Villamil-Ortiz, J. G., Arias-Londoño, J. D., & Cardona-Gómez, G. P. (2018). Inverse Phosphatidylcholine/Phosphatidylinositol Levels as Peripheral Biomarkers and Phosphatidylcholine/Lysophosphatidylethanolamine-Phosphatidylserine as Hippocampal Indicator of Postischemic Cognitive Impairment in Rats. Frontiers in neuroscience, 12, 989.
73. Ahsanul Haque, M., Omori, N., Md Sheikh, A., Yano, S., Osago, H., Mitaki, S., Kalam Azad, A., Sakai, H., Michikawa, M., & Nagai, A. (2023). Analysis of the time-

dependent changes of phospholipids in the brain regions of a mouse model of Alzheimer's disease. Brain research, 1800, 148197.

74. Xu, Z., Shabestari, S. K., Barannikov, S., Bieniek, K. F., Blurton-Jones, M., Palavicini, J. P., & Han, X. (2024). Microglia-Dependent and Independent Modulation of Brain Lipid Metabolism in Alzheimer's Disease Revealed by Pharmacological and Genetic Microglial Depletion. bioRxiv, 2024-11.

75. Nitsch, R. M., Blusztajn, J. K., Pittas, A. G., Slack, B. E., Growdon, J. H., & Wurtman, R. J. (1992). Evidence for a membrane defect in Alzheimer disease brain. Proceedings of the National Academy of Sciences of the United States of America, 89(5), 1671–1675.

76. Mapstone, M., Cheema, A. K., Fiandaca, M. S., Zhong, X., Mhyre, T. R., MacArthur, L. H., Hall, W. J., Fisher, S. G., Peterson, D. R., Haley, J. M., Nazar, M. D., Rich, S. A., Berlau, D. J., Peltz, C. B., Tan, M. T., Kawas, C. H., & Federoff, H. J. (2014). Plasma phospholipids identify antecedent memory impairment in older adults. Nature medicine, 20(4), 415–418.

77. Xicoy, H., Brouwers, J. F., Wieringa, B., & Martens, G. J. M. (2020). Explorative Combined Lipid and Transcriptomic Profiling of Substantia Nigra and Putamen in Parkinson's Disease. Cells, 9(9), 1966.

78. Lobasso, S., Tanzarella, P., Vergara, D., Maffia, M., Cocco, T., & Corcelli, A. (2017). Lipid profiling of parkin-mutant human skin fibroblasts. Journal of cellular physiology, 232(12), 3540–3551.

79. Mapstone, M., Cheema, A. K., Fiandaca, M. S., Zhong, X., Mhyre, T. R., MacArthur, L. H., Hall, W. J., Fisher, S. G., Peterson, D. R., Haley, J. M., Nazar, M. D., Rich, S. A., Berlau, D. J., Peltz, C. B., Tan, M. T., Kawas, C. H., & Federoff, H. J. (2014). Plasma phospholipids identify antecedent memory impairment in older adults.

80. Seet, R. C., Lee, C. Y., Lim, E. C., Tan, J. J., Quek, A. M., Chong, W. L., Looi, W. F., Huang, S. H., Wang, H., Chan, Y. H., & Halliwell, B. (2010). Oxidative damage in Parkinson disease: Measurement using accurate biomarkers. Free radical biology & medicine, 48(4), 560–566.

81. Chiurchiù, V., Tiberi, M., Matteocci, A., Fazio, F., Siffeti, H., Saracini, S., ... & Sancesario, G. (2022). Lipidomics of bioactive lipids in Alzheimer's and Parkinson's diseases: where are we?. International journal of molecular sciences, 23(11), 6235.

82. yurina, Y. Y., Polimova, A. M., Maciel, E., Tyurin, V. A., Kapralova, V. I., Winnica, D. E., Vikulina, A. S., Domingues, M. R., McCoy, J., Sanders, L. H., Bayır, H., Greenamyre, J. T., & Kagan, V. E. (2015). LC/MS analysis of cardiolipins in substantia nigra and plasma of rotenone-treated rats: Implication for mitochondrial dysfunction in Parkinson's disease. Free radical research, 49(5), 681–691.

83. Yin F. (2023). Lipid metabolism and Alzheimer's disease: clinical evidence, mechanistic link and therapeutic promise. The FEBS journal, 290(6), 1420–1453.

84. Wood, P. L., Medicherla, S., Sheikh, N., Terry, B., Phillipps, A., Kaye, J. A., Quinn, J. F., & Woltjer, R. L. (2015). Targeted Lipidomics of Fontal Cortex and Plasma Diacylglycerols (DAG) in Mild Cognitive Impairment and Alzheimer's Disease: Validation of DAG Accumulation Early in the Pathophysiology of Alzheimer's Disease. Journal of Alzheimer's disease : JAD, 48(2), 537–546.

85. Dakterzada, F., Benítez, I. D., Targa, A., Carnes, A., Pujol, M., Jové, M., Mínguez, O., Vaca, R., Sánchez-de-la-Torre, M., Barbé, F., Pamplona, R., & Piñol-Ripoll, G. (2023). Cerebrospinal fluid lipidomic fingerprint of obstructive sleep apnoea in Alzheimer's disease. Alzheimer's research & therapy, 15(1), 134.

86. Burgess, B. L., McIsaac, S. A., Naus, K. E., Chan, J. Y., Tansley, G. H., Yang, J., Miao, F., Ross, C. J., van Eck, M., Hayden, M. R., van Nostrand, W., St George-Hyslop, P., Westaway, D., & Wellington, C. L. (2006). Elevated plasma triglyceride levels precede amyloid deposition in Alzheimer's disease mouse models with abundant A beta in plasma. Neurobiology of disease, 24(1), 114–127.

87. Espina, A., Mendoza, E., & Lao, A. (2022). Modelling the Effects of Medium-Chain Triglycerides on Cerebral Ketone Body Metabolism. Frontiers in Systems Biology, 2, 907957.

88. Sun, L., Ye, K. X., Wong, H. L. K., Wang, L., Lim, S. L., Chao, Y. X., Zhang, C., Yap, K. Z., & Feng, L. (2023). The Effects of Medium Chain Triglyceride for Alzheimer's Disease Related Cognitive Impairment: A Systematic Review and Meta-Analysis. Journal of Alzheimer's disease : JAD, 94(2), 441–456.

89. Hillebrandt, H. L., Dias, C. B., Barin, E. S., Chatterjee, P., Shah, T. M., Basci, A. M., Kaplan. J., Sohrahi, H. R., & Martins, R. N. (2021). Cognition may improve with medium-chain triglyceride oil supplementation: A pilot study. Alzheimer's & Dementia, 17, e055702.

90. Lee, A., Yoo, H. J., Kim, M., Kim, M., Choi, J. H., Lee, C., & Lee, J. H. (2019). Effects of equivalent medium-chain diacylglycerol or long-chain triacylglycerol oil intake via muffins on postprandial triglycerides and plasma fatty acids levels. Journal of functional foods, 53, 299-305.

91. Watanabe, Y., Kasuga, K., Tokutake, T., Kitamura, K., Ikeuchi, T., & Nakamura, K. (2021). Alterations in Glycerolipid and Fatty Acid Metabolic Pathways in Alzheimer's Disease Identified by Urinary Metabolic Profiling: A Pilot Study. Frontiers in neurology, 12, 719159.

92. Di Paolo, G., & Kim, T. W. (2011). Linking lipids to Alzheimer's disease: cholesterol and beyond. Nature reviews. Neuroscience, 12(5), 284–296.

93. Feringa, F. M., & van der Kant, R. (2021). Cholesterol and Alzheimer's Disease; From Risk Genes to Pathological Effects. Frontiers in aging neuroscience, 13, 690372.

94. Liu, Y., Zhong, X., Shen, J., Jiao, L., Tong, J., Zhao, W., Du, K., Gong, S., Liu, M., & Wei, M. (2020). Elevated serum TC and LDL-C levels in Alzheimer's disease and mild cognitive impairment: A meta-analysis study. Brain research, 1727, 146554.

95. Beydoun, M. A., Beason-Held, L. L., Kitner-Triolo, M. H., Beydoun, H. A., Ferrucci, L., Resnick, S. M., & Zonderman, A. B. (2011). Statins and serum cholesterol's associations with incident dementia and mild cognitive impairment. Journal of epidemiology and community health, 65(11), 949–957.

96. Phillips, G. R., Hancock, S. E., Brown, S. H. J., Jenner, A. M., Kreilaus, F., Newell, K. A., & Mitchell, T. W. (2020). Cholesteryl ester levels are elevated in the caudate and putamen of Huntington's disease patients. Scientific reports, 10(1), 20314.

Chapter 5

Comprehensive plasma lipidome profiling of pre-adolescent children using untargeted LC/MS- A study from Hokkaido

5.1 Introduction

Lipids play essential roles in human health, serving as key components of both cellular and extracellular structures. They contribute significantly to cell membrane integrity, function, energy storage, thermal insulation, and protection [1]. Lipid metabolites also serve as vital mediators in cellular communication and metabolic regulation within the body. Disruptions in lipid metabolism are linked to a wide range of chronic diseases, including CVD, cancer, and genetic lipid pathway disorders, all of which pose significant health risks [2]. In early childhood, lipid metabolism plays a crucial role in growth, body composition development, and overall child development, with lasting effects on long-term health outcomes [3]. The metabolism of dietary lipids, particularly cholesterol, during this critical period can significantly impact children's health, potentially influencing rates of morbidity and mortality [4]. To assess disease risk, plasma lipid profiles are routinely analyzed by measuring total cholesterol, TGs, high-density lipoprotein cholesterol (HDL-C), and low-density lipoprotein cholesterol (LDL-C) levels [5].

Human plasma contains a vast array of molecular lipid species, alongside nucleic acids, amino acids, and carbohydrates, exhibiting remarkable functional and chemical diversity [6]. These lipids are present in concentrations ranging from μM to mM and encompass multiple lipid classes, including FAs, GLs, GPs, SPs, STs, and PRs [7]. Plasma lipid metabolites are intricately involved in numerous biological pathways and are increasingly recognized as biomarkers that reflect disease progression and responses to therapeutic interventions [8]. Plasma concentrations of total TG, HDL-C, and LDL-C serve as critical indicators and potential causes of cardiometabolic disease risk [9]. Consequently, these lipoprotein-related biomarkers are routinely assessed in clinical practice, and the associated molecular pathways are key targets of first-line drugs for the prevention of cardiometabolic diseases [10]. Beyond traditional lipids, several lipid subclasses in plasma- including TGs, GPs, SPs, and CEs- have been identified as diagnostic indicators for various diseases. For example, altered levels of these lipids have been associated with AD [11], while LPC has been implicated in cancer risk [12], and specific SPs species have proven useful in evaluating therapeutic response in genetic disorders such as Niemann-Pick C1 disease [13]. Alterations in plasma lipid metabolism are modulated by a complex interplay of dietary habits, physical activity levels, and

genetic predispositions [14,15]. Supporting this, earlier studies have demonstrated that both dietary intake and physical activity can beneficially modify the FFAs profiles in plasma, particularly in children aged 6 to 8 years [16]. Additionally, a study by Martin et al. revealed a significant upregulation of LPC species in the plasma of obese women following physical exercise, underscoring the responsiveness of specific lipid subclasses to lifestyle interventions [17]. A study by Zhang et al. demonstrated that structured exercise training significantly elevates the levels of ether-linked alkylPC and TGs in the plasma of healthy male adolescents [18]. Additionally, genetic variability plays a critical role in modulating the plasma lipidome, with specific genetic loci being associated with distinct lipid species that contribute to CVD risk [19]. Previous investigations into the plasma lipidome of children have primarily concentrated on individual lipid classes. A recent cohort-based analysis assessed plasma samples from healthy adolescents by quantifying total cholesterol, HDL-C, and TGs levels through standard enzymatic assays. The findings revealed a decrease in total cholesterol concentrations between ages 9 and 16 in girls and a more pronounced reduction from ages 10 to 17 in boys. LC/MS is a robust and widely utilized analytical platform in plasma lipidomics. For instance, in one study, lipids were extracted from dried blood spot samples obtained from children across various age groups (0–10 days, 2–18 months, and 3–13 years) using the Bligh–Dyer method and subsequently analyzed via LC/MS. The results identified 16 lipid species from multiple lipid subclasses that exhibited statistically significant variations among the age groups. Notably, lipid species containing linoleic acid were markedly reduced in 0–10 days groups, with a progressive increase observed in the 2–18 months and 3–13 years cohorts [21]. LC/MS technique has also been employed to investigate plasma lipidomic profiles in Chinese male adolescents aged 14–16 years, comparing obese individuals with their normal-weight counterparts. In this study, plasma lipids were extracted using a modified Folch method. The analysis revealed a total of 328 lipid species spanning 24 lipid classes and subclasses. A notable finding was the significant reduction in LPCs in the plasma of obese adolescents compared to normal-weight controls, indicating a strong inverse association between LPC levels and adolescent obesity [22].

Existing studies on plasma lipidomics in healthy children provides limited insights into how factors such as age, sex, and body weight modulate lipid metabolism and contribute to lifestyle-associated health outcomes. To date, no comprehensive lipidomic

investigations have been conducted specifically on Japanese preadolescent populations. Therefore, it is of particular interest to characterize the plasma lipidome of Japanese children and examine its variability in relation to age, sex, and body weight. Hence, in the present study, we employed HPLC/LTQ-Orbitrap-MS to perform a comprehensive lipidomic profiling of plasma samples collected from preadolescent Japanese children (n = 342), aged 9 to 12 years, including both boys and girls. The overall study design is illustrated in **Figure 5.1A**. To our knowledge, this represents the first large-scale investigation exploring the plasma lipidome in Japanese preadolescents, with a specific focus on variations associated with age, sex, and body weight.

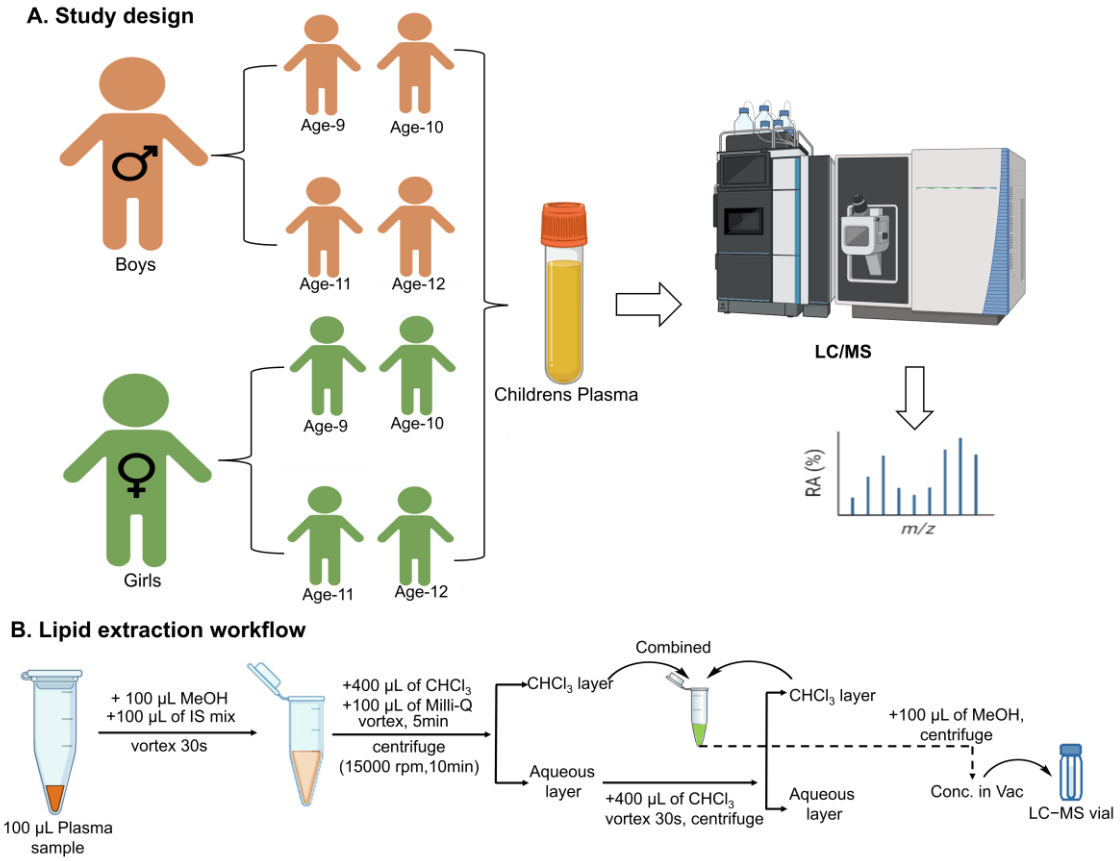

Figure 5.1: A. Overview of study design for plasma lipidomics in preadolescent children. **B.** Schematic representation of total lipid extraction workflow from plasma samples.

5.2 Materials and Methods

5.2.1 Chemicals and reagents

The materials used in this study, including solvents and internal standards, were the same as those described in **Chapter 2, Section 2.1**.

5.2.2 Sample information of pre-adolescent children's plasma samples

Non-fasting plasma samples were obtained from participants in the Hokkaido Study on Environment and Children's Health, a part of the Hokkaido Cohort [23], and stored at -80°C. The participant selection criteria for sample collection were previously described in our study [24]. The cohort consisted of 342 healthy preadolescent children (n = 181 boys and 161 girls) aged 9 to 12 years, residing in Sapporo City, Hokkaido, Japan. Height and body weight measurements were taken on the same day as blood collection at pediatric clinics. A summary of the demographic information for the preadolescent children is provided in **Table 5.1**. Written informed consent was obtained from all parents, and the children themselves provided assent after being informed of the study's purpose and procedures.

Table 5.1: Characteristics of participants enrolled in the Hokkaido study (Mean±SD).

	Age (years old)	**Height (cm)**	**Weight (kg)**	**POW (%)**
Boys	9 (n = 68)	134.9 ± 5.0	31.8 ± 6.1	1.40 ± 13.56
(n = 181)	10 (n = 63)	139.0 ± 6.4	35.0 ± 8.3	2.31 ± 16.90
	11 (n = 20)	148.3 ± 6.5	41.8 ± 8.1	2.69 ± 18.54
	12 (n = 30)	150.6 ± 9.4	44.2 ± 9.8	5.12 ± 17.81
Girls	9 (n = 46)	136.1 ± 5.7	30.2 ± 5.9	-5.18 ± 11.72
(n = 161)	10 (n = 70)	140.4 ± 7.0	34.6 ± 8.1	0.07 ± 14.04
	11 (n = 16)	151.0 ± 5.0	39.5 ± 5.8	-6.83 ± 10.05
	12 (n =29)	151.5 ± 6.5	42.6 ± 8.4	-2.75 ± 12.69

5.2.3 Lipid extraction from plasma samples

Non-fasting plasma samples (n = 342) from pre-adolescent boys and girls aged 9 to 12 years were subjected to total lipid extraction. The detailed extraction workflow is shown in **Figure 5.1B**. The samples were collected and stored at -80°C for subsequent analysis. A 100 µL of plasma sample was used for the lipid extraction using the modified Folch technique, as described previously in **Chapter 2, Section 2.2.4.**

5.2.4 LC/MS analysis of plasma samples

The LC/MS conditions employed for lipid analysis in both negative and positive ion mode in this chapter were identical to those previously described in **Chapter 2, Section 2.2.5**.

5.2.5 Lipid annotation and quantification

The processing of LC/MS data, lipid identification, and quantification were performed using MS-DIAL software (version 4.9), with peak processing and integration further refined using Xcalibur 2.2 software (Thermo Fisher Scientific Inc.), as described previously in **Chapter 4, Section 4.2.6.**

5.2.6 Statistical analysis

The data processing and visualization have been done, as described previously in **Chapter 2, Section 2.2.7**. Statistical analyses, including OPLS-DA and ordinary two-way ANOVA, were conducted as described in **Chapter 4 section 4.2.6**. Further, sparse partial least squares discriminant analysis (sPLS-DA) was performed using the web platform MetaboAnalyst 5.0 (https://www.metaboanalyst.ca, accessed on January 4, 2024). Power analysis was performed using G*Power version 3.1.9.7 software. All data are presented as mean ± SEM.

5.3 Results

5.3.1 Multivariate analysis and sex-specific lipid profiling of plasma samples from pre-adolescent children

In this study, pre-adolescent children were grouped by gender, and plasma samples were collected for lipid extraction. An untargeted lipidomic analysis was carried out using HPLC/LTQ-Orbitrap-MS. **Figure 5.2** displays the lipid classes identified in the plasma samples from the pre-adolescent children, along with their corresponding

multivariate analysis. Power calculations were performed to assess the adequacy of the sample size. The analysis comparing the bodyweight-based groups showed a power value of 0.99, supporting the sufficiency of the sample size for this comparison. In contrast, the comparison between boys and girls yielded a low power value of 0.15, suggesting that the sample size for gender-based comparisons may be inadequate.

Analysis of plasma samples from pre-adolescent children identified a total of 219 lipid species across several lipid classes (**Figure 5.2A**). The lipid species included 53 TGs, 35 PEs, 31 FAs, 18 PIs, 18 PCs, and 14 Cer. Multivariate analysis using OPLS-DA revealed similar lipid profiles in both boys and girls, as shown in **Figure 5.2B**. The OPLS-DA models, T score [1] and T score [2], accounted for 23.4% of the total variance in the data, with T score [1] explaining 20.5%. Score plots and the corresponding feature importance box plot (S-plot) were used to assess the variable influence within the OPLS-DA model. Lipid species with larger positive or negative loading scores have a greater influence on the orthogonal components. **Figure 5.2C** highlights that specific TG molecular species, such as TG (10:0/16:0/18:1), TG (12:0/12:0/18:1), TG (16:0/16:0/18:1), and TG (16:0/18:1/18:1), show higher positive loading scores in boys.

A volcano plot was generated to illustrate the relationship between $-\log_{10}$(p-value) and $\log_2$(fold change), highlighting the lipid molecular species that were significantly and markedly altered between the plasma lipidomes of boys and girls (**Figure 5.2D**). The results reveal that certain lipid species exhibited notably higher concentrations in boys compared to girls. Specifically, lipids such as PE (16:0/20:5), PE (15:1/20:5), TG (10:0/12:0/18:1), TG (10:0/10:0/18:1), and TG (10:0/12:0/18:2), which are prominently marked in red on the right side of the plot, were significantly elevated in boys. Conversely, no significant downregulation of lipid molecules was observed in the plasma between boys and girls.

The lipid biosynthesis pathway analysis, based on KEGG pathways (https://www.genome.jp/kegg/pathway.html), is presented in **Appendix Figure 5.1**. The biosynthetic origins of the identified lipid classes have been described in the previous **Chapter 4, Section 4.4.** Our lipidomic profiling revealed differences in specific lipid biosynthesis pathways between the plasma lipidomes of boys and girls. Notably, there were no significant differences in FFAs levels between the two groups. However, a decrease in HexCer and SM levels was observed in girls compared to boys, which may

be attributed to the downregulation of the SPs biosynthesis pathway in females. A similar pattern was noted for GPs and GLs. These findings offer valuable insights into sex-specific lipid metabolism and the regulatory mechanisms involved.

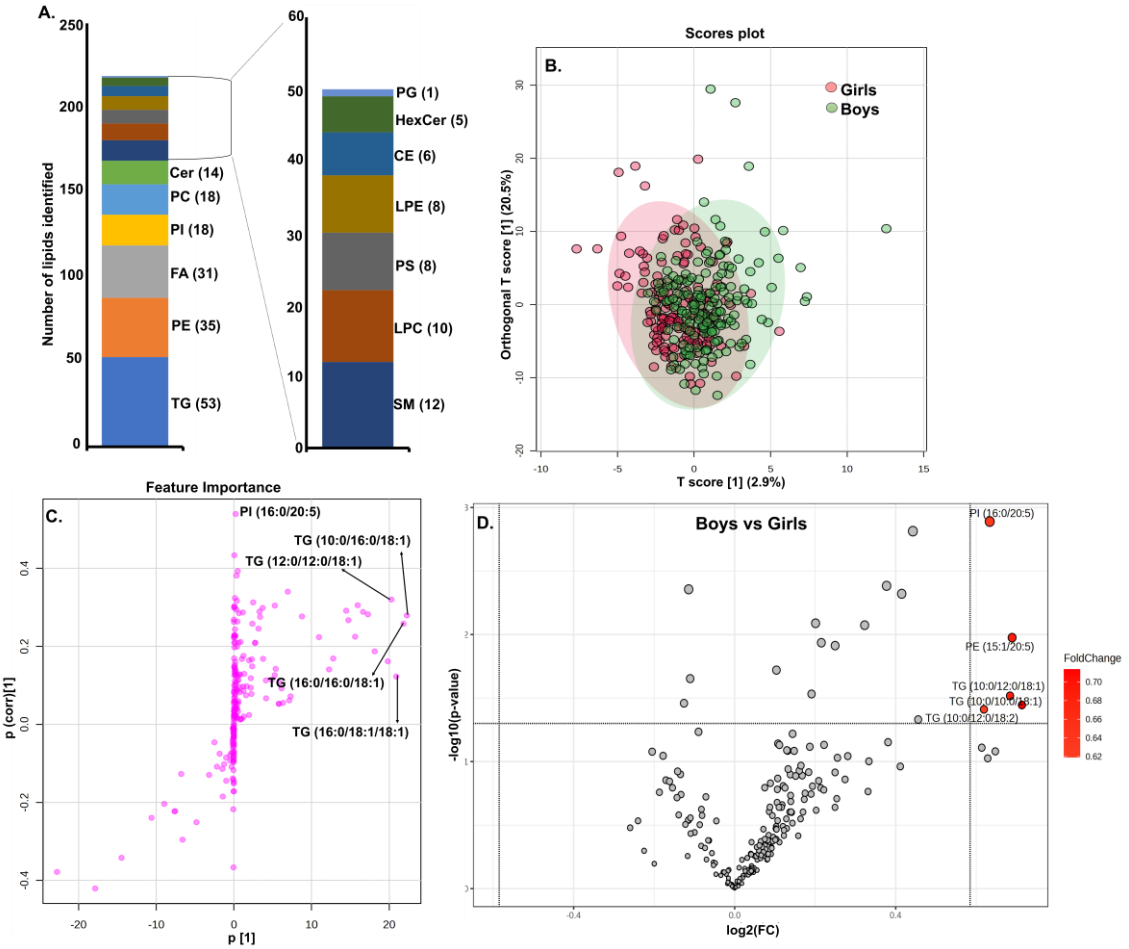

Figure 5.2: A. Distribution of lipid classes detected in plasma samples of preadolescent children. **B.** Orthogonal partial least squares discriminant analysis (OPLS-DA) score plot showing group separation between boys and girls based on plasma lipid profiles. **C.** Loading plot illustrating key lipid contributors differentiating the sexes. **D.** Volcano plot highlighting significantly dysregulated lipids ($p < 0.05$) between male and female preadolescent groups.

5.3.2 Variation in plasma fatty acyl levels across different age groups in pre-adolescent children

Figure 5.3 illustrates significant changes in FAs levels across different age groups in the plasma lipidomes of both boys and girls. The violin plots represent the average

concentrations of SFAs, MUFAs, and PUFAs, including ω-3 and ω-6 PUFAs for each group. Interestingly, there were no statistically significant differences in the overall levels of SFAs, MUFAs, and PUFAs between boys and girls (**Figure 5.3A**). Despite the known benefits of PUFAs on metabolic health, no significant changes were observed in the levels of ω-3 and ω-6 PUFAs in either sex (**Figure 5.3B**). However, distinct variations in FAs levels were noted when examining different age groups (9, 10, 11, and 12 years). Notably, a significant increase in SFA levels was observed in the plasma of 9-year-old boys, with a greater rate of increase compared to other age groups. Conversely, a marked decrease in SFA levels was observed in boys aged 11 years, indicating age-dependent changes in FAs profiles.

Notably, no significant changes were observed in the levels of MUFAs and PUFAs (both ω-3 and ω-6 PUFAs) in either boys or girls (**Figure 5.3C and 5.3D**). In the girls' group, a significant increase in SFA levels was observed in the 9-year-old cohort when compared to the other age groups. Remarkably, the rate of increase in SFA levels for the 9-year-old girls was notably higher than that observed in the other age groups, similar to the pattern seen in the boys' group. However, aside from the 9-year-old group, no significant variations were found in SFA, MUFA, or PUFA levels among the other age groups of girls. The MUFA and PUFA levels showed no significant changes across the different age groups of girls (**Figures 5.3E and 5.3F**). Overall, SFA levels in the 9-year-old group, regardless of sex, were higher compared to the other age groups. Nevertheless, no significant changes were observed in MUFA or PUFA levels across age groups in either boys or girls.

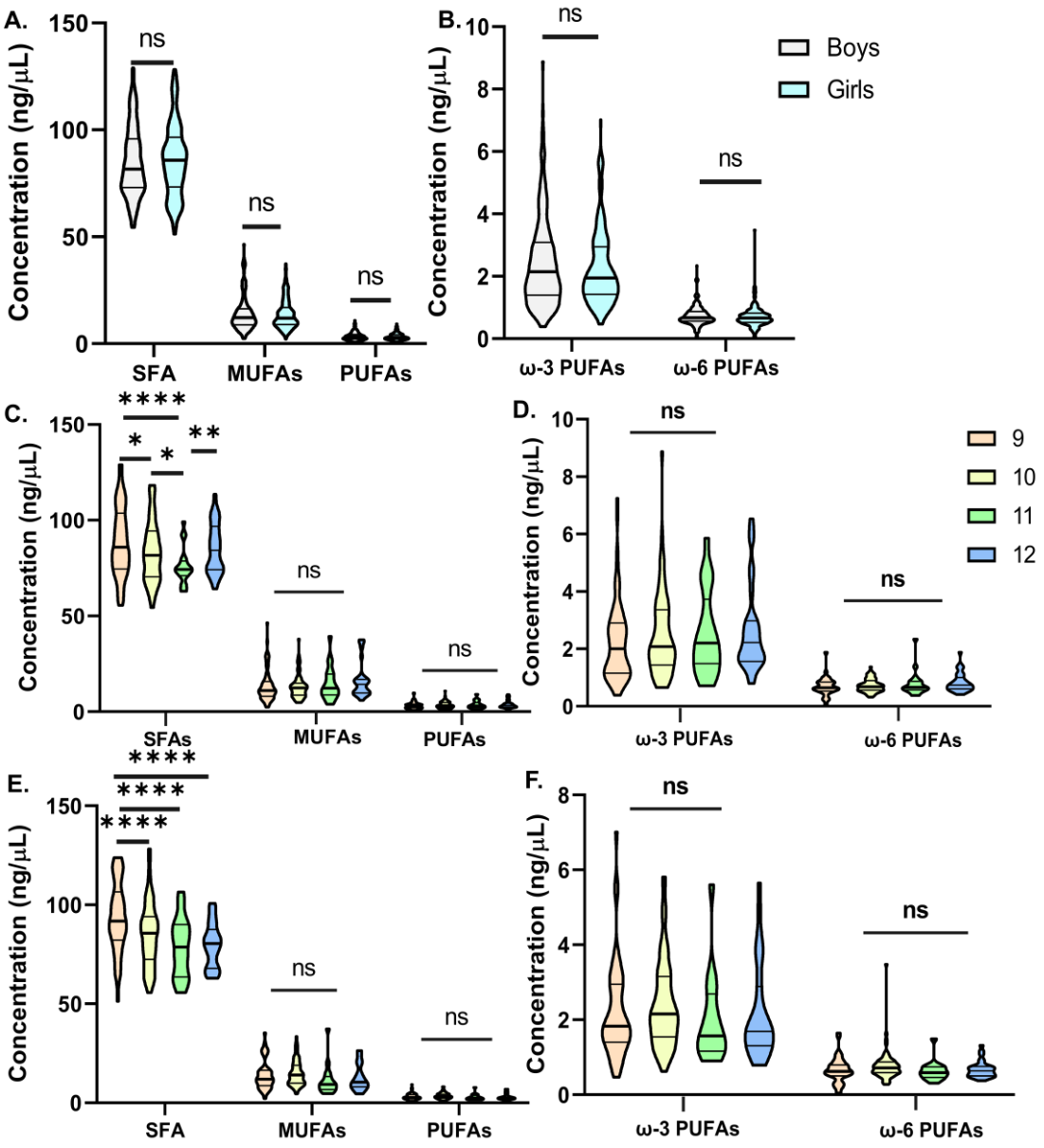

Figure 5.3: **A.** Changes in SFA, MUFA, and PUFA levels between boys and girls. **B.** Distribution of ω-3 and ω-6 PUFAs by sex. **C.** Age-related changes in SFA, MUFA, and PUFA levels among boys. **D.** Age-related changes in ω-3 and ω-6 PUFAs in boys. **E.** Age-related changes in SFA, MUFA, and PUFA levels among girls. **F.** Age-related changes in ω-3 and ω-6 PUFAs in girls. (Ordinary two-way ANOVA, ****$p < 0.0001$, **$p < 0.01$, *$p < 0.05$, 0.1 (ns), saturated fatty acids (SFAs), monounsaturated fatty acids (MUFAs), and polyunsaturated fatty acids (PUFAs)).

5.3.3 Age-dependent variations in plasma lipidome at the subclass levels in pre-adolescent children

Lipid molecular species were categorized according to their subclass levels, and the relative abundances of lipidomic alterations by age in both sexes are shown in **Figure 5.4.** The line graph displays the mean ± SEM of the individual concentrations of each molecular species across the age groups, representing the concentration of each lipid subclass. SPs, including Cer, HexCer, and SM, were significantly elevated in the 10-year-old group of both sexes compared to other age groups. GPs, such as PE, were notably increased in the 11-year-old group in both boys and girls, while no significant changes were found in the 9-, 10-, and 12-year-old groups. Similarly, PI levels were significantly higher in the 10-year-old age group in both sexes. PS lipids were significantly elevated in the 12-year-old children, with lower levels observed in the 9-year-old group of both boys and girls. No significant changes were noted in LPC, lysophosphatidylethanolamine (LPE), or PC levels across the different age groups.

Furthermore, GLs, particularly TG, showed a significant increase in the 12-year-old age group in both boys and girls compared to the other age groups. As illustrated in **Figure 5.4**, significant variations in lipid subclasses were observed in the 10- and 12-year-old age groups for both boys and girls. In summary, elevated levels of Cer, HexCer, SM, and PI are distinctive markers for the 10-year-old group of children across both sexes, while elevated TG and PS levels serve as potential indicators for differentiating boys and girls within the 12-year-old age group. **Appendix Figure 5.2 and 5.3** show volcano plots that represent the relationship between -log10(p-value) and log2(fold change), helping to highlight significantly altered lipid molecular species within the plasma lipidomes of boys and girls across different age groups. Specifically, in the 10-year-old group, Cer (d18:1/23:1) was notably upregulated in both boys and girls, while HexCer (d18:1/16:0) levels decreased in the 11- and 12-year-old groups for both sexes.

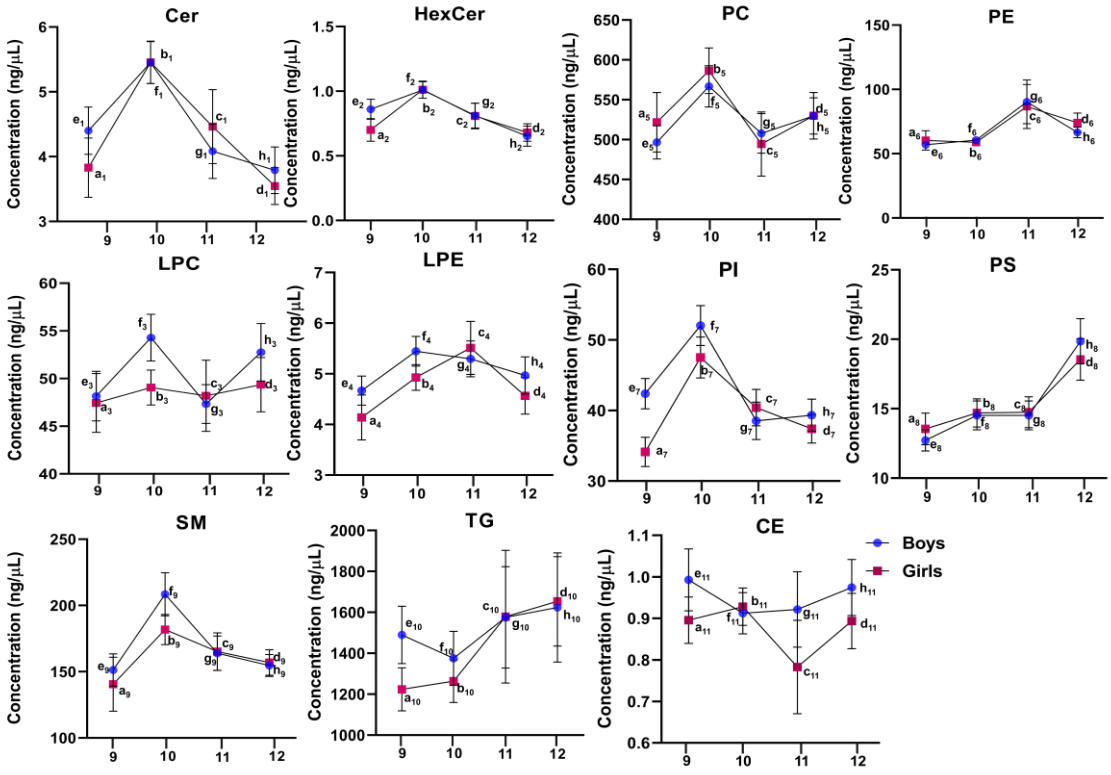

Figure 5.4: Age-associated changes in plasma lipid subclasses among preadolescent children. Lipidomic variations are illustrated across the 9-, 10-, 11-, and 12-year age groups for both sexes. Data for girls are represented in red, and boys in blue. Statistical significance was assessed using ordinary two-way ANOVA ($p < 0.05$ considered statistically significant). Significant differences in lipid subclasses are as follows: Cer: girls (a1–b1, b1–d1), boys (f1–h1); HexCer: girls (a2–b2, b2–d2), boys (f2–h2); PE: girls (a6–c6, b6–c6), boys (e6–g6, f6–g6); PI: girls (a7–b7), boys (e7–f7, f7–g7, f7–h7); PS: girls (a8–d8), boys (e8–h8, f8–h8); SM: boys (e9–f9). No significant differences were observed in LPC, LPE, PC, TG, and CE levels ($p > 0.05$, ns).

5.3.4 Impact of percentage of overweight (POW) status on the plasma lipidome of pre-adolescent children

The percentage of overweight (POW) is determined using age- and sex-specific bodyweight-for-height standards, which are utilized to define childhood obesity in Japan [25]. POW is calculated using the formula: [measured weight (kg) - standard weight (kg) / standard weight (kg)] × 100. Children were classified into three groups based on POW: UW for POW ≤ -20%, normal range (NR) for POW between -20% and +20%, and OW

for POW ≥ +20% (**Table 5.2**). The cluster correlation analysis of the top fifty significantly altered lipids across the UW, NR, and OW groups is presented in **Figure 5.5A**. Compared to the UW and NR groups, the OW group showed higher levels of most TGs. Notably, TG (10:0/10:0/18:1) exhibited a significant increase in the OW group.

In **Figure 5.5B**, the multivariate sPLS-DA score plot displays the distribution of annotated lipids across different weight categories. Components 1 and 2 together account for 23.5% of the total variance, with Component 1 explaining 19.1%. This analysis highlights the separation of lipid profiles among the sample groups. Notably, the UW and NR groups show overlapping clusters, indicating that there are minimal differences in lipid composition between these two groups. However, the OW group forms distinct clusters, suggesting significant lipidomic differences compared to both the UW and NR groups. **Figure 5.5C** shows volcano plots for the plasma lipidome of NR and OW children, illustrating the significant and large alterations in lipid molecular species based on -log10(p-value) versus log2(FC). The analysis reveals that most TGs, particularly those composed of capric acid chains, such as TG (10:0/10:0/18:1), are upregulated in the OW group. To assess the diagnostic potential of these lipids in distinguishing OW from NR, ROC curve analysis was performed. Among all the discriminatory lipids, TG (10:0/10:0/18:1) exhibited the highest AUC value of 0.7279 (95% confidence interval (CI): 0.6377–0.8181), as shown in **Figure 5.5D**.

Table 5.2: Classification of children based on POW (%)

	Boys (n = 181)			**Girls (n = 161)**		
Age	POW (%)			POW (%)		
(years old)	Under weight	Normal Range	Over weight	Under weight	Normal Range	Over weight
9	2	57	9	3	42	1
10	0	53	10	3	60	7
11	0	16	4	2	14	0
12	1	24	5	1	26	2

POW, percentage of overweight. Underweight: Children with POW < -20%; Normal range: Children with POW between -20% and 20%; Overweight: Children with POW ≧ +20%.

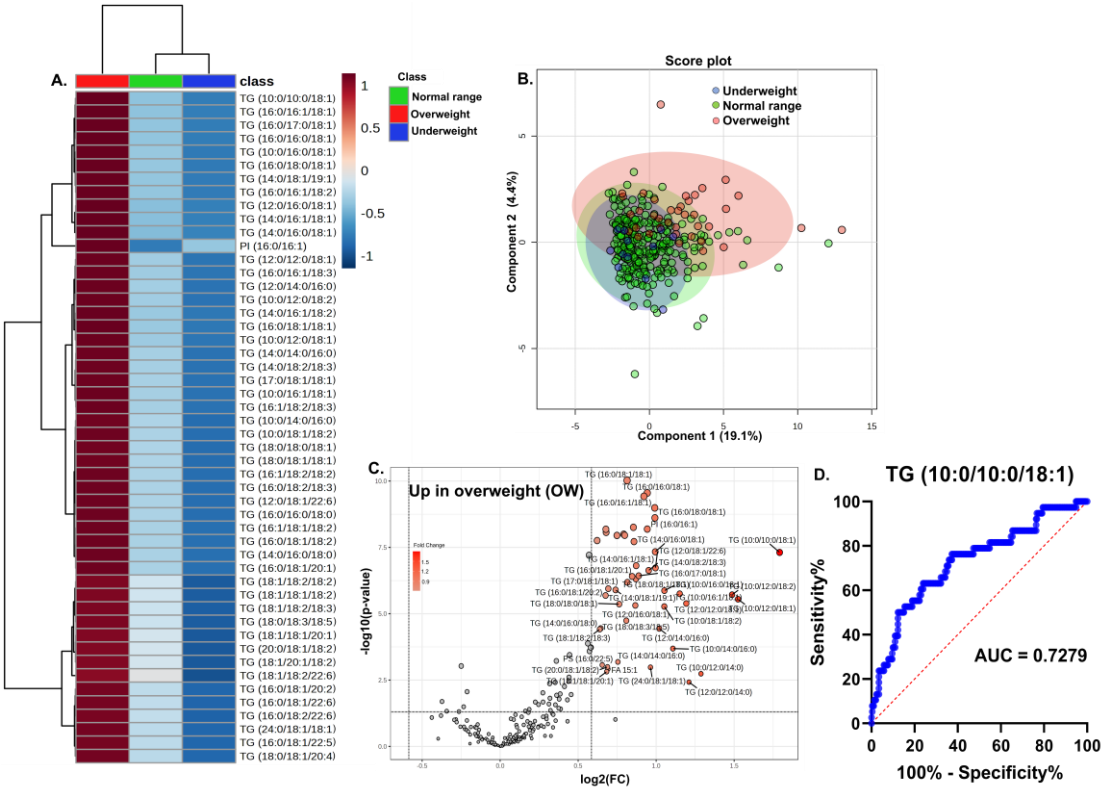

Figure 5.5: Plasma lipidomic alterations across underweight (UW), normal range (NR), and overweight (OW) preadolescent children. **A.** Hierarchical cluster correlation heatmap of the top 50 significantly altered lipid species ($p < 0.05$) among UW, NR, and OW groups. Red indicates higher, and blue indicates lower lipid abundance. **B.** Sparse partial least squares discriminant analysis (sPLS-DA) score plot showing group separation based on plasma lipid profiles. **C.** Volcano plot depicting differentially expressed lipids between NR and OW groups (t-test, $p < 0.05$). **D.** Receiver operating characteristic (ROC) curve highlighting TG (10:0/10:0/18:1) as a potential discriminator between NR and OW groups, showing the highest area under the curve (AUC)

4.4 Discussion

Human blood plays a critical role as a biomarker in both clinical and research settings [26]. Plasma, a self-renewing biological fluid, is easy to collect and poses minimal health risks [27,28]. In recent years, MS-based lipidomics techniques have become widely adopted for the identification and quantification of hundreds to thousands of lipid species in plasma [29]. However, before investigating lipidomic changes related to disease, it is important to first understand the natural variability of the lipidome in

healthy individuals, taking into account factors such as age, sex, and body weight. Several studies have demonstrated that these factors, including sex, age, and weight, play significant roles in shaping the plasma lipid profile over time [30]. The findings of this study are represented in a lipid biosynthesis pathway, as shown in **Appendix Figure 5.1**. The biosynthetic origins of the identified lipid classes have been described in **Chapter 4 Section 4.4.**

SFAs are known to play critical roles in regulating protein activation, protein-membrane interactions, and gene transcription, which are essential for metabolism and various biological functions [31]. As shown in **Figure 5.3**, no significant differences in SFA levels were observed between boys and girls in the study. However, a distinct pattern emerged when the data were stratified by age groups. Notably, the 9-year-old group exhibited significantly higher levels of SFAs compared to the other age groups in both boys and girls. In contrast, SFA levels showed a decreasing trend with advancing age across both sexes. Previous research has demonstrated that FFAs, are elevated in plasma samples from younger age groups, such as newborns, and also tend to be higher in females [32-34]. In a study focusing on various age groups, from newborns to young adults, plasma samples revealed elevated levels of SFA levels in younger age groups compared with other age groups [32]. Our results from plasma samples of pre-adolescent children are consistent with earlier studies. Additionally, in line with a previous analysis of serum samples, no significant difference in SFA levels was found between boys and girls [35]. The higher SFA levels observed in younger individuals compared to older ones can be linked to several factors, such as differences in diet, metabolism, hormonal changes associated with growth and development, and variations in physical activity levels [36]. These factors likely contribute to the elevated plasma SFA levels seen in younger individuals. On the other hand, MUFAs play an important role in improving cholesterol levels, reducing inflammation, regulating blood sugar, supporting weight management, and enhancing the absorption of fat-soluble vitamins. PUFAs, particularly ω-3 and ω-6, are beneficial for cognitive function, mood regulation, TGs levels, blood pressure, blood clot prevention, and overall eye and skin health [37]. In our study, there were no significant differences in the levels of total MUFAs and PUFAs, including ω-3 and ω-6, between boys and girls, or across different age groups in children (**Figure 5.3**). These results are consistent with previous studies that reported similar PUFAs levels in blood

samples from a large cohort of 160,000 individuals ranging from 10 to 99 years of age [38]. The consistency in FAs profiles across demographic categories can likely be attributed to common physiological factors, similar hormonal influences, stable dietary habits, genetic predispositions, and methodological aspects that affect FA metabolism and distribution [39]. While the exact cause of this consistency remains unclear, multiple factors could contribute to the stable FAs composition observed in previous studies. Additionally, when compared to blood samples from adults and newborns, the total levels of MUFAs in children's samples were significantly lower [40].

GPs are essential components of cell membranes and serve as precursors for signaling molecules that play a critical role in various cellular and physiological functions [6]. Plasmalogens, a specific type of GPs, are known for their antioxidant properties, providing protective effects on cells, plasma, and tissues by reducing oxidative stress [41]. Our analysis revealed distinct differences in lipid classes across age groups for both boys and girls (**Figure 5.4**). PEs, which are the second most abundant PLs class in cells and biofluids [42], played a significant role in differentiating age groups in both sexes. Specifically, PE molecular species were elevated in the 11-year-old group, while PSs species showed an increase in the 12-year-old group compared to the 9-year-old group across both sexes. Notably, PE (O-17:1/20:4) and PE (O-18:2/20:5) displayed patterns similar to those observed in previous studies of blood samples from children aged 0–13 years [21]. Previous research on serum samples from healthy individuals revealed an increase in specific molecular species of PE in elderly and young Japanese individuals of both sexes [35]. Moreover, a recent study identified a sex-dependent, age-related increase in PLs, including PC and PE, with a more pronounced rise in females compared to males. This age-related increase may be attributed to a combination of physiological and developmental factors, such as hormonal changes, shifts in dietary habits, metabolic adjustments associated with growth, and biological processes occurring during puberty [33]. Additionally, genetic and environmental factors could further influence the distinct lipid profiles observed in different age groups [43].

SPs are essential components of cell membranes and function as signaling molecules within cells [44]. Notably, low levels of certain SM molecular species have been associated with an increased risk of T2D, CVD, and NDs [45,46]. Age was also strongly correlated with Cer and HexCer species, which are produced via an alternative

de novo sphingolipid synthesis pathway [3]. Cer and HexCer play a vital role in maintaining the integrity, function, and adaptability of cell membranes, which are critical for cellular and tissue health [47]. In our study, we observed that the levels of Cer, SM, and HexCer were elevated in the plasma samples of 10-year-old boys and girls (**Figure 5.4**). A previous study observed that SM levels were higher in elder females compared to elder males, while the levels between young and elderly females remained similar. The study also found that young children with lower sex hormone levels displayed sex-related differences in plasma SM concentrations. In contrast, Cer species showed age-related increases in serum samples from male subjects [48]. Additionally, certain SM molecular species, such as SM 32:1, were found to be reduced in individuals with T2D [45].

TG that contains SFAs are metabolized through β-oxidation in the mitochondria, a process that becomes less efficient with age due to the impaired activity of β-oxidation enzymes [49]. A recent study has highlighted that higher levels of certain TG molecular species are associated with an increased risk of type 2 diabetes (T2D) [35,50]. It was also found that elder individuals tend to have higher serum levels of these TG species compared to younger individuals, which aligns with the results observed in this study. Additionally, the plasma concentrations of TG species, particularly TG (10:0/10:0/18:1), were found to be higher in boys compared to girls. Despite this, the precise role of lipid species in obesity-related metabolic changes is still not fully understood [51]. In this study, samples were categorized based on their POW. The data showed that the majority of TG species, such as TG (10:0/10:0/18:1), were significantly higher in the OW group compared to the NR and UW groups (**Figure 3.5**). These findings are in agreement with previous studies linking increased TG levels to overweight status [52], reinforcing the strong connection between TG levels and body weight.

The choice between fasting and non-fasting samples for lipid measurements is largely dependent on the clinical context. For example, non-fasting samples are preferred when diagnosing metabolic syndrome or assessing initial risks in untreated primary prevention patients. On the other hand, fasting samples are typically required for patients with a family history of genetic hyperlipidemia [53]. Non-fasting lipid measurements offer several advantages, including simplifying blood sampling for both patients and clinicians, which can lead to improved patient compliance with lipid testing. Nordestgaard et al.. conducted a study that showed fasting is not routinely necessary for determining lipid

profiles. They suggested that non-fasting blood samples can be effectively used for assessing plasma lipid profiles [54]. A study by de Vries et al. further supported the use of non-fasting lipid profiles, indicating that they are acceptable for determining lipid-lowering therapy, assessing CVD risk, and addressing discrepancies between primary and lipid disorders [55]. Additionally, a prospective study involving 26,509 healthy women in the United States found that non-fasting blood TG levels were more strongly associated with cardiovascular events than fasting TG levels [56]. Szternel et al. conducted a study that established reference values for non-fasting lipid parameters in healthy children aged 9-11 years, underscoring the significance of non-fasting lipid measurements for assessing CVD risk in pediatric populations [57]. Similarly, a study of 356 French-Canadian children aged 6 to 13 years provided reference intervals for lipid markers, taking into account age, sex, and puberty stage, further supporting the use of non-fasting plasma samples for screening purposes [58]. These studies collectively emphasize the importance of obtaining non-fasting blood lipid levels, highlighting their relevance in clinical assessments compared to fasting samples. Therefore, despite the relatively small sample size, our study presents the first report on non-fasting plasma lipid profiles in a Japanese pediatric population.

This study provides important insights into the lipid classes present in plasma samples from pre-adolescent children, categorized by sex, age, and weight groups, along with a detailed analysis of lipid composition. However, several limitations must be acknowledged. One such limitation is the semi-quantitative nature of the reported lipid concentrations, which are not absolute values. Additionally, the use of non-fasting plasma samples in this study may introduce variability in lipid profiles. The lipid composition in plasma can be influenced by various factors, including diet, physical activity, genetic predispositions, and family history, none of which were accounted for in this study. Additionally, while a range of molecular species from SPs, GLs, and FAs were identified in the plasma samples from both boys and girls, the exact mechanisms driving their metabolism remain unclear. Despite these limitations, this study provides a thorough lipid profiling of plasma from preadolescent children, highlighting variations across sex, age, and percentage of overweight groups. A key strength of this research is the use of untargeted LC/MS, which enabled the identification of capric acid-containing TG as a

potential plasma biomarker for childhood obesity. However, further validation is needed to establish the clinical significance and reproducibility of these findings.

4.5 Conclusion

In this study, lipid profiles in plasma samples from pre-adolescent children were compared across different sexes, age groups, and weight categories. The findings revealed unique lipid composition patterns within the 9-12-year-old age range for both boys and girls. Significant differences in SFA levels were observed, particularly between the 9-year-old children and those in other age groups. Moreover, certain SPs such as Cer, HexCer, and SM, and PLs like PI were found to be more abundant in the plasma of children aged 10 compared to other age groups. In addition, plasma TG and PS levels were found to increase within the 9 to 12-year age range. Notably, children classified as OW showed elevated TG levels compared to those in the NR, with TG (10:0/10:0/18:1) emerging as a potential biomarker for childhood obesity. In summary, this study revealed significant lipidome variations, demonstrating the utility of untargeted lipid profiling using HPLC/LTQ-MS for comprehensive lipid analysis in pre-adolescent plasma samples. The findings provide valuable insights into sex, age, and weight-specific lipid metabolism patterns in pre-adolescent children.

References

1. Amin, K. A., Homeida, A. M., El Mazoudy, R. H., Hashim, K. S., & Garelnabi, M. (2019). Dietary Lipids in Health and Disease. Journal of lipids, 2019, 5729498.
2. Yoon, H., Shaw, J. L., Haigis, M. C., & Greka, A. (2021). Lipid metabolism in sickness and in health: Emerging regulators of lipotoxicity. Molecular cell, 81(18), 3708–3730.
3. Koletzko, B., Demmelmair, H., & Socha, P. (1998). Nutritional support of infants and children: supply and metabolism of lipids. Bailliere's clinical gastroenterology, 12(4), 671–696.
4. Uauy, R., & Castillo, C. (2003). Lipid requirements of infants: implications for nutrient composition of fortified complementary foods. The Journal of nutrition, 133(9), 2962S–72S.
5. GBD 2016 Causes of Death Collaborators (2017). Global, regional, and national age-sex specific mortality for 264 causes of death, 1980-2016: a systematic analysis for the Global Burden of Disease Study 2016. Lancet (London, England), 390(10100), 1151–1210.
6. Quehenberger, O., & Dennis, E. A. (2011). The human plasma lipidome. The New England journal of medicine, 365(19), 1812–1823.
7. Fahy, E., Subramaniam, S., Murphy, R. C., Nishijima, M., Raetz, C. R., Shimizu, T., Spener, F., van Meer, G., Wakelam, M. J., & Dennis, E. A. (2009). Update of the LIPID MAPS comprehensive classification system for lipids. Journal of lipid research, 50 Suppl(Suppl), S9–S14.
8. Maekawa, K., Okemoto, K., Ishikawa, M., Tanaka, R., Kumagai, Y., & Saito, Y. (2017). Plasma Lipidomics of Healthy Japanese Adults Reveals Gender- and Age-Related Differences. Journal of pharmaceutical sciences, 106(9), 2914–2918.
9. Eichelmann, F., Sellem, L., Wittenbecher, C., Jäger, S., Kuxhaus, O., Prada, M., Cuadrat, R., Jackson, K. G., Lovegrove, J. A., & Schulze, M. B. (2022). Deep Lipidomics in Human Plasma: Cardiometabolic Disease Risk and Effect of Dietary Fat Modulation. Circulation, 146(1), 21–35.
10. Hegele, R. A., & Tsimikas, S. (2019). Lipid-Lowering Agents. Circulation research, 124(3), 386–404.

11. Kim, M., Nevado-Holgado, A., Whiley, L., Snowden, S. G., Soininen, H., Kloszewska, I., Mecocci, P., Tsolaki, M., Vellas, B., Thambisetty, M., Dobson, R. J. B., Powell, J. F., Lupton, M. K., Simmons, A., Velayudhan, L., Lovestone, S., Proitsi, P., & Legido-Quigley, C. (2017). Association between plasma ceramides and phosphatidylcholines and hippocampal brain volume in late onset Alzheimer's disease. Journal of Alzheimer's Disease, 60(3), 809-817.

12. Kühn, T., Floegel, A., Sookthai, D., Johnson, T., Rolle-Kampczyk, U., Otto, W., von Bergen, M., Boeing, H., & Kaaks, R. (2016). Higher plasma levels of lysophosphatidylcholine 18:0 are related to a lower risk of common cancers in a prospective metabolomics study. BMC medicine, 14, 13.

13. Fan, M., Sidhu, R., Fujiwara, H., Tortelli, B., Zhang, J., Davidson, C., Walkley, S. U., Bagel, J. H., Vite, C., Yanjanin, N. M., Porter, F. D., Schaffer, J. E., & Ory, D. S. (2013). Identification of Niemann-Pick C1 disease biomarkers through sphingolipid profiling. Journal of lipid research, 54(10), 2800–2814.

14. Eichelmann, F., Prada, M., Sellem, L., Jackson, K. G., Salas Salvadó, J., Razquin Burillo, C., Estruch, R., Friedén, M., Rosqvist, F., Risérus, U., Rexrode, K. M., Guasch-Ferré, M., Sun, Q., Willett, W. C., Martinez-Gonzalez, M. A., Lovegrove, J. A., Hu, F. B., Schulze, M. B., & Wittenbecher, C. (2024). Lipidome changes due to improved dietary fat quality inform cardiometabolic risk reduction and precision nutrition. Nature medicine, 30(10), 2867–2877.

15. Latino, F., Cataldi, S., Carvutto, R., De Candia, M., D'Elia, F., Patti, A., Bonavolontà, V., & Fischetti, F. (2021). The Importance of Lipidomic Approach for Mapping and Exploring the Molecular Networks Underlying Physical Exercise: A Systematic Review. International journal of molecular sciences, 22(16), 8734.

16. Venäläinen, T. M., Viitasalo, A. M., Schwab, U. S., Eloranta, A. M., Haapala, E. A., Jalkanen, H. P., de Mello, V. D., Laaksonen, D. E., Lindi, V. I., Ågren, J. J., & Lakka, T. A. (2016). Effect of a 2-y dietary and physical activity intervention on plasma fatty acid composition and estimated desaturase and elongase activities in children: the Physical Activity and Nutrition in Children Study. The American journal of clinical nutrition, 104(4), 964–972.

17. San Martin, R., Brandao, C. F. C., Junqueira-Franco, M. V. M., Junqueira, G. P., de Freitas, E. C., de Carvalho, F. G., Rodrigues, C. H. P., Aguesse, A., Billon-Crossouard,

S., Krempf, M., Croyal, M., & Marchini, J. S. (2022). Untargeted lipidomic analysis of plasma from obese women submitted to combined physical exercise. Scientific reports, 12(1), 11541.

18. Zhang, H., Liu, J., Cui, M., Chai, H., Chen, L., Zhang, T., Mi, J., Guan, H., & Zhao, L. (2023). Moderate-intensity continuous training has time-specific effects on the lipid metabolism of adolescents. Journal of translational internal medicine, 11(1), 57–69.

19. Tabassum, R., Rämö, J. T., Ripatti, P., Koskela, J. T., Kurki, M., Karjalainen, J., Palta, P., Hassan, S., Nunez-Fontarnau, J., Kiiskinen, T. T. J., Söderlund, S., Matikainen, N., Gerl, M. J., Surma, M. A., Klose, C., Stitziel, N. O., Laivuori, H., Havulinna, A. S., Service, S. K., Salomaa, V., … Ripatti, S. (2019). Genetic architecture of human plasma lipidome and its link to cardiovascular disease. Nature communications, 10(1), 4329.

20. Dai, S., Fulton, J. E., Harrist, R. B., Grunbaum, J. A., Steffen, L. M., & Labarthe, D. R. (2009). Blood lipids in children: age-related patterns and association with body-fat indices: Project HeartBeat!. American journal of preventive medicine, 37(1 Suppl), S56–S64.

21. Ferreira, H. B., Melo, T., Rocha, H., Paiva, A., Domingues, P., & Domingues, M. R. (2023). Lipid profile variability in children at different ages measured in dried blood spots. Molecular omics, 19(3), 229–237.

22. Wang, Y., Jiang, C. T., Song, J. Y., Song, Q. Y., Ma, J., & Wang, H. J. (2019). Lipidomic Profile Revealed the Association of Plasma Lysophosphatidylcholines with Adolescent Obesity. BioMed research international, 2019, 1382418.

23. Kishi, R., Sasaki, S., Yoshioka, E., Yuasa, M., Sata, F., Saijo, Y., Kurahashi, N., Tamaki, J., Endo, T., Sengoku, K., Nonomura, K., Minakami, H., & Hokkaido Study on Environment and Children's Health (2011). Cohort profile: the Hokkaido study on environment and children's health in Japan. International journal of epidemiology, 40(3), 611–618.

24. Goudarzi, H., Ikeda-Araki, A., Bamai, Y. A., Ito, S., Inao, T., Yokota, I., Miyashita, C., Kishi, R., & Konno, S. (2023). Potential determinants of T helper 2 markers and their distribution in school-aged children. Allergology international : official journal of the Japanese Society of Allergology, 72(1), 100–106.

25. Masubuchi, R., Noda, M., Yoshida, S., & Kawakami, K. (2022). Longitudinal study of body mass index and percentage of overweight in Japanese children grouped by maturity. Endocrine journal, 69(4), 451–461.

26. Montoliu, I., Scherer, M., Beguelin, F., DaSilva, L., Mari, D., Salvioli, S., Martin, F. P., Capri, M., Bucci, L., Ostan, R., Garagnani, P., Monti, D., Biagi, E., Brigidi, P., Kussmann, M., Rezzi, S., Franceschi, C., & Collino, S. (2014). Serum profiling of healthy aging identifies phospho- and sphingolipid species as markers of human longevity. Aging, 6(1), 9–25.

27. Yang, K., & Han, X. (2016). Lipidomics: Techniques, Applications, and Outcomes Related to Biomedical Sciences. Trends in biochemical sciences, 41(11), 954–969.

28. Burla, B., Arita, M., Arita, M., Bendt, A. K., Cazenave-Gassiot, A., Dennis, E. A., Ekroos, K., Han, X., Ikeda, K., Liebisch, G., Lin, M. K., Loh, T. P., Meikle, P. J., Orešič, M., Quehenberger, O., Shevchenko, A., Torta, F., Wakelam, M. J. O., Wheelock, C. E., & Wenk, M. R. (2018). MS-based lipidomics of human blood plasma: a community-initiated position paper to develop accepted guidelines. Journal of lipid research, 59(10), 2001–2017.

29. Brügger B. (2014). Lipidomics: analysis of the lipid composition of cells and subcellular organelles by electrospray ionization mass spectrometry. Annual review of biochemistry, 83, 79–98.

30. Lamichhane, S., Ahonen, L., Dyrlund, T. S., Kemppainen, E., Siljander, H., Hyöty, H., Ilonen, J., Toppari, J., Veijola, R., Hyötyläinen, T., Knip, M., & Oresic, M. (2018). Dynamics of Plasma Lipidome in Progression to Islet Autoimmunity and Type 1 Diabetes - Type 1 Diabetes Prediction and Prevention Study (DIPP). Scientific reports, 8(1), 10635.

31. Legrand, P., & Rioux, V. (2010). The complex and important cellular and metabolic functions of saturated fatty acids. Lipids, 45(10), 941–946.

32. Jakobik, V., Burus, I., & Decsi, T. (2009). Fatty acid composition of erythrocyte membrane lipids in healthy subjects from birth to young adulthood. European journal of pediatrics, 168(2), 141–147.

33. Slade, E., Irvin, M. R., Xie, K., Arnett, D. K., Claas, S. A., Kind, T., Fardo, D. W., & Graf, G. A. (2021). Age and sex are associated with the plasma lipidome: findings from the GOLDN study. Lipids in health and disease, 20(1), 30.

34. Schienkiewitz, A., Truthmann, J., Ernert, A., Wiegand, S., Schwab, K. O., & Scheidt-Nave, C. (2019). Age, maturation and serum lipid parameters: findings from the German Health Survey for Children and Adolescents. BMC public health, 19(1), 1627.
35. Kawanishi, N., Kato, Y., Yokozeki, K., Sawada, S., Sakurai, R., Fujiwara, Y., Shinkai, S., Goda, N., & Suzuki, K. (2018). Effects of aging on serum levels of lipid molecular species as determined by lipidomics analysis in Japanese men and women. Lipids in health and disease, 17(1), 135.
36. Te Morenga, L., & Montez, J. M. (2017). Health effects of saturated and trans-fatty acid intake in children and adolescents: Systematic review and meta-analysis. PloS one, 12(11), e0186672.
37. Kharazmi-Khorassani, J., Ghafarian Zirak, R., Ghazizadeh, H., Zare-Feyzabadi, R., Kharazmi-Khorassani, S., Naji-Reihani-Garmroudi, S., Kazemi, E., Esmaily, H., Javan-Doust, A., Banpour, H., Mohammadi-Bajgiran, M., Besharatlou, M. R., Ferns, G. A., Hashemi, M., & Ghayour-Mobarhan, M. (2021). The role of serum monounsaturated fatty acids (MUFAs) and polyunsaturated fatty acids (PUFAs) in cardiovascular disease risk. Acta bio-medica : Atenei Parmensis, 92(2), e2021049.
38. Harris, W. S., Pottala, J. V., Varvel, S. A., Borowski, J. J., Ward, J. N., & McConnell, J. P. (2013). Erythrocyte omega-3 fatty acids increase and linoleic acid decreases with age: observations from 160,000 patients. Prostaglandins, leukotrienes, and essential fatty acids, 88(4), 257–263.
39. Ponnampalam, E. N., Sinclair, A. J., & Holman, B. W. B. (2021). The Sources, Synthesis and Biological Actions of Omega-3 and Omega-6 Fatty Acids in Red Meat: An Overview. Foods (Basel, Switzerland), 10(6), 1358.
40. Risé, P., Tragni, E., Ghezzi, S., Agostoni, C., Marangoni, F., Poli, A., Catapano, A. L., Siani, A., Iacoviello, L., Galli, C., IDEFICS Consortium, & CHECK group (2013). Different patterns characterize Omega 6 and Omega 3 long chain polyunsaturated fatty acid levels in blood from Italian infants, children, adults and elderly. Prostaglandins, leukotrienes, and essential fatty acids, 89(4), 215–220.
41. Lee, J., & Choe, E. (2011). Effects of phospholipids on the antioxidant activity of α-tocopherol in the singlet oxygen oxidation of canola oil. New biotechnology, 28(6), 691–697.

42. Calzada, E., Onguka, O., & Claypool, S. M. (2016). Phosphatidylethanolamine Metabolism in Health and Disease. International review of cell and molecular biology, 321, 29–88.

43. Wong, M. W., Thalamuthu, A., Braidy, N., Mather, K. A., Liu, Y., Ciobanu, L., Baune, B. T., Armstrong, N. J., Kwok, J., Schofield, P., Wright, M. J., Ames, D., Pickford, R., Lee, T., Poljak, A., & Sachdev, P. S. (2020). Genetic and environmental determinants of variation in the plasma lipidome of older Australian twins. eLife, 9, e58954.

44. Khavandgar, Z., & Murshed, M. (2015). Sphingolipid metabolism and its role in the skeletal tissues. Cellular and molecular life sciences : CMLS, 72(5), 959–969.

45. Holland, W. L., & Summers, S. A. (2008). Sphingolipids, insulin resistance, and metabolic disease: new insights from in vivo manipulation of sphingolipid metabolism. Endocrine reviews, 29(4), 381–402.

46. Gonzalez-Covarrubias, V., Beekman, M., Uh, H. W., Dane, A., Troost, J., Paliukhovich, I., van der Kloet, F. M., Houwing-Duistermaat, J., Vreeken, R. J., Hankemeier, T., & Slagboom, E. P. (2013). Lipidomics of familial longevity. Aging cell, 12(3), 426–434.

47. Yang, F., & Chen, G. (2022). The nutritional functions of dietary sphingomyelin and its applications in food. Frontiers in nutrition, 9, 1002574.

48. Avela, H. F., & Sirén, H. (2020). Advances in lipidomics. Clinica chimica acta; international journal of clinical chemistry, 510, 123–141.

49. Rhee, E. P., Cheng, S., Larson, M. G., Walford, G. A., Lewis, G. D., McCabe, E., Yang, E., Farrell, L., Fox, C. S., O'Donnell, C. J., Carr, S. A., Vasan, R. S., Florez, J. C., Clish, C. B., Wang, T. J., & Gerszten, R. E. (2011). Lipid profiling identifies a triacylglycerol signature of insulin resistance and improves diabetes prediction in humans. The Journal of clinical investigation, 121(4), 1402–1411.

50. Rangel-Huerta, O. D., Pastor-Villaescusa, B., & Gil, A. (2019). Are we close to defining a metabolomic signature of human obesity? A systematic review of metabolomics studies. Metabolomics : Official journal of the Metabolomic Society, 15(6), 93.

51. Rauschert, S., Uhl, O., Koletzko, B., Kirchberg, F., Mori, T. A., Huang, R. C., Beilin, L. J., Hellmuth, C., & Oddy, W. H. (2016). Lipidomics Reveals Associations of

Phospholipids With Obesity and Insulin Resistance in Young Adults. The Journal of clinical endocrinology and metabolism, 101(3), 871–879.

52. Mousa, A., Naderpoor, N., Mellett, N., Wilson, K., Plebanski, M., Meikle, P. J., & de Courten, B. (2019). Lipidomic profiling reveals early-stage metabolic dysfunction in overweight or obese humans. Biochimica et biophysica acta. Molecular and cell biology of lipids, 1864(3), 335–343.

53. Driver, S. L., Martin, S. S., Gluckman, T. J., Clary, J. M., Blumenthal, R. S., & Stone, N. J. (2016). Fasting or Nonfasting Lipid Measurements: It Depends on the Question. Journal of the American College of Cardiology, 67(10), 1227–1234.

54. Nordestgaard, B. G., Langsted, A., Mora, S., Kolovou, G., Baum, H., Bruckert, E., Watts, G. F., Sypniewska, G., Wiklund, O., Borén, J., Chapman, M. J., Cobbaert, C., Descamps, O. S., von Eckardstein, A., Kamstrup, P. R., Pulkki, K., Kronenberg, F., Remaley, A. T., Rifai, N., Ros, E., … European Atherosclerosis Society (EAS) and the European Federation of Clinical Chemistry and Laboratory Medicine (EFLM) joint consensus initiative (2016). Fasting is not routinely required for determination of a lipid profile: clinical and laboratory implications including flagging at desirable concentration cut-points-a joint consensus statement from the European Atherosclerosis Society and European Federation of Clinical Chemistry and Laboratory Medicine. European heart journal, 37(25), 1944–1958.

55. de Vries, M., Klop, B., & Castro Cabezas, M. (2014). The use of the non-fasting lipid profile for lipid-lowering therapy in clinical practice - point of view. Atherosclerosis, 234(2), 473–475.

56. Bansal, S., Buring, J. E., Rifai, N., Mora, S., Sacks, F. M., & Ridker, P. M. (2007). Fasting compared with nonfasting triglycerides and risk of cardiovascular events in women. JAMA, 298(3), 309–316.

57. Szternel, Ł., Kwasigroch, M., Murawska, K., Dereziński, T., & Sypniewska, G. (2020). The cut-off values for non-fasting routine lipid parameters in presumably healthy 9–11-year-old children. Medical Research Journal, 5(1), 15-18.

58. Bouhour, S., Plantefève, R., Gillet, V., Abolghasemi, A., Bouchouirab, F. Z., Baccarelli, A. A., Takser, L., & Çaku, A. (2024). Establishing non-fasting reference values for plasma lipids levels based on age, sex, and puberty stage in a French-Canadian pediatric population. Lipids in health and disease, 23(1), 54.

Chapter 6

Discovery of wakame-derived bioactive compounds for obesity control: targeting sphingomyelin synthase (SMS)

6.1 Introduction

Obesity has emerged as a global epidemic and a major public health burden, primarily due to its strong association with a wide spectrum of chronic metabolic disorders, including T2D mellitus, CVD, non-alcoholic fatty liver disease, and various cancers [1]. The World Health Organization WHO estimates that more than 650 million adults worldwide are classified as overweight or obese, accounting for one in eight individuals living with obesity (https://www.who.int/news-room/fact-sheets/detail/obesity-and-overweight). Despite the availability of lifestyle interventions and pharmacological therapies, the global prevalence of obesity continues to rise, highlighting the urgent need for novel, safe, and effective therapeutic strategies. Emerging evidence indicates that dysregulation of lipid metabolism plays a crucial role in the development of obesity and related metabolic disorders. SPs are a major class of lipids, comprising diverse metabolites that play a key role in regulating various cellular processes and physiological functions [2]. Alterations in sphingolipid metabolism have been linked to various metabolic disorders such as obesity, abnormal lipid profiles, insulin resistance, CVD, and T2D [3]. One of the key enzymes involved in sphingolipid metabolism is sphingomyelin synthase (SMS), which catalyzes the conversion of Cer and PC into SM and DG [4].

In mammals, SMS is expressed in three isoforms: SMS1, SMS2, and SMSr [5]. Although SMS1 and SMS2 share approximately 57% sequence similarity and have identical enzyme activities, but different subcellular locations [6]. SMS1 functions predominantly in the Golgi apparatus, whereas SMS2 operates at the plasma membrane [7,8]. Recent studies in a murine model have shown that SMS deficiency inhibits the progression of atherosclerosis [9], insulin resistance [10], and obesity [11], whereas *in vitro* SMS suppression attenuates endotoxin-mediated macrophage inflammation and atherosclerosis [12]. Therefore, targeting SMS represents a potential therapeutic approach for treating metabolic disorders, including obesity, and the identification of effective SMS inhibitors offers a promising strategy for discovering novel anti-obesity agents. The discovery of potent SMS inhibitors remains in its nascent phase, with only a limited number of both natural and synthetic molecules reported so far [13]. Among natural sources, ginkgolic acid (GA) from Ginkgo biloba leaves [14], and malabaricanes A-C and E, derived from the fruits of M. cinnamomea [15], have demonstrated potent SMS-inhibitory activity. However, GA is associated with toxicity concerns, limiting its

potential for further development as a therapeutic drug [16]. These limitations emphasize the urgent need to discover new, safer, and more efficacious SMS inhibitors, especially those derived from natural products.

Marine organisms, particularly seaweeds, constitute a largely underexplored but promising source of novel SMS inhibitors. Seaweed has been an essential part of traditional diets, particularly in East Asia, where it is consumed in various forms. It has also been used in traditional medicine to address various disorders, owing to its rich nutrient profile and bioactive compounds [17]. Recent studies suggest that seaweed consumption is associated with a reduced risk of CVD and plays a crucial role in promoting longevity, particularly in Japanese populations where seaweed is a regular component of the diet [18, 19]. Although seaweed offers various health benefits, its therapeutic potential in obesity management, especially through the regulation of lipid metabolism, remains limited.

In this study, we aim to investigate the bioactive potential of *Undaria pinnatifida* (wakame), a brown seaweed, by specifically assessing the anti-obesity properties of its bioactive compounds, with a particular focus on their ability to inhibit SMS. The results were further validated through *in-silico* molecular docking and dynamics simulation studies. This study underscores the potential of wakame-derived bioactive compounds as natural SMS inhibitors, offering new insights into the development of functional foods and nutraceuticals for obesity management and other metabolic disorders.

6.2 Materials and Methods

6.2.1 Materials

Dried wakame seaweed was sourced from a commercial vendor based in Sapporo, Japan. LC/MS-grade solvents, including isopropanol, chloroform, and methanol, were procured from Wako Pure Chemical Industries, Ltd (Osaka, Japan). Ammonium acetate (1 mol/L, eluent additive for LC/MS) was purchased from Sigma-Aldrich (St Louis, MO, USA). Deuterated chloroform ($CDCl_3$) was purchased from Kanto Chemical Co., Ltd. C6-Cer (d18:1/6:0) and C6-SM (d18:1/6:0) were purchased from Avanti Polar Lipids, Inc. (Alabaster, USA). The protease inhibitor cocktail (EDTA-free) was sourced from Nacalai Tesuque, Inc. (Kyoto, Japan), while bovine serum albumin (BSA) was purchased from

Thermo Fisher Scientific (Tokyo, Japan). Thin-layer chromatography (TLC) silica gel plates of 0.2 mm thickness were purchased from Merck KGaA, Darmstadt, Germany.

6.2.2 NMR and LC/MS analysis

NMR spectra of the purified compound were acquired using a JEOL 400 MHz spectrometer maintained at 25 °C, utilizing $CDCl_3$ as the solvent and tetramethylsilane (TMS) as the IS. Chemical shift values (δ) are reported in parts per million (ppm), and coupling constants (J) are given in Hertz (Hz), referenced to $CDCl_3$ (^1H at δ 7.26 ppm) and TMS. The LC/MS analysis of the purified compound employed for HRMS analysis in negative ion mode as described in **Chapter 2, Section 2.2.5.**

6.2.3 Extraction of *Undaria pinnatifida* (wakame)

The extraction protocol applied to *U. pinnatifida* (wakame) was adapted from a conventional method previously employed for isolating daurichromenic acid from the traditional Chinese medicinal plant Rhododendron dauricum [20]. One kilogram of commercially procured dried wakame was finely ground using a mechanical mill and transferred into a 2-liter beaker. The powdered seaweed was subjected to three successive extractions with 2 L of methanol at room temperature, each lasting 24 hours. The combined methanol extracts were then concentrated under reduced pressure. The resulting residue was dissolved in 500 mL of 20% MeOH in Milli-Q and subsequently partitioned three times with 200 mL each of hexane, diethyl ether (Et_2O), and ethyl acetate (EtOAc). Following solvent evaporation, the residues from hexane, Et_2O, EtOAc, and water were evaluated for SMS activity. Further assessment of their activity was conducted using an SMS inhibition assay. The active fraction was further purified through column chromatography using Silica Gel 60 N (spherical, neutral) with a particle size of 40–50 μm (Kanto Chemicals) to isolate the purified SMS inhibitor.

6.2.4 Cell culture and protein assay

HeLa cells stably expressing human SMS1 or SMS2 (hSMS1 or hSMS2) were cultured in Minimum Essential Medium supplemented with 10% (v/v) fetal bovine serum and 1% penicillin-streptomycin-neomycin antibiotic mixture, with all components obtained from Thermo Fisher Scientific (Tokyo, Japan). These cells were kept at 37 °C in a moisture-controlled atmosphere with 5% carbon dioxide. To determine cellular protein

content, cells were collected by centrifugation at 1000 rpm for 10 min and stored at –80 °C until further analysis. For protein quantification, the cell pellet was resuspended in 1 mL of 20 mM Tris buffer (pH 7.5) and vortexed thoroughly. An aliquot of 25 µL from the resulting lysate was dispensed into a 96-well microplate in triplicate. The assay reagent was prepared by mixing reagents A and B from the Bicinchoninic Acid Protein Assay Kit (Thermo Fisher Scientific) in a 50:1 ratio, and 200 µL of this reagent was added to each well. The plate was incubated at 37 °C for 30 min, after which absorbance was measured at 562 nm using a Wallac 1420 ARVO Mx microplate reader. A standard curve was created using serial dilutions of bovine serum albumin from a 2000 µg/mL stock to concentrations of 2000, 1000, 100, 10, 1, and 0.1 µg/mL in phosphate-buffered saline. The absorbance values of these standards were measured under the same conditions and used to estimate the protein concentrations of the cell lysates. All cell handling and protein assay procedures were conducted following previously published protocols without modification [21].

6.2.5 *In-vitro* SMS assay

The *in vitro* SMS activity assay was carried out based on a previously reported LC-MS/MS-based method developed by our team [21]. For the assay, HeLa/hSMS1 and HeLa/hSMS2 cells were lysed in a buffer containing 20 mM Tris-HCl (pH 7.5) supplemented with a Complete™ protease inhibitor cocktail, followed by sonication for 5 seconds, and the resulting lysates were adjusted to a protein concentration of 0.1 µg/µL. Briefly, 100 µL of an aliquot of each cell lysate with a known protein concentration was transferred into a 1.5-mL Eppendorf tube in quadruplicate, and 1 µL of the inhibitor (initial concentration: 10 mg/mL in DMSO) was added. These mixtures were incubated at 37 °C for 30 min, followed by the addition of 1 µL of C6-Cer (5 µM solution in ethanol). The enzymatic reactions were allowed to proceed for an additional 60 min at 37 °C. To stop the reaction, 350 µL of a chloroform: methanol mixture (2:1, v/v) was added. The samples were vortexed at 1300 rpm for 10 min and centrifuged at 15,000 rpm for 5 min. The lower chloroform phase, containing lipids, was carefully transferred to a new Eppendorf tube. The organic solvents were evaporated under reduced pressure at 4 °C. The dried lipid residues were redissolved in 100 µL of methanol, vortexed for 5 min, and centrifuged again at 15,000 rpm for 10 min. The resulting supernatants were transferred

into LC vials and analyzed on a TSQ Quantum Access triple quadrupole MS (Thermo Fisher Scientific, Waltham, MA, USA) operating in positive electrospray ionization mode. Data acquisition and processing were performed using Xcalibur 2.2 software to extract ion chromatograms and quantify signal intensities for C6-Cer and C6-SM. All procedures followed the established assay protocol without any modifications [21].

6.2.6 *In-silico* molecular docking studies

Molecular docking studies were conducted using previously optimized structural models of the SMS1 and SMS2 enzymes developed by our research group. The purpose of this analysis was to evaluate the interaction between the EPA and the refined SMS1 and SMS2 protein structures, employing AutoDock Vina version 1.5.6 [22]. The 2D molecular structure of EPA was first constructed using the Marvin JS tool and subsequently converted into PDB format. Ligand preparation was carried out in AutoDock Vina, and the structures were saved in PDBQT format for docking analysis. The optimized SMS1 and SMS2 proteins were accessed in PDB format, with associated molecules eliminated during the protein configuration enhancement procedure. Hydrogen atoms were added to the protein structures using AutoDock Vina 1.5.6. A defined grid box was established to target the active site of each receptor. For SMS1, the grid center was set at x = 3.16, y = 1.03, and z = 11.48; for SMS2, the coordinates were x = 12.25, y = 4.58, and z = –6.05. Molecular docking analysis was carried out with AutoDock Vina, and the binding affinities were expressed in kcal/mol [22]. The binding interactions were evaluated and visualized using Biovia Discovery Studio 2021 software [23].

6.2.7 *In-silico* molecular dynamic studies

To further validate the binding stability of the protein-ligand complex, molecular dynamics (MD) simulations were performed using the Desmond module from the Schrödinger software suite (version 2020-2) [24]. These simulations aimed to assess the conformational stability of EPA within the binding sites of SMS1 and SMS2 proteins. The simulation system was built by embedding the protein-ligand complex in a cubic simulation box solvated with TIP3P water molecules and solvating it using a simple point charge model. The OPLS3 force field was applied to prepare the protein-ligand complex and to examine the molecular interactions [25]. To neutralize the system, a small number of sodium ions (Na^+) and salt molecules were incorporated. The entire system was then

subjected to energy minimization, applying a convergence threshold defined in kcal·mol^{-1}·Å. Following this, equilibration was carried out under an NPT ensemble for a duration of 100 ns. A subsequent 20 ns MD simulation was conducted under NPT ensemble conditions. The pressure was maintained at 1 bar using the Martyna-Tobias-Klein barostat, while temperature control at 300 K was achieved with a Nose-Hoover thermostat. The focus of the analysis was on evaluating the stability of the protein-ligand interactions, as well as assessing the root mean square deviation (RMSD), root mean square fluctuations (RMSF), and the occupancy of hydrogen bonds with the residues [26, 27].

6.3 Results

6.3.1 Extraction of *Undaria pinnatifida* (wakame)

The extraction of *U. pinnatifida* (wakame) was performed using the method described earlier. The initial methanol extraction yielded 29.6 g of crude extract. To assess its potential as an inhibitor of SMS, an SMS inhibition assay was conducted at a concentration of 100 µg/mL. The extract demonstrated substantial inhibitory activity against both SMS1 and SMS2, with more than 90% inhibition observed in each case. The methanol extract was further fractionated using liquid-liquid partitioning with solvents of varying polarity, including hexane, ethyl acetate, diethyl ether, and water. The resulting solvent fractions were concentrated, yielding 9.8 g of hexane extract, 3.3 g of ether extract, 2.8 g of ethyl acetate extract, and 3.0 g of water extract. Each of these fractions was then assessed for SMS inhibition activity. Notably, the hexane fraction displayed the most potent inhibitory effect, achieving more than 90% inhibition for both SMS1 and SMS2. A summary of the methanol extraction, solvent partitioning, and initial SMS inhibition assay results is shown in **Figure 6.1**.

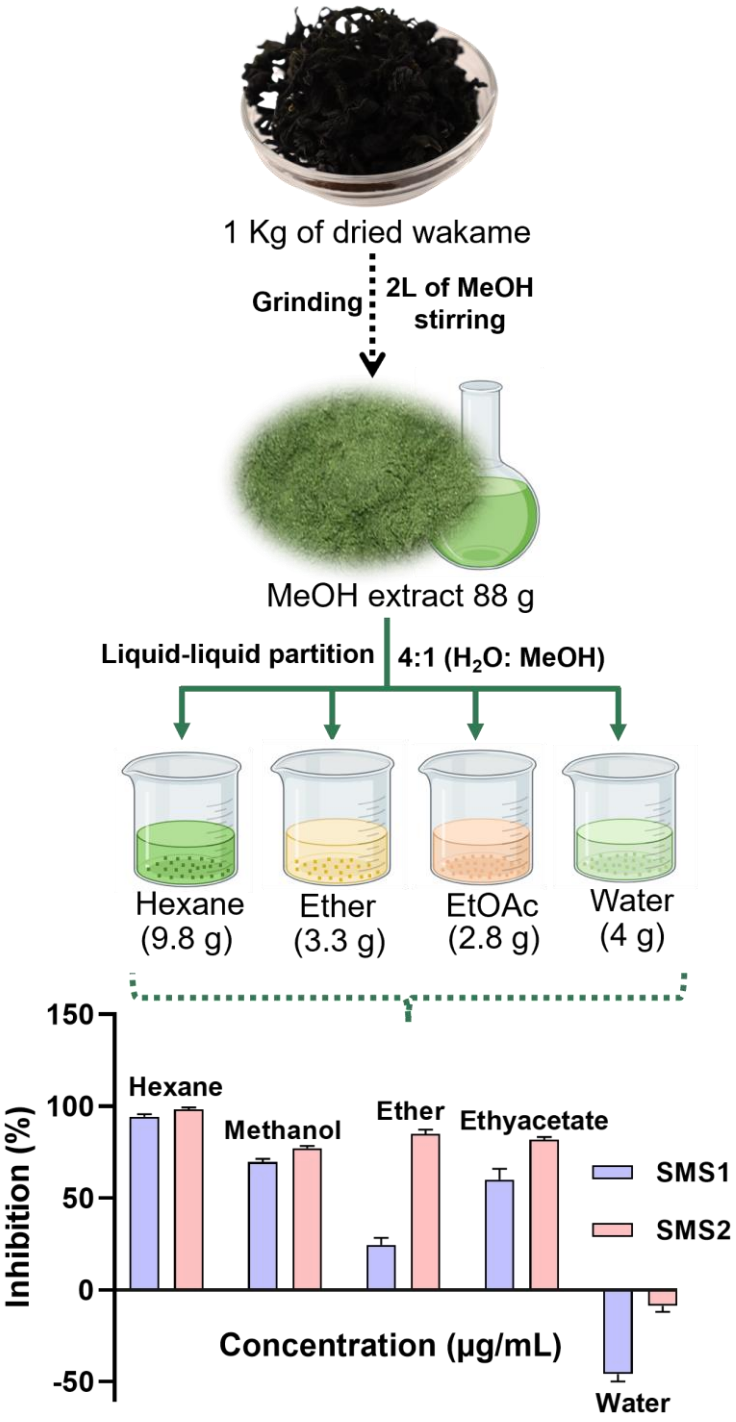

Figure 6.1: Methanol extraction and liquid-liquid partition of *Undaria pinnatifida* (wakame) with weights and SMS inhibition assay results.

6.3.2 Separation and Isolation of the active compound

To obtain the bioactive compound from the potent hexane fraction of wakame, silica gel column chromatography was utilized, a widely applied technique for separating, fractionating, and purifying natural compounds. A silica-packed column was prepared using hexane as the mobile phase, and the separation process was guided by TLC with a hexane-to-ethyl acetate solvent system (4:1 v/v). The initial separation resulted in ten subfractions, each comprising a mixture of compounds. These subfractions were then subjected to SMS inhibition assays to determine their bioactivity. Among the ten, Fraction 7 demonstrated the most significant inhibitory effect, achieving more than 90% inhibition for both SMS1 and SMS2. The detailed isolation and separation of the hexane fraction are shown in **Appendix Figure 6.1**. The separation details, inhibition assay results, and corresponding TLC profiles of ten subfractions are presented in **Appendix Figure 6.1A**. Despite its strong inhibitory activity, fraction ten remained a mixture of compounds. Therefore, it was further purified through a second round of column chromatography under the same solvent conditions, which resulted in four distinct subfractions: 7a, 7b, 7c, and 7d. SMS inhibition assay performed on this purified subfraction revealed that fraction 7c exhibited the highest inhibitory activity against both SMS1 and SMS2. However, subfraction 7c remained a mixture of compounds. The separation of compounds in subfraction 7c through conventional column chromatography was challenging due to the similar polarity of the compounds, revealed by TLC analysis. To overcome this limitation and achieve better separation, preparative TLC (PTLC) was employed using a chloroform-to-methanol solvent system (9.8:0.2 v/v) as the mobile phase. The PTLC results in the successful separation of subfraction 7c-1. TLC analysis confirmed that subfraction 7c-1 contained a single spot, indicating a purified compound. The detailed separation process, inhibition results, and TLC profiles of subfractions of fraction 7 are shown in **Appendix Figure 6.1B**. From 1 kg of wakame, 4 mg of purified subfraction 7c-1 was obtained, corresponding to an overall yield of 0.004%. This stepwise purification process successfully led to the identification of a potent SMS inhibitor from wakame. The structure of this bioactive compound was further characterized using various analytical techniques.

6.3.3 Identification and characterization of the purified compound

The identification of the potent compound responsible for SMS inhibition in the purified compound from wakame was carried out using UHPLC-LTQ Orbitrap MS. The analysis was performed in negative ion mode, allowing the detection of $[M-H]^-$ precursor ions for subsequent analysis. Comprehensive mass spectral analysis revealed that the active fraction was a mixture of long-chain FFAs, with FA 20:5 as the major isomer. High-resolution mass spectra confirmed the presence of these compounds, while the MS/MS spectra confirm their fragmentation behaviors, are represented in **Figure 6.2**. In the purified compound, FA 20:5 eluted at an RT of 12.61 min, closely matching the retention time of the standard EPA eluting at 12.50 min. FA 20:5 in the purified compound was detected and ionized to yield an $[M-H]^-$ ion at *m/z* 301.2144. Furthermore, MS^2 analysis revealed a characteristic fragment ion at m/z 257, corresponding to the loss of CO_2 (44 Da), consistent with the fragmentation pattern observed for the standard EPA. These confirm the presence of EPA as a major isomer in the purified compound. The EIC and mass spectra of both the standard and purified compound, represented in **Figures 6.2A and 6.2B**, respectively. Additionally, HRMS analysis identified the presence of other long-chain FFAs, specifically FA 20:4 and FA 18:4, in the purified mixture. Similar CO_2 loss fragmentation patterns were observed in the MS^2 spectra of these FFAs, confirming their identities. Based on peak intensities, the relative ratio of FA 18:4, FA 20:5, and FA 20:4 in the mixture was approximately 1:2:1. Structural confirmation was further achieved through ^1H NMR spectra are represented in **Appendix Figure 6.2**. Both the purified compound and standard EPA were analyzed at 400 MHz. The ^1H NMR spectrum of the purified compound exhibited the following chemical shifts and coupling constants: δ 5.39 (10H, m), 2.82 (8H, m), 2.38 (2H, t, J = 8 Hz), 2.09 (4H, m), 1.73 (2H, m), and 0.98 (3H, t, J = 8 Hz) (**Figure S2A**). In comparison, the ^1H NMR spectrum of the standard EPA showed the following chemical shifts: δ 5.39 (10H, m), 2.82 (8H, m), 2.37 (2H, t, J = 8 Hz), 2.13 (4H, m), 1.72 (2H, m), and 0.98 (3H, t, J = 8 Hz) (**Figure S2B**). Although the purified fraction was a mixture of long-chain FFAs, the NMR spectral analysis confirmed that FA 20:5 was the predominant isomer, indicating its major contribution within the mixture.

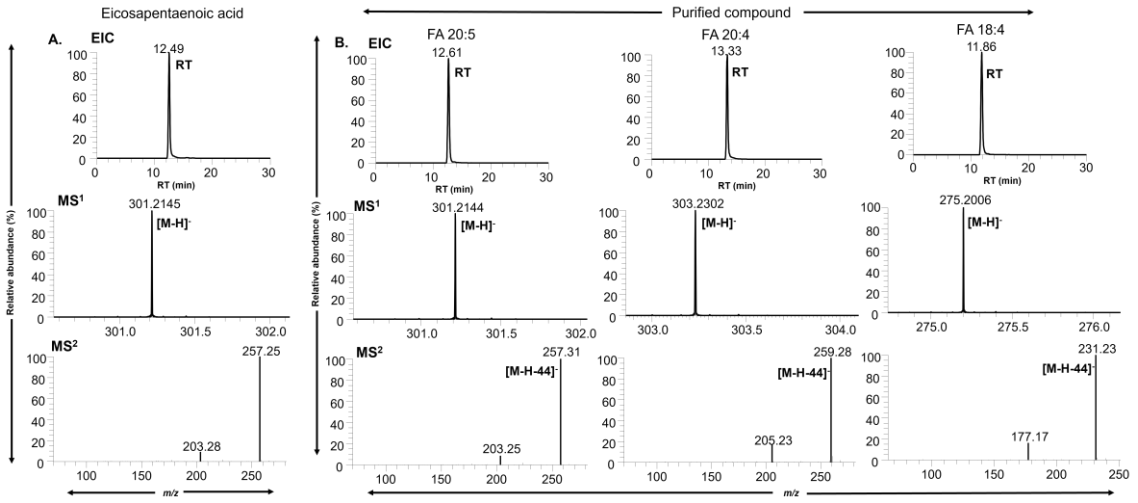

Figure 6.2: Extracted ion chromatogram (EIC), MS^1 and MS^2 spectra of **A.** Standard eicosapentaenoic acid (EPA) **B.** FA 20:5 **C.** FA 20:4 **D.** FA 18:4 in the purified compound.

6.3.4 *In-vitro* SMS inhibition assay for the purified compound.

To assess the inhibitory potential of the purified compound, which was confirmed to be a mixture of long-chain FFAs with FA 20:5 as a major isomer. The SMS inhibition assay was performed for the purified compound at different concentrations. The inhibitory potential of the purified compound was determined by its half-maximal inhibitory concentrations (IC_{50}) for both SMS1 and SMS2. These values were calculated using a cell-based assay coupled LC-MS/MS technique previously developed and reported by our group. This method allows for accurate quantification of Cer and SM levels and provides a detailed analysis of enzyme inhibition at various concentrations of purified compound. As shown in **Figure 6.3A**, the calculated IC_{50} for the purified compound was 10 µM for SMS1 and 6.5 µM for SMS2, indicating that the mixture of essential FFAs shows a potent inhibition for both enzymes. These results are compared with the standard EPA by calculating their IC_{50} value for both SMS and SMS2, as shown in **Figure 6.3B**.

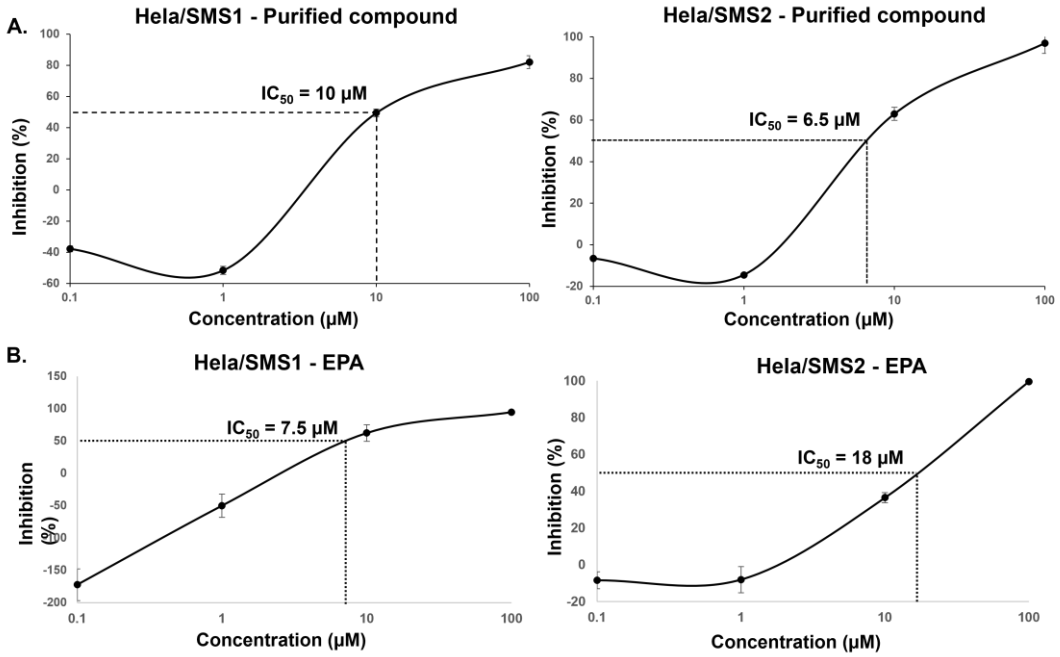

Figure 6.3: *In-vitro* SMS assay results and their IC_{50} for both hSMS1 and hSMS2 of **A.** Purified compound. **B.** Standard eicosapentaenoic acid

6.3.5 *In-silico* molecular docking analysis of FA 20:5 with SMS1 and SMS2

To validate the *in-vitro* findings, *in-silico* molecular docking studies were performed using the optimized protein structures of SMS1 and SMS2, as previously reported by our group. The docking analysis revealed that FA 20:5 exhibited strong binding affinities toward the active sites of both SMS isoforms. The calculated binding energies were -7.1 kcal/mol for SMS1 and -6.4 kcal/mol for SMS2, indicating favourable and stable interactions. The binding interaction modes were further visualized using Discovery Studio Visualizer, and the docking results are presented in **Figure 6.4A**. Notably, FA 20:5 was found to form conventional hydrogen bonds with key amino acid residues ALA325 and Pi–alkyl interaction with HIS 285, PHE 184, PHE 242, and HIS 274 in the active site of SMS1. For SMS2, FA 20:5 exhibited a conventional hydrogen bond with ARG286 and multiple non-covalent interactions, including alkyl and Pi–alkyl interactions, suggesting a stable and specific binding configuration **(Figure 6.4B).**

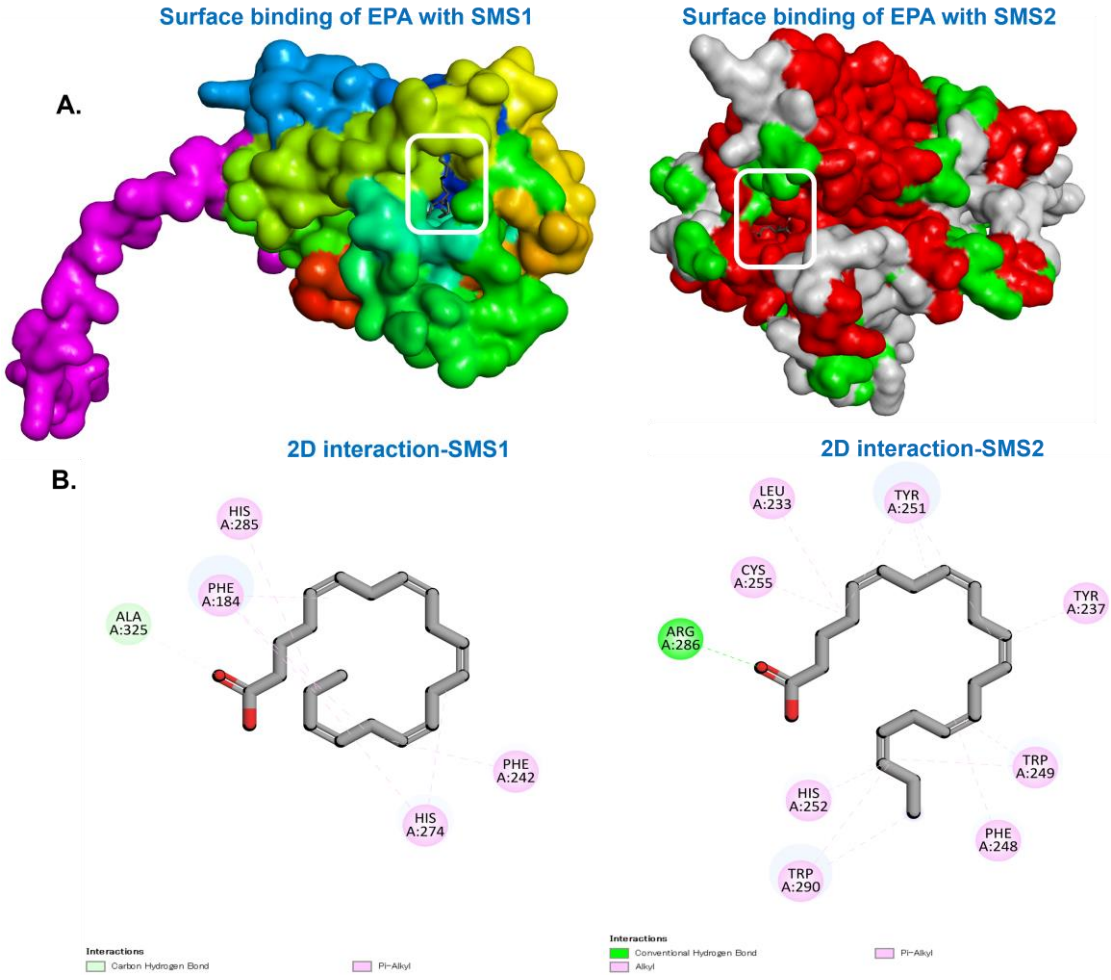

Figure 6.4: *In-silico* molecular docking analysis of eicosapentaenoic acid with hSMS1 and hSMS2 proteins indicates **A.** EPA binding to the surface of SMS1 and SMS2 proteins. **B.** Two-dimensional interaction of EPA with the SMS1 and SMS2 proteins.

6.3.6 *In-silico* molecular dynamics simulation analysis of FA 20:5 with SMS1 and SMS2

6.3.6.1 Root Mean Square Deviation (RMSD) Analysis

To evaluate the stability of the protein–ligand complexes, MD simulations were performed, and the root-mean-square deviation (RMSD) of the protein Cα atoms was analyzed. In the FA 20:5–SMS1 complex, RMSD values ranged from 2.0 Å to 3.2 Å. The system achieved initial stability after approximately 25 ns and exhibited minor fluctuations between 40–50 ns. Thereafter, the complex regained and maintained stable conformational behavior from 55 ns up to 100 ns. A final stable trajectory was observed beyond 100 ns, indicating strong ligand binding and overall system stability. In the case

of the FA 20:5–SMS2 complex, RMSD values ranged from 2.0 Å to 4.5 Å. The system showed consistent stability from 0 to 40 ns, followed by a phase of divergence between 45–80 ns. Stability was re-established between 80–90 ns, and despite a slight deviation towards 100 ns, the complex ultimately stabilized again beyond 100 ns. Both complex systems demonstrated acceptable fluctuations in RMSD throughout the simulation period, indicative of dynamic yet stable protein–ligand interactions. The average RMSD profiles of both systems are depicted in **Figure 5A**.

6.3.6.2 Root Mean Square Fluctuation (RMSF) Analysis

To assess residue-level fluctuations within the protein–ligand complexes, root mean square fluctuation (RMSF) analysis was performed. In the FA 20:5–SMS1 complex, the average RMSF value was approximately 2.5 Å, with increased flexibility observed at specific residue ranges—namely, residues 30–40, 100–125, 130–140, and 215–230. Similarly, in the FA 22:1–SMS2 complex, a higher average RMSF of approximately 5.0 Å was recorded. Distinctly elevated fluctuations were detected in the residue ranges 40–50, 110–160, and 195–210. Both complexes demonstrated characteristic fluctuation profiles, as depicted in **Figure 5B**. The comparative RMSF analysis indicates that ligand binding significantly affects the dynamic behavior of specific protein regions. These findings suggest that the binding of FA 20:5 contributes to the overall structural stabilization of SMS1 and SMS2, respectively, which demonstrated favourable docking results.

6.3.6.3 Occupancy of Hydrogen bond interaction

In the FA 20:5–SMS1 complex, a consistent hydrogen bond was observed with the HIS285 residue, occurring in approximately 25% of the simulation trajectory. In contrast, the FA 20:5–SMS2 complex exhibited a more persistent hydrogen bond interaction with ARG311, present in over 100% of the simulation frames, indicating that multiple hydrogen bonds were formed and maintained concurrently throughout the simulation period. The persistence of these interactions across a significant portion of the simulation trajectory reinforces the ligand's stabilizing effect on the protein structures. Additional amino acid interactions contributing to complex stabilization are illustrated in **Figure 5C**. Collectively, these findings confirm the crucial role of hydrogen bonding in

mediating the high binding affinity and stability of the FA 20:5- SMS1 and SMS2 complexes.

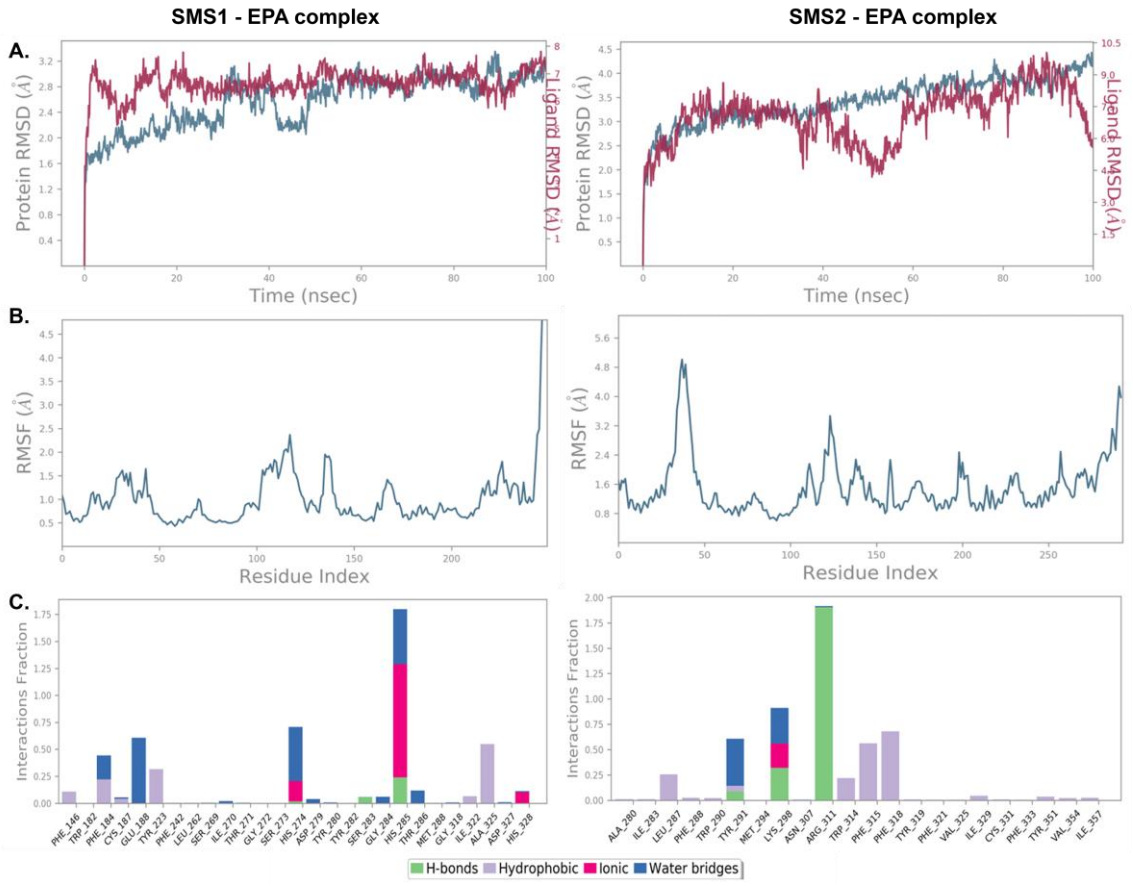

Figure 6.5: Molecular dynamics simulation of **A.** Root mean square deviation (RMSD) analysis of SMS1 and SMS2 with EPA complexes. **B.** Root mean square fluctuation (RMSF) analysis of SMS1 and SMS2 with EPA complexes. **C.** Occupancy of hydrogen bond analysis of SMS1 and SMS2 with EPA complexes.

6.4 Discussion

The present study aimed to explore the anti-obesity potential of *U. pinnatifida* (wakame) by identifying natural inhibitors of SMS, a key enzyme involved in lipid metabolism and implicated in the development of metabolic disorders. SMS is the last enzyme involved in the SM biosynthesis and plays a crucial role in signal transduction and protein sorting within lipid raft domains [28]. Dysregulation of SMS activity has been associated with several metabolic abnormalities, including insulin resistance and hepatic steatosis [29]. Previous studies have shown that SMS inhibition in mouse models can significantly

improve liver steatosis, positioning SMS as a viable therapeutic target for treating obesity-related metabolic syndromes [30]. Therefore, targeting SMS represents a promising strategy for modulating sphingolipid-mediated metabolic dysfunctions associated with obesity and related syndromes. Prior studies have primarily focused on synthetic SMS inhibitors, such as tricyclodecan-9-yl-xanthogenate (D609) and other selective compounds targeting SMS1 and SMS2 isoforms [31, 32]. Although these synthetic inhibitors have demonstrated efficacy in reducing SMS activity, their clinical translation has been hindered by high cytotoxicity and unfavourable safety profiles [32]. In light of these limitations, naturally derived SMS inhibitors have garnered attention as potentially safer alternatives; however, research in this area remains limited.

A prior study reported daurichromenic acid, a potent SMS inhibitor isolated from the hexane fraction of the traditional Chinese medicinal plant Rhododendron dauricum [20]. These findings are consistent with our results, where the hexane fraction of wakame exhibited notable SMS inhibitory activity, underscoring the effectiveness of this extraction approach for identifying bioactive compounds. Wakame, a staple in traditional Japanese cuisine, is known to be rich in essential minerals, vitamins, and dietary fibers [33]. Furthermore, previous studies have shown that consumption of EPA-rich fish oil and wakame significantly lowers serum and liver triacylglycerol levels compared to standard diets [34]. Our study shows that subfraction 7c-1, containing a bioactive compound, exhibits potent SMS inhibition activity, indicating that subfraction 7c-1 may contain EPA.

Based on subsequent purification, SMS assay, and structural characterization of subfraction 7c-1 (the most active subfraction), revealed active compound is a mixture of FFAs, with EPA as the major bioactive compound responsible for SMS inhibition. Although earlier studies had identified similar compounds through total lipid extraction, they lacked in-depth structural characterization [35]. In contrast, our study utilized comprehensive LC-MS and NMR techniques, supported by direct comparisons with authentic standards, to confirm the structure and identity of the bioactive components. Furthermore, the SMS inhibition assay was performed on the purified EPA-rich fraction, and the results align well with previously reported results for Gingkolic acid, which was evaluated using the same SMS inhibition assay method [21]

EPA is a well-known ω-3 bioactive lipid which are well recognized for its anti-inflammatory and cardioprotective effects [36]. Recent rodent model studies have demonstrated EPA's efficacy in improving metabolic outcomes in both type 1 and type 2 diabetes [37-39]. Another study also revealed the beneficial effect of EPA supplements on metabolic parameters, including glucose and glycosylated haemoglobin in type 2 diabetic patients [40]. Additionally, studies have demonstrated that combined intake of ω-3 and ω-6 FFAs has been linked to improved outcomes in obesity-related comorbidities, such as atherosclerotic cardiovascular disease and mental health disorders [41, 42]. Recent cross-sectional data analysis revealed a linear relation between ω-3 and ω-6 FFAs intakes, which significantly lowers the body fat percentage [43]. These collective findings are in line with our observations regarding SMS inhibition of purified compound.

To our knowledge, this is the first study reporting the identification of anti-obesity bioactive compounds from wakame targeting SMS. Nevertheless, several limitations must be acknowledged. The presence of multiple FFAs species in the active fraction posed challenges for chromatographic separation and structural elucidation, especially in identifying double bonds in highly unsaturated compounds. Additionally, the limited availability of commercial standards constrained definitive compound identification for some constituents.

6.5 Conclusion

This study highlights *Undaria pinnatifida* (wakame) as a promising natural source of SMS inhibitors, with FA 20:5 identified as the major bioactive compound exhibiting potent inhibitory activity against both SMS1 and SMS2 isoforms. Utilizing a multidisciplinary approach- comprising *in-vitro* enzymatic assays, *in-silico* molecular docking and dynamics simulations, and advanced structural characterization through LC/MS and NMR- we confirmed the efficacy of FA 20:5 in modulating sphingolipid metabolism. These findings offer valuable insights into the potential development of functional foods or nutraceuticals derived from wakame for the management of lipid-related metabolic disorders. However, further *in-vivo* studies and targeted formulation strategies will be essential to substantiate the therapeutic potential of FA 20:5 as a dietary intervention for obesity and associated metabolic diseases.

References

1. Jaacks, L. M., Vandevijvere, S., Pan, A., McGowan, C. J., Wallace, C., Imamura, F., Mozaffarian, D., Swinburn, B., & Ezzati, M. (2019). The obesity transition: stages of the global epidemic. The lancet. Diabetes & endocrinology, 7(3), 231–240.
2. Dong, J., Liu, J., Lou, B., Li, Z., Ye, X., Wu, M., & Jiang, X. C. (2006). Adenovirus-mediated overexpression of sphingomyelin synthases 1 and 2 increases the atherogenic potential in mice. Journal of lipid research, 47(6), 1307–1314.
3. Hammad, S. M., & Lopes-Virella, M. F. (2023). Circulating sphingolipids in insulin resistance, diabetes and associated complications. International Journal of Molecular Sciences, 24(18), 14015.
4. Zhang, Y., Lin, F., Deng, X., Wang, R., & Ye, D. (2011). Molecular Modeling of the Three-Dimensional Structure of Human Sphingomyelin Synthase. Chinese Journal of Chemistry, 29(8), 1567-1575.
5. Chiang, Y. P., Li, Z., Chen, Y., Cao, Y., & Jiang, X. C. (2021). Sphingomyelin synthase related protein is a mammalian phosphatidylethanolamine phospholipase C. Biochimica et Biophysica Acta (BBA)-Molecular and Cell Biology of Lipids, 1866(11), 159017.
6. Chen, Y., Yurek, D. A., Yu, L., Wang, H., Ehsani, M. E., Qian, Y. W., Konrad, R. J., Jiang, X. C., Kuo, M. S., Cao, G., & Wang, J. (2013). Development of a quantitative biochemical and cellular sphingomyelin synthase assay using mass spectrometry. Analytical biochemistry, 438(1), 61–66.
7. Gault, C. R., Obeid, L. M., & Hannun, Y. A. (2010). An overview of sphingolipid metabolism: from synthesis to breakdown. Advances in experimental medicine and biology, 688, 1–23.
8. Yeang, C., Varshney, S., Wang, R., Zhang, Y., Ye, D., & Jiang, X. C. (2008). The domain responsible for sphingomyelin synthase (SMS) activity. Biochimica et biophysica acta, 1781(10), 610–617.
9. Li, Z., Fan, Y., Liu, J., Li, Y., Huan, C., Bui, H. H., Kuo, M. S., Park, T. S., Cao, G., & Jiang, X. C. (2012). Impact of sphingomyelin synthase 1 deficiency on sphingolipid metabolism and atherosclerosis in mice. Arteriosclerosis, thrombosis, and vascular biology, 32(7), 1577–1584.

10. Li, Z., Zhang, H., Liu, J., Liang, C. P., Li, Y., Li, Y., Teitelman, G., Beyer, T., Bui, H. H., Peake, D. A., Zhang, Y., Sanders, P. E., Kuo, M. S., Park, T. S., Cao, G., & Jiang, X. C. (2011). Reducing plasma membrane sphingomyelin increases insulin sensitivity. Molecular and cellular biology, 31(20), 4205–4218.

11. Koh, E. H., Yoon, J. E., Ko, M. S., Leem, J., Yun, J. Y., Hong, C. H., Cho, Y. K., Lee, S. E., Jang, J. E., Baek, J. Y., Yoo, H. J., Kim, S. J., Sung, C. O., Lim, J. S., Jeong, W. I., Back, S. H., Baek, I. J., Torres, S., Solsona-Vilarrasa, E., Conde de la Rosa, L., … Lee, K. U. (2021). Sphingomyelin synthase 1 mediates hepatocyte pyroptosis to trigger non-alcoholic steatohepatitis. Gut, 70(10), 1954–1964.

12. Lou, B., Dong, J., Li, Y., Ding, T., Bi, T., Li, Y., Deng, X., Ye, D., & Jiang, X. C. (2014). Pharmacologic inhibition of sphingomyelin synthase (SMS) activity reduces apolipoprotein-B secretion from hepatocytes and attenuates endotoxin-mediated macrophage inflammation. PloS one, 9(7), e102641.

13. Deng, X., Lin, F., Zhang, Y., Li, Y., Zhou, L., Lou, B., Li, Y., Dong, J., Ding, T., Jiang, X., Wang, R., & Ye, D. (2014). Identification of small molecule sphingomyelin synthase inhibitors. European journal of medicinal chemistry, 73, 1–7.

14. Swamy, M. M. M., Murai, Y., Ohno, Y., Jojima, K., Kihara, A., Mitsutake, S., Igarashi, Y., Yu, J., Yao, M., Suga, Y., Anetai, M., & Monde, K., (2018). Structure-inspired design of a sphingolipid mimic sphingosine-1-phosphate receptor agonist from a naturally occurring sphingomyelin synthase inhibitor. Chemical communications (Cambridge, England), 54(90), 12758–12761.

15. Othman, M. A., Yuyama, K., Murai, Y., Igarashi, Y., Mikami, D., Sivasothy, Y., Awang, K., & Monde, K. (2019). Malabaricone C as Natural Sphingomyelin Synthase Inhibitor against Diet-Induced Obesity and Its Lipid Metabolism in Mice. ACS medicinal chemistry letters, 10(8), 1154–1158.

16. Liu, Z. H., & Zeng, S. (2009). Cytotoxicity of ginkgolic acid in HepG2 cells and primary rat hepatocytes. Toxicology letters, 187(3), 131–136.

17. Wells, M. L., Potin, P., Craigie, J. S., Raven, J. A., Merchant, S. S., Helliwell, K. E., Smith, A. G., Camire, M. E., & Brawley, S. H. (2017). Algae as nutritional and functional food sources: revisiting our understanding. Journal of applied phycology, 29(2), 949–982.

18. Kishida, R., Yamagishi, K., Muraki, I., Sata, M., Tamakoshi, A., Iso, H., & JACC Study Group (2020). Frequency of Seaweed Intake and Its Association with Cardiovascular Disease Mortality: The JACC Study. Journal of atherosclerosis and thrombosis, 27(12), 1340–1347.

19. Murai, U., Yamagishi, K., Sata, M., Kokubo, Y., Saito, I., Yatsuya, H., Ishihara, J., Inoue, M., Sawada, N., Iso, H., Tsugane, S., & JPHC Study Group (2019). Seaweed intake and risk of cardiovascular disease: the Japan Public Health Center-based Prospective (JPHC) Study. The American journal of clinical nutrition, 110(6), 1449–1455.

20. Deepak, H. V., Swamy, M. M. M., Murai, Y., Suga, Y., Anetai, M., Yo, T., Kuragano, M., Uwai, K., Tokuraku, K., & Monde, K. (2020). Daurichromenic Acid from the Chinese Traditional Medicinal Plant Rhododendron dauricum Inhibits Sphingomyelin Synthase and Aβ Aggregation. Molecules (Basel, Switzerland), 25(18), 4077.

21. Sundaraswamy, P. M., Minami, Y., Jayaprakash, J., B Gowda, S. G., Takatsu, H., Gowda, D., Shin, H. W., & Hui, S. P. (2024). A facile method for monitoring sphingomyelin synthase activity in HeLa cells using liquid chromatography/mass spectrometry. The Analyst, 149(12), 3293–3301.

22. Nanjundaswamy, S., Jayashankar, J., Renganathan, R. R. A., Karthik, C. S., Mallesha, L., Mallu, P., & Rai, V. R. (2022). Pyridine coupled pyrazole analogues as lethal weapon against MRSA: An in-vitro and in-silico approach. Microbial pathogenesis, 166, 105508.

23. Gogoi, B., Chowdhury, P., Goswami, N., Gogoi, N., Naiya, T., Chetia, P., Mahanta, S., Chetia, D., Tanti, B., Borah, P., & Handique, P. J. (2021). Identification of potential plant-based inhibitor against viral proteases of SARS-CoV-2 through molecular docking, MM-PBSA binding energy calculations and molecular dynamics simulation. Molecular diversity, 25(3), 1963–1977.

24. Nanjundaswamy, S., Jayashankar, J., Chethana, M. H., Renganathan, R. A., Karthik, C. S., Ananda, A. P., Nagashree, S., Mallu, P., & Rai, V. R. (2022). Design, synthesis, and in-silico studies of pyrazolylpyridine analogues: A futuristic antibacterial contender against coagulase positive superbug-MRSA. Journal of Molecular Structure, 1255, 132400.

25. Kubaib, A., Afroze, N. N., Imran, P. M., Natarajan, P., Balu, D., & Ansari, A. (2024). Insights into the binding mechanism of 2, 5-substituted 4-pyrone derivatives as

therapeutic agents for fused dimeric interactions: A computational study using QTAIM, dynamics and docking simulations of protein–ligand complexes. International Journal of Quantum Chemistry, 124(3), e27330.

26. Shah, A. A., Ahmad, S., Yadav, M. K., Raza, K., Kamal, M. A., & Akhtar, S. (2024). Structure-based virtual screening, molecular docking, molecular dynamics simulation, and metabolic reactivity studies of quinazoline derivatives for their anti-EGFR activity against tumor angiogenesis. Current Medicinal Chemistry, 31(5), 595-619.

27. Jayashankar, J., Ningaraju, G. N., Nanjundaswamy, S., Rajabathar, J. R., Karnan, M., Karthik, C. S., & Mallu, P. (2024). An in-silico investigation of volatile compounds in Tulsi and Ginger as a potent inhalant for SARS-CoV-2 treatment. Journal of the Iranian Chemical Society, 21(2), 479-502.

28. Li, Z., Hailemariam, T. K., Zhou, H., Li, Y., Duckworth, D. C., Peake, D. A., Zhang, Y., Kuo, M. S., Cao, G., & Jiang, X. C. (2007). Inhibition of sphingomyelin synthase (SMS) affects intracellular sphingomyelin accumulation and plasma membrane lipid organization. Biochimica et biophysica acta, 1771(9), 1186–1194.

29. Lee, M., Lee, S. Y., & Bae, Y. S. (2023). Functional roles of sphingolipids in immunity and their implication in disease. Experimental & molecular medicine, 55(6), 1110–1130.

30. Li, Y., Dong, J., Ding, T., Kuo, M. S., Cao, G., Jiang, X. C., & Li, Z. (2013). Sphingomyelin synthase 2 activity and liver steatosis: an effect of ceramide-mediated peroxisome proliferator-activated receptor γ2 suppression. Arteriosclerosis, thrombosis, and vascular biology, 33(7), 1513–1520.

31. Luberto, C., & Hannun, Y. A. (1998). Sphingomyelin synthase, a potential regulator of intracellular levels of ceramide and diacylglycerol during SV40 transformation. Does sphingomyelin synthase account for the putative phosphatidylcholine-specific phospholipase C?. The Journal of biological chemistry, 273(23), 14550–14559.

32. Deng, X., Lin, F., Zhang, Y., Li, Y., Zhou, L., Lou, B., Li, Y., Dong, J., Ding, T., Jiang, X., Wang, R., & Ye, D. (2014). Identification of small molecule sphingomyelin synthase inhibitors. European journal of medicinal chemistry, 73, 1–7.

33. Taboada, M. C., Millán, R., & Miguez, M. I. (2013). Nutritional value of the marine algae wakame (Undaria pinnatifida) and nori (Porphyra purpurea) as food supplements. Journal of Applied Phycology, 25, 1271-1276.

34. Murata, M., Sano, Y., Ishihara, K., & Uchida, M. (2002). Dietary fish oil and Undaria pinnatifida (wakame) synergistically decrease rat serum and liver triacylglycerol. The Journal of nutrition, 132(4), 742-747.

35. Dawczynski, C., Schubert, R., & Jahreis, G. (2007). Amino acids, fatty acids, and dietary fibre in edible seaweed products. Food chemistry, 103(3), 891-899.

36. Koutsaliaris, I. K., Pantazi, D., Tsouka, A. N., Argyropoulou, O., Tellis, C. C., & Tselepis, A. D. (2024). Differential Effect of Omega-3 Fatty Acids on Platelet Inhibition by Antiplatelet Drugs In Vitro. International Journal of Molecular Sciences, 25(18), 10136.

37. Mohan, I. K., & Das, U. N. (2001). Prevention of chemically induced diabetes mellitus in experimental animals by polyunsaturated fatty acids. Nutrition, 17(2), 126-151.

38. Suresh, Y., & Das, U. N. (2003). Long-chain polyunsaturated fatty acids and chemically induced diabetes mellitus. Effect of omega-3 fatty acids. Nutrition (Burbank, Los Angeles County, Calif.), 19(3), 213–228.

39. Jacobo-Cejudo, M. G., Valdés-Ramos, R., Guadarrama-López, A. L., Pardo-Morales, R. V., Martínez-Carrillo, B. E., & Harbige, L. S. (2017). Effect of n-3 Polyunsaturated Fatty Acid Supplementation on Metabolic and Inflammatory Biomarkers in Type 2 Diabetes Mellitus Patients. Nutrients, 9(6), 573.

40. Maki, K. C., Dicklin, M. R., & Kirkpatrick, C. F. (2021). Saturated fats and cardiovascular health: Current evidence and controversies. Journal of clinical lipidology, 15(6), 765-772.

41. Gao, X., Su, X., Han, X., Wen, H., Cheng, C., Zhang, S., Li, W., Cai, J., Zheng, L., Ma, J., Liao, M., Ni, W., Liu, T., Liu, D., Ma, W., Han, S., Zhu, S., Ye, Y., & Zeng, F. F. (2022). Unsaturated Fatty Acids in Mental Disorders: An Umbrella Review of Meta-Analyses. Advances in nutrition (Bethesda, Md.), 13(6), 2217–2236.

42. Yang, Z., Lan, Y., Yang, K., Zhang, J., Chen, L., Meng, T., Wu, M., & Lu, X. (2025). Omega-3 and omega-6 fatty acids: Inverse association with body fat percentage and obesity risk. Nutrition research (New York, N.Y.), 135, 32–41.

Conclusion remarks

This thesis utilized untargeted lipidomics as a powerful platform for investigating diverse physiological and pathological conditions, like alcohol-associated gut dysbiosis, neurodegenerative diseases, childhood obesity, and the discovery of bioactive lipids from marine resources. The detailed analyses of diverse sample types through the application of high-resolution HPLC/LTQ-MS, coupled with advanced data processing, enabled the identification of novel lipid species, elucidation of metabolic signatures, and discovery of potential diagnostic and therapeutic lipid biomarkers.

Chapter 2 was focused on the impact of ethanol consumption on gut lipid metabolism using colon flush samples from both male and female mice. Distinct sex-specific alterations in lipid classes such as FFAs, SPs, and GPs were observed, with specific upregulation of PG (O-15:1/15:0) and PE (O-18:2/15:0) in EF mice. The reduction of FAHFAs in female mice highlighted the vulnerability of anti-inflammatory lipid pathways under alcohol-induced stress. These findings emphasize the intricate sex-dependent mechanisms governing gut lipid regulation and suggest new leads for understanding the pathophysiology of alcohol-related gastrointestinal disorders.

Building upon the exploration of gut lipidome diversity, **Chapter 3** delved into the identification of novel FAHFA-derived lipid species in human fecal samples. Using advanced LC/MS techniques, this work reported for the first time the presence of MFAHFAs, specifically EA and CLA esters of long-chain hydroxy fatty acids, in the human gut. These lipids likely originate from microbial or host-microbe interactions and may hold physiological or diagnostic relevance. The detection of both abundant and rare SFAHFAs and MFAHFAs sheds light on the complexity of gut-associated lipid metabolism and expands the lipidome landscape relevant to intestinal and metabolic health.

Chapter 4 focused on lipid dysregulation in NDs. In the first part, untargeted lipidomics of saliva, plasma, and fecal samples from older adults across stages of cognitive impairment revealed distinct alterations in lipid class distributions and ω6/ω3 fatty acid ratios. Lipid species such as FA 18:3, FA 22:5, and CE 18:2 emerged as promising stage-specific biomarkers, while increased TG-MCFAs in fecal samples were indicative of early

cognitive decline (MCI). Further stratification by sex and body weight provided additional insight into lipidomic variability in MCI patients. In the second part, deep lipidomic profiling of postmortem brain tissue from patients with AD, PD, and HD revealed strong disease-specific signatures. A total of 291 lipid species were profiled across different brain regions, with clear group separation observed via OPLS-DA analysis. Volcano plot and ROC analyses identified AHexCer (d(O-18:1)18:1/15:0;O), PC (O-22:5/19:3), and PS (O-17:0/22:6) among the top differentiators of disease states. The sex- and brain region-specific lipid alterations further emphasized the influence of biological variables in lipid-mediated neurodegeneration and provided molecular insight into the heterogeneous nature of these disorders.

In **Chapter 5**, the lipidomics of pre-adolescent children explained how sex, age, and weight status influence plasma lipid metabolism. Differences in SPs and PLs were observed across age groups, with a notable rise in TG and PS levels between ages 9 and 12. Children classified as overweight exhibited elevated TG levels, particularly TG (10:0/10:0/18:1), which emerged as a potential lipid biomarker for early-onset obesity. This study contributes to the understanding of early metabolic shifts during childhood and supports the use of untargeted lipidomics in pediatric populations to monitor and predict metabolic health trajectories.

Chapter 6 described the discovery of a potent SMS inhibitor from the edible seaweed *U. pinnatifida* (wakame), highlighting the translational potential of lipidomics in therapeutic discovery. Using a multidisciplinary approach combining *in-vitro* SMS assay, LC/MS, and NMR-based structural elucidation, and *in-silico* molecular docking and dynamics simulations, FA 20:5 was identified as the principal bioactive molecule with strong inhibitory effects on SMS1 and SMS2 isoforms. Given the pivotal role of SMS in SPs metabolism and obesity pathogenesis, these findings provide a basis for developing functional foods or nutraceutical interventions targeting obesity.

Overall, this thesis illustrates the versatility of untargeted lipidomics in capturing biologically relevant lipid changes across tissues, fluids, species, and diseases. It highlights novel lipid biomarkers, identifies new bioactive lipid species, and demonstrates the relevance of lipidomic profiling in both basic and translational research. The

integration of sex-, age-, disease-, and tissue-specific lipid data across studies not only enriches our understanding of lipid metabolism but also emphasizes the potential of lipidomics in precision medicine. Future studies should focus on the targeted validation of candidate biomarkers and functional elucidation of novel lipid species, with an emphasis on integrating lipidomics with genomics, proteomics, and metabolomics for a more holistic view of disease mechanisms and therapeutic potential.

Appendix

Supplementary information for Chapter 1

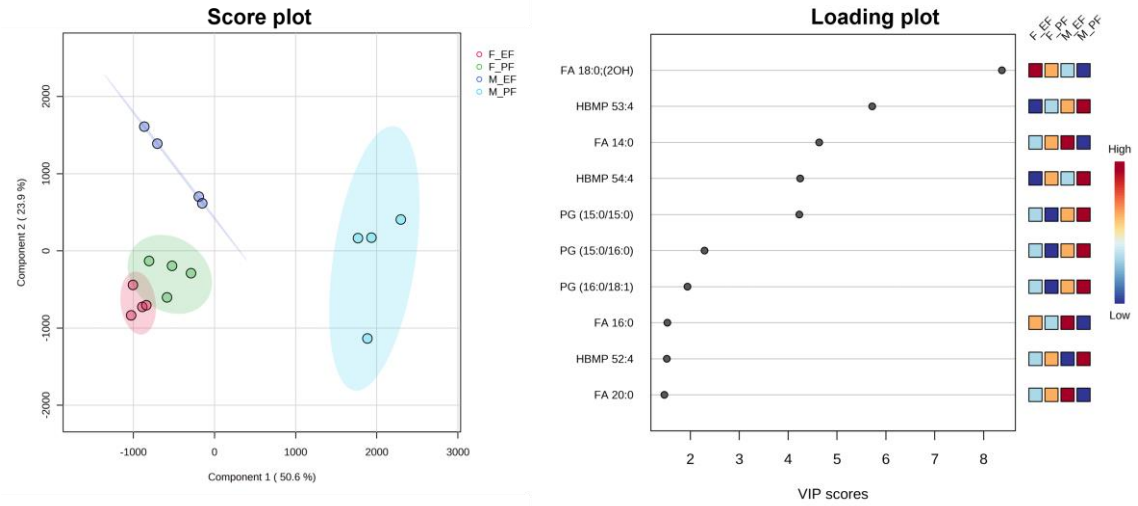

Figure 2.1: PLS-DA score plot (up) and their variable importance in projection (VIP) scores (down).

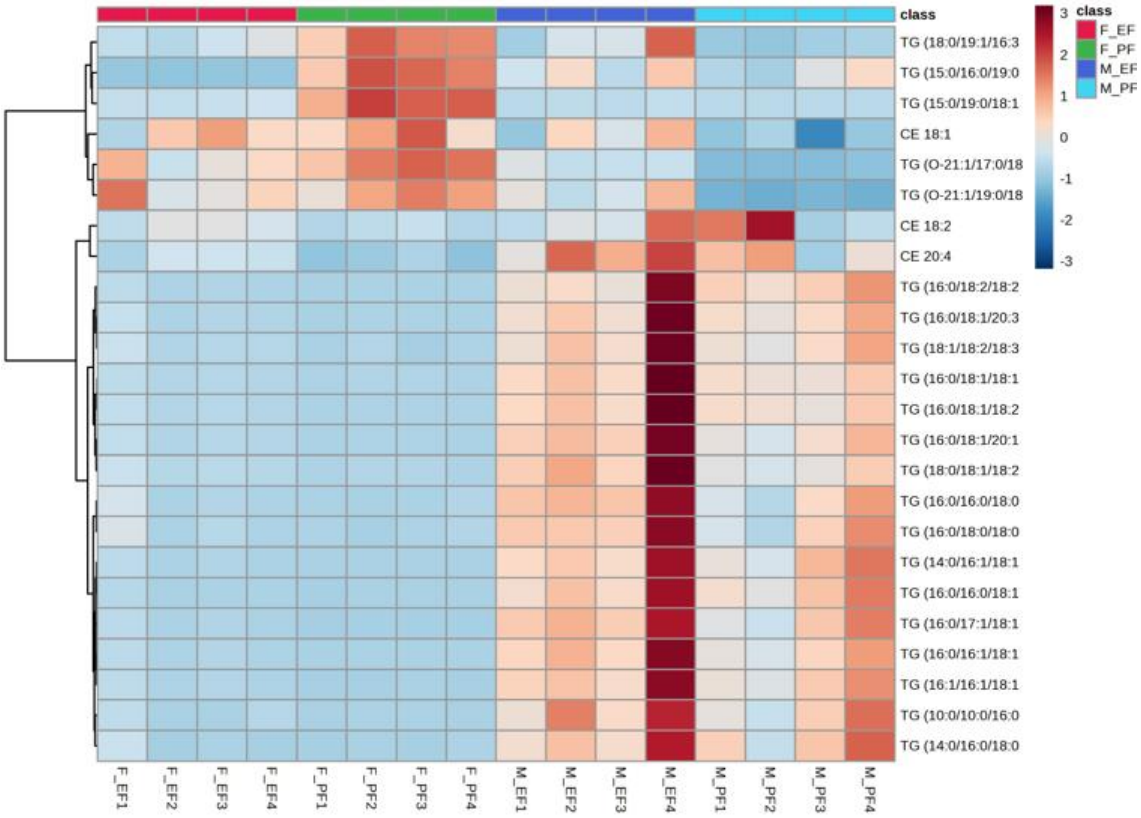

Figure 2.2: Hierarchical cluster correlation analysis of TG (clustering method: ward, distance measure: Euclidean)

Supplementary information for Chapter 4

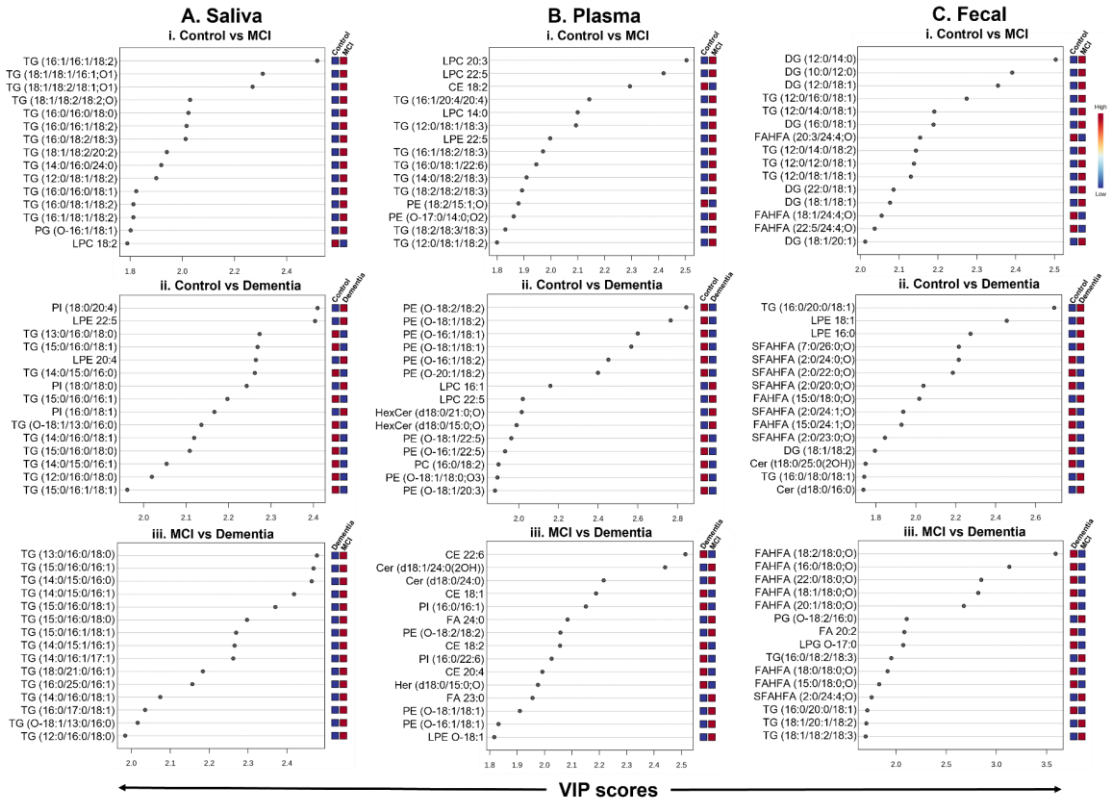

Figure 4.1: Multivariate analysis of all lipid molecular species identified in saliva, plasma, and fecal samples of control, MCI, and dementia groups of older adults. **A.** OPLS-DA loading plot of the saliva samples representing: (i) control vs MCI groups, (ii) control vs dementia groups, (iii) MCI vs dementia groups. **B.** OPLS-DA loading plot of the plasma samples representing: (i) control vs MCI groups, (ii) control vs dementia groups, (iii) MCI vs dementia groups. **C.** OPLS-DA loading plot of the fecal samples representing: (i) control vs MCI groups, (ii) control vs dementia groups, and (iii) MCI vs dementia groups.

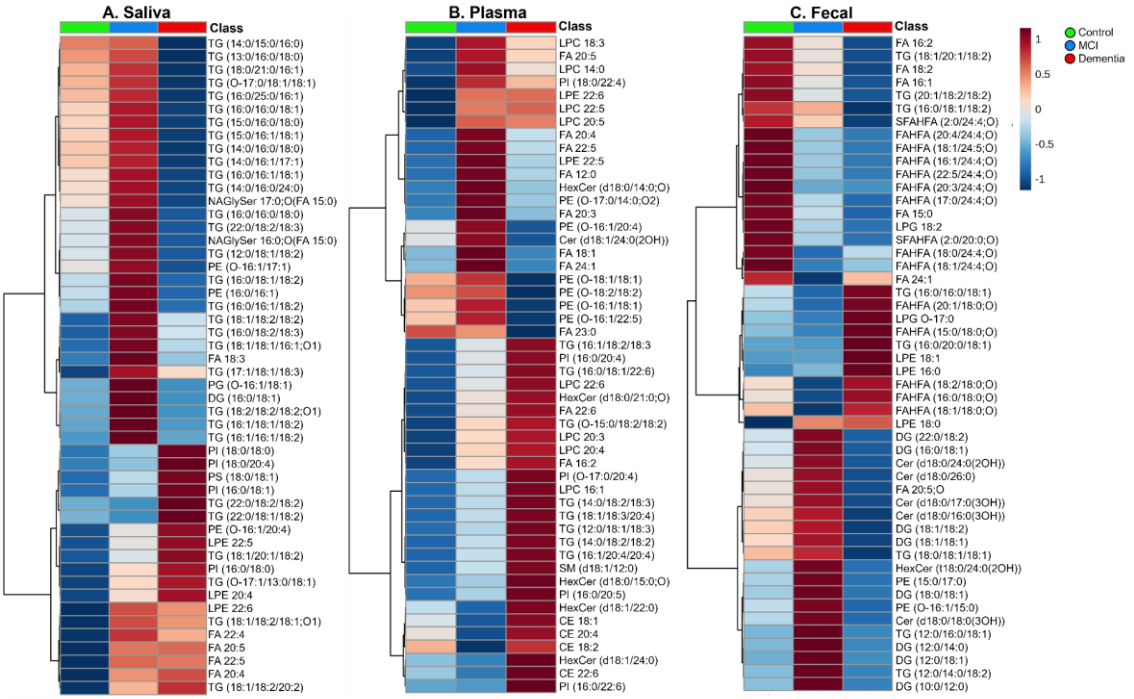

Figure 4.2: Heatmaps of the top 50 altered lipid molecular species in control, MCI, and dementia groups of saliva, plasma, and fecal samples of older adults.

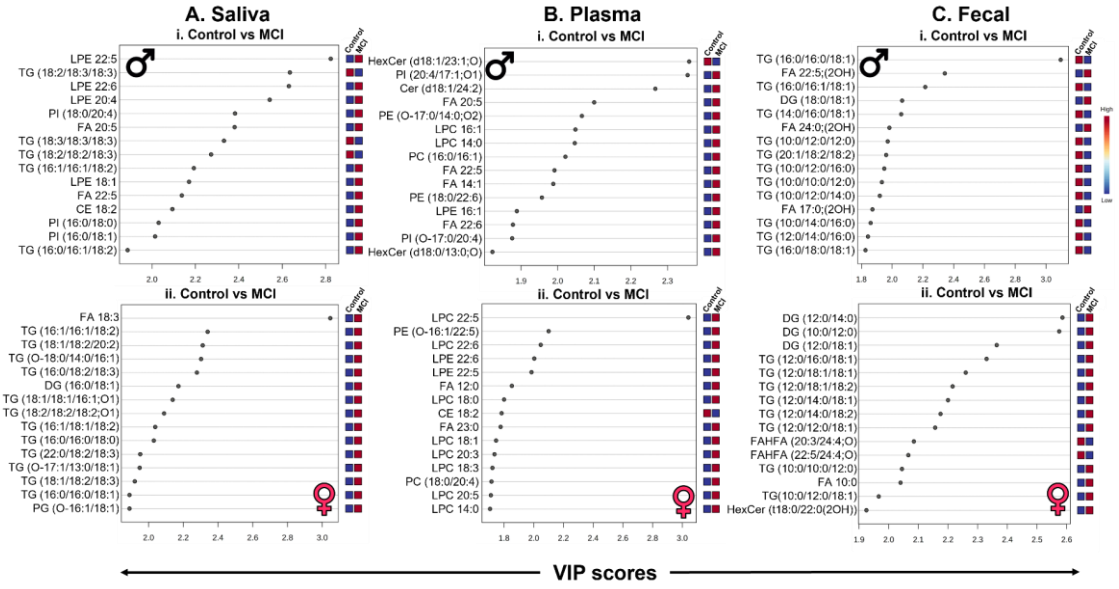

Figure 4.3: Sex-specific lipidome alternation in control and MCI groups of saliva, plasma, and fecal samples. **A.** OPLS-DA loading plot analysis of control and MCI groups of saliva samples for: (i) male participants, (ii) female participants, **B.** OPLS-DA loading plot analysis of control and MCI groups of plasma samples for:(iii) male participants, (iv) female participants, **C.** OPLS-DA loading plot analysis of control and MCI groups of fecal samples for: (v) male participants, and (vi) female participants.

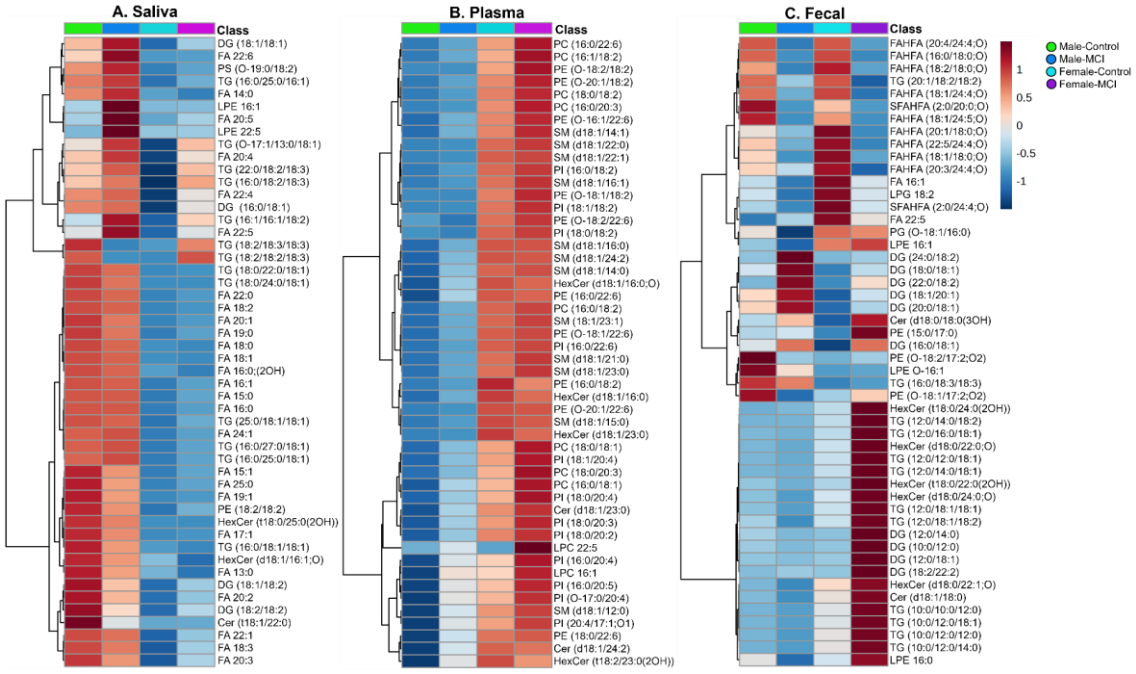

Figure 4.4: Heatmaps of the top 50 altered lipid molecular species in both the sex groups of control and MCI groups across saliva, plasma, and fecal samples of older adults.

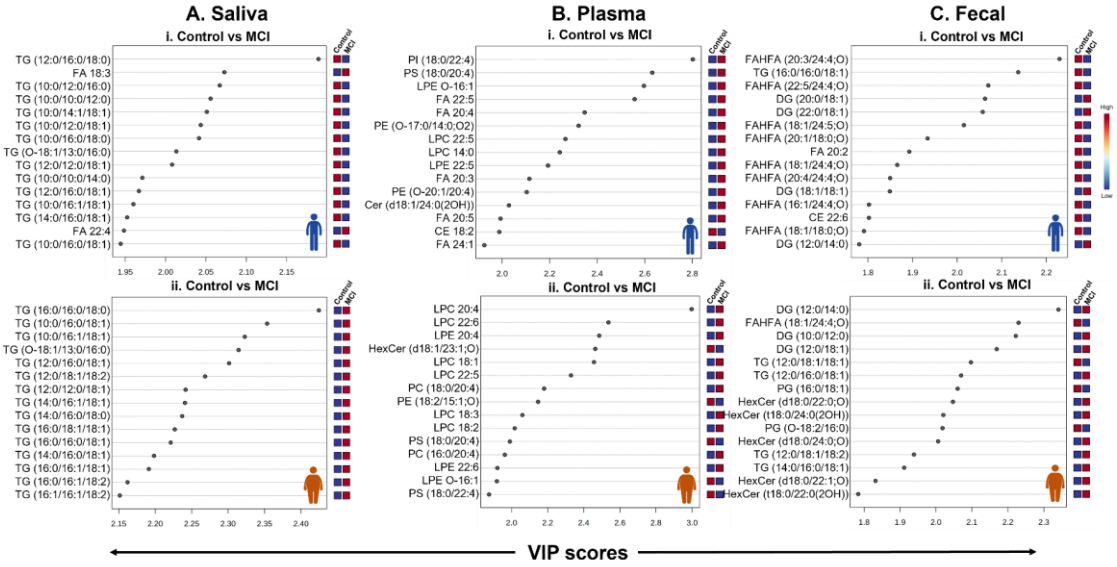

Figure 4.5: Weight-specific lipidome alternation in control and MCI groups of saliva, plasma, and fecal samples. **A.** OPLS-DA loading plot analysis of control and MCI groups of saliva samples for: (i) NW participants, (ii) OW participants, **B.** OPLS-DA loading plot analysis of control and MCI groups of plasma samples for:(iii) NW participants, (iv) OW participants, **C.** OPLS-DA loading plot analysis of control and MCI groups of fecal samples for: (v) NW participants, and (vi) OW participants.

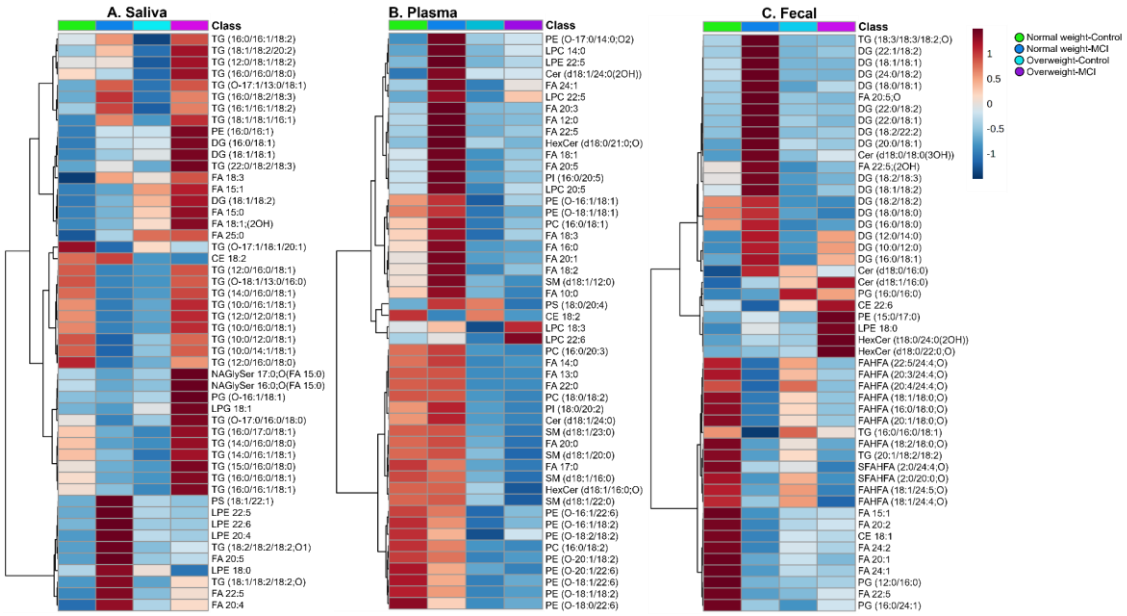

Figure 4.6: Heatmaps of the top 50 altered lipid molecular species in both the weight groups of control and MCI groups across saliva, plasma, and fecal samples of older adults.

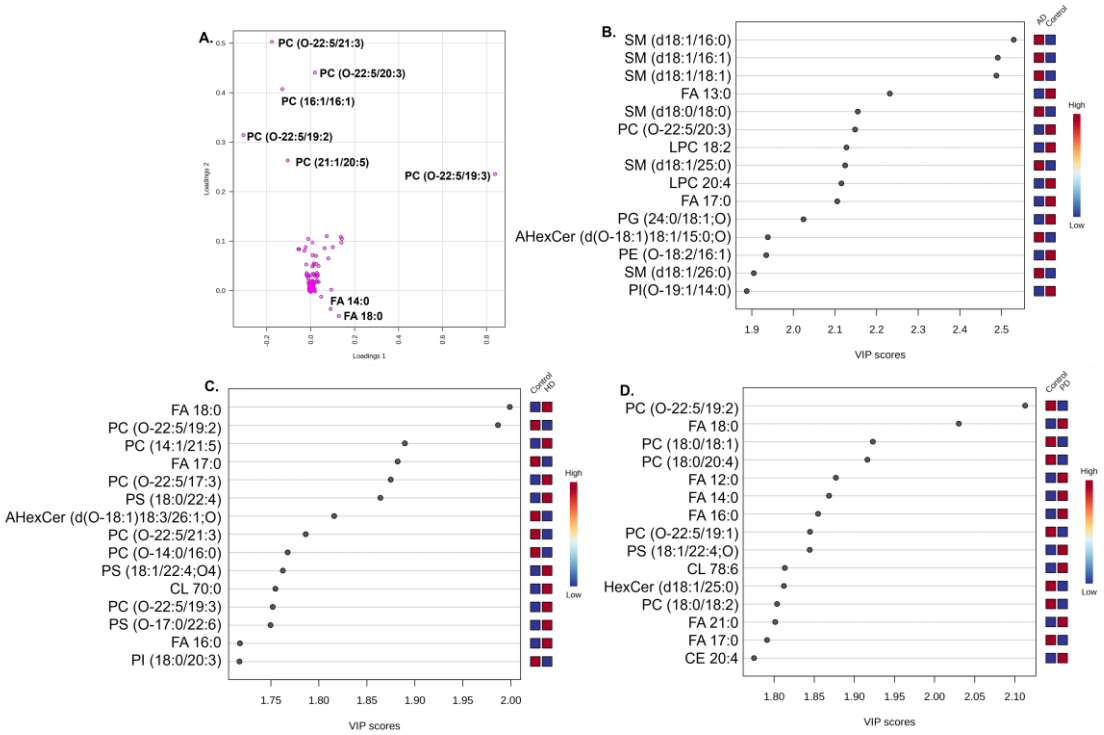

Figure 4.7: Multivariate analysis of all lipid molecular species identified brain tissue samples of HV, AD, HD, and PD samples of NDs. **A.** sPLS-DA loading plot of the brain tissue samples from the HV, AD, HD, and PD groups **B.** OPLS-DA loading plot of the brain tissue samples representing HV vs AD groups. **C.** OPLS-DA loading plot of the brain tissue samples representing HV vs HD groups. **D.** OPLS-DA loading plot of the brain tissue samples representing HV vs PD groups.

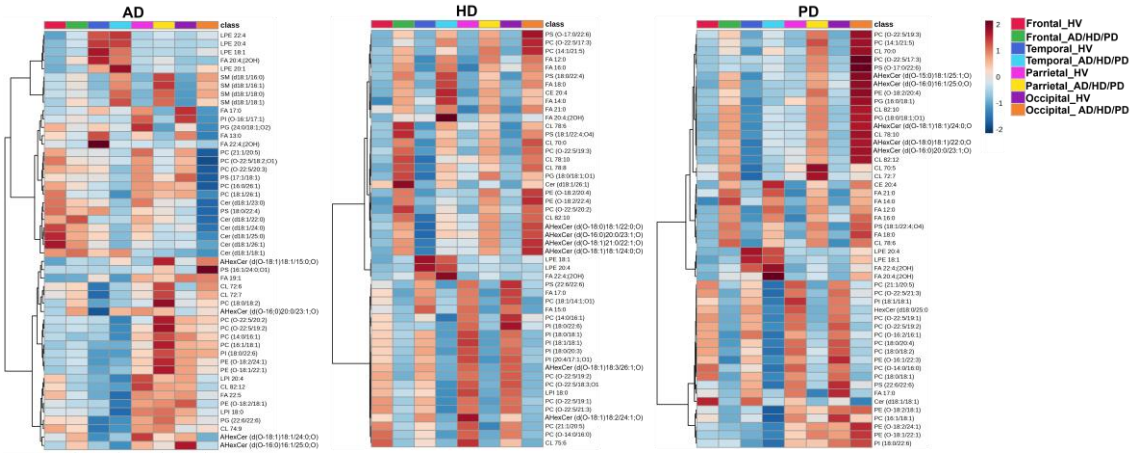

Figure 4.8: Heatmap of top 50 significantly altered lipids ($p < 0.05$) in region-specific groups across the brain tissue samples of HV, AD, HD, and PD participants.

Table 4.1: Significantly altered lipids between HV vs AD ($p < 0.05$).

Top candidates	Fold change (FC)	Log_2FC
PS (16:1/24:0;O1)	4.2471	2.0865
AHexCer (d(O-18:1)18:1/15:0;O)	2.4862	1.3139
PG (24:0/18:1;O2)	0.42552	-1.2327
PI (O-16:1/17:1)	0.42397	-1.238
PC (O-22:5/19:3)	0.40122	-1.3175
LPC 18:2	0.35891	-1.4783
FA 22:4;(2OH)	0.33439	-1.5804
LPC 17:2	0.28541	-1.8089

Table 4.2: Significantly altered lipids between HV vs HD (p <0.05).

Top candidates	FC	Log_2FC	Top candidates	FC	Log_2FC
PC (O-22:5/17:3)	24.698	4.6263	PS (18:0/22:4)	2.0137	1.0098
PS (O-17:0/22:6)	23.477	4.5532	LPI 18:1	0.49703	-1.0086
CE 18:2	4.8147	2.2675	PC (O-14:0/16:0)	0.49674	-1.0094
CE 20:4	3.8571	1.9475	PI (O-19:0/20:3)	0.48787	-1.0354
SPB 18:1;O2	3.5467	1.8265	LPI 18:0	0.47298	-1.0802
FA 18:0	3.4213	1.7745	PC (O-22:5/18:3;O1)	0.43017	-1.217
FA 20:4;(2OH)	3.3708	1.7531	PI (18:1/18:1)	0.42766	-1.2255
PC (14:1/21:5)	3.3003	1.7226	PC (21:1/20:5)	0.38622	-1.3725
CE 18:1	3.2335	1.6931	PI (18:0/20:3)	0.3833	-1.3834
PC (O-22:5/19:3)	2.6206	1.3899	PC (18:1/14:1;O1)	0.32845	-1.6063
CE 22:6	2.4435	1.2889	PC (O-22:5/19:2)	0.31871	-1.6497
CL 74:5	2.3006	1.202	PI (20:4/17:1;O1)	0.31799	-1.6529
CL 78:8	2.1146	1.0804	PS (22:6/22:6)	0.28796	-1.7961
CL 82:12	2.0989	1.0696	CL 75:6	0.24127	-2.0513
PE (O-18:2/22:4)	2.0334	1.0239	AHexCer (d(O-18:1)18:2/24:1;O)	0.16811	-2.5726
CL 72:7	2.0265	1.019	AHexCer (d(O-18:1)18:3/26:1;O)	0.080106	-3.642
CL 70:0	2.0194	1.0139	AHexCer (d(O-18:1)18:1/15:0;O)	0.012992	-6.2662

Table 4.3: Significantly altered lipids between HV vs PD (p <0.05).

Top candidates	FC	Log_2FC	Top candidates	FC	Log_2FC
PS (O-17:0/22:6)	15.437	3.9483	CL 78:10	2.1314	1.0918
PC (O-22:5/17:3)	7.4632	2.8998	FA 14:0	2.1251	1.0875
CE 18:2	4.5912	2.1989	CL 70:4	2.0452	1.0322
CE 20:4	3.9017	1.9641	Cer (d18:1/18:1)	0.47897	-1.062
PC (14:1/21:5)	3.7333	1.9004	HexCer (t18:1/23:1(2OH))	0.47645	-1.0696
CE 18:1	3.4768	1.7978	PC (O-22:5/19:1)	0.46526	-1.1039
CE 22:6	3.2248	1.6892	PI (20:4/17:1;O1)	0.46478	-1.1054
FA 20:4;(2OH)	2.9519	1.5616	PS (22:6/22:6)	0.44092	-1.1814
FA 18:0	2.7426	1.4555	PE (18:1/16:1;O2)	0.40791	-1.2937
FA 20:5	2.633	1.3967	PC (18:1/14:1;O1)	0.38417	-1.3802
SPB 18:1;O2	2.5011	1.3225	AHexCer (d(O-18:1)18:2/24:1;O)	0.38339	-1.3831
PC (O-22:5/19:3)	2.4466	1.2908	PC (O-22:5/19:2)	0.36559	-1.4517
PG (18:0/18:1;O1)	2.4416	1.2878	HexCer (d18:0/25:0)	0.35277	-1.5032
CL 82:10	2.3214	1.215	PC (21:1/20:5)	0.32255	-1.6324
FA 18:0;(2OH)	2.222	1.1518	AHexCer (d(O-18:1)18:3/26:1;O)	0.23321	-2.1003
PS (18:1/22:4;O4)	2.2125	1.1457	AHexCer (d(O-18:1)18:1/15:0;O)	0.020291	-5.623
PS (18:0/18:0;O)	2.1963	1.1351			

Supplementary information for Chapter 5

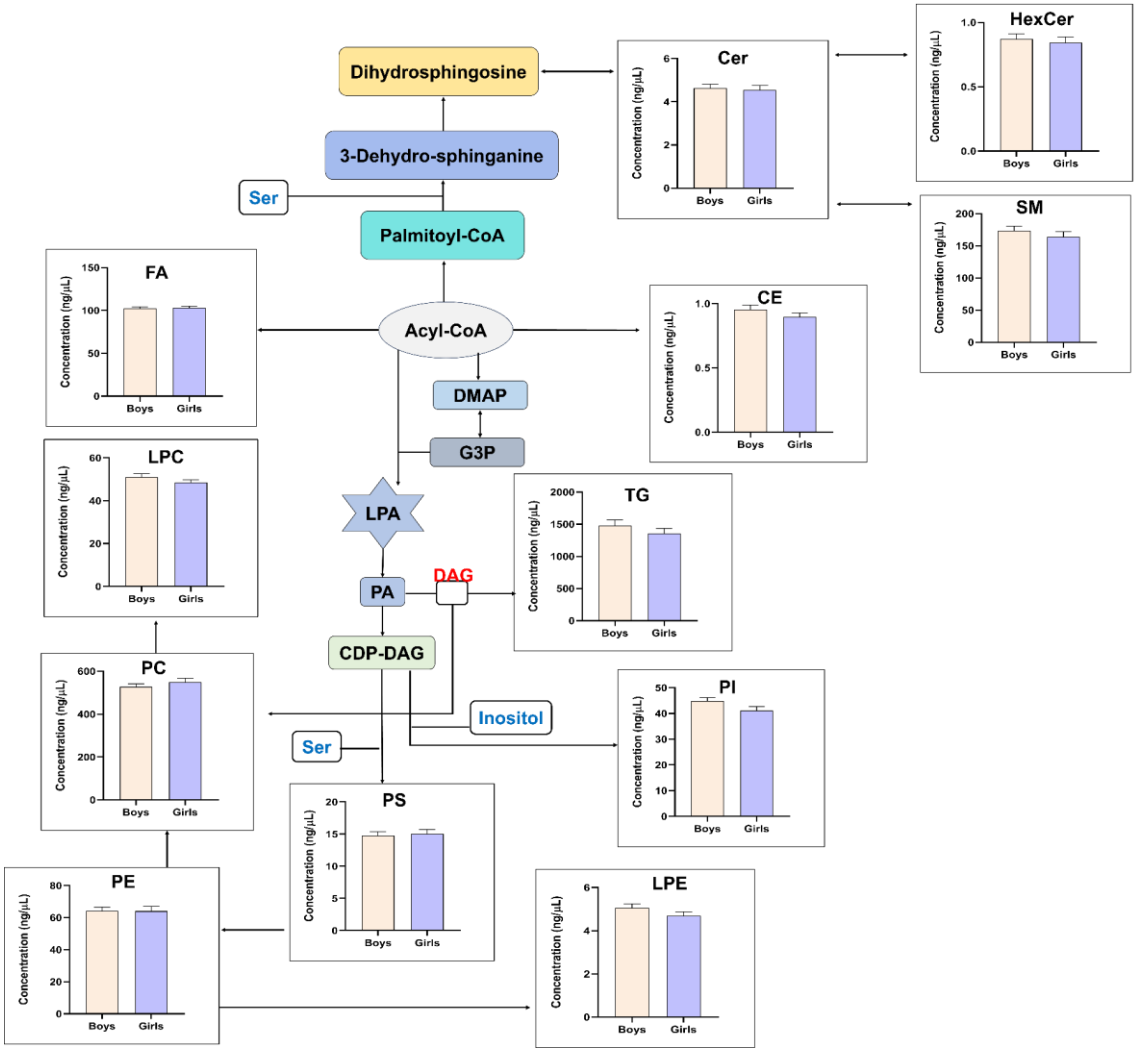

Figure 5.1: Analysis of lipid biosynthesis pathways in boys and girls. The data is represented as mean ± SEM. The Y-axis represents the concentration of the lipid sub-class in ng/µL and the X-axis represents different sex groups. Where the abbreviations are as follows: Acetyl Coenzyme A (Acetyl Co A), Fatty Acids (FAs), Dihydroxyacetone Phosphate (DHAP), Glycerol-3-Phosphate (G3P), Lysophosphatidic Acid (LPA), Phosphatidic acid (PA), Cytidine Diphosphate Diacylglycerol (CDP-DAG), Phosphatidylinositol (PI), Phosphatidylethanolamine (PE), Lyso-phosphatidylethanolamine(LPE), Phosphatidylcholine(PC), Lyso-phosphatidylcholine(LPC), Phosphatidylserine(PS), Diacylglycerol (DAG), Triacylglycerol (TG), Serine (Ser), Ceramide(Cer), Hexosylceramide(HexCer) and Sphingomyelin (SM).

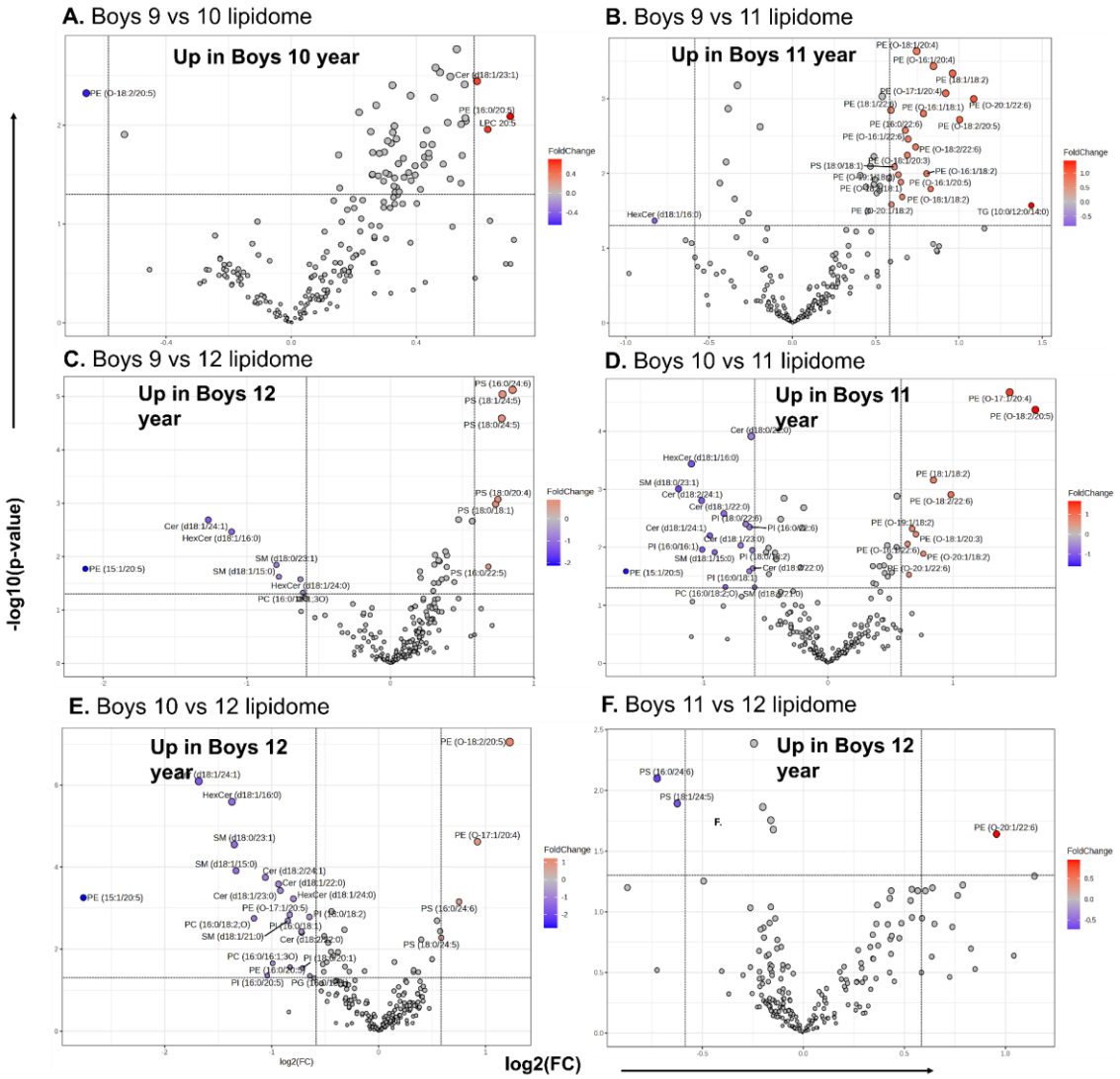

Figure 5.2: Volcanic plot representing significantly altered lipids (t-test, $p < 0.05$) in the plasma samples of boys **A.** Boys in the 9 vs. 10 years age group. **B.** Boys in the 9 vs. 11 age group. **C.** Boys in the 9 vs. 12 age group. **D.** Boys in the 10 vs. 11 age group. E. Boys in the 10 vs. 12 age group. F. Boys in the 11 vs. 12 age group.

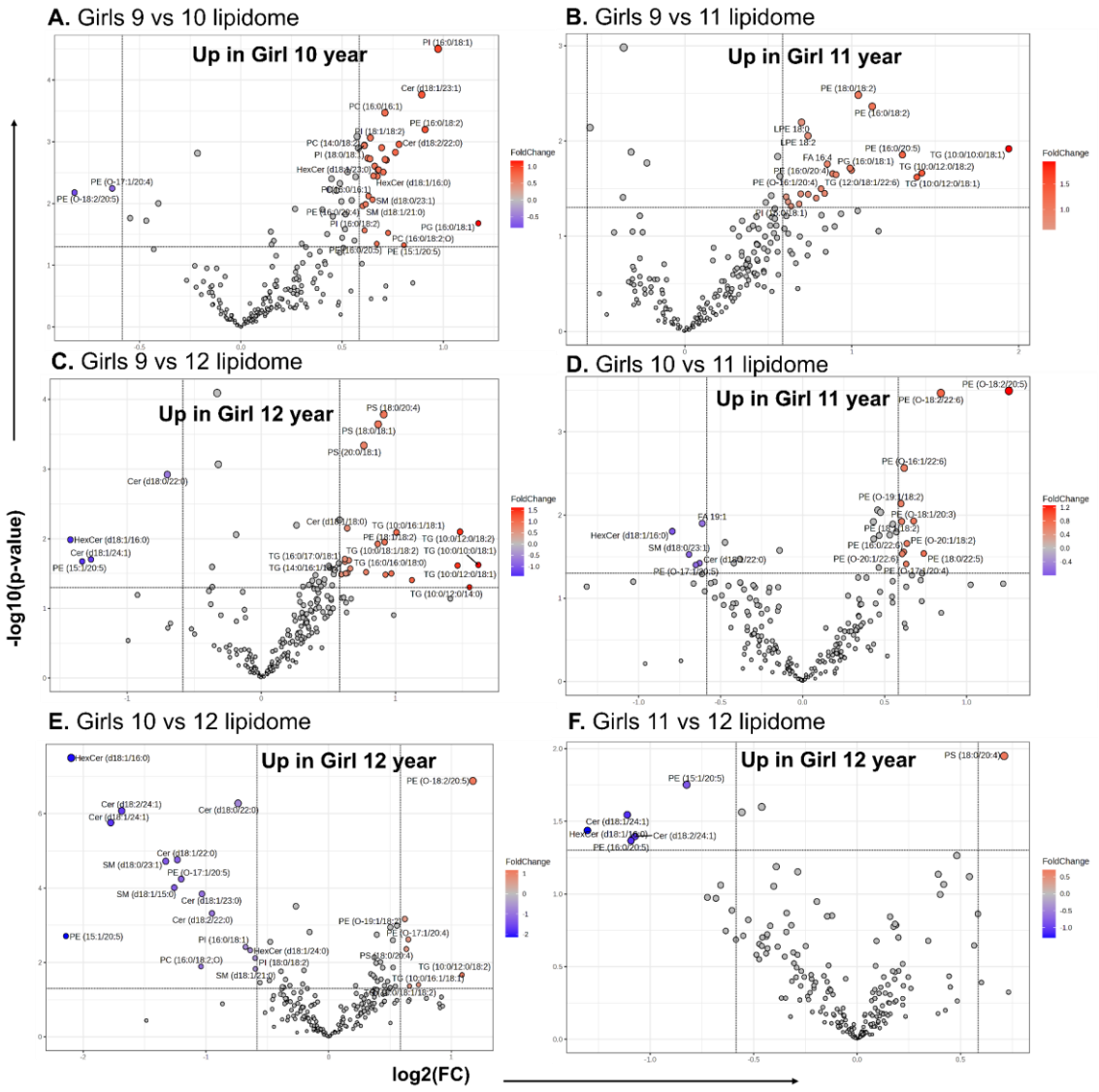

Figure 5.3: Volcanic plot representing significantly altered lipids (t-test, $p < 0.05$) in the plasma samples of girls **A.** Girls in the 9 vs. 10 age group. **B.** Girls in the 9 vs. 11 age group. **C.** Girls in the 9 vs. 12 age group. **D.** Girls 10 vs. 11 age group. E. Girls in the 10 vs. 12 age group. F. Girls in the 11 vs. 12 age group.

Supplementary information for Chapter 6

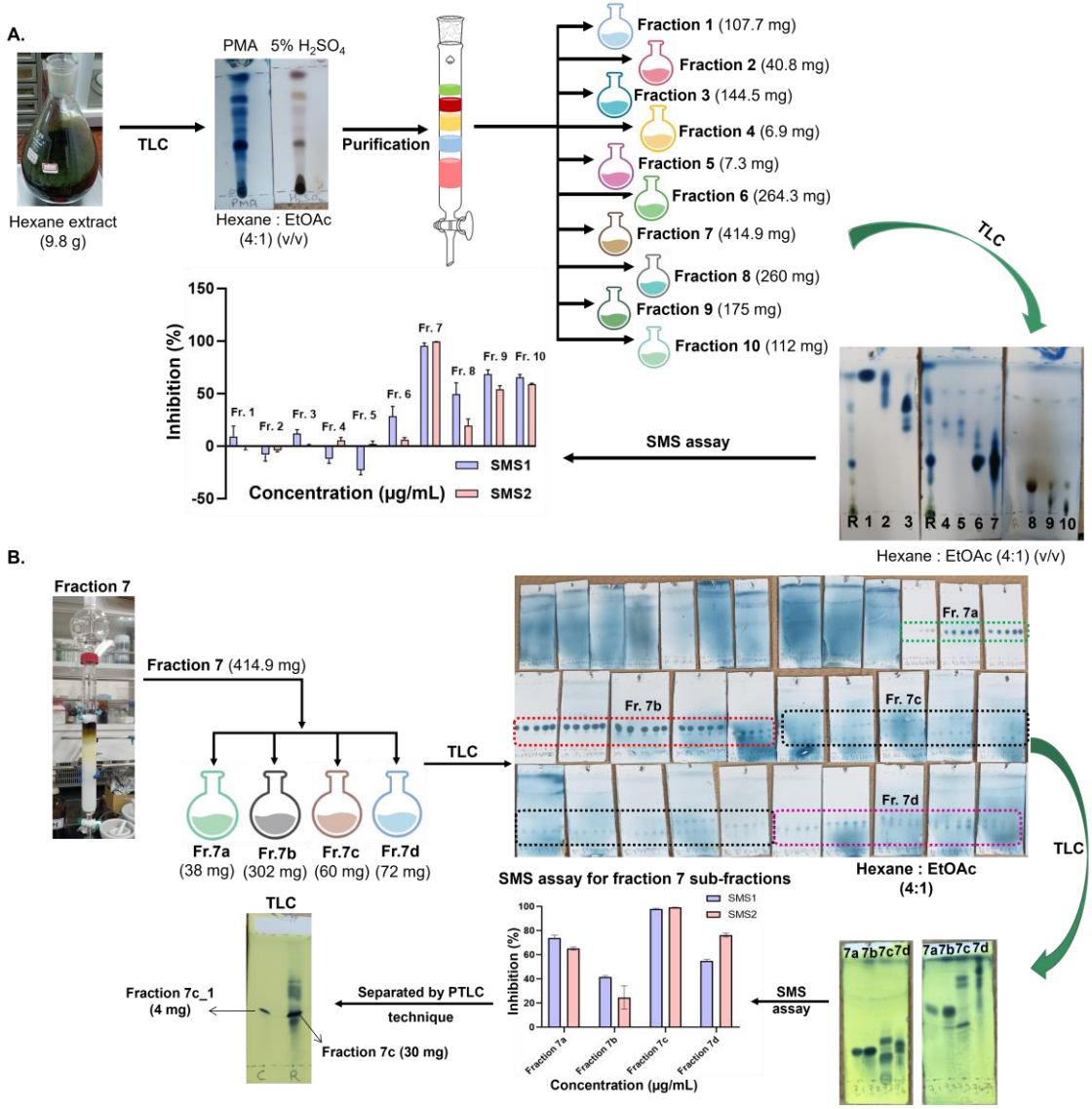

Figure 6.1: Detailed separation, purification, and SMS assay results of wakame: **A.** Isolation, separation, and SMS assay results of the hexane fraction. **B.** Isolation, separation, and SMS assay results of fraction 7.

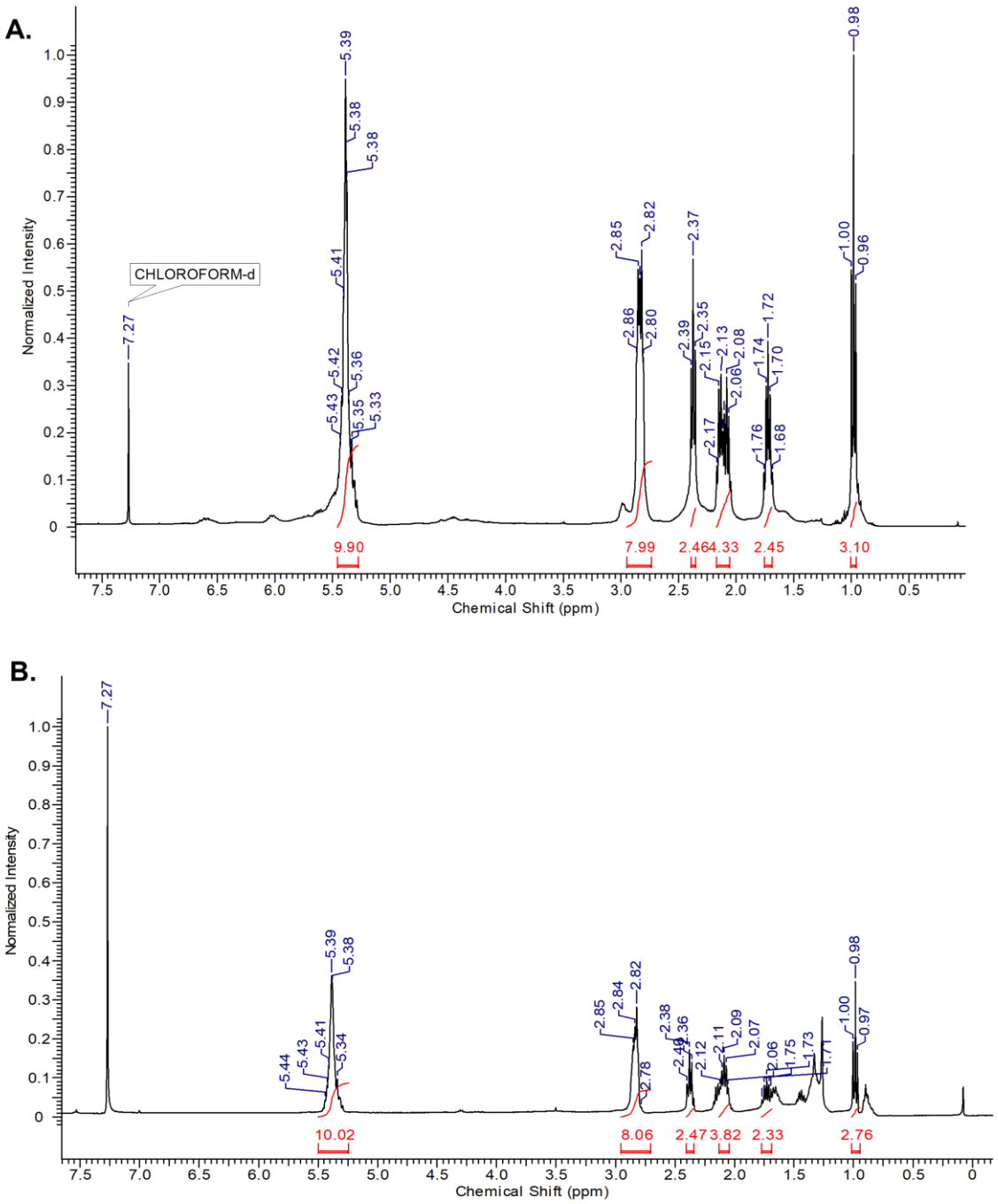

Figure 6.2: [1]H-NMR of **A.** Eicosapentaenoic acid (EPA). **B.** Purified compound